Independent mode protection of three ended power systems

Daniel, J. S.

Award date:
1991

Awarding institution:
University of Bath

INDEPENDENT MODE PROTECTION OF THREE ENDED POWER SYSTEMS

submitted by J. S. Daniel

for the degree of PhD.

of the University of Bath

1991

ProQuest LLC
789 East Eisenhower Parkway
P.O. Box 1346
Ann Arbor, MI 48106-1346

ACKNOWLEDGEMENT

The author would like to express his deep appreciation for the help and advice of so many people in the production of this work and to the Science and Engineering Research Council for providing a grant covering tuition fees and subsistence.

Those deserving special mention are my supervisors: Prof. A. T. Johns and Dr. R. K. Aggarwal; members of the Power Systems Group during my time at Bath: Dr. M. Martin, Dr A. Barker and Dr. D. Trip; staff of the University of Bath Computing Centre and of the University of Bristol Computing Centre.

During my time at the University of Newcastle the author would like to thank the Computing Department for use of facilities as an external student, and the Department of Electrical and Electronic Engineering for use of facilities and in particular Prof A. Jack for encouragement to get this work completed. The surface plots in Chapter 6 were drawn using UNIMAP.

CONTENTS

SUMMARY

This thesis investigates the simulation and relaying scheme requirements for three ended feeder protection using a combination of directional relays (DRs) and independent mode relays (IMRs). The IMR is triggered by a forward decision from its associated DR. Faults on particular Teed feeder configurations having a combination of short feedrounds between weak sources can cause incorrect operation of the directional scheme. The IMR is designed to operate for these cases.

The IMR algorithm derives and compares estimates of the fault–point voltage magnitude: one is constructed using pre–fault quantities; the other using superimposed quantities. Signals are combined in a novel way to reduce encroachment by earth fault detectors. The comparison algorithm is relatively insensitive to local source capacity and fault point on wave for solid faults. but there are limitations at high values of fault resistance. The minimum operation time is 11 ms: reach stability is considered more important than operating speed for the cases where the DR detects an internal fault as external.

The IMR design features checks to prevent false tripping during abnormal operating conditions. These are simple to define and implement if superimposed components are available.

There are also significant problems in applying directional relays to Teed feeders due to the uneven distribution of fault current between the ends and uneven desensitisation of relays. A design of directional relay has been developed which uses one directional discriminant and variable thresholds to ensure co–ordination of sensitivities at each of the ends. A new design of variable threshold algorithm was developed.

Work has also been done to make the power system simulation more accurate and efficient in generating series of studies in which pre–fault conditions and fault point on wave are varied. Displaying relay results as surfaces plotted against these two variables seems the best way to present their characteristics.

ABBREVIATIONS

AVR	Automatic voltage regulator
CT	Current transformer
CVT	Capacititor voltage transducer
DFT	Discrete Fourier Transform
DR	Directional relay
EHV	Extra high voltage
EMTP	Electromagnetic transient Program
FFT	Fast Fourier Transform
IMR	Independent mode relay
PLC	Power line carrier
p.u.	per unit
ROM	Read only memory
UHV	Ultra high voltage
VLTA	Variable level threshold algorithm

UNITS

A	Amperes
GVA	Giga Volt Ampere
Hz	Hertz
kHz	kilo Hertz
MVA	Mega Volt Ampere
V	Volts
VAR	Volt Ampere reactive

SYMBOLS

CONVENTION: Bold symbols refer to matrices; italic symbols to scalars or complex numbers. Suffices for bold and italic symbols are distinct.

'	(Prime) indicates modified version of a variable or matrix, or transient quantity i.e. X_d', T_d' according to context.

"	Indicates modified version of a primed variable or matrix, or sub–transient quantity i.e. X_d", T_d" according to context.
α	Frequency shift constant (positive real number).
a(t), A(ω)	Time domain signal and spectrum
β	thickness
b(t), B(ω)	Time domain signal and spectrum
c(t)	Time domain current
C	Current discriminant
C, C	Laplace or frequency domain current
δ	skin depth
$\delta(t)$	delta (impulse) function
D	Group delay
Dt	time sample duration
Dw	half frequency sample interval
e, E, E	emf
$\varepsilon(t)$	Envelope function
ϕ	Angle
f	frequency
f(t), F(ω)	Time domain (input) signal and spectrum, or (time domain) impulse and frequency response
F	Fault point F
FT	Feeder between fault and Tee point
g(t), G(ω)	Time domain signal and spectrum, or (time domain) impulse and frequency response
h	complex number causing 120^0 rotation in frequency domain
h(t)	Unit step function.
I	Current
I	Unit matrix
j	Complex number: $j^2 = -1$

k	integer or reach setting constant according to context
K	Constant used in mutual inductance model
$\Lambda_x, \Lambda_y, \Lambda_z$	Integrals giving time delay windowing functions
L	Inductance
m	Integer sometimes specifying a digital filter property.
n,N	Integers
P	Busbar P
P	Permittivity
PF, PT	Feeder between busbar P and F, and between P and Tee point.
PQ, PR	Feedrounds between P and Q,R
Q	Busbar Q
QT, QR	Feeder between busbar Q and Tee point, feedround between Q and R
$\rho(t)$	Critical phase angle, i.e. fault point on wave that would produce maximum filtered voltage at time t after the fault
r	Variable defining time within observation time window or root of cubic equation according to context.
R	Busbar R
RT	Feeder between busbar R and Tee point
$R, \boldsymbol{R}$	Resistance
σ	conductivity
s	Laplace domain independent variable.
S	Constant used in mutual inductance model
$\Sigma_x, \Sigma_y, \Sigma_z$	Sums of frequency spectrum points.
t	Time: (independent variable).
T	Particular time: Upper bound of observation time window, time constant or duration of one sample according to context.
T_{ir}	VLTA threshold: first suffix refer to voltage or current; second to forward or reverse quantities.
u	Variable

$U(\omega)$	Spectrum of time domain signal $u(t)$.
v_b	Backward voltage travelling wave
v_f	Forward voltage travelling wave
v_m	Voltage produced by superimposed current in a mimic inductance.
$v(t)$	Time domain voltage
$V, \boldsymbol{V}$	Laplace or frequency domain voltage
ω	Angular frequency (radians per second).
W	Particular value of angular frequncy
W_0	Angular frequency of power system
x	Independent variable
x_0, x_1, x_2, x_3	Data points
X	Reactance (usually combined with suffix).
$X(\omega)$	Spectrum of time domain signal $x(t)$.
ψ	Angle
y	Dependent variable
y_0, y_1, y_2, y_3	Function values at data points
$Y(\omega)$	Spectrum of time domain signal $y(t)$.
$\boldsymbol{Y}$	Admittance matrix
z	Independent variable
$\boldsymbol{Z}$	Impedance matrix

SUBSCRIPTS

CONVENTION: The following subscripts apply except where variable and subscript have already been explicitly defined. Combinations of two or more subscripts, i.e. pq denotes value of section of line between those locations or combination of properties as appropriate.

012	Sequence vector or matrix
0,1,2	Sequence components
abc	Vector or matrix relating to phase quantities
a	Armature resistance as in R_a

a,b,j,k,l,m	sets of rows and columns forming sub–matrices
a,b,c,d,e	Components of $y(t)$
ae,be,ce	Relating to (compensated) phase quanitities
bc,ac,ab	Relating to line quantities
d,q	direct and quadrature axis values (applied to reactances)
f	Value at fault point or pertaining to fault.
l	leakage (applied to reactances)
p,q,r	Value at busbars P, Q, R
s	Value pertaining to source at that point.
ss	Pre–fault value
sup	Superimposed component
t	Value at Tee point

CHAPTER 1

INTRODUCTION

1.1 AIMS

1.1.1 SCOPE

In any protection project, there are usually four main areas in which work is necessary:

1) Specification of system performance requirements and assessment of how well these are satisfied by the final design.

2) Specification of relaying principles and communication requirements.

3) Detailed design of relay.

4) Simulation of relay signals.

Seven objectives are outlined in the following subsections.

1.1.2 SYSTEM PERFORMANCE REQUIREMENTS

The main aim of this project is to provide better protection for single circuit Teed feeders on power systems. Specific objectives are:

1) To achieve single cycle fault clearance for severe faults.

2) To enable a greater variety of Tee configurations to be protected.

It is difficult sensibly to quantify the worst configuration which one should be able to protect. However, reasonable targets are those studied by Johns and Aggarwal [1] and here reproduced as Fig 1.1.

For comparison purposes, the easiest Teed feeder to protect has the following properties:

a) The line distance from the Tee point to each busbar is the same.

b) Each busbar has the same (high) source capacity.

c) Connections between busbars which do not pass via the Tee point (feedrounds) either do not exist or are very much longer than internal connections. For double circuit Teed feeders, an unfaulted parallel circuit produces a similar effect to a feedround having the same length as the internal path.

1.1.3 RELAYING SCHEME CONSIDERATIONS

In unit protection schemes, the fault clearance time is heavily dependent on the communication channel speed (bandwidth). Microwave or fibre optic links have a very large bandwidth, but the performance of cheaper more conventional communication channels such as power line carrier (PLC) may be unacceptably slow. However, if faults close to the busbars (close up faults) are detected with separate high speed independent mode relays (IMR) which trip the local circuit breaker, then a PLC unit scheme would be significantly improved. High speed operation requires:

a) That only locally available measurands are used.

b) That the measuring algorithm be optimised for speed rather than accuracy.

The protected zone would accordingly have to be smaller than in distance schemes, since transient over reach past a remote busbar must be avoided at all costs.

It is vital to clear close up faults quickly, since generally the nearer a fault is to a busbar, the greater the voltage depression and reduction in power which may be exported and hence the greater threat to system stability. It was for this reason that Chamia and Lieberman [2] incorporated an independent mode feature in their directional relay (DR) design.

When Teed feeders are to be protected with a DR scheme, an IMR is required to ensure correct operation, rather than as a means of improving performance for close up faults. In some Tee configurations (with unequal arm lengths, short feed rounds and an adverse combination of busbar source capacities), it is possible for internal faults close to one busbar to cause fault current to flow out of the Tee at another busbar. This 'feed round problem' (mentioned by Johns and Aggarwal [1]) causes one of the DRs to detect the fault as 'reverse' and issue a block signal preventing operation of the unit scheme. Additional communication channels (for intertrip signals) are necessary to overcome this problem. Objectives identified in this section are:

3) To test whether such circumstances can be rendered unimportant by the intertrips issued by IMRs at each busbar.

4) To assess the improvement in directional relaying performance provided

by IMRs in plain feeder applications. Note that intertripping would not be necessary in such cases.

1.1.4 PROCESSING OF RELAY SIGNALS

The information available at a relaying location consists of the three phase voltages and the three line currents, all of which are distorted by transducer errors. From these signals it is required to deduce the direction of the disturbance and whether the fault is within the protected zone. The separation of these tasks allows each to be performed more efficiently. In particular, determination of the direction of a disturbance allows the algorithm for (b) to incorporate the following features:

a) Pre–fault information may be discarded, since the earliest time of fault incidence is known from the operation of the DR.

b) A non–directional protection characteristic may be used, since fault direction is already known. This is a particular advantage as close up faults appear near the centre of the protection characteristic in the measured impedance plane rather than towards the edge.

An objective identified in this subsection is:

5) To test algorithms incorporating these features.

The actual waveforms that are used to make an impedance measurement are not pure sinusoids. There is distortion and corruption of the following kinds:

a) For most faults the voltage transducer (CVT) will contribute a slowly decaying transient to the voltage signal.

b) For most faults there will be exponentially decaying components in the power system current waveforms.

c) Travelling wave signals will also be present on both voltage and current signals, and have magnitudes which are not simply related to the (desired) power frequency magnitudes.

d) Cables, shunt and series capacitive line compensation, and static VAR compensators tend to lower the frequency of power system resonances, making them less

easily distinguishable from the power frequency components [3].

e) There are various sources of 'noise' caused by wideband processes which contribute to the relaying waveforms components which cannot be summarily neglected. The sources include switching transients and various non–linear consequences thereof, i.e. corona, transformer saturation and surge arrester activity. There is also 'noise' produced by the relay, e.g. analogue to digital quantisation error.

f) There are longer term non–linearities, such as arc voltage, transformer and generator magnetising currents and transducer saturation, which may cause the measurands to be appreciably non–sinusoidal.

The objective identified in this subsection is:

6) To consider the above phenomena and include their effects in simulations if likely to be significant.

1.1.5 SIMULATION

Simplifications are needed to make any modelling problem feasible, but the risk of omitting some important phenomenon is always present. Judgement is required to assess what level of accuracy and efficiency are appropriate at each stage of the project. In the early stages, a crude model may suffice to eliminate unpromising strategies, but more realism will be required at later stages. The four criteria are:

a) Costs of computer time and storage.

b) Actual simulation turn round time.

c) Simulation techniques available.

d) Accuracy required.

It will be shown that linear or linearised power system models allow useful work to be done on relay design, and hence frequency domain analysis may be applied to the network as a whole. However, improvements are possible in a number of areas:

a) Simulation of generator dynamics by a resistance in series with a reactance is inadequate. The sub–transient time constant is of the order of 30 ms. which is short enough to affect some aspects of relay performance.

b) The un–modified Inverse Fourier Transform technique can be made to work with reasonable efficiency and offers the advantage that it is unnecessary to express circuit impedances as functions of complex frequency. This is discussed by Dommel [4]. Another advantage is that Lanczos' sigma factor may not be required in order to filter Gibb's oscillations [5a].

c) The output from a relay simulation study consists of data showing whether a relay operated, and if so, how long it took. The input data is much more complicated, but still expressible numerically. The need to organise results into a form suitable for storage in a database imposes a structure on the program and makes a series of runs in which one parameter is varied (to produce two dimensional graphs) the norm.

d) In a series of runs it is possible to make use of network linearity to generate power system waveforms for any point on wave by linear combination of outputs at two different points on wave (e.g. 0^0 and 90^0, but not 0^0 and 180^0). This technique was mentioned by Dommel in his reply to discussion of a paper [4]. When the fault type is such that the superimposed signals depend only on one phasor, i.e single phase to earth and phase faults, the combination of two post fault waveforms (e.g. at 0^0 and 90^0 POW) may also be used to efficiently generate waveforms in which the pre–fault loading is varied.

Objectives identified in this subsection are:

7) To attempt to produce an un–modified Fourier transform technique incorporating methods to efficiently produce sets of results.

1.2 BACKGROUND TO SYSTEM PERFORMANCE REQUIREMENTS

Improvements in protection design are needed to cope with the following changes in power system design:

1) Smaller urban power stations are being closed down in the UK, leaving large centres of generation and load interconnected by long transmission lines. Abroad this circumstance is even more pronounced: some load and generation centres are separated by as much as 1500 km.

2) Modern large generators have lower p.u. inertia and higher p.u. transient reactance than smaller machines [6].

3) Extensions or reinforcements of the transmission grid requiring further transmission lines or substations are resisted due to capital expense and environmental impact.

4) On long transmission lines abroad, it is becoming more common to attach distribution transformers (without EHV side circuit breakers) at intermediate locations [7].

5) Extensions to the existing grid by connecting new feeders directly to an existing line, rather than building a substation at the junction or routing the new feeder back to an existing substation are being proposed and built. These Teed feeders are obviously much cheaper to build but have particular protection problems [8].

Each of the above changes makes it more likely that synchronisation between a generator and the rest of the grid could be lost in the event of a fault. Several ways of enhancing system stability exist:

1) Making the generator excitation system respond more quickly.

2) Reducing turbine power by means of fast valving.

3) Shunting affected generators with electrical braking resistors.

4) Using single pole reclosure schemes.

5) Reducing maximum fault clearance time (to one power cycle period) [9].

When a fault is on the system, each of the above options attempts either to reduce the mechanical power supplied to the generator or increase the electrical power which it can deliver to the system.

Option (1) has usually been pursued to the practical limit (static thyristor exciters) at crucial power stations. Options (2) and (3) are expensive: requiring additional or uprated hardware. Single pole reclosure would improve stability for single phase to ground faults, but for very severe three phase faults there would be no improvement over conventional protection schemes.

The most attractive option is to reduce the fault clearance time, although there may be extra cost in replacing or up–rating the circuit breakers to meet the higher current breaking duty. However, this is usually preferable to utilising important transmission lines inef-

ficiently (i.e. with transient stability considerations reducing maximum permissible power transfer to much less than the limits imposed by steady state stability requirements or resistive heating and thermal effects).

1.3 BACKGROUND TO RELAYING SCHEMES

There are essentially two types of protection schemes:

1) Non–unit schemes, in which a determination of whether a fault is present in the protected zone is made using only measurands derived locally. A communication channel may also be present to accelerate tripping at the remote end.

a) Distance relaying uses voltage and current signals measured at a single relaying location to determine whether the impedance to a fault lies within the protection characteristic in the impedance plane. Various different zones may be defined for a single relay with tripping times for outer zones deliberately delayed or made dependent on signals received via the communication channel in order to maintain co-ordination with other relays [10].

b) Over current relaying also makes use of only local measurands to generate either zero or negative sequence current components. The scheme relies on a low value of local source impedance to give forward/reverse discrimination and protection zone definition. The latter is necessarily less precise than that given by a distance relay [11].

2) Unit schemes depend entirely on a data communication channel between relaying locations. Ultra high speed relaying schemes are usually of this sort. Two types of scheme have been described:

a) Differential relaying: in which the currents at each end of a plain feeder are measured and the coded value transmitted to a processor at one or both ends. The values are compared and if they differ sufficiently then a trip is initiated. Communications requirements may be reduced by combining the three line currents into one signal before coding, but this has the disadvantage that certain unusual types of fault cannot be detected [12].

b) Directional relaying: in which the direction of a disturbance from the re-

laying location is ascertained using voltage and current signals. If the fault direction is 'reverse' then a block signal is issued [13].

The minimum relay operating times for faults initiated at various points on wave, and the effects of system noise on relays are discussed by Phadke [14]. Directional relays can be compared to over–reaching distance relays (in a blocking scheme), but their performance is superior due to the use of superimposed components.

The blocking scheme of communication used in directional relaying has the following advantages:

1) The relay nearer to the fault operates first, unlike the behaviour in permissive over–reach schemes where it is often the last to operate [14a].

2) There is no need to signal through a fault with power line carrier communication equipment, since signalling is only required for external disturbances.

3) Minimal coding security is needed for a block signal (compared to an intertrip signal), and hence communication delay and bandwidth requirement are small.

4) Only one blocking frequency is needed for plain or Teed feeders.

5) Since decisions rather than data are being communicated, the bandwidth and channel attenuation demands are much less onerous than for differential protection.

Communications requirements become a major consideration when directional relaying is applied to Teed feeders, as intertrip channels are required in addition to the blocking channel. Due to the higher security requirement for an intertrip channel and the need to signal through a fault (when using PLC), it is not desirable to have a common intertrip channel [15]] i.e. each transmitter communicating with both remote receivers on the same frequency. Hence, either:

1) Two complete sets of communication hardware must be fitted at each relaying location (to allow simultaneous transmission on different frequencies), or:

2) Two sets must be fitted at only one location and intertrip signals from the other ends received and retransmitted there.

The latter scheme is cheaper but would often result in a longer delay before all circuit breakers had operated. If intertrip signalling is dispensed with altogether, then the trip-

ping of one circuit breaker might cause the other relays to trip (sequentially) when they detected that disturbance, but, this process would be slow and uncertain, since directional relays do not recover full sensitivity immediately after a fault.

Distance protection of Teed feeders is possible for a limited range of configurations, though restrictions on load flow are often required to prevent incorrect operation in protection zones 2 and 3. If this is not acceptable, then, short of reconfiguring the whole system, it is possible to insert one set of CTs at the junction of the longest arm with the other arms and protect that arm using differential relaying [16].

True three ended differential schemes have been proposed, but they require the wide bandwidth of a fibre optic link [1] or a microwave link [17].

Protection of transmission lines which have transformers (without intervening circuit breakers) at intervals between the busbars also presents problems, in that it becomes difficult to distinguish between healthy and faulted network impedances. However the problems are not so acute as those of Teed feeders and conventional relaying together with operational restrictions may suffice [7].

1.4 BACKGROUND TO RELAY DESIGN

Two techniques will be discussed in this section:

1) Impedance measurements as carried out in distance relaying.

2) Directional determination as used in 'travelling wave' or 'superimposed component' relays.

1.4.1 IMPEDANCE MEASUREMENT

When a fault occurs it acts as a broad band source of electromagnetic energy, and in principle, the line impedance could be measured at any frequency. In practice, the signals to be measured are assumed to be at power frequency. (The energy spectrum corresponding to the change in relaying signals due to the fault peaks around power frequency, so the choice is not unreasonable.)

At power frequency and assuming ideal transposition of the transmission line, there exist two different values of relay to fault impedance:

1) Zero sequence component or earth mode.

2) Positive or negative sequence component: same value for each.

It is difficult to isolate positive or negative sequence voltage and current as the defining phase to sequence transformation relates phasors (or frequency domain objects) by complex coefficients. The time domain implementation requires frequency invariant phase shifts over a wide frequency band (theoretically infinite).

Another difficulty is that it is impossible to generate measurands which exclude the effects of zero sequence line impedance for faults which involve earth. All that can be done is to compensate using an assumption as to the ratio of the zero to the positive sequence line impedance. Measurands which would seem to exclude zero sequence quantities, e.g. Clarke components of voltage and current, actually introduce an extra dependence on zero sequence source impedance.

Generally two techniques are advanced for extracting the desired (sinusoidal) power frequency signals:

1) Time domain filtering or computer relaying, which includes least squares estimation [18], Kalman filters [19] and finite Fourier transform techniques [20]. These have the advantage of explicitly finding the real and imaginary parts of the impedance, allowing the protection characteristic to be a complicated shape e.g. a quadrilateral, in the complex impedance plane. However, all the techniques seem to be very sensitive to low frequency exponential decays.

2) Frequency domain filtering, which involves passing signals through a low pass or band pass filter such that higher frequency components are greatly attenuated. Considerable effort has gone into assessing what the filter cut off frequency should be, since the lower it is, the longer the filter group delay and relay operating time [21].

In conventional distance relaying, the protection characteristic is defined by phase or amplitude comparison of two signals: each being the sum of voltage derived from the system and the voltage across a mimic impedance. More elaborate impedance characteristics are possible with a larger number of signals, and improved performance for close up faults by the use of cross polarisation [22].

Distance relaying techniques are now mature and well understood in terms of steady state performance, i.e. protection characteristics are defined as areas in the complex impedance plane. When the effects of transients (other than at power frequency) become troublesome, extra filtering is used, but this increases the group delay and hence the operating time (even if greater rejection of only low frequency terms is required). Narrowing the relay response bandwidth also extends the duration in which the effects of pre–fault measurands are significant. The use of directional relays to ensure that measurement only uses post fault information promises a means of overcoming the consequent degradation in performance.

1.4.2 SUPERIMPOSED COMPONENTS

Directional relays use the superimposed current and voltage components at a relaying point to determine the direction of a disturbance from that point. Superimposed components are obtained by subtracting the steady state quantities from the measured quantities. However, since there are always perturbations on a power system, there may be some argument as to the precise definition of the steady state quantities. In effect there are two definitions of superimposed components: the theoretical and the practical. In theory (and simulation) it is possible to specify and subtract the pre fault steady state components.

Practical implementations of superimposed component extraction do not attempt to use a precise definition of a steady state quantity but derive the superimposed component by passing the measured quantity through a filter which has a notch at the assumed frequency of the steady state component. The bandwidth of the notch determines the duration of the superimposed component for step changes in either power frequency amplitude and/or phase of the measured signal. (A step change in signal frequency or mismatch of the notch frequency would cause a continuous output.) It is possible to make the notch frequency track the measured frequency in digital implementations [23].

The physical interpretation of a superimposed quantity is relevant to its use. Fault incidence on a network may be represented either as:

1) A change in circuit configuration at fault time, (which treatment is not

amenable to linear analysis): Fig 1.2a, or,

2) The post fault circuit configuration existing for all time, together with voltage sources in the fault path which make the fault current equal to zero before the fault: Fig 1.2b

Provided the network is linear, the latter treatment may be simplified by separating the voltage sources which exist on the network into two sets:

1) Those existing for all time: Fig 1.2c

2) Those which change at fault time: Fig 1.2d

The system response is equal to the sum of the responses to these separate excitations.

The response to the first set of excitations is simply the pre fault condition of the network, produced by assigning the pre–fault excitations to the generators. The values of the voltage sources at the fault point are found by solving the network assuming they are open circuit.

The second set of voltage sources consists of zero excitation to the generators (for all time) together with sources at the fault point which are zero before the fault and have a finite value at and after the fault time. This value is chosen to satisfy the post fault conditions, i.e. to make the post fault sum of the fault path source voltages zero.

It can be seen that synthesizing the superimposed network quantities isolates the network response to the second set of sources, which has a number of advantages:

1) The only excitation is at the fault point.

2) If the Thevenin equivalent reactance of the network at a relaying point is generated (looking in either direction), then it will be found to be predominantly inductive.

Superimposed quantities therefore represent the effect of sources at the fault point injecting current into a network dominated by inductive reactance, and the direction of the fault can be deduced by comparing polarities of the voltage and the differential of the current. Strictly, the above explanation applies only to the theoretical definition of superimposed components.

1.4.3 DIRECTIONAL RELAYING PRINCIPLES

Superimposed component relays were originally called travelling wave relays [2], and attempted to recreate and compare the forward and backward travelling waves V_f, V_b arising from a fault. Assuming that the transmission line is lossless and has frequency invariant parameters, this may be done by forming the following quantities:

$$V_f = V - CR \qquad\qquad V_b = V + CR$$

Where R is a surge resistance, and V and C are combinations of superimposed voltage and current.

For a short period after the fault (of the order of two wave transit times for the line), comparing these two quantities gives an unambiguous indication of fault direction. V_f should be zero and V_b finite for a forward fault, and vice versa for a reverse fault. Travelling wave reflections after this short period, which is inadequate to allow a definite decision in the presence of noise and transducer delays, may not satisfy the directional criterion. Low pass filtering was therefore added to remove some of the noise, and, perhaps unexpectedly, it worked well. The forward and backward waveforms now looked like power frequency waveforms and a much longer discriminative time was available. Gradually it became apparent that the value of the 'modal surge impedance ' R was by no means critical, and it was renamed 'current mixing factor' [24]. The travelling wave connection had disappeared except in theoretical justification of the technique [13].

Engler et al. [25] have developed a different directional relaying principle. Two discriminant signals are formed from the superimposed voltage V and a voltage produced V_m by the superimposed current C in a mimic inductance L:

$$V_m = L\frac{dC}{dt} \qquad\qquad V_f' = V - V_m \qquad\qquad V_b' = V + V_m$$

If L is the inductance of the local source then V_m is either equal to, or equal and opposite to, V, giving the magnitude criterion that V_f' should be zero and V_b' large for a forward fault and vice versa for a reverse fault. Even if the value of L were not so happily chosen then the relative magnitudes of V_f' and V_b' would still allow directional discrimination.

Since the superimposed current starts from zero at the fault time, for most of the first quarter cycle of power frequency the filtered current and its differential, i.e. *Vm* in this principle and *CR* in Johns [13], have the same polarity and hence cause similar behaviour in the respective discriminants.

In theory Engler's principle is better since the magnitude relation is maintained for all time (in the absence of current clipping). Practically there may be little difference, since a directional relay should operate within a quarter of a power cycle period. However, an additional check is needed in Johns' formulation to prevent incorrect operation when the magnitude relation becomes invalid. Dommel and Michels [26] use a rather more complicated set of discriminants to ensure that their magnitude criterion is maintained for all time. Using the rate of change of relaying voltage in a discriminant seems less satisfactory than using rate of change of current, since travelling waves are more pronounced on voltage signals.

Rajendra and McLaren's travelling wave principle [27] does actually use travelling wave properties but requires voltage transducers having an extended high frequency response which increases scheme cost. The authors also draw attention to the difficulty of interpreting relaying signals that occur on Teed feeders (due to multiple reflections.)

1.5 BACKGROUND TO SYSTEM MODELLING

1.5.1 INTRODUCTION

The system may be considered to be composed of the following components:

1) Power transmission lines.
2) Transformers.
3) Generators.
4) The arc at the fault point.
5) Circuit breakers and switches.
6) Load.
7) VAR compensation or series compensation.
8) Reactors.

Modelling will be restricted to components (1–4). Other components (7,8) are assumed not to exist on the protected network or not to operate or vary during the simulation time window (5,6). Such simplifications are necessary if simulation results are to be produced within an acceptable timescale and at acceptable cost. It is believed that the neglected phenomena do not critically affect relay performance.

1.5.2 TRANSMISSION LINE MODELLING

Most power transmission line modelling refers the work of Carson [28] who derived impedance formulae which take into account the finite conductivity of the earth, which causes the parameters to be frequency dependent. Wise [29] has shown that finite earth conductance also requires a correction to be applied to the admittance per unit length parameters of the idealised model. However this correction will be omitted as it is not significant below 10 kHz. and transducer frequency responses band limit the relaying signals much below that.

The effects of corona [30] which causes a non–linear variation of line capacitance with voltage will be neglected. Power transmission lines are designed so that corona does not occur at working voltages, but it may be present under faulted conditions due to over–voltages on un–faulted conductors. Switching operations also cause over–voltages, but the response of the relaying scheme to such disturbances will not be studied.

There are two approaches to simulation of a system which includes transmission lines with frequency variant parameters:

1) Time domain simulation. Three techniques have been proposed:

a) Convolution models.

b) State variable (including recursive convolution) models.

c) z transform models.

2) Frequency domain simulation. Two techniques have been proposed:

a) Fourier Transform method.

b) Modified Fourier Transform method.

1.5.2.1 CONVOLUTION MODELS

Much of the work in this area has been done to interface a line model with frequency variant parameters to the Bonneville Power Administration Electromagnetic Transients Program (EMTP) [31], which uses state variables to define the behaviour of lumped parameter components.

The first attempt was made by Budner [32] who found the modal admittances and transfer admittances of a multi–conductor line as a function of frequency and then derived weighting coefficients for a convolution model using the inverse Fourier Transform. A large number of coefficients have to be found as the impulse responses take many travelling wave transit times to decay.

A major improvement was made by Snelson [33] who modelled a line terminated in frequency invariant matching resistances rather than open circuited. The coefficients in the model now represent forward and backward voltage transfer ratios rather than admittances, and far fewer are required since reflections from the ends of the line are much reduced.

This method was modified by Meyer and Dommel [4] to utilise the trapezoidal integration routine existing in the EMTP and hence allow larger time steps. Ametani [34] proposed linearly interpolating between a subset of convolution coefficients as an alternative way of reducing the computational workload.

1.5.2.2 STATE VARIABLE MODELS

Semlyen and Dabuleanu [35] derive a formulation based on Duhamel's integral which they term recursive convolution. The voltage change at one end of the line (with a matched termination) is found as the convolution (with a set of coefficients) of the voltage changes at the other end. The coefficients are produced by modelling the line step response as the sum of a number of exponential decays. To attempt to reproduce the low frequency characteristics of the line surge impedance, an exponential decay modelling the step response of the matching termination admittance is included.

The formulation is equivalent to finding the poles with the largest residues in the respective responses and associating state variables with them. Three exponentials were initially used to model the voltage step transfer admittance and one for the matching termination admittance, but subsequent experience [36] showed this gave unacceptable error at zero and power frequencies and the order of the fit had to be increased. Triezenberg [37] noted a similar problem in his much simpler attempt to model power transmission lines using state variables. Finding more poles more accurately or more efficiently has now emerged as the central issue in this field, as a number of papers testify [38,39].

1.5.2.3 z TRANSFORM MODELS

The z transform method of simulating electromagnetic transients [40] is a variation on the theme of the previous paragraph (1.5.2.2). The procedure is to fit rational functions of z to the step transfer and termination admittance functions of the line in the z domain using a least squares algorithm. The time domain transform of the rational function is then computed. The order of the functions is quite low and the technique corresponds to fitting a few poles. Originally the bilinear transform was used but it was found unsatisfactory.

It is an advantage with this technique if the time step is an integral sub–multiple of the travelling wave transit time (as with Semlyen's recursive convolution technique), but this limitation is overcome (in both cases) by using interpolation formulae. Most of the computational effort in both techniques is spent in fitting rational functions or finding poles; the actual simulation times are proportional to the number of time steps (rather than the number squared for conventional convolution).

1.5.2.4 FOURIER TRANSFORM METHOD

Provided that each circuit element is linear or may be represented by a linearised model, then their frequency responses may be combined to obtain transfer functions of the network at any frequency. The spectra of the exciting functions (usually generator or fault point voltages) can often be simply calculated; hence the output spectra (voltages and currents at relaying locations) may be found, and, by application of the inverse Fourier Transform, the time domain signals. There are three difficulties though:

1) Often the transfer function of the network is not a closed algebraic expression, and a numerical rather than an algebraic inverse Fourier Transform method needs to be used.

2) The usual idealised time domain exciting signals (steps or sinusoids instantaneously applied) have frequency spectra which contain poles on the jω axis and generalised functions (delta functions), which require algebraic treatment.

3) The transfer function may have peaks at certain frequencies which require detailed numerical treatment which would be inappropriate for the whole spectrum. This conflicts with the requirement of the Fast Fourier Transform (FFT) [41] for uniformly spaced data points.

Lego and Sze [42] addressed some of these problems. As they show in the Appendix to their paper (and in Appendix 1), the spectrum of a unit step (in the time domain) consists of two components:

1) A delta function.

2) A pole at zero frequency.

Their method treats the delta function in a special way, but unnecessarily assumes that the network transfer function is of such a form that the pole will not cause numerical problems. Once this defect is remedied the method may be extended to instantaneously applied sinusoids as hinted by Lanczos [43].

1.5.2.5 MODIFIED FOURIER TRANSFORM METHOD

Despite the possibility of removing impulses and poles on the jω axis from a frequency spectrum, the difficulty of localised peaks (e.g. at travelling wave frequencies) remains, which require a small frequency sampling interval for the spectrum to be accurately represented. The problem is particularly acute in over voltage studies, where a very wide frequency bandwidth has to be considered. The modified Fourier Transform technique, described in a series of papers [5a–d], was developed to overcome this problem.

In essence, the technique involves a change of angular frequency variable from ω to ω–jα. Provided that the frequency response of the network can be obtained in terms of com-

plex frequency, the excitation and output spectra can be found as functions of $\omega - j\alpha$ and the time domain signals evaluated. However for transmission lines with frequency variant parameters, the component of the line impedance due to the earth return path cannot be directly found in such a form. If this component is given by:

$$Z(\omega) = R(\omega) + j\omega L(\omega)$$

Then strictly, curve fitting should be used to obtain:

$$Z(\omega - j\alpha) = R(\omega - j\alpha) + (\alpha + j\omega)L(\omega - j\alpha)$$

However, this is troublesome to do and the following approximation is usually made:

$$Z(\omega - j\alpha) \approx R(\omega) + (\alpha + j\omega)L(\omega)$$

An attempt has been made [44a] to show that this is not an approximation, but despite early misgivings [44b], the approximation does not seem to cause unacceptable errors.

A point not emphasised in the literature is that there are two quite distinct methods of obtaining a time domain output using the modified Fourier Transform in an observation time window $0 < t < T$:

1) The integration method: in which the exciting signal $x(t)$ is equal to a physically realisable signal $f(t)$ for all time:

$$x(t) = f(t) = 0 \qquad t < 0 \qquad\qquad x(t) = f(t) \qquad t \geq 0$$

Both the input and output spectra are continuous, and the output time domain signal should (in theory) represent the actual output signal for all time.

2) The series method: in which the exciting signal $x(t)$ is equal to $f(t)$ only during the observation time window:

$$x(r + mT) = f(r)\exp(\alpha mT)$$

$$t = r + mT \qquad 0 \leq r < T \qquad m = \ldots, -2, -1, 0, 1, 2, \ldots$$

The input signal is not zero for $t < 0$ and it is not equal to $f(t)$ for $t > T$. The input and output spectra consist of a series of impulses at angular frequencies:

$$\alpha + j\left(\frac{2\pi n}{T}\right) \qquad\qquad n = \ldots, -2, -1, 0, 1, 2, \ldots$$

In Ametani's developed modified formulation [45], the expression for the input signal is given by:

$$x(r+mT) = (-1)^m f(r)\exp(\alpha mT)$$

And the spectrum lines occur at angular frequencies:

$$\alpha + j\left(\frac{\pi n}{T}\right) \qquad n = \ldots,-3,-1,1,3,\ldots$$

It can be seen from the expressions for the input waveform that there is likely to be a large step change in value at $t=T$, which, when the frequency spectrum is truncated, may cause Gibb's oscillations in the time domain. These can be reduced by multiplying the truncated frequency by Lanczos' sigma function, though this has the side effect of artificially reducing the rate of rise of steep wave fronts. The integration method of finding the time domain output does not have this discontinuity (though there is still likely to be one at $t=0$) and the physically unrealisable low pass filtering implicit in the use of the sigma factor may be omitted.

Inclusion of transducer frequency responses in frequency domain simulations would improve both accuracy and efficiency of the simulation for the following reasons:

1) The low pass nature of such responses would reduce frequency truncation effects.

2) The two stage process of obtaining relaying signals described by Johns et al. [46] requires that the upper half of the network frequency spectrum be zero so that an unaliassed signal can be presented to the transducer simulation. If the transducer response were included then this restriction would no longer apply.

When the modified Fourier Transform is used, almost invariably the problem is being formulated in terms of the series method, despite statements about numerical or trapezoidal integration. If the integration method is actually used then the solution accuracy is likely to be lower within the observation time window, but it should converge to a steady state outside it (which the series method will not do). Another point not made in the literature is that the spectrum values for the exciting waveform need to be found in

different ways. A discrete Fourier Transform over the time window $0 < t < T$ should be used for the series method, but a continuous one over all time for the integration method.

1.5.3 TRANSFORMER MODELLING

The magnetising current of transformer cores has a non–sinusoidal component [47] due to the hysterisis and non–linearity of the magnetising characteristic. Under normal working conditions the transformer is designed to operate as a linear device, but when over–voltages occur, the core may be driven into saturation causing a large increase in magnetising current. If the capacitance in parallel with the transformer is sufficiently large (due to cables and/or compensating capacitors) then it is also possible that ferroresonance could occur.

Much work has been done on time domain modelling of transformers [48,49,50,51] with over–voltage studies in view, but for fault studies, where the line voltage tends to fall, a simple linear (frequency domain) model consisting of a leakage reactance and perhaps the linearised magnetising reactance (if accuracy at zero frequency is required).

The power frequency harmonics in the magnetising current cannot be produced in a frequency domain simulation. If it was desired to study their effects on a relay then the simplest way would probably be to include harmonic current sources at the busbars, (once the transformer working conditions had been found).

1.5.4 GENERATOR MODELLING

1.5.4.1 INTRODUCTION

In principle the whole of the electrical, excitation, mechanical and governing system of a generator is involved when electrical conditions at its terminals change. For relaying purposes many of these sub–systems are usually ignored as their time constants greatly exceed protection operating times (2 to 20 ms.). This simplification process must be undertaken with care, since a relay must behave correctly not only for a short time after a fault, but also through the subsequent series of fault clearance circuit breaker operations. Inclusion of exciter, automatic voltage regulator (AVR) loop and possibly turbine tor-

sional resonance models in the simulation might be required for this, but will not be attempted here.

Even the more modest task of checking that the protection behaves correctly in the interval between fault inception and the first circuit breaker operation (say 20 ms.) requires some modelling of the sub–transient decay of generator armature current and hence a more sophisticated generator model than a reactance and resistance in series (as is conventional practice).

1.5.4.2 PAST WORK

There have been many attempts to model generators: one of the most useful was that of Park [52] who derived differential equations in a reference frame rotating with the generator rotor. This allowed the machine to be represented as sets of windings (with resistances and leakage inductances) disposed about the direct axis (through the poles) and the quadrature axis (perpendicular to the poles for a 2 pole machine).

The evaluation of (actual or imputed) winding parameters has been controversial. the following techniques have been attempted:

1) To calculate leakage reactances from design data using formulae such as those proposed by Kilgore [53]. Though these simple formulae and parameter definitions suffice for switchgear specification, more complicated design data models [54,55] have been developed for stability studies.

2) To measure the transfer functions between a small sinusoidal signal injected into the AVR and terminal voltages and currents while the machine is connected to or isolated from the grid [56]. This is the most satisfactory method, but due to the non–linearity of the generator, the frequency response is dependent on the magnitude of the disturbing signal. Fitting a model using lumped parameter circuits usually comprises two stages:

a) Finding a pole zero approximation to the desired response.

b) Assigning values to circuit elements. This is the more difficult stage as sophisticated techniques i.e. in non–linear optimisation, have to be used to get acceptable

results.

The possibility of using experimental results directly has been demonstrated by Johns and El–Kateb [57], but the frequency domain formulation appears unpromising at first, since the assumption of generator linearity does not reflect the highly saturated operating conditions.

3) To obtain the standstill frequency response of the generator by using a power amplifier to drive the windings directly [58,59]. Doubts have been expressed whether the frequency response obtained id representative of the machine under operating conditions.

4) To switch transmission lines connected to the generator in and out of the network and record system waveforms, which are usually used to check model predictions, as the transmission network characteristics are unlikely to be known precisely.

5) To apply a step change to the AVR voltage reference and record the resulting armature voltages and currents. This is often used to check model performance, since although the frequency response can be derived from the data, corruption by noise is much worse than in direct frequency response measurements (where the measurement bandwidth can be made to peak sharply about the chosen frequency). However, where on–line frequency response measurements are forbidden due to concern about torsional resonances, this method may have to be used.

6) To apply a short circuit to the machine terminals and record the armature and field current waveforms [60]. The test only provides information on direct axis positive sequence parameters. The quadrature axis parameters are rather more difficult to find, and (where they exist) are generally assumed to equal those of the direct axis, except in the case of the synchronous reactance where small differences can cause large changes in predicted field current for normal (saturated) operating conditions.

Review has been made of the various ways of deriving generator parameters as some of the results will be used in a frequency domain model. The high frequency behaviour of solid iron (skin effect) is simple to model in the frequency domain, but requires a large number of state variables in the time domain. However, some major assumptions need

to be made;

1) That only the generator mutual reactance saturates and that other reactances are unaffected by operating conditions. This assumption is common in time domain formulations [61].

2) That the direct and quadrature axes have the same reactance and saturate equally. (This also removes any dependence on rotor angle.) This assumption will produce errors in the post fault steady state conditions of the generator, but such errors would be small compared to the armature current immediately after the fault.

3) That the effective mutual reactance is linear and its value may be found from the (saturated values before and after the fault.

4) That the generator speed is constant throughout the study. This assumption is common to all frequency domain models.

5) That the field voltage applied to the generator is constant, (i.e. does not rise due to AVR action). The problem in making the simulation more realistic is that there are unavoidable non–linearities in the derivation of the terminal voltage feedback for the AVR and in the excitation system. The assumption of a constant field voltage is common in protection work.

1.5.5 ARC SIMULATION

An arc has a highly non–linear resistance and hence it cannot be modelled accurately in the frequency domain. Several equations describing arc behaviour exist, but modelling them in the time domain has proved to be computationally expensive.

For relaying purposes faults are assumed to conform to one of two archetypes:

1) Low resistance fault caused by flashover across an arcing horn on a transmission tower or between phase conductors. The arc is relatively short and has a low voltage drop of approximately 5 kV [62], and can be modelled either as a short circuit or a low linear resistance (less than 2.5 Ohm).

2) High resistance fault: possibly caused by arcing to nearby vegetation. Very little data exists since such faults either evolve into something more serious or extinguish themselves. If the line protection does operate then there may be slight physical

damage to determine where or whether a fault occurred. In the absence of data and for the sake of simplicity, the fault resistance will be modelled as linear.

TEED FEEDER CONFIGURATIONS

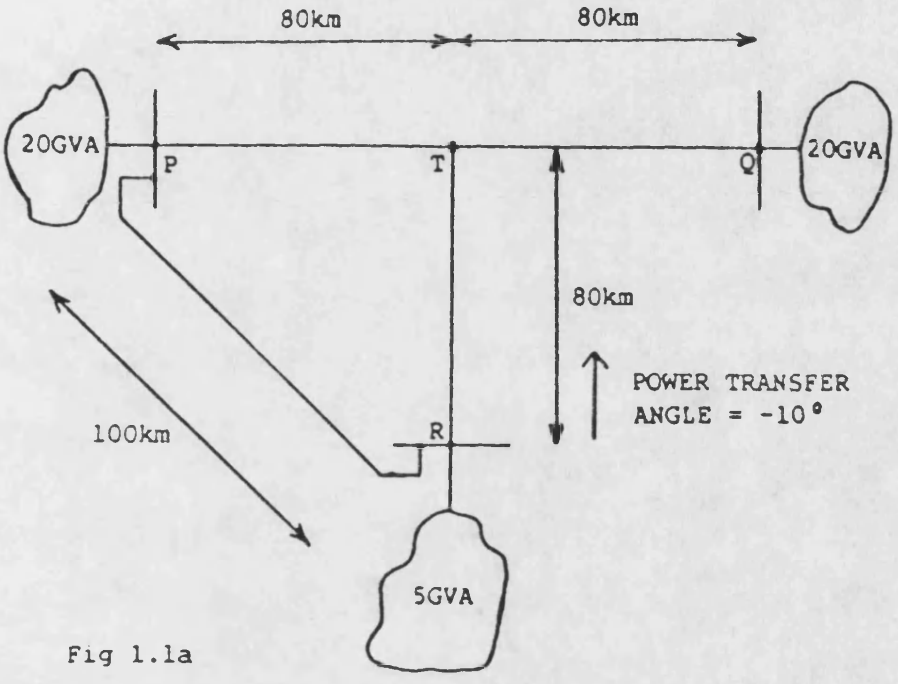

Fig 1.1a

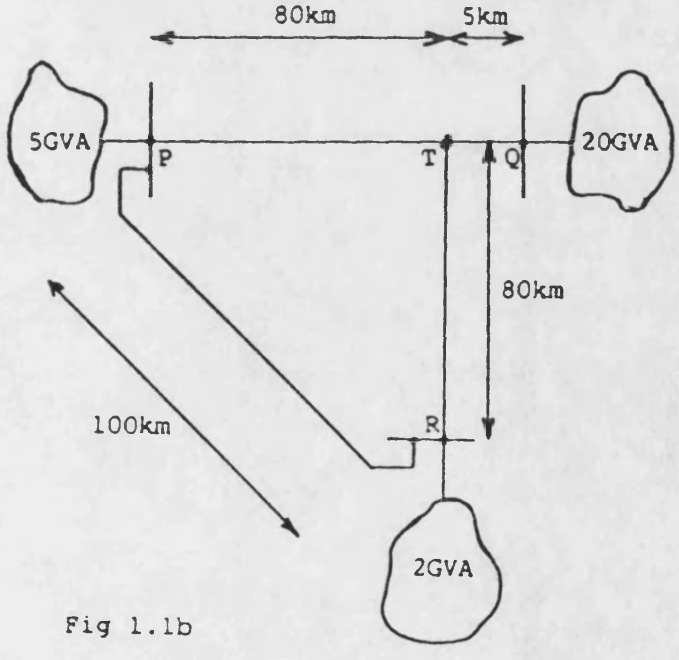

Fig 1.1b

THE PRINCIPLE OF SUPERPOSITION APPLIED TO A FAULTED NETWORK

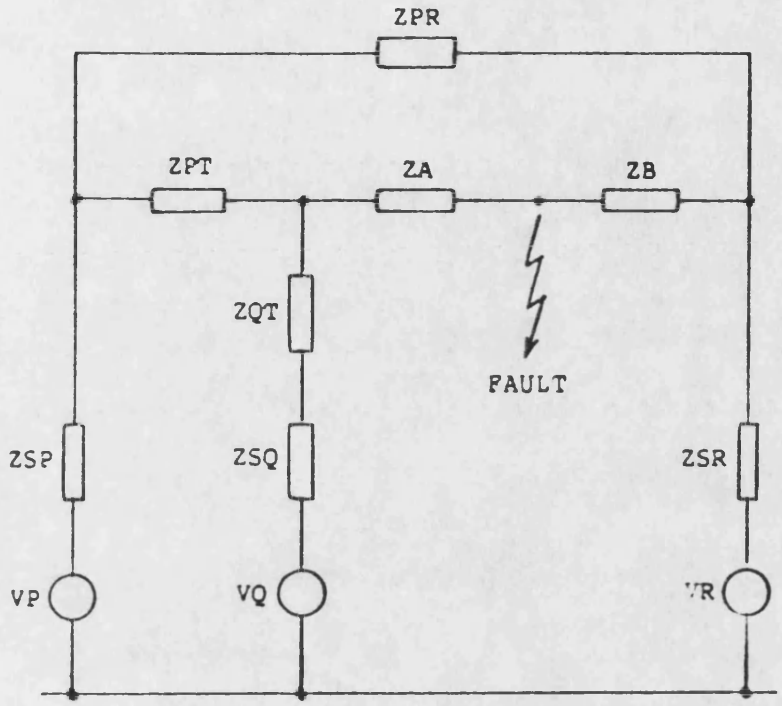

Fig 1.2a

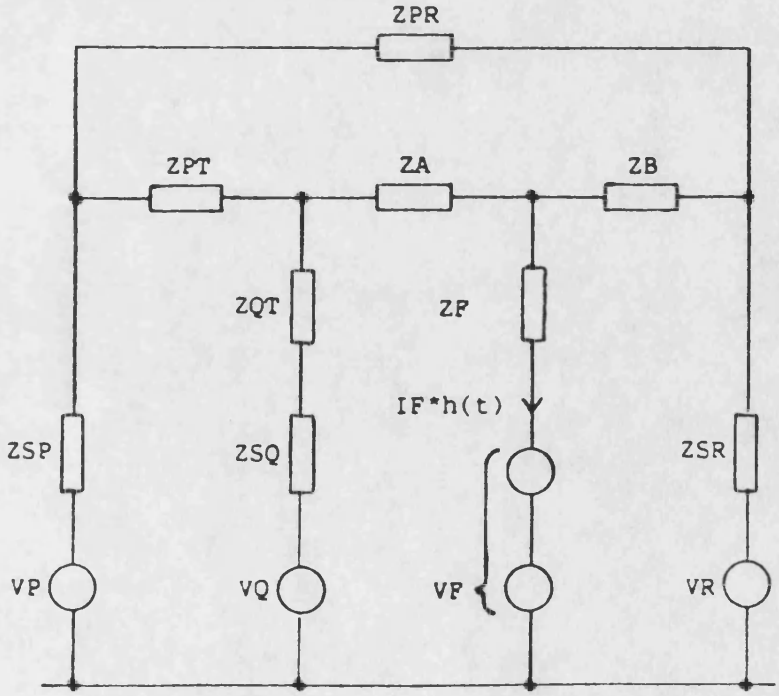

Fig 1.2b

THE PRINCIPLE OF SUPERPOSITION APPLIED TO A FAULTED NETWORK

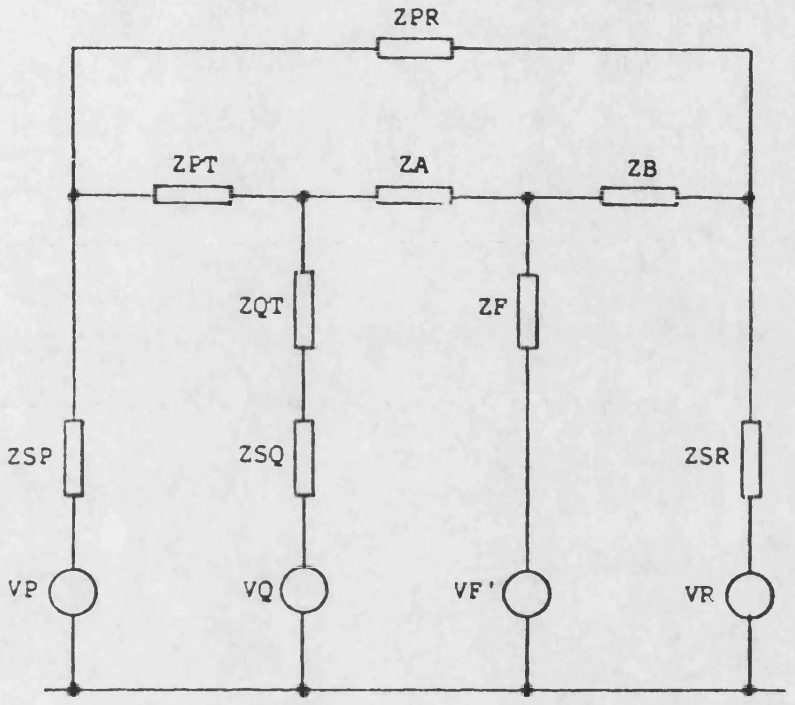

Fig 1.2c

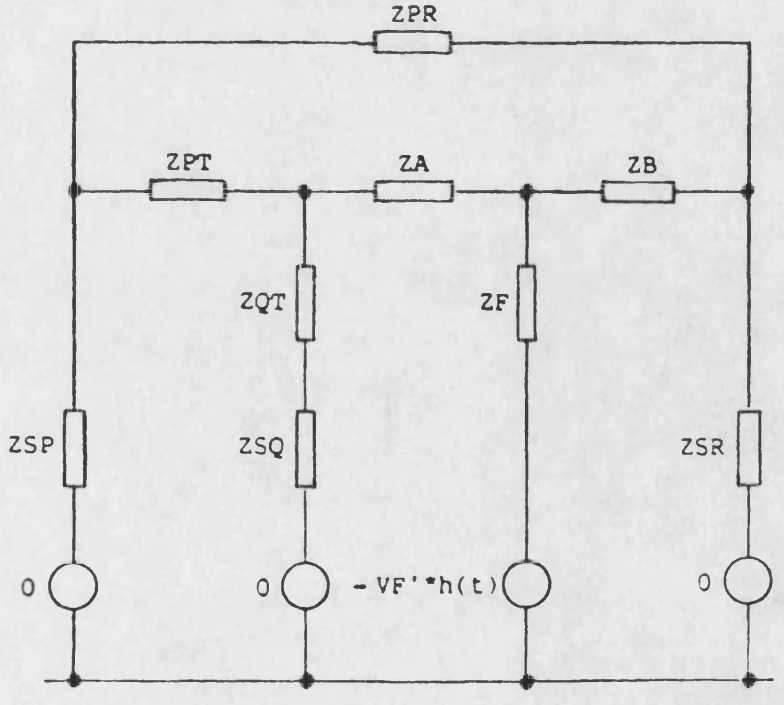

Fig 1.2d

CHAPTER 2

SIMULATION

2.1 INTRODUCTION

This chapter covers the modelling of power system components and their incorporation into a frequency domain simulation program.

In order to obtain the current and voltage spectra at a relaying point, it is necessary to find the transfer response between the fault point (where the voltage spectrum is known), and the relaying point. At a particular frequency, each physical component may be represented by an admittance (or impedance) matrix, relating voltages and currents at its terminals. These matrices are combined into the system matrix (by ensuring that Kirchoff's laws are satisfied) and the transfer functions (at a particular frequency) may be found by solving the matrix.

2.1.1 CONSTRUCTION OF SYSTEM MATRIX

Nodal analysis will be used to solve the network at each frequency, since with an admittance formulation, extra links between nodes may be added easily, making the program very flexible. This flexibility is needed, since for a single–circuit three ended system simulation, (if external faults and cases with one circuit breaker open are also to be considered), there are no fewer than 11 different faulted configurations. These are drawn in Figs 2.1 to 2.11. Note that this number neglects configurations which may be transformed into those drawn by permutation of busbar labels.

Faults occurring at the busbars or at the Tee point cannot be simulated by inputting a zero distance into a general simulation program: the special cases have to be dealt with individually. A twelfth configuration (which models two sections of plain feeder joined together (Fig 2.12)) is also included. For any configuration, as many as 9 sets of relaying quantities may be obtained from each fault simulation, most of which will usually be of no interest. Care in program design will avoid having to sift routinely through a massive output file, for the sake of the few occasions when all the information is required.

The problems of setting up the system matrix (to model a certain configuration) and specifying the output are linked, in that the sub–matrices used to construct the system matrix are also needed to derive line currents from the nodal (busbar) voltages. The efficient utilisation of these sub–matrices is one of the prime requirements in the program design. The organisation of input data and program function will be briefly discussed for one of the most useful configurations.

Configuration 1 is defined as a Teed feeder with a fault on PQ (Fig 2.1). The system matrix is set up with the fault position nodes occupying the first block of 3 rows (and columns), busbar P the next 3, busbar Q the next 3, busbar R the next 3, and the Tee point occupies the final 3. The total matrix size is (15*15), and all the above information is implied when configuration 1 is specified in the input data.

Seven lengths are input, which are interpreted for this configuration as PF, FT, QT, RT, PQ, QR, RP. The last three lengths refer to links external to the Tee, and if any of these is input as zero, then that link is deemed not to exist. At a certain frequency each of these lengths will generate two (3*3) admittance matrices Y_{aa}, Y_{ab} which relate the voltages and currents (inward flowing) at the ends of the link. (The derivation of these matrices is discussed in a later section.)

$$\begin{bmatrix} C_a \\ C_b \end{bmatrix} = \begin{bmatrix} Y_{aa} & Y_{ab} \\ Y_{ab} & Y_{aa} \end{bmatrix} \begin{bmatrix} V_a \\ V_b \end{bmatrix}$$

Each of the links is now coded as three numbers, indicating which blocks of nodes terminate the link and where the matrices defining the link admittances are stored. The Y_{aa} matrices are stored sequentially in an array with dimension (3*3*7), and the Y_{ab} matrices similarly. Hence the link PF would be coded as (2,1,1), indicating that the second block of three nodes is to be connected to the first block of three nodes, and the relevant matrices are in the first position of each storage array. The code could equally well have been (1,2,1). The link RT would be coded as (4,5,4) or (5,4,4). These codes are assigned by the program in response to the choice of configuration; they are not fed in as data.

The system matrix is set up by combining the admittance matrices of all the links, and has been partitioned into (3*3) matrices since this makes the working clearer. Starting from a system matrix in which all the elements are zero, the links PF and PQ will be added (as an example of the method):

$$\begin{bmatrix} C_f \\ C_p \\ C_q \\ C_r \\ C_t \end{bmatrix} = \begin{bmatrix} Y_{aapf} & Y_{abpf} & 0 & 0 & 0 \\ Y_{abpf} & Y_{aapf} + Y_{aapq} & Y_{abpq} & 0 & 0 \\ 0 & Y_{abpq} & Y_{aapq} & 0 & 0 \\ 0 & 0 & 0 & 0 & 0 \\ 0 & 0 & 0 & 0 & 0 \end{bmatrix} \begin{bmatrix} V_f \\ V_p \\ V_q \\ V_r \\ V_t \end{bmatrix}$$

When the other links have been added, the source admittances are added along the diagonal matrices of the partitioned matrix. i.e. instead of $Y_{aapf} + Y_{aapq}$, there would be $Y_{aapf} + Y_{aapq} + Y_{sp}$.

2.1.2 OUTPUT SPECIFICATION

Once the system matrix has been set up and solved at a certain frequency, the line currents can be found from the nodal voltages. The sets of relaying quantities to be output are coded in the same way as the links used in setting up the matrix. If, say, the voltage at busbar R were required with the current RT, (to simulate the inputs to a relay on RT at R), then the code (4,5) (for configuration 1) would be specified in the data. The order is now significant: if (5,4) were specified, the voltage at the Tee point and the current TR would be obtained.

Only two numbers need to be specified for each current, since the program compares the input code (and its transpose) with the links data. If a match is found, then the current will be calculated using the matrices indexed, if not, then a flag is set, causing the current output to be zero

2.1.3 SOLUTION OF SYSTEM MATRIX

In the following method, it is essential that the faulted phases are at the very top of the system matrix. In general permutations of matrix rows and columns are necessary to achieve this. (Naturally the voltage and current vectors would be similarly permuted). Since the matrix may have to be constructed, permuted and solved for many hundred fre-

quencies, it is very desirable that this process be made efficient. A position in an array may be defined by assigning the index 1 to the top left hand element, 2 to the one below it, 16 to the first element in the second column (for a (15*15) matrix), etc. Similarly indices may be assigned to the elements in the arrays holding the Y_{aa}, Y_{ab} and source admittance matrices. For every frequency the mapping between these indices and the permuted system matrix indices will be the same. Therefore a list of index pairs may be constructed from:

1) The coding of the links implicit in the configuration choice.

2) The input data as to the existence of external links.

3) The permutation necessary to bring the faulted phases to the top of the matrix.

Once this list has been assembled, the matrix may be constructed very rapidly. The faulted phases are brought to the top of the matrix since superimposed sources only exist at the fault point on the faulted phases and only at those nodes will current be injected. The matrix equation may be partitioned:

$$\begin{bmatrix} C_j \\ 0 \end{bmatrix} = \begin{bmatrix} Y_{jj} & Y_{jk} \\ Y_{kj} & Y_{kk} \end{bmatrix} \begin{bmatrix} V_j \\ V_k \end{bmatrix}$$

Where C_j is a column vector of 1,2 or 3 elements, depending on fault type. This equation may be much simplified by expressing V_k in terms of V_j:

$$V_k = -Y_{kk}^{-1} Y_{kj} V_j = Y_{kj'} V_j$$

Hence,

$$C_j = (Y_{jj} + Y_{jk} Y_{kj'}) V_j = Y_{jj'} V_j$$

For earth faults with zero fault resistance this solves the matrix, since the V_j are the known spectrum components of the applied source.

It is possible to avoid matrix inversion altogether by applying the above process one row at a time (starting with the bottom row). The matrix is partitioned such that the suffix $_1$ applies to the last row and column, and the suffix $_m$ applies to the rest of the matrix. The inverted matrix Y_{ll}^{-1} then is the reciprocal of a complex number and V_l becomes depend-

ent on all voltages above it, i.e V_m:

$$V_l = \left(\frac{-1}{Y_{ll}}\right) Y_{lm} V_m = Y_{lm'} V_m$$

$$C_m = (Y_{mm} + Y_{lm} Y_{ml'}) V_m = Y_{mm'} V_m$$

The procedure may now be repeated with $Y_{mm'}$ as the starting point, and continued until $Y_{jj'}$ is obtained, having reduced the matrix size by one node each time.

A necessary refinement to this is to exchange the lth row with the row in the range $j+1,l$, which has the largest element in its lth column, before eliminating it. This does not affect the right hand side of the equation, since both injected currents will be zero, but minimises the value of Y_{ll}^{-1}, and therefore improves accuracy. Exchanging columns to the same end does however require a record to be made, since an inverse permutation eventually has to be performed to restore the original variable order. Though this involves extra work, the record may be used to permute the matrix before solution to reduce permutations required during solution. The routines are already needed to bring faulted phases to the top, and frequency domain analysis requires the repeated solution of similar matrices. A convenient point at which to record the permutations undergone in solution is after the superimposed power frequency quantities have been determined.

If the elements $Y_{lm'}$ are substituted for Y_{lm} as each row is processed, then each element of V_k will be defined by:

$$V_k = Y_{kj'} V_j + Y_{kk'} V_k$$

Where $Y_{kk'}$ is a matrix which is zero on and above the leading diagonal. Further substitution will allow the expression of V_k as a function of the V_j alone. This may seem more complicated than inverting a sub–matrix or even inverting the system matrix. However it is simpler and more accurate (due to fewer operations) than a general purpose inversion routine.

2.1.4 FAULT RESISTANCE

When fault resistance exists, further steps are needed, since the voltage at the fault point differs from the applied source, due to the resistive voltage drop. If the source voltage E_j and the fault voltage V_j can be linked by an equation:

$$\mathbf{V_j = E_j - R_f C_j}$$

Then V_j may be found by the following steps:

$$\mathbf{C_j = Y_{jj'}\left(E_j - R_f C_j\right)}$$

$$\mathbf{E_j = Y_{jj'}^{-1}\left(I + Y_{jj'} R_f\right) C_j}$$

$$\mathbf{V_j = \left(I - R_f\left(I + Y_{jj'} R_f\right)^{-1}\right) E_j}$$

The resistance matrix R_f may be constructed easily for faults which are in effect combinations of single phase to earth faults. For more complicated situations, its derivation is rather less obvious, but it is shown in Appendix 2 that the equation linking E_j and V_j can always be constructed for faults involving earth.

2.1.5 PHASE TO PHASE FAULTS

For these faults, the treatment given in the previous section is not valid: sources need to be inserted between faulted phases rather than between the faulted phases and earth. The formulation is described in Appendix 3, together with extensions of this technique to include making and breaking series network connexions.

2.1.6 STORAGE CONSIDERATIONS

At each of many hundreds of frequencies, say 15 voltages and 9 currents are produced, which occupy a lot of memory when stored as double precision complex variables. Using large arrays to store data can cause a lot of swapping between main and virtual memory (page faults). This program uses arrays as temporary stores which are repeatedly written to direct access disc files and then refilled as more spectrum points are obtained. When all the frequencies have been run through, there will be say 24 direct access files, each containing the voltage or current spectrum of the 3 nodes at a point on the network.

The output for a series of simulations in which only the fault point on wave is varied may be generated economically by forming the weighted sum of stored outputs from two simulations, in which fault point on wave incidence differed by ninety degrees. It is also desirable to generate the spectrum of the second point on wave simultaneously with the first one, since although the excitation is different, the matrix construction and solution steps are identical. This doubles the storage requirement, and strengthens the argument for using direct access files.

It is possible to save computer time in other ways when multiple runs require variation of fault type or resistance, by reducing the system matrix, such that all the rows are dependent on the top 3 rows, i.e. the system matrix is reduced as if a three phase fault were to be simulated, and then storing $Y_{jj'}$, $Y_{kj'}$ matrices at each frequency. These may then be further reduced for other types of fault excitation, and/or fault resistance specifications.

Once a set of relaying quantities has been derived (and as many as are specified by the input data are possible), then the variables may be printed out or fed directly into a relay simulation. The outputs from the latter are collated in a comprehensive way as described in a later section.

2.2 FREQUENCY DOMAIN FORMULATION

2.2.1 INTRODUCTION

Past work using frequency domain power system simulation [1,23,46], has used the modified Fourier Transform as described by Day et al.[5]. Inclusion of transducer and more realistic generator models would require the following work:

1) Curve fitting to generate frequency responses as a function of $\alpha+j\omega$ rather than $j\omega$.

2) Assessment of simulation accuracy, which may be done in two ways:

a) By varying simulation parameters until extra computational effort produces little change in the answers obtained.

b) By comparing simulations with results of guaranteed accuracy.

Although it is less work simply to vary simulation parameters, weaknesses due to the modified Transform technique itself would not be exposed: i.e.

1) The accuracy of the curve fitting process is not tested.

2) In the most efficient (i.e. Fast Fourier Transform) formulation of the technique, the simulation parameters are not independent: the observation time T, truncation frequency W, frequency shift constant a and number of frequency (and time) domain samples N are linked by the following approximate equations:

a) $\alpha T = 1$

b) $W = 2\pi N/T$

c) Variation of the simulation parameters changes the physical situation modelled rather than the accuracy with which a modelled situation is interpreted. The distinction is subtle, but means that it is more difficult to obtain repeatable results with different simulation parameters for the series (compared to the integration) formulation.

Inclusion of a transducer model would probably make a power system simulation better behaved in that the added high frequency roll off would make the truncation frequency a less critical parameter (provided it exceeded the roll off frequency). The same cannot be said if the transducer model is excluded, since a transmission line has a large bandwidth and altering the truncation frequency will affect the time domain simulation output.

Since many changes are going to be made, it is considered necessary to have an independent reference by which results may be judged (as was done when the modified Fourier transform technique was developed). Therefore formulation and solution of a power system model using the unmodified numerical Fourier transform is required, since the frequency variance of the transmission line parameters forbids an algebraic formulation over the frequency range of interest.

2.2.2 NUMERICAL INTEGRATION

Two precautions need to be observed when using numerical integration techniques:

1) That the integrand may be adequately represented by sampling.

2) That the inevitable truncation of the integration range (for integrals with infinite range) does not lead to unacceptable errors.

For an inverse Fourier transform, the integrand in question is the frequency spectrum of a disturbance multiplied by a phase shift $exp(j\omega t)$ and integrated from negative to positive infinite frequency. Since only real time domain exciting signals and physically realisable networks will be used, the value of the spectrum at a negative frequency will be the complex conjugate of that at the corresponding positive frequency. Taking twice the real part of the integral over the frequency range zero to infinity will therefore equal the integral over the full range but with the advantage that only the spectrum for positive frequencies need be considered.

The principle of superposition (which assumes network linearity) may be used to represent the disturbance as a change in amplitude of a voltage source at the fault location. In a previously undisturbed network, the source voltage changes from zero (pre–fault) to a power frequency sinusoid, and it is a spectrum similar to this which needs to be integrated. Initially, however it is easier to consider the spectrum of a unit step rather than a sinusoid applied at zero time.

2.2.3 SPECTRUM OF A UNIT STEP

A unit step in the time domain is defined as follows:

$$x(t) = 0 \qquad -\infty < t \leq 0$$

$$x(t) = 1 \qquad 0 < t < \infty$$

It may be considered as the sum of two signals (assuming network linearity) both in the time and frequency domains:

$$x(t) = x_a(t) + x_b(t) \qquad\qquad X(\omega) = X_a(\omega) + X_b(\omega)$$

The components are:

1) A constant (even) signal of amplitude 0.5.

$$x_a(t) = 0.5 \qquad -\infty < t < \infty \qquad\qquad X_a(\omega) = \pi\delta(\omega)$$

2) An odd signal of amplitude 0.5:

$$x_b(t) = -0.5 \qquad -\infty < t \leq 0$$

$$x_b(t) = 0.5 \qquad 0 < t < \infty$$

This has a spectrum:

$$X_b(\omega) = \frac{1}{j\omega}$$

Note that a delta function does not figure in the Laplace or modified Fourier Transforms of a time domain step. Obviously such a component needs special treatment when numerical integration is to be attempted. Lego and Sze (41) separated the response to the first and second components and obtained the network step response:

$$Y(\omega) = F(\omega)X(\omega) = F(0)X_a(\omega) + F(\omega)X_b(\omega)$$

$$y(t) = \frac{F(0)}{2} + \int_{-\infty}^{\infty} \frac{F(\omega)\exp(j\omega t)}{j\omega} df$$

Note that F(w) is the transfer function of the network studied, and there may be numerical problems at zero frequency if it contains a pole or even if it remains non zero. This limitation may be overcome by grouping the terms as follows:

$$G(\omega) = \frac{F(\omega) - F(0)}{j\omega}$$

$$y(t) = F(0)x(t) + \int_{-\infty}^{\infty} G(\omega)\exp(j\omega t) df \qquad (1)$$

Note that:

$$\lim_{\omega \to 0} G(\omega) = -j\left[\frac{d}{d\omega}F(\omega)\right]_0$$

This is not necessarily zero, but is certainly finite, and hence the integral may be found numerically. For the case where the transfer function contains a pole at the origin the expression (1) becomes:

$$y(t) = \lim_{\omega \to 0}(j\omega t F(\omega)) + \int_{-\infty}^{\infty} G(\omega)\exp(j\omega t) df$$

Truncation of the integration range should equally affect the first term (since that contains high frequency components). If the spectrum is to be truncated at $\omega = W$, then the correct form of the first term may be derived as follows:

$$x_a(t) = \int_0^{\infty} \frac{\sin(\omega t)}{\omega} df$$

$$Si(u) = \int_0^{u} \frac{\sin(z)}{z} dz$$

Hence, expression (1) becomes

$$y(t) = F(0)\left(\frac{1}{2} + \frac{Si(Wt)}{\pi}\right) + \int_{-\infty}^{\infty} G(\omega)\exp(j\omega t)df$$

The function *Si(u)* is the Sine Integral and is a well known, easily calculated function [63]). Separating a frequency spectrum into a part containing the poles (which is evaluated algebraically) and a residual (which is evaluated numerically) was mentioned by Morched et al. [64].

2.2.4 SPECTRUM OF STEPPED SINUSOID

The spectrum of a time domain sinusoid may be found by applying Euler's identities and the frequency shift theorem to the spectrum of a step *x(t)*. A superimposed sinusoidal waveform at frequency *Wo* may be represented (without any loss of generality) by the time domain signal *u(t)*:

$$\cos(W_0 t + \phi) = \cos(W_0 t)\cos(\phi) - \sin(W_0 t)\sin(W_0 t)$$

$$\cos(W_0 t) = \frac{\exp(jW_0 t) + \exp(-jW_0 t)}{2}$$

$$\sin(W_0 t) = \frac{\exp(jW_0 t) - \exp(-jW_0 t)}{2j}$$

$$a(t) = x(t)\exp(jW_0 t) \qquad b(t) = x(t)\exp(-jW_0 t)$$

$$A(\omega) = \frac{1}{j(\omega - W_0)} + \pi\delta(\omega - W_0) \qquad B(\omega) = \frac{1}{j(\omega + W_0)} + \pi\delta(\omega + W_0)$$

$$u(t) = x(t)\cos(W_0 t + \phi) = \frac{\big(a(t) + b(t)\big)\cos(\phi) + \big((a(t) - b(t)\big)\sin(\phi)}{2}$$

$$= \frac{a(t)\exp(j\phi) + b(t)\exp(-j\phi)}{2}$$

$$U(\omega) = \frac{A(\omega)\exp(j\phi) + B(\omega)\exp(-j\phi)}{2}$$

$$= \frac{j\omega\cos(\phi) - W_0\sin(\phi)}{W_0^2 - \omega^2}$$

$$+ \frac{\pi}{2}\big(\exp(j\phi)\delta(\omega - W_0) + \exp(-j\phi)\delta(\omega + W_0)\big)$$

The spectrum *A(w)* is derived from first principles in Appendix 1. The output spectrum is defined by:

$$Y(\omega) = F(\omega)U(\omega)$$

The need to integrate the impulses and discontinuities in the spectrum $Y(\omega)$ may be removed by splitting the time domain output $y(t)$ into two parts:

$$y(t) = y_a(t) + y_b(t) \qquad Y(\omega) = Y_a(\omega) + Y_b(\omega)$$

$$Y_a(\omega) = F(W_0)\exp(j\phi)\left(\frac{1}{j(\omega - W_0)} + \frac{\pi\delta(\omega - W_0)}{2}\right)$$

$$+ F(-W_0)\exp(-j\phi)\left(\frac{1}{j(\omega + W_0)} + \frac{\pi\delta(\omega + W_0)}{2}\right)$$

$$Y_b(\omega) = \exp(j\phi)\frac{F(\omega) - F(W_0)}{j(\omega - W_0)} + \exp(-j\phi)\frac{F(\omega) - F(-W_0)}{j(\omega + W_0)}$$

As might be realised, $y_a(t)$ consists of an sinusoid similar to the exciting signal (though attenuated and phase shifted by the network transfer function). When the range of integration is not infinite, then a term corresponding to the integral over the omitted range needs to be subtracted from the time domain output; this term will be denoted $y_c(t)$, i.e.

$$y(t) = y_a(t) + y_b(t) + y_c(t)$$

The value of the correction term is most easily found by considering the following quantities:

$$y_d(t) = \int_W^\infty \frac{\omega \sin(\omega t)}{W_0^2 - \omega^2} d\omega \qquad y_e(t) = \int_W^\infty \frac{W_0 \cos(\omega t)}{W_0^2 - \omega^2} d\omega$$

These quantities are most easily found by dividing the integration range into a number of intervals, and integrating numerically using an interpolation polynomial to approximate the denominator of the integrand. The correction term is then found:

$$y_c(t) = \frac{1}{\pi} \mathrm{Re}\left(F(W_0)\exp(j\phi) y_d(t) + F(-W_0)\exp(-j\phi) y_e(t)\right)$$

The correction delays and decreases the slope of $y_a(t)$ near t=0. As such, it becomes insignificant as time increases and only a few values need to be computed, which are dependent on the choice of W, W_0 and ϕ. However, if the correction coefficients have been computed for two values of ψ (differing by 90^0), then the correction for any value of ϕ is derivable as their weighted sum.

2.2.5 DIVISION OF SPECTRUM

Although the continuous spectrum $Y_b(w)\exp(j\omega t)$ does not contain any poles (on the $j\omega$ axis) or impulses, the accuracy achieved in its numerical integration will be dependent on the smoothness of the spectrum and the integration interval used. It would be inefficient to use the same length interval over the whole spectrum, since certain localised features would require this length to be very small. These features arise in the following ways:

1) From spectrum features around zero frequency. The lumped line inductance and resistance will give rise to a term $k/(\alpha+j\omega)$ in the output current spectrum, (corresponding to an exponential decay $k\exp(-\alpha t)$ in the time domain). The constant α is quite small and results in a sharp peaking of the spectrum around zero frequency.

2) From features of the generator model. When transient and sub–transient time constants are modelled then sharp peaks or troughs occur in the output spectra around power frequency.

3) Resonances or anti–resonances corresponding to travelling wave frequencies on transmission lines.

The former two cases are more serious than the last, as the degree of peaking in the frequency spectrum is dependent on the length of the associated time constant of the time domain component, which may run into seconds for the generator. However it is known precisely where those problems occur, i.e. around zero and power frequencies.

The travelling wave peaks are less sharp, but their centre frequencies are dependent on system configuration and may occur over a wide frequency range. Since they cannot sensibly be specified in data, a four stage process is required to accurately integrate the high frequency spectrum:

1) A relatively coarse frequency scan is made (with a frequency interval which would be appropriate if there were no travelling waves; i.e. about the same as used in the Modified Fourier Transform method).

2) The travelling wave frequencies are located by finding the largest differences between adjacent spectrum samples.

3) Additional fine frequency scans are carried out within the intervals which have been identified.

4) As shown in the next section, when a spectrum is integrated with a coarse frequency interval, it is possible to consider the result as an accurate integration of a piecewise linear spectrum. Hence by integrating the coarse spectrum and adding to that the integral of the fine spectrum minus interpolated values from the coarse spectrum, greater accuracy may be achieved.

This process could also be used to treat the peaks around zero and power frequencies, but since their location is known, the simpler procedure of dividing the spectrum into segments, and finding the time domain contribution from each segment, will be used. The formulation of the integration routine allows this: the last spectrum point of the previous segment is the first in the present segment.

2.2.6 INTEGRATION TECHNIQUE

Each segment of the spectrum (taken between angular frequencies W_1 and W_2) is divided into an integral number N of intervals (of width $2Dw$).

$$W_2 - W_1 = 2NDw$$

Within each interval several treatments are possible:

1) To treat the spectrum as having a constant value within each interval (i.e. the mean of the interval endpoint values).

2) To treat the spectrum as varying linearly between endpoint values.

3) To interpolate between the endpoints using low order Lagrange interpolation polynomials (generated with 3 or 4 data points).

4) To fit piecewise continuous polynomials (splines) over the whole segment. This will be much more accurate than the previous option since continuity of slope is guaranteed (for cubic or higher splines), but polynomial generation and implementation of the interpolation is much more time consuming.

It will be shown that the Fourier Transform of a segment of a spectrum for any of the first three approaches can be separated into two components:

1) Boundary terms due to the fact that the general representation of the spectrum within an interval cannot be used at the ends of the segment: i.e. information from outside the segment would be needed. Different expressions have to be used there, and cause additional terms (which increase in number and complexity with the interpolation polynomial degree).

2) The main term which is the product of:

a) The discrete inverse Fourier Transform of the equally spaced spectrum samples (multiplied by a frequency shift term if the initial frequency W_1 does not equal zero).

b) An envelope factor which is a function of time, spectrum sampling interval $2Dw$ and the complexity of interpolation formula used.

This may be illustrated by developing the expressions for the time domain output when the spectrum is treated as constant and then as varying linearly within each interval.

The inverse transform of a segment of the spectrum $Y_b(\omega)$ is:

$$g(t) = \frac{1}{\pi}\mathrm{Re}\left(\int_{W_1}^{W_2} G(\omega)\exp(j\omega t)d\omega \right)$$

Where the integrand is:

$$G(\omega) = \frac{Y_b(W_1 + 2nDw) + Y_b(W_1 + (2n+2)Dw)}{2}$$

Where n is the integral part of $(\omega - W_1)/(2Dw)$. The complex exponential may be separated into two factors:

$$\exp(j\omega t) = \exp(j(\omega - (2n+1)Dw)t)\exp(j(2n+1)Dwt)$$

Using this result, the time domain output may be expressed as the real part of the product of a continuous integral $\Lambda_x(t)$, a discrete sum $\Sigma_x(t)$ and a base frequency term:

$$g(t) = \frac{1}{\pi}\mathrm{Re}(\Lambda_x(t)\Sigma_x(t)\exp(jW_1 t))$$

$$\Lambda_x(t) = \int_{-Dw}^{Dw} \frac{\exp(j\omega t)}{2} d\omega = \frac{\sin(Dwt)}{t} \qquad \Lambda_x(0) = Dw$$

$$\Sigma_x(t) = \sum_{i=0}^{i=N-1} (Y_b(W_1 + 2iDw) + Y_b(W_1 + (2i+2)Dw))\exp(j(2i+1)Dwt)$$

The sum may be separated as follows:

$$\Sigma_x(t) = \exp(jDwt)\sum_{i=0}^{i=N-1} (Y_b(W_1 + 2iDw)\exp(j2iDwt)$$

$$+ \exp(-jDwt)\sum_{i=1}^{i=N} (Y_b(W_1 + 2iDw)\exp(j2iDwt)$$

Using Euler's identities and writing:

$$\Sigma_z(t) = \sum_{i=0}^{i=N} (Y_b(W_1 + 2iDw)\exp(j2iDwt)$$

They may be combined as follows:

$$\Sigma_x(t) = 2\cos(Dwt)\Sigma_z(t)$$

$$-Y_b(W_2)\exp(j(W_2-W_1+Dw)t)-Y_b(W_1)\exp(-jDwt)$$

This approximation is, of course, not ideal. A piecewise linear approximation would certainly be better, and may be obtained for little extra complexity. The division of the spectrum into intervals is retained, but equality with the actual spectrum is preserved at the interval endpoints, which are joined by linear segments. This is equivalent to adding the following integral to the previous result:

$$g_1(t)=\frac{1}{\pi}\mathrm{Re}\left(\int_{W_1}^{W_2}G_1(\omega)\exp(j\omega t)d\omega\right)$$

Where the integrand is:

$$G_1(\omega)=\left(Y_b((2n+2)Dw)-Y_b(2nDw)\right)\frac{\omega-(2n+1)Dw}{2Dw}$$

As before, the contribution to the time domain may be separated into the real part of the product of an integral, a sum and a frequency term:

$$g_1(t)=\frac{1}{\pi}\mathrm{Re}\left(\Lambda_y(t)\Sigma_y(t)\exp(jW_1t)\right)$$

$$\Lambda_y(t)=\int_{-Dw}^{Dw}\frac{\omega\exp(j\omega t)}{2Dw}d\omega=\frac{1}{jt}\left(\cos(Dwt)-\frac{\sin(Dwt)}{Dwt}\right)\qquad\Lambda_y(0)=0$$

$$\Sigma_y(t)=\sum_{i=0}^{i=N-1}(Y_b(W_1+2iDw)-Y_b(W_1+(2i+2)Dw))\exp(j(2i+1)Dwt)$$

The sum may be decomposed into a more familiar form as follows:

$$\Sigma_y(t)=\exp(-jDwt)\sum_{i=1}^{i=N}(Y_b(W_1+2iDw)\exp(j2iDwt)$$

$$-\exp(jDwt)\sum_{i=0}^{i=N-1}(Y_b(W_1+2iDw)\exp(j2iDwt)$$

They may be combined as follows:

$$\Sigma_y(t)=-2j\sin(Dwt)\Sigma_z(t)$$

$$+Y_b(W_2)\exp(j(W_2-W_1+Dw)t)-Y_b(W_1)\exp(-jDwt)$$

Combining the two sums and time domain windows gives:

$$g(t) + g_1(t) = \frac{1}{\pi}\mathrm{Re}\Big(\big(\Lambda_x(t)\Sigma_x(t) + \Lambda_y(t)\Sigma_y(t)\big)\exp(jW_1t)\Big)$$

$$\Lambda_x(t)\Sigma_x(t) = \frac{\sin(2Dwt)}{t}\Sigma_z(t)$$

$$-Y_b(W_1)\Lambda_x(t)\exp(-jDwt) - Y_b(W_2)\Lambda_x(t)\exp(j(W_2 - W_1 + Dw)t)$$

$$\Lambda_y(t)\Sigma_y(t) = -\frac{\sin(2Dwt)}{t}\Sigma_z(t) + \frac{2}{Dw}\left(\frac{\sin(Dwt)}{t}\right)^2\Sigma_z(t)$$

$$-Y_b(W_1)\Lambda_y(t)\exp(-jDwt) - Y_b(W_2)\Lambda_y(t)\exp(j(W_2 - W_1 + Dw)t)$$

Summing these two expressions produces a great simplification:

$$\Lambda_x(t)\Sigma_x(t) + \Lambda_y(t)\Sigma_y(t) = \frac{2}{Dw}(\Lambda_x(t))^2\Sigma_z(t)$$

$$-\big(\Lambda_x(t) + \Lambda_y(t)\big)Y_b(W_1)\exp(-jDwt)$$

$$-\big(\Lambda_x(t) - \Lambda_y(t)\big)Y_b(W_2)\exp(j(W_2 - W_1 + Dw)t)$$

Though the terms look complicated, there is a high degree of commonality in them, which makes evaluation fairly easy. The complex exponentials may be generated recursively, and sine and cosine functions by taking real and imaginary parts thereof. The Fast Fourier Transform algorithm may be used to implement the discrete inverse Fourier Transform $\Sigma_z(t)$ provided the following conditions are met:

1) $$W_2 - W_1 = \frac{2\pi}{Dt}$$

2) $$N + 1 = 2^m$$

Where Dt is the output time step required (or an integral sub–multiple thereof) and m is a positive integer.

Further refinements to the integration procedure may be attempted, e.g. representing the spectrum by a quadratic polynomial over each interval, but the number of boundary terms and sums required increases, making the option unattractive.

2.2.7 SEGMENTATION DETAILS

The zero frequency point is not found, since the line parameter evaluation routine would need a test and a special algorithm to find it. Instead a spectrum point $A+jB$ is found at a low frequency W_s, e.g. 0.001 rads/sec. The spectrum at zero frequency is assumed to consist of the real part A of the low frequency spectrum.

The first segment therefore consists of just two points and its contribution to the time domain output is:

$$\frac{1}{\pi t}\left\{A\sin(W_s t) + B\left(\cos(W_s t) - \frac{\sin(W_s t)}{W_s t}\right)\right\}$$

This is twice the real part of the inverse transform of the positive frequency spectrum (i.e. assumes that the spectrum for negative is the complex conjugate of that for positive frequencies).

The next segment consists of perhaps 6 rads/sec divided into an arbitrary number of intervals. The Fast Fourier Transform (FFT) algorithm is not suited to inverting a narrow bandwidth spectrum to give time domain output at a high sampling rate, but the only alternative, the Discrete Fourier Transform (DFT), requires a lot of computer time for even a very modest number of points.

The number of points required to be calculated using the DFT be significantly reduced by noticing that, for a narrow bandwidth spectrum about a low centre frequency, the angular change (for any frequency component) between time domain points is low, allowing the possibility of interpolation between points in the time domain, as is discussed in the next section.

The spectrum between about 2 Hz. and say 100 Hz. may be divided into as many segments as seen fit (with the width of the segment and interval within the segment decreasing as power frequency is approached). Between 100 Hz. and the truncation frequency, a final segment is added, which is integrated using the FFT.

The first frequency sample in the FFT is treated as if it occurred at zero frequency, and the FFT complex time domain output is frequency shifted (by multiplying with a complex

exponential). The FFT imposes constraints between the time domain sampling rate Dt and the integration interval in the frequency domain $2Dw$, which inevitably means that the truncation frequency does not match the time domain sampling frequency. This is of little importance provided circuit elements have been included to attenuate high frequency components in the output spectra.

It is possible to vary the parameters for this segment, but usually only by a factor which is a power of two. (e.g. The integration interval may be halved by doubling the number of points N+1, (which also doubles the observation time, but keeps the maximum frequency W almost the same). Alternatively truncation effects may be investigated by doubling N+1, but keeping the same integration interval, and only using every second time domain point.)

Finer adjustment of the integration parameters in segments integrated using the DFT is possible. There is one precaution though: the frequency samples should be arranged to straddle power frequency (preferably symmetrically). Apart from this the spectrum may be divided into an arbitrary number of DFT segments with an arbitrary number of points. It will also be necessary to specify the DFT time domain sampling rate, as this is not constrained when interpolation between time domain points is used.

2.2.8 INTERPOLATION

The accuracy of interpolation depends on the algorithm used (i.e. how many data points are used to generate an interpolated point) and on the nature of the function to be interpolated. When the inverse transform of a frequency spectrum is to be interpolated, the greatest distortion will be suffered by the highest frequency component in the spectrum. The distortion may be assessed by interpolating a sinusoid with various angular spacings between data points. Interpolation rules using two, three and four points will be considered with a spacing of 18 degrees between data points. The formulae are:

Two point (linear) interpolation:

$$y = \frac{(x-x_1)y_1 - (x-x_2)y_2}{(x_2-x_1)}$$

Three point interpolation:

$$y = \frac{(x-x_1)(x-x_2)y_0}{(x_0-x_1)(x_0-x_2)} + \frac{(x-x_0)(x-x_2)y_1}{(x_1-x_0)(x_1-x_2)} + \frac{(x-x_0)(x-x_1)y_2}{(x_2-x_0)(x_2-x_1)}$$

Four point interpolation:

$$y = \frac{(x-x_1)(x-x_2)(x-x_3)y_0}{(x_0-x_1)(x_0-x_2)(x_0-x_3)} + \frac{(x-x_0)(x-x_2)(x-x_3)y_1}{(x_1-x_0)(x_1-x_2)(x_1-x_3)}$$

$$+ \frac{(x-x_0)(x-x_1)(x-x_3)y_2}{(x_2-x_0)(x_2-x_1)(x_2-x_3)} + \frac{(x-x_0)(x-x_1)(x-x_2)y_3}{(x_3-x_0)(x_3-x_1)(x_3-x_2)}$$

Where (x_0,y_0), (x_1,y_1), (x_2,y_2), (x_3,y_3) are the co-ordinates of four data points.

In each case interpolation will only be carried out for $x_1<x<x_2$ and the maximum error will occur at the mid–point of this range ($x = (x_1 + x_2)/2$). The formulae for the mid–point simplify to:

2 point: $y = (y_1 + y_2)/2$

3 point: $y = (-y_0 + 6y_1 + 3y_2)/8$

4 point: $y = (-y_0 + 9y_1 + 9y_2 - y_3)/16$

Error estimates may be obtained by evaluating (cos(x)), where (x) equals zero or ninety degrees, and the error will be expressed as a percentage of unity.

Data points: –27, –9, 9, 27 degrees used to interpolate value of cosine at 0 degrees.

Rule	Value	Error (%)
2 point	0.9877	1.23
3 point	0.9998	0.023
4 point	0.9998	0.023

Data points: 63, 81, 99, 117 degrees used to interpolate value of cosine at 90 degrees.

Rule	Value	Error (%)
2 point	0	0
3 point	0.00191	0.019
4 point	0	0

The four point rule is chosen since it seems a good compromise between complexity and accuracy. If the 0.023% distortion is permissible then the time domain sampling rate for the DFT must be at least 20 times the highest frequency in the spectrum segment.

2.2.9 OPTIMISATION

The saving from using interpolation is approximately the ratio of the final time domain sampling rate to the DFT sampling rate. This saving will be maximised if a frequency shift is applied to the whole segment to bring its centre frequency to zero. A DFT is performed on this shifted spectrum and intermediate points generated by interpolation. The whole time domain output may then be frequency shifted to cancel the original frequency shift.

The maximum frequency in the shifted spectrum is only half its bandwidth, and a DFT may be performed as easily on a spectrum centred at zero frequency as on one centred at any other frequency. The extra work in shifting the time domain output is one complex multiplication per point, but this allows the DFT time domain sampling rate to be reduced. Four complex multiplications and additions are required to produce each interpolated point as against $N+1$ for each DFT point. Hence there is a clear saving for segments containing more than 5 points. The interpolation distortion may be reduced by increasing the ratio of DFT sampling rate to maximum frequency in segment:

Ratio	Error (%)
20	2.3×10^{-2}
40	1.42×10^{-3}
50	5.84×10^{-4}
80	8.91×10^{-5}

2.2.10 EXTENDED OBSERVATION TIMES

Since the formulation imposes no rigid time window on the validity of the output (merely the accuracy with which it is integrated), output may be produced for times greater than the observation time T of the FFT. Segments integrated using the FFT will have the largest integration interval in the frequency domain and hence will be the most critical constituent of the time domain output. The unwindowed FFT output is periodic:

$$f(t + nT) = f(t) \qquad n = 0, 1, 2, 3, \ldots.$$

The output of the integration routine is not, however, due to the time domain windowing

factor, which has different values and slopes at $t=0$ and $t=nT$. Error is still present: as may be seen from the time domain output always being zero at $t=nT$, irrespective of the spectrum. However, providing the integration interval has been well chosen, (T is large enough), the true output should have decayed significantly and the error relative to the maximum output should be small.

The important point is that output may be generated for $t > T$, since there are no discontinuities in the output from the FFT segment to obscure the longer term effects from segments integrated over smaller frequency intervals.

2.3 APPLICATION TO POWER SYSTEM

2.3.1 DERIVATION OF LINE PARAMETERS

Transmission lines are characterised by distributed parameters, which cause the voltages and currents on the line to be related by partial differential equations. The coefficients of these equations will not be constants, since the resistive terms increase with frequency due to the skin effect. The coefficients will also depend on the current distribution between conductors. Distributions using earth as a path for current return will have very different parameters from distributions in which current only flows in conductors.

At a single frequency, the partial differential equations in time and distance may be reduced to differential equations with constant coefficients in distance only. These coefficients are the series impedance per unit length $\boldsymbol{Z}$ matrix and the shunt admittance per unit length $\boldsymbol{Y}$ matrix. For a single circuit line with one earth wire, the matrix dimension is (4*4), but since it is known that, for all faults, the voltage of the earth wire will remain very close to zero, and that the current in the earth return path need not be found, the matrix dimension may be reduced to (3*3).

The line parameters are derived using the formulae given by Shorrocks and Wedepohl [65], but the reduction process mentioned, i.e. inverting the (4*4) matrix, discarding the last row and column and then inverting again, is inefficient and inaccurate, since the symmetry of the matrix is destroyed by numerical errors, greatly reducing the accuracy with which the eigenvalues and eigenvectors can be found at a later stage.

A far better procedure is to reduce the size of the matrix one row at a time (as was done to solve the system matrix in a previous section), since this retains the symmetry of the matrix and is also very much quicker. The reduced impedance per unit length and admittance per unit length matrices are used to find the admittance matrices of any length of line, as described in the next section.

2.3.2 ADMITTANCE FORMULATION

At a certain frequency, the matrix equations describing voltage and current distributions as a function of line length x are:

$$\frac{d\mathbf{V}(x)}{dx} = -\mathbf{Z}\mathbf{C}(x) \qquad (2)$$

$$\frac{d\mathbf{C}(x)}{dx} = -\mathbf{Y}\mathbf{V}(x)$$

The above equations may be combined to give:

$$\frac{d^2\mathbf{V}(x)}{dx^2} = \mathbf{Z}\mathbf{Y}\mathbf{V}(x) = \mathbf{S}^{-1}\mathbf{G}\mathbf{S}\mathbf{V}(x)$$

Where S is the eigenvector matrix, and G is the associated diagonal eigenvalue matrix: both are complex. If Q is the diagonal matrix of the complex square roots of the eigenvalues, (either sign of square root may be taken):

$$\mathbf{G} = \mathbf{Q}^2$$

Then the differential equation has the solution:

$$\mathbf{V}(x) = \mathbf{S}^{-1}(\cosh(\mathbf{Q}x)\mathbf{S}\mathbf{A} + \sinh(\mathbf{Q}x)\mathbf{S}\mathbf{B})$$

Where A, B are vectors to be determined by the end conditions. The hyperbolic sine or cosine of a diagonal matrix is the diagonal matrix of the hyperbolic sines or cosines of the diagonal elements. Writing:

$$\mathbf{Y}_0 = \mathbf{Z}^{-1}\mathbf{S}^{-1}$$

Rearranging equation (2) gives:

$$\mathbf{C}(x) = \mathbf{Z}^{-1}\frac{d\mathbf{V}(x)}{dx} = \mathbf{Y}_0\mathbf{Q}(\sinh(\mathbf{Q}x)\mathbf{S}\mathbf{A} + \cosh(\mathbf{Q}x)\mathbf{S}\mathbf{B})$$

It is required to derive matrices which express the currents C_a, C_b flowing into the ends of the line in terms of the voltages V_a, V_b at the ends of the line :

$$\begin{bmatrix} C_a \\ C_b \end{bmatrix} = \begin{bmatrix} Y_{aa} & Y_{ab} \\ Y_{ba} & Y_{aa} \end{bmatrix} \begin{bmatrix} V_a \\ V_b \end{bmatrix}$$

Vectors A, B will be eliminated by imposing boundary conditions, which for a line of length l are:

$$x = 0: \quad V_a = V(0); \quad C_a = C(0)$$

$$x = l: \quad V_b = V(l); \quad C_b = -C(l)$$

The negative sign in the second current boundary condition is due to the current convention adopted: currents flowing inwards at the ends of the line. Using the following abbreviations:

$$P = S^{-1}\cosh(Ql)S \qquad U = S^{-1}\sinh(Ql)S \qquad T = Y_0QS$$

The boundary conditions are imposed:

$$\begin{bmatrix} -TB \\ T(UA+PB) \end{bmatrix} = \begin{bmatrix} Y_{aa} & Y_{ab} \\ Y_{ba} & Y_{bb} \end{bmatrix} \begin{bmatrix} A \\ PA+UB \end{bmatrix}$$

These equations may be rewritten:

$$\begin{bmatrix} 0 \\ 0 \end{bmatrix} = \begin{bmatrix} Y_{aa}+Y_{ab}P & Y_{ab}U+T \\ Y_{ba}+Y_{bb}P-TU & Y_{bb}-TP \end{bmatrix} \begin{bmatrix} A \\ B \end{bmatrix}$$

Since vectors A, B are arbitrary, there are four conditions to be met:

$$Y_{bb} = TU^{-1}P \qquad Y_{ab} = -TU^{-1} \qquad Y_{aa} = Y_{bb} \qquad Y_{ab} = Y_{ba}$$

Hence, only two matrices Y_{aa}, Y_{ab} are required:

$$Y_{aa} = Y_0Q\coth(Ql)S \qquad Y_{ab} = -Y_0Q\,\mathrm{cosech}(Ql)S$$

Note that these values do not change if Q is replaced by $-Q$.

The Y_0, S matrices and the diagonal elements of matrix Q represent the total output from the evaluation and eigenvector decomposition of the line parameters at a particular fre-

quency. The Y_{aa}, Y_{ab} matrices are easily calculated from this data, which could either be stored as a data set (together with data at the other spectrum sampling frequencies needed for a simulation), or calculated each time the program was run and stored for use in subsequent parameter iterations.

2.3.3 EIGENVECTOR DECOMPOSITION OF A MATRIX

For a single circuit line, the complex matrix ZY has dimension (3*3) and it would be possible to find the eigenvalues by solving algebraically the (cubic) characteristic equation. However the method would not be applicable to double circuit lines, since sixth order polynomials cannot be solved algebraically. The method used instead is to construct a (6*6) real matrix A from four (3*3) real matrices. If the real and imaginary parts of the ZY matrix are found as real (3*3) matrices U, Q, then:

$$\mathbf{ZY} = \mathbf{U} + j\mathbf{Q} \qquad \mathbf{A} = \begin{bmatrix} \mathbf{U} & -\mathbf{Q} \\ \mathbf{Q} & \mathbf{U} \end{bmatrix}$$

This matrix has all the eigenvalues of the original complex matrix and in addition their complex conjugates. The matrix is first converted into a Hessenberg form (i.e. zero below the first sub–diagonal) and then the eigenvalues are found. The eigenvalues which equal those of the complex matrix may be selected since it is known that the latter have positive imaginary parts. This may be demonstrated for an uncoupled system where R, L, C are diagonal, and each element is positive:

$$\mathbf{Z} = \mathbf{R} + j\omega\mathbf{L} \qquad \mathbf{Y} = j\omega\mathbf{C} \qquad \mathbf{ZY} = -\omega^2\mathbf{LC} + j\omega\mathbf{RC}$$

The result follows, since ZY is identical with its eigenvalue matrix.

Once the eigenvalues have been obtained, the eigenvectors may be calculated by solving the complex equation:

$$\mathbf{B} = \mathbf{ZY} \qquad [\mathbf{B} - \mathbf{V}]\mathbf{E} = \mathbf{0}$$

$$\begin{bmatrix} b_{11}-v & b_{12} & b_{13} \\ b_{21} & b_{22}-v & b_{23} \\ b_{31} & b_{32} & b_{33}-v \end{bmatrix} \begin{bmatrix} e_1 \\ e_2 \\ e_3 \end{bmatrix} = \begin{bmatrix} 0 \\ 0 \\ 0 \end{bmatrix}$$

Since only the ratio of eigenvector components is important, components may be arbitrarily assigned as unity. (This will almost always be valid). Let e_1 be so assigned. The matrix equation can now be rewritten:

$$\begin{bmatrix} b_{22}-\nu & b_{23} \\ b_{32} & b_{33}-\nu \end{bmatrix}\begin{bmatrix} e_2 \\ e_3 \end{bmatrix} = \begin{bmatrix} -b_{21} \\ -b_{31} \end{bmatrix}$$

Hence allowing e_2, e_3 to be found by inverting the matrix on the left hand side.

Despite its simplicity, this is a very inaccurate technique. With double precision complex arithmetic, and the reduction of the Z matrix from (4*4) to (3*3) accomplished by matrix inversion, the error in reconstructing the ZY matrix from its eigenvalues and eigenvectors is of the order of one part in 10^8. With the Z matrix reduced by row by row elimination and the eigenvectors found by the following technique, the error drops to the order of one part in 10^{13}.

The disadvantage with the previous technique is that only two rows of the matrix are used to evaluate the eigenvector ratio. The application of row by row elimination uses all of the matrix. The element with the largest modulus is permuted into the bottom right hand corner. e_3 is then expressed as a function of e_1, e_2, allowing a (2*2) matrix operating on e_1, e_2, to equate to zero. Let this matrix be A

$$\begin{bmatrix} a_{11} & a_{12} \\ a_{21} & a_{22} \end{bmatrix}\begin{bmatrix} e_1 \\ e_2 \end{bmatrix} = \begin{bmatrix} 0 \\ 0 \end{bmatrix}$$

The process may be repeated for e_2 unless both a_{12} and a_{22} are zero, in which case e_1 is zero, and e_2 may be set to unity. Normally e_1 may be set to unity and e_2, e_3 calculated by back substitution. The eigenvectors for the three eigenvalues constitute the columns of the S^{-1} matrix mentioned in 2.3.2.

2.4 SOURCE SIMULATION

2.4.1 INTRODUCTION

There exists a wide variety of source conditions which may be produced by equipment connected to a busbar. The most obvious is a generator and associated transformer.

Usually the magnetising reactance of the transformer is neglected, allowing the positive (and negative) sequence leakage reactances to be lumped in with those of the generator. The star–delta transformer connexion forbids the flow of zero sequence current in a generator, and therefore the zero sequence source impedance will depend solely on the transformer and its earthing arrangements.

The ratio of zero to positive sequence source impedance will be quite different from the previous case if there is no local generation, or if there is an open circuited transformer. Similar comments apply to the ratio of reactance to resistance (X/R), for positive and zero sequence currents. A sufficient number of source configurations need to be available to cope with these unusual cases.

2.4.2 GENERATOR SIMULATION

The power frequency armature current amplitude $c(t)$ resulting from a short circuit test is assumed to obey the following equation, in which e is the open circuit voltage:

$$c(t) = \frac{e}{X_d} + e\left(\frac{1}{X_d'} - \frac{1}{X_d}\right)\exp\left(\frac{-t}{T_d'}\right) + e\left(\frac{1}{X_d''} - \frac{1}{X_d'}\right)\exp\left(\frac{-t}{T_d''}\right)$$

X_d is the synchronous reactance and determines the final short circuit current. This parameter is well understood, as it may be related to the physical reluctance of the generator flux circuit under open (or short) circuit conditions. It is responsible for only a small proportion of the total fault current.

X_d' is the transient reactance which represents the effect of the field winding on armature currents, and T_d' is the transient time constant associated with the reactance.

X_d'' is the sub–transient time constant, which is the least understood but most used parameter in protection work. Fortunately it is largely composed of the armature leakage reactance X_l, which is well understood, e.g. X_l=.155 p.u., X_d''=.186 p.u. for High Marnham No 1., which is a 222 MVA machine.

In the conventional model (Fig 2.13), the difference is assumed to be supplied by the leakage reactance of one or possibly more damper windings which mimic the effects of eddy currents in the solid rotor. Associated with each leakage reactance is a damper resistance,

which is basically adjusted until a reasonable match between the sub–transient time constant T_d'' in the model and reality is achieved.

The negative sequence parameters are much simpler to deal with, since the generator looks to them like a simple reactance with a value approximately equal to the sub–transient reactance. There will be no zero sequence components reaching the generator, due to the star–delta transformer connexion.

2.4.3 SIMPLE GENERATOR MODEL

For most protection work, it would be desirable to avoid the complexity of a full model. The first and simplest option is to simulate the generator as the series combination of the armature resistance, a resistance associated with losses in the rotor, and the sub–transient reactance (for both positive and negative sequence armature components). This produces a constant amplitude alternating component of fault current which is approximately valid only immediately after the fault. Neither the sub–transient nor transient decays are modelled, and since the losses in the rotor are frequency dependent, it is unlikely that a frequency independent resistance will adequately model this effect.

Such a model may be useful in the early stages of relay testing, but it is inappropriate for the application studies of anything except relays which are insensitive to source parameters and operate very quickly

2.4.4 AN EMPIRICAL MODEL

The theoretical short circuit transient behaviour of a generator can be empirically modelled once the similarity between it and the behaviour of a notch filter is appreciated.

In Appendix 4, it is shown that a change in the amplitude of a signal at notch frequency (applied to a notch filter) will give an output which looks like an exponentially decaying component at notch frequency. (The decay time constant is dependent on the bandwidth of the notch). Hence, using the principle of superposition, the required behaviour could be constructed by combining two notch filters and three reactances as drawn in Fig 2.14a, or one notch filter and two reactances if the transient decay is neglected (Fig 2.14b).

The above discussion has merely been concerned with single phase power frequency components: the situation is slightly more complicated when differences between positive and negative sequence quantities also need to be modelled. Essentially the notch filter response must be modified such that there is only one complex pole, occurring at W_0 for positive sequence components. A corresponding branch for negative sequence components (with a only one pole at $-W_0$ must also be provided. It can be checked that the frequency response of this combination for negative frequencies (or values of the Laplace variable s is the complex conjugate of that for positive frequencies. This is a necessary condition for the model to be realisable physically.

In Appendix 5, it is shown that positive sequence quantities are dependent on $\omega-W_0$, and negative sequence quantities are dependent on $\omega+W_0$, or in terms of the Laplace variable $s-jW_0$; and $s+jW_0$ respectively.

The model is drawn in Fig 2.15. The real constant α will determine the bandwidth of the notch and hence the associated time constant. This model can be implemented using the Laplace Transform method and separating the output transform into a series of partial fractions. The output would accurately reflect the behaviour of the curve which was fitted to the three phase short circuit current, but without shedding any light on the mechanisms producing the effects.

It is rather more difficult to set up a physically representative generator model, but the effort is worthwhile in that not only the effects but the mechanisms by which the effects are produced are modelled, resulting in greater understanding and confidence.

2.4.5 FULL MODEL

Conventional models of generators have tended to use the *d,q* description of parameters, which enables rotor saliency and different saturation in the direct and quadrature axes to be modelled. However, these features are not of principal importance for relaying simulations, for which a simpler frequency domain model is more appropriate. Many of the features of a frequency domain model (in which rotor quantities are referred to the stator) may be carried over from a direct axis model in a *d,q* generator representation (Fig 2.13):

1) Stator components: armature resistance R_a and leakage reactance X_l.

2) Field winding components: resistance R_{fd} and leakage reactance X_{fd}.

3) Mutual inductance between rotor and stator. This gives rise to the synchronous reactance X_d.

4) Notional damper windings to model eddy currents in rotor body.

5) Actual damper windings. (These are rare on large generators) Note that all these components are frequency invariant, though in a time domain formulation they may be functions of time (if saturation is modelled).

A frequency domain model for a 2 pole generator rotating at W_0 rads/sec is drawn in Fig 2.16. All the inductances and resistances are frequency independent but positive and negative sequence quantities experience different impedances due to the rotation of the rotor. The apparent frequency on the rotor W_a of a stator frequency ω is $\omega - W_0$ for positive sequence currents, and $\omega - W_0$ for negative sequence currents, (as shown in Appendix 5). The transformation ratio for per unit quantities between the stator and rotor is 1:1 for current, and $\omega : W_a$ for voltage and frequency, which result in ratios of 1:1 for inductances in the rotor and $\omega : W_a$ for resistances.

Despite the complexity of the full model, the treatment of eddy current effects by one or possibly two lumped parameter circuits is an unsatisfactory makeshift imposed by the constraints of time domain modelling. Frequency domain modelling easily caters for frequency variant components, which simplify and improve the high frequency accuracy of the model.

2.4.6 MUTUAL INDUCTANCE MODELLING

Hammond [66] has described how the skin effect introduces frequency dependence into the effective permeance m of an iron core. Neglecting saturation and hysterisis (for the moment), he arrives at the formula:

$$\mu = P\frac{\tanh((1+j)z)}{(1+j)z} \qquad z = \frac{\beta}{\delta} \qquad \delta = \sqrt{\frac{2}{\sigma P}}$$

Where P is an absolute permeability; β is a thickness (of iron); δ is the skin depth at fre-

quency ω; σ is the conductivity of iron. The real and imaginary parts of the complex permeability may be separated:

$$\frac{1}{\mu} = \frac{1}{A(z)} + \frac{1}{jB(z)}$$

$$A(z) = \frac{P}{z}\left(\frac{\cosh(2z) - \cos(2z)}{\sinh(2z) + \sin(2z)}\right) \qquad \lim_{z \to 0} A(z) = P \qquad \lim_{z \to \infty} A(z) = \frac{P}{z}$$

$$B(z) = \frac{P}{z}\left(\frac{\cosh(2z) - \cos(2z)}{\sinh(2z) - \sin(2z)}\right) \qquad \lim_{z \to 0} B(z) \to \infty \qquad \lim_{z \to \infty} B(z) = \frac{P}{z}$$

These parts may be modelled as a mutual reactance $j\omega A(z)$ in parallel with a loss resistance $\omega B(z)$. An allowance may be made for hysterisis by reducing the loss resistance, (which increases the loss angle). This model assumes that the effective length of the flux path is independent of frequency, and requires modification when a generator rotor is to be modelled.

At very low frequencies the flux essentially travels across the diameter of the rotor; at slightly higher frequencies it is forced towards the circumference, and at high frequencies it has to negotiate the profile produced by the rotor teeth. (In the last regime most of the flux is likely to cross the slots and contribute to a leakage rather than the mutual inductance.) The model may be reduced to three parameters:

1) The synchronous reactance X_d.

2) A corner frequency K..

3) A phase shift factor S, which multiplies the parallel resistance $B(z)$.

$$X_d = \omega P \qquad z = \sqrt{\frac{\omega}{K}}$$

The values of these parameters are most conveniently found by comparison with published results. The paper by Sharma et al. [55] provides useful data. Fig 2.17 uses data taken from Fig 4.3 of that paper corresponding to the experimentally measured d–axis armature–field mutual inductance at open–circuit rated voltage. (Note that the caption has been transposed with that of the previous diagram in the paper.) Since correspondence

at zero apparent frequency is desirable, the synchronous reactance X_d is chosen to be 0.9p.u. The solid curves on Fig 2.17a,b represent the transfer function of the model for parameter choices ($S = 0.5$; $K = 1.96, 2.56, 3.24$), and those on Fig 2.17c,d represent the transfer function for parameter choices ($K = 2.56$; $S = 0.4, 0.5, 0.6$). As can be seen, the fit is quite good for ($K = 2.56$; $S = 0.5$) and these parameters will be used in the model.

2.4.7 SATURATION

There is a need to model saturation effects, since the behaviour of a generator to small changes in armature (or field) current, under normal (saturated) working conditions, can be very different to that for large changes. Assumptions made are:

1) Field excitation is constant.

2) Voltages, voltage depressions and currents are all positive sequence, power frequency components which are measured once transient effects have subsided.

3) Faults remain on the system until steady conditions exist.

4) Saliency effects will be neglected.

5) The synchronous reactance X_d is assumed to be a function of the modulus of the difference between the field current C_f and armature current C_a phasors.

6) The terminal voltage V is assumed to obey the following phasor equation:

$$V = jX_dC_f - (Ra + j(X_d + X_l))C_a$$

Using these assumptions, (and the open circuit voltage against field current characteristic curve), it is possible to iterate on to nominal working points for both pre– and post– fault conditions. These 'steady state' conditions determine the apparent synchronous reactance seen by the fault: If the machine remains saturated after the fault, then the synchronous reactance will appear low; if large fault currents have caused a large terminal voltage depression, then the synchronous reactance will be larger, possibly approaching that used to set up the pre–fault conditions.

2.4.8 STEADY STATE CALCULATION

As described earlier, the system matrix is constructed to a certain pattern for each configuration, with the fault point nodes at the top. For the steady state calculation, this ar-

rangement is not suitable since the excitation is applied at the busbars and not at the fault point. However, the same routines (with different parameters) may be used to permute the busbar nodes to the top of the matrix.

It is possible to simulate rotating loads (e.g. induction machines) connected to the busbars by considering them as unexcited synchronous machines (with different parameters). Remote sources of generation (not modelled explicitly elsewhere in the program) may also be included at a busbar by lumping the admittance of the combination of the remote generators and tie lines together, and adding it to the local source admittance.

If there is no local or remote generation feeding into a busbar, then the voltages (and load angles) there cannot be arbitrarily assigned: i.e. the busbar nodes must be considered as unenergised and are not permuted to the top of the system matrix.

Once the energised nodes have been brought to the top, the technique of row by row elimination (described earlier), is applied to express the voltages at the unenergised nodes as functions of the excitation at the energised nodes. It is required to set the positive sequence component at each energised busbar to a certain level, and to simulate power flow by specifying the power angle between busbars.

The total busbar voltage (including negative and zero sequence components produced by positive sequence currents in the feeders) is unknown. Each generator may be considered as a pure positive sequence voltage source behind a reactance, but the alternative representation as an unknown positive sequence current source in parallel with a reactance is more suitable for nodal analysis. The injected current then appears directly on the left hand side of the matrix equation, and the associated reactances are included in the system admittance matrix, (as they are in the transient calculation). The matrix equation describing the phase quantities (with the energised busbar nodes permuted to the top left hand corner of the matrix) is:

$$\begin{bmatrix} C_b \\ 0 \end{bmatrix} = \begin{bmatrix} Y_{bb} & Y_{bx} \\ Y_{xb} & Y_{xx} \end{bmatrix} \begin{bmatrix} V_b \\ V_x \end{bmatrix}$$

Where V_b, C_b are busbar phase quantities and V_x are the uninvolved or unenergised

nodes. The injected current vector I_b (dimension $3n$) should consist of n positive sequence sets. A square matrix P (with the same dimension as the admittance matrix) is constructed on the following pattern. (The case for a (6*6) matrix is shown.):

$$\mathbf{P} = \begin{bmatrix} 1 & 0 & 1 & 0 & 1 & 0 \\ h^2 & 0 & h & 0 & 1 & 0 \\ h & 0 & h^2 & 0 & 1 & 0 \\ 0 & 1 & 0 & 1 & 0 & 1 \\ 0 & h^2 & 0 & h & 0 & 1 \\ 0 & h & 0 & h^2 & 0 & 1 \end{bmatrix}$$

$$\mathbf{Q} = \mathbf{P}^{-1} = \frac{1}{3}\mathbf{P}^{t} *$$

Hence the sequence voltages $[V_1, V_2, V_0]$ and currents $[C_1, C_2, C_0]$ are related to the previously obtained phase quantities as follows:

$$\begin{bmatrix} \mathbf{E}_1 \\ \mathbf{E}_2 \\ \mathbf{E}_0 \end{bmatrix} = \mathbf{PE} \qquad\qquad \mathbf{C} = \mathbf{Q}\begin{bmatrix} \mathbf{C}_1 \\ \mathbf{C}_2 \\ \mathbf{C}_0 \end{bmatrix}$$

Hence the sequence source currents and voltages obey the following equation:

$$\begin{bmatrix} \mathbf{C}_{b1} \\ 0 \\ 0 \\ 0 \\ 0 \\ 0 \end{bmatrix} = \mathbf{QYP}\begin{bmatrix} \mathbf{E}_{b1} \\ \mathbf{E}_{x1} \\ \mathbf{E}_{b2} \\ \mathbf{E}_{x2} \\ \mathbf{E}_{b0} \\ \mathbf{E}_{x0} \end{bmatrix}$$

Writing,

$$\mathbf{A} = \mathbf{QYP} = \begin{bmatrix} \mathbf{A}_{jj} & \mathbf{A}_{jk} \\ \mathbf{A}_{kj} & \mathbf{A}_{kk} \end{bmatrix}$$

The procedures used to reduce the matrix dimension may be applied again giving the equations:

$$\mathbf{C}_{b1} = \mathbf{A}_{jj}'\mathbf{E}_{b1}$$

$$\begin{bmatrix} E_{b1} \\ E_{x1} \\ E_{b2} \\ E_{x2} \\ E_{b0} \\ E_{x0} \end{bmatrix} = A_{kj}' E_{b1}$$

After which the phase voltages may be recovered by pre–multiplying with matrix ***P***.

Once the system voltages have been found, the magnitude of the fault point voltage (for single phase or phase to phase faults) is stored and the whole set of voltages is rotated to achieve the correct fault point on wave.

Assuming that the busbar voltages comprise positive sequence sets slightly eases computation, but causes the pre– and post–fault calculations to use different system models. Imposition of a set of busbar voltages implies that the negative and zero sequence reactances of the generator/transformer combinations are zero before the fault. (Zero and negative sequence currents exist in an unfaulted network since the transmission line conductors cannot be transposed).

2.4.9 CALCULATION OF SYNCHRONOUS INDUCTANCE

The calculation in the previous section gives the positive sequence components of armature current and terminal voltage. A positive sequence excitation phasor for to a particular busbar C_j which is an element of the vector C_{b1} may be iteratively derived from these for the local source (modelled as Fig 2.18) at each busbar. If remote sources are modelled, then these are assumed not to contribute any pre–fault current, (except when the local source is absent). Post–fault conditions require several steps:

1) The system matrix is set up (with excitation supplied at energised busbars) and the fault represented as follows:

a) If the fault resistance between a phase and earth is zero, then the row and column representing that phase at the fault point are simply removed.

b) For a zero resistance phase to phase fault, the two rows affected are replaced by a row which is their sum. The affected columns are similarly treated.

c) Non–zero fault resistances may be readily incorporated into a nodal sys-

tem matrix.

2) The system matrix is then reduced to give relations between busbar voltages and currents.

3) The matrix equation relating the positive sequence components of busbar voltage E_{b1} and current C_{b1} is obtained by pre– and post–multiplying with the P and Q matrices described in the previous section. For each source the phasors E_b and C_b are selected

4) Remote sources are modelled more simply than a local busbar source. The steady state model used is simply a positive sequence voltage source E_{br}, (for which the magnitude and phase are known from the pre–fault calculation), in series with an assigned reactance. This reactance is combined with the tie line reactance to derive an admittance phasor Y_{rb} linking remote source current C_r with busbar voltage E_b and remote source excitation:

$$C_r = Y_{rb}(E_{rb} - E_b)$$

Hence, at a particular busbar (tied to m remote sources) the current contributions from each C_r may be summed to give the total remote positive sequence source current C_t:

$$C_t = \sum_{r=1}^{r=m} C_r = \sum_{r=1}^{r=m} Y_{rb}E_{rb} - \left(\sum_{r=1}^{r=m} Y_{rb}\right)E_b = B - Y_t$$

5) The vector C_t is formed from the elements C_t at each busbar, and similarly for vectors B and Yt. The current supplied by the local sources at the busbars with be defined as C_l:

$$\mathbf{C_l = C_b - C_t = (A_{jj}' + Y_t)E_b - B}$$

Writing,

$$\mathbf{Z_t = [A_{jj}' + Y_t]^{-1}}$$

The voltage across the mutual inductance for the local sources V_m is now formed:

$$\mathbf{V_m = E_b + X_lC_l = Z_tB + (Z_t + X_l)C_l}$$

6) The voltage across the mutual reactance of the generator model (Fig 2.18)

is given by:

$$V_m = (C_m + C_l)X_d$$

Where X_d is a function of the current C_m–C_l assumed earlier. Hence a solution for X_d may be obtained iteratively from the two equations defining V_m.

7) The magnitudes of the current C_m–C_l obtained for the pre– and post–fault conditions define the operating points on the assumed operating characteristic. Hence, the ratio of change of open circuit voltage to change in current magnitude between these points gives a value of inductance which should be used in the transient calculation. See Fig 2.19.

This procedure has not been implemented, since doing a series of runs in which different values of synchronous inductance are used would probably cover the same ground.

2.4.10 POWER FLOW

When it is required to obtain a series of runs varying power flow and/or busbar voltages, then computer time can be saved by noting that these affect only the phase and magnitude of the single superimposed source at the fault point (for single phase to earth or phase to phase faults). Hence if two simulations with fault points on wave differing by 90 degrees are available, then the post–fault response to any phase and magnitude variations to the pre–fault voltage may be generated by forming weighted sums of the reference simulations. The pre–fault calculation must be repeated in full for each different pre–fault condition, since it is used to derive the phase shift and amplitude of the fault point voltage for the post–fault calculation.

The technique only applies to components which are dependent on a single source applied at the fault point, and cannot be legitimately applied to double phase to earth or three phase faults, as their post–fault spectra depends on two or more sinusoids, (which will be affected by different amplitude and phase factors for a change in busbar voltage or pre–fault power flow).

2.5 TRANSDUCER AND RELAY INTERFACE SIMULATION

For analogue filters such as a second order Butterworth, the frequency response $G(w)$ exists as a known function:

$$G(\omega) = \frac{W_n^2}{W_n^2 + \sqrt{2}\, j\omega W_n - \omega^2}$$

Where W_n is the cutoff angular frequency The response may therefore be easily calculated and combined with the spectra of the power system waveforms at frequencies determined by the simulation. The frequency response for various cut–off frequencies is shown in Fig 2.20.

The transfer function of the CVT is not so easily expressed as an explicit function of frequency, (without the recourse of curve fitting). However, given data points, (which are sufficiently closely spaced), cubic spline interpolation (using NAG routines E01BAF and E02BBF) may be used to derive the response at any frequency. A typical CVT frequency response has been published by Stalewski [67], and a comparison of actual and model time domain responses by Hughes [68]. The gain and phase of the model used in the simulation are shown in Fig 2.21.

The current transformer is not usually simulated, since its high frequency response is level beyond the cut off frequency of the pre–filters used in relays. Its low frequency response however, shows a zero at zero frequency, and it is advantageous to include this to reduce the current output spectrum peak occurring there.

A simple model is:

$$G(\omega) = \frac{j\omega T}{(1 + j\omega T)}$$

Where T is a time constant which ranges between 60 ms. and 1s. for linear CTs, but may be much longer if ungapped or anti–remanence CTs are used [69]. If a transactor is used as a CT burden, then its time constant is much shorter than this and the CT time constant may be neglected. The frequency responses of CT burdens with various X/R ratios, but the impedance normalised to 1 Ohm at power frequency are shown in Fig 2.22.

In the frequency domain program the transducers may be simulated by multiplying the output spectrum by their frequency responses. Saturation of CTs may be approximately simulated by operations on the time domain signals which include the transducer filtering. Usually the relay pre–filtering (which reduces aliassing in the analogue to digital conversion process) would be lumped in with the transducer frequency response. When current clipping occurs, this treatment is not strictly correct, but for the relatively high filter cut–off frequencies which will be used, the error should not be significant.

POWER SYSTEM CONFIGURATIONS (1 - 6)

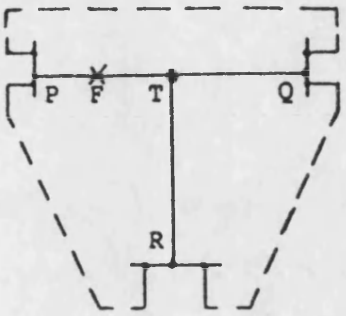

Fig 2.1

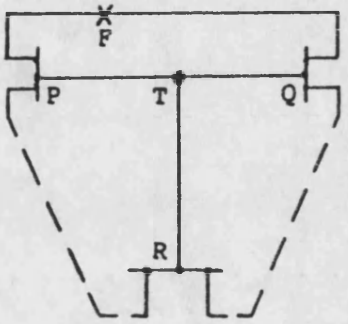

Fig 2.2

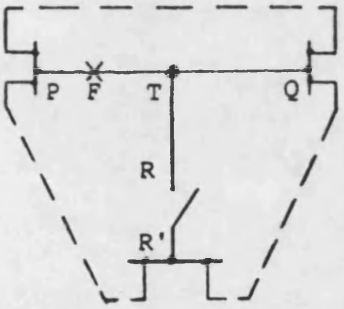

Fig 2.3

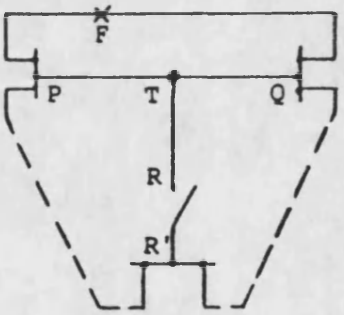

Fig 2.4

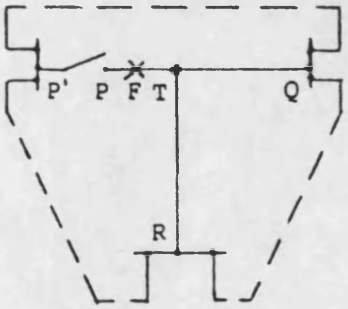

Fig 2.5

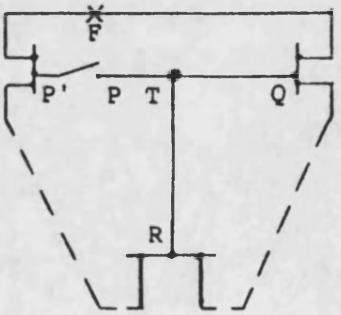

Fig 2.6

POWER SYSTEM CONFIGURATIONS (7 - 12)

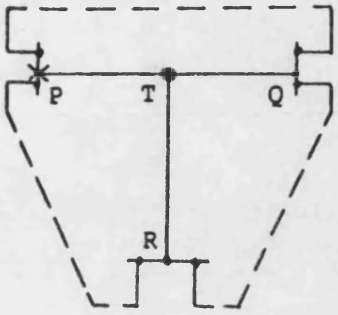

Fig 2.7

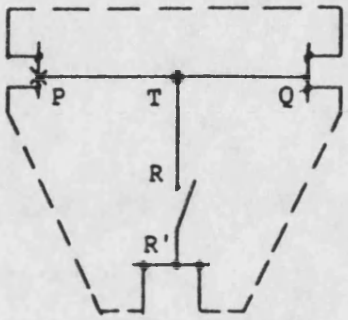

Fig 2.8

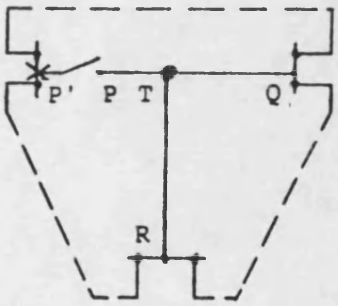

Fig 2.9

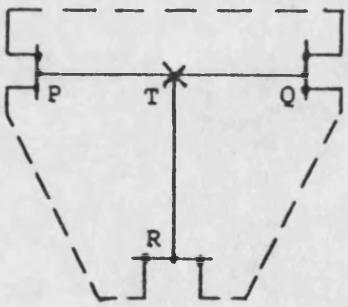

Fig 2.10

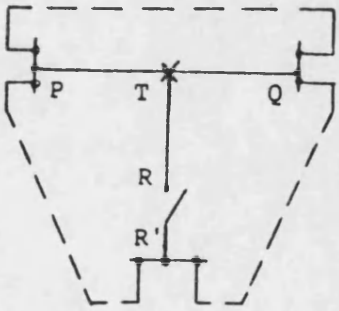

Fig 2.11

Fig 2.12

CONVENTIONAL (d,q) GENERATOR MODEL

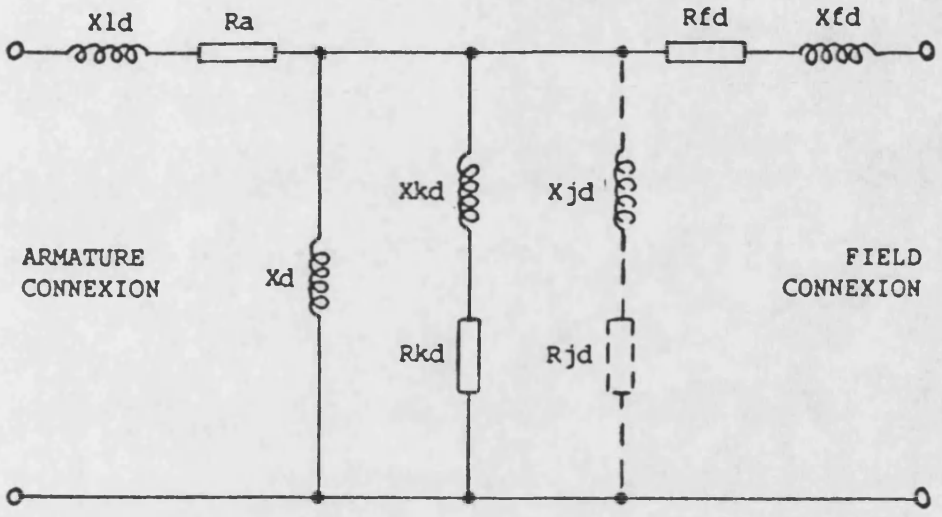

Fig 2.13a DIRECT AXIS MODEL

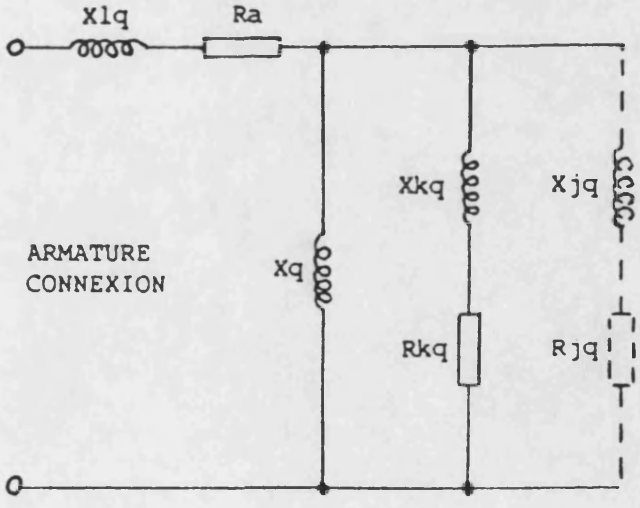

Fig 2.13b QUADRATURE AXIS MODEL

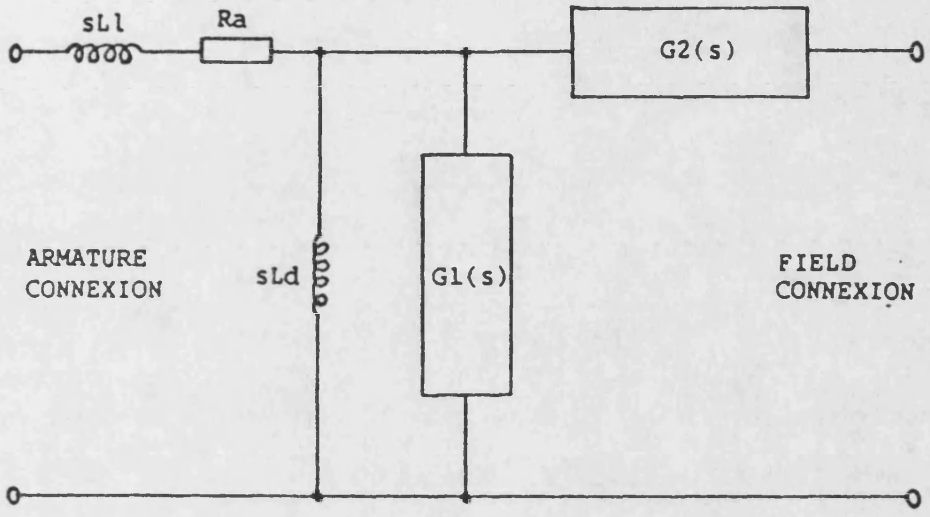

Fig 2.14a COMPLETE MODEL

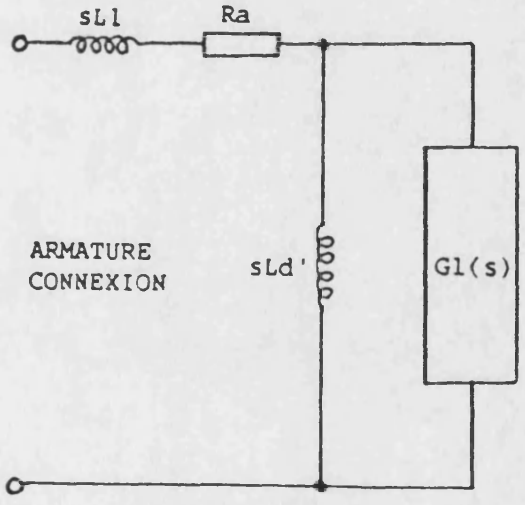

Fig 2.14b SIMPLIFIED MODEL

$$G1(s) = \frac{s(Ld' * Ld'')}{(Ld' - Ld'')} * \frac{(s^2 + Wo^2 + a^2)}{(s^2 + Wo^2)}$$

$$G2(s) = \frac{s(Ld * Ld')}{(Ld - Ld')} * \frac{(s^2 + Wo^2 + b^2)}{(s^2 + Wo^2)}$$

EMPIRICAL SEQUENCE MODELS

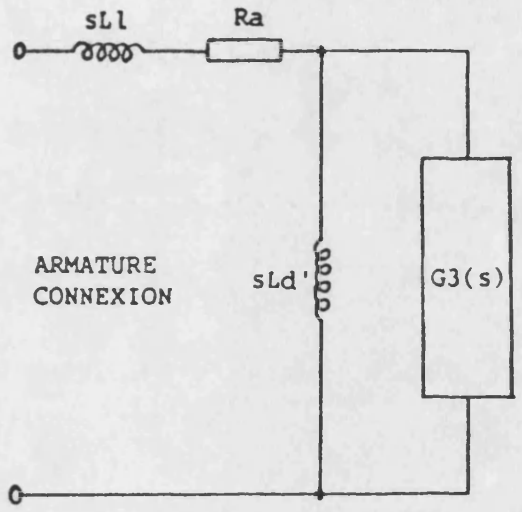

Fig 2.15a POSITIVE SEQUENCE MODEL

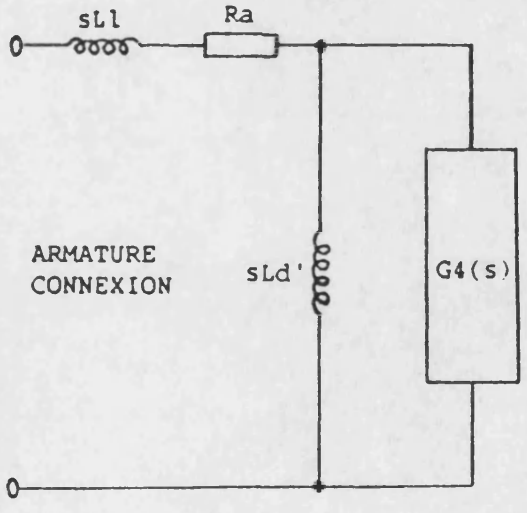

Fig 2.15b NEGATIVE SEQUENCE MODEL

$$G3(s) = \frac{s(Ld' * Ld'')}{(Ld' - Ld'')} * \frac{(s - jWo - a)}{(s - jWo)}$$

$$G4(s) = \frac{s(Ld' * Ld'')}{(Ld' - Ld'')} * \frac{(s + jWo - a)}{(s + jWo)}$$

FREQUENCY DOMAIN MODEL

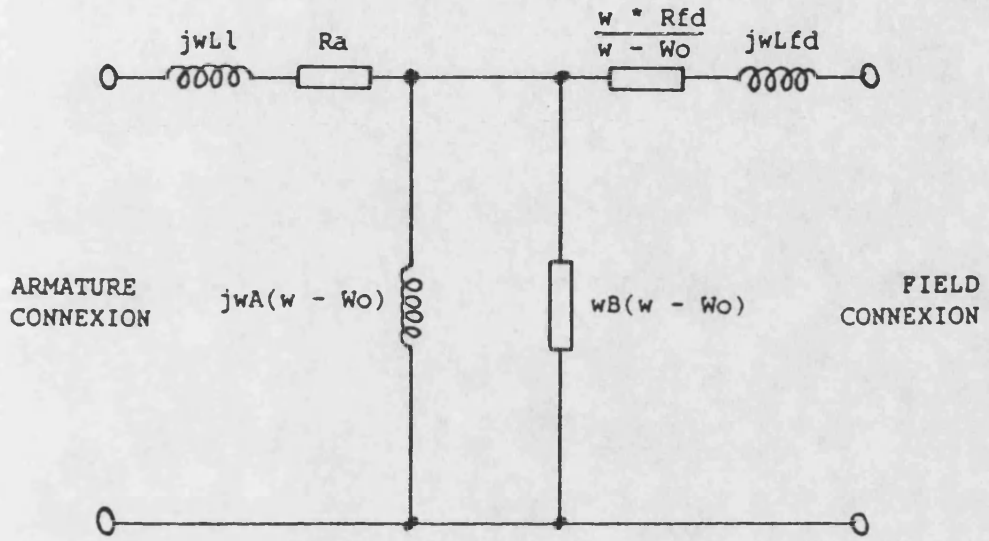

Fig 2.16a POSITIVE SEQUENCE MODEL

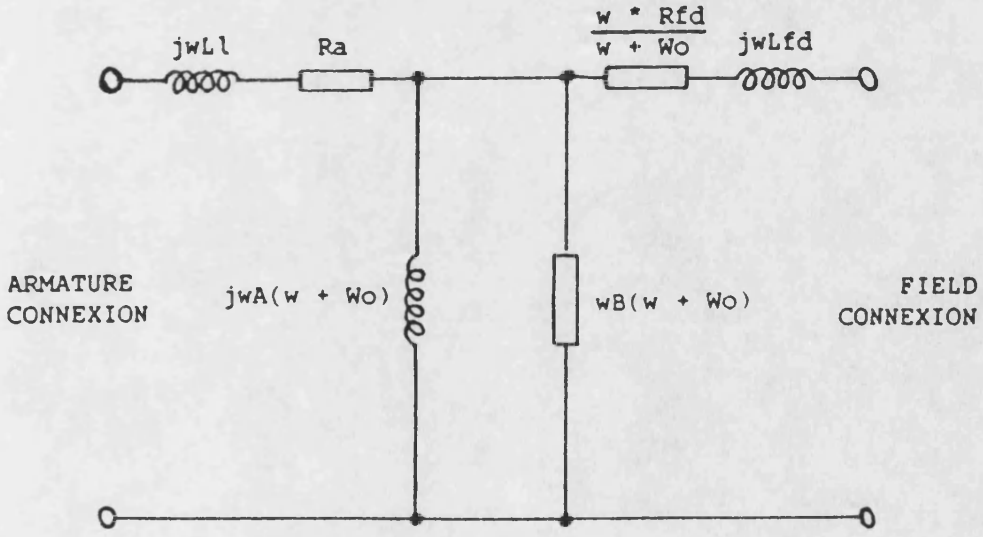

Fig 2.16b NEGATIVE SEQUENCE MODEL

COMPARISON OF MUTUAL INDUCTANCE MODEL WITH MEASURED RESULTS

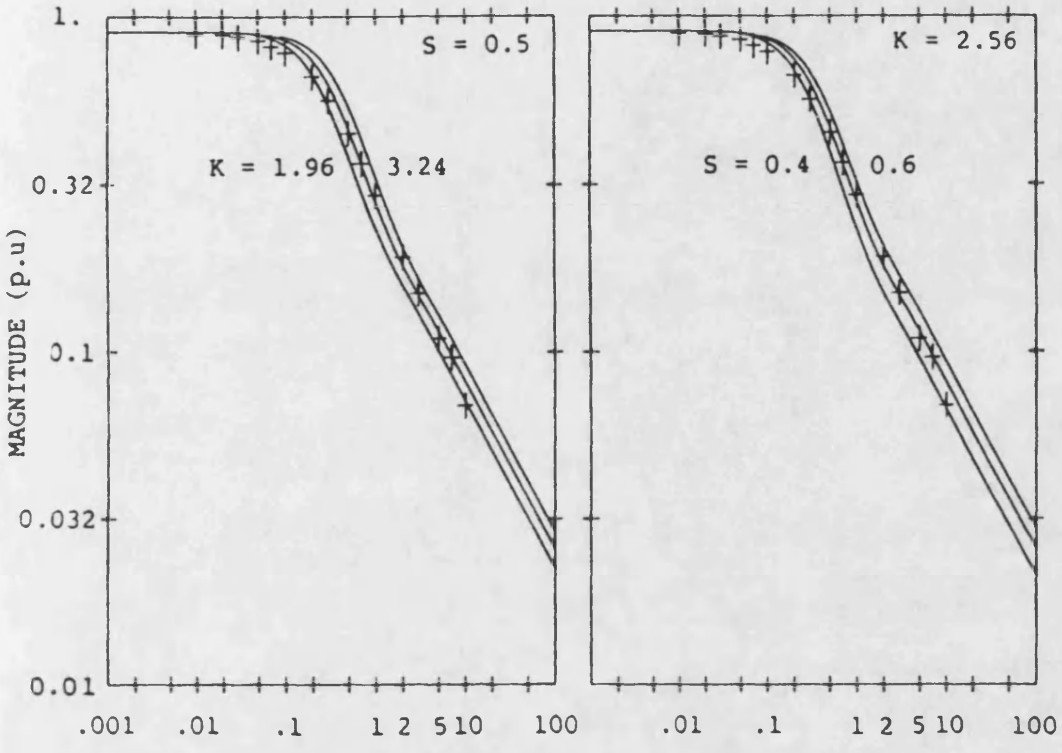

Fig 2.17a FREQUENCY (Hz.)

Fig 2.17c FREQUENCY (Hz.)

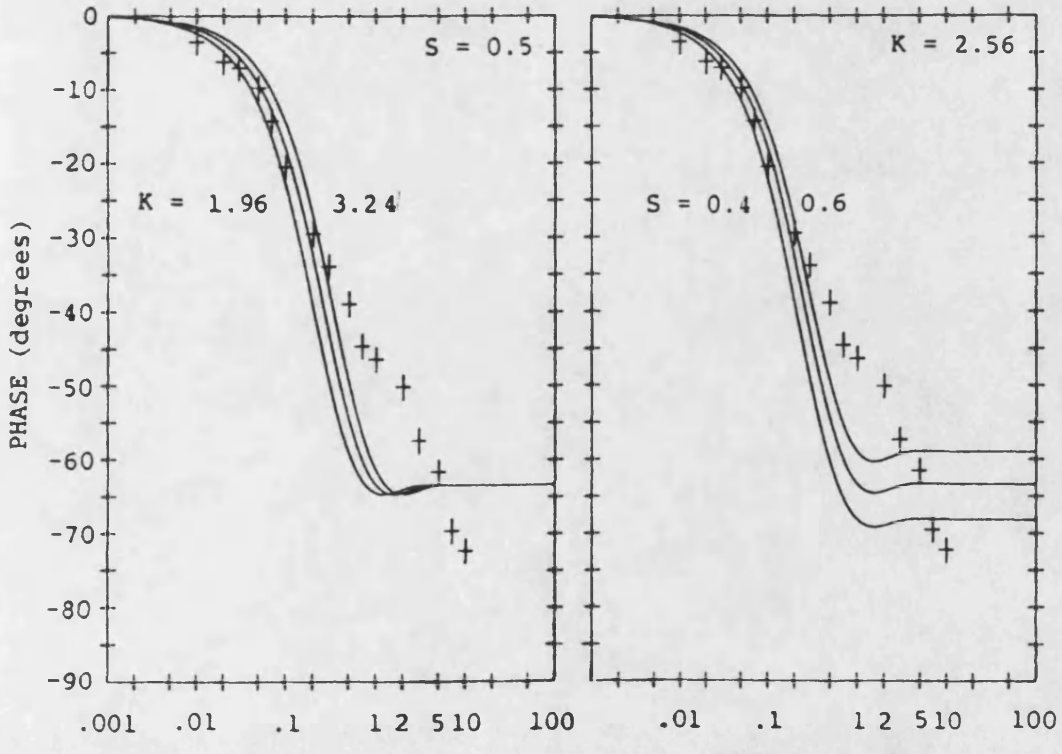

Fig 2.17b FREQUENCY (Hz.)

Fig 2.17d FREQUENCY (Hz.)

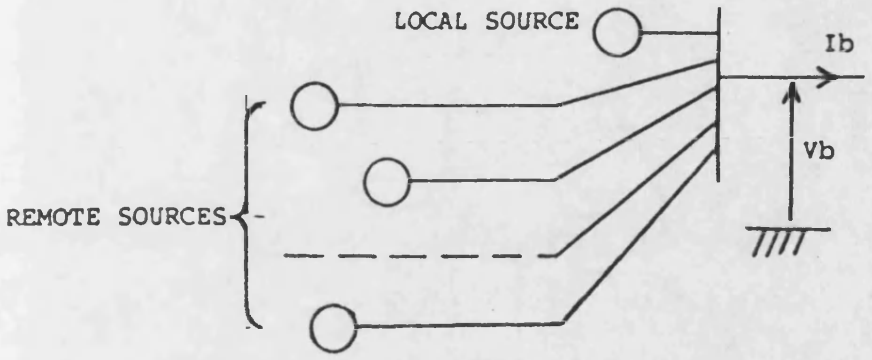

Fig 2.18a THREE PHASE DIAGRAM OF BUSBAR CONNEXIONS

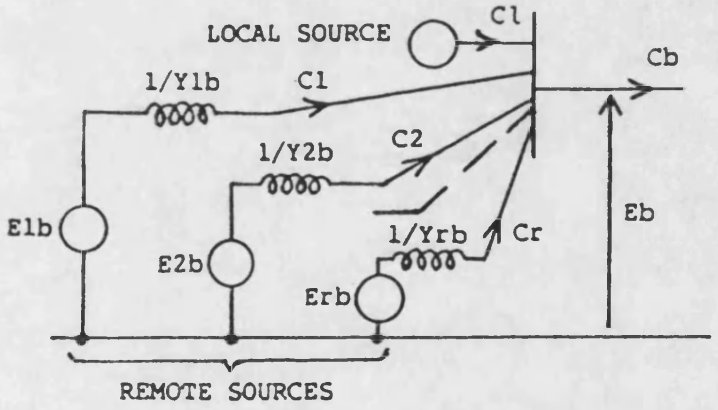

Fig 2.18b POSITIVE SEQUENCE BUSBAR MODEL

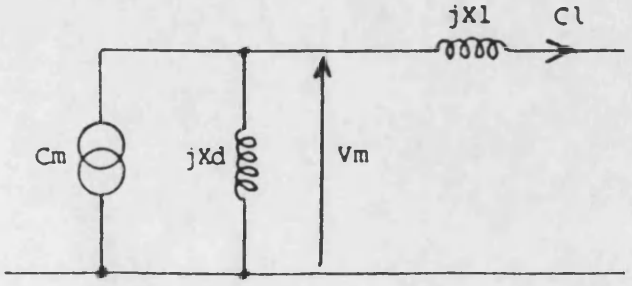

Fig 2.18c POSITIVE SEQUENCE LOCAL SOURCE MODEL

SATURATION MODEL

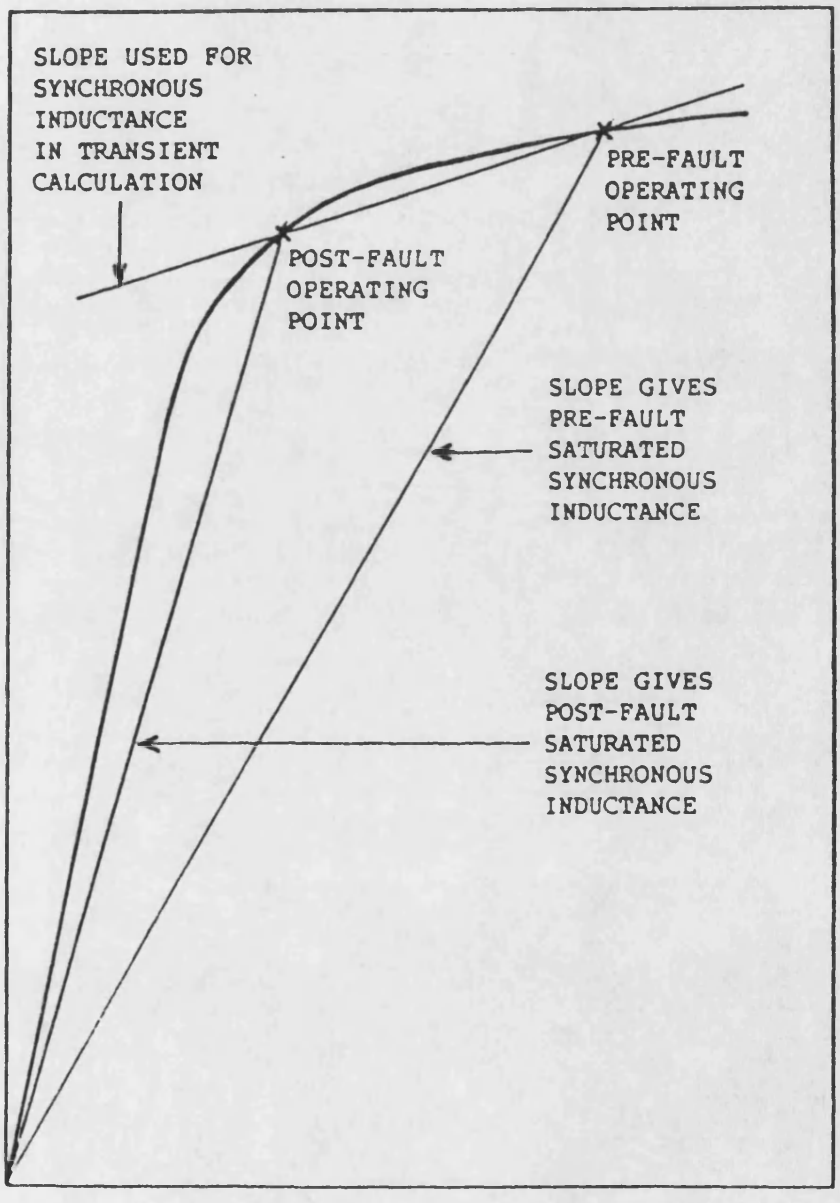

Fig 2.19

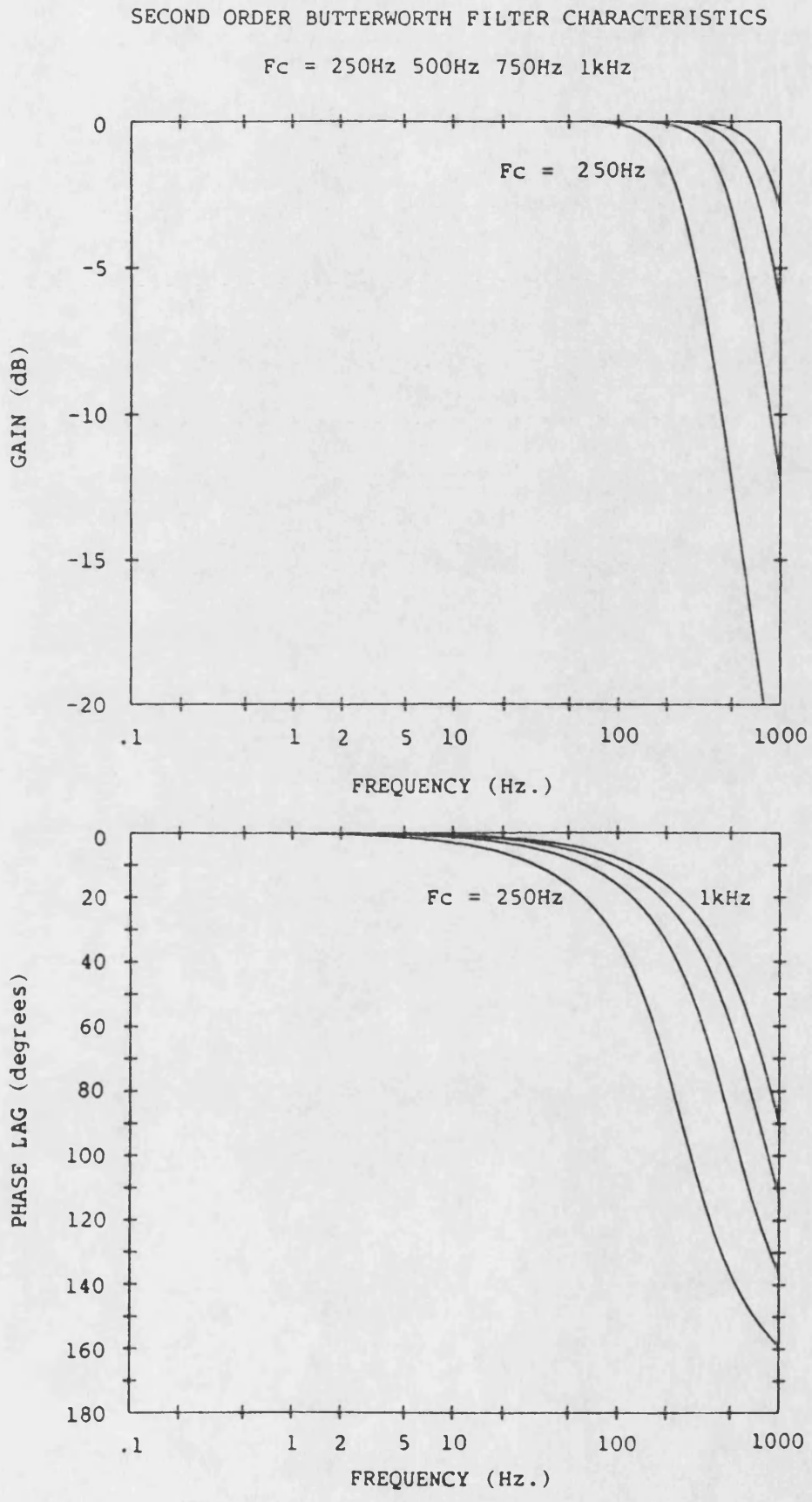
SECOND ORDER BUTTERWORTH FILTER CHARACTERISTICS
Fc = 250Hz 500Hz 750Hz 1kHz
GAIN (dB)
0
-5
-10
-15
-20
Fc = 250Hz
.1
1
2
5
10
100
1000
FREQUENCY (Hz.)
PHASE LAG (degrees)
0
20
40
60
80
100
120
140
160
180
Fc = 250Hz
1kHz
.1
1
2
5
10
100
1000
FREQUENCY (Hz.)

Fig 2.20

Fig 2.21 CVT CHARACTERISTICS

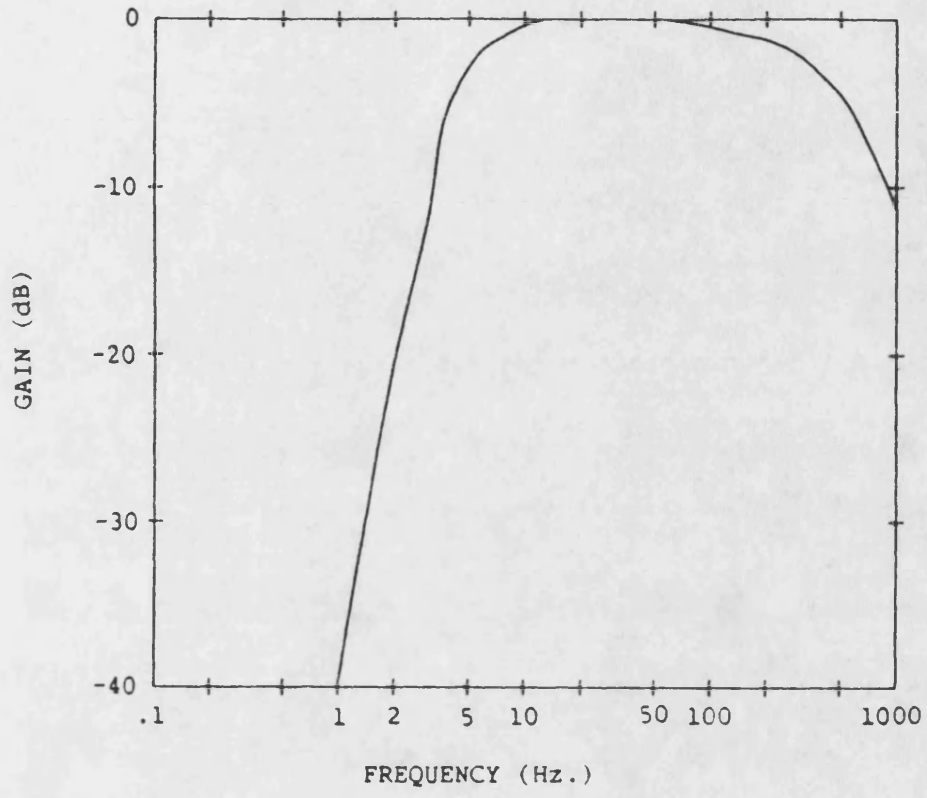

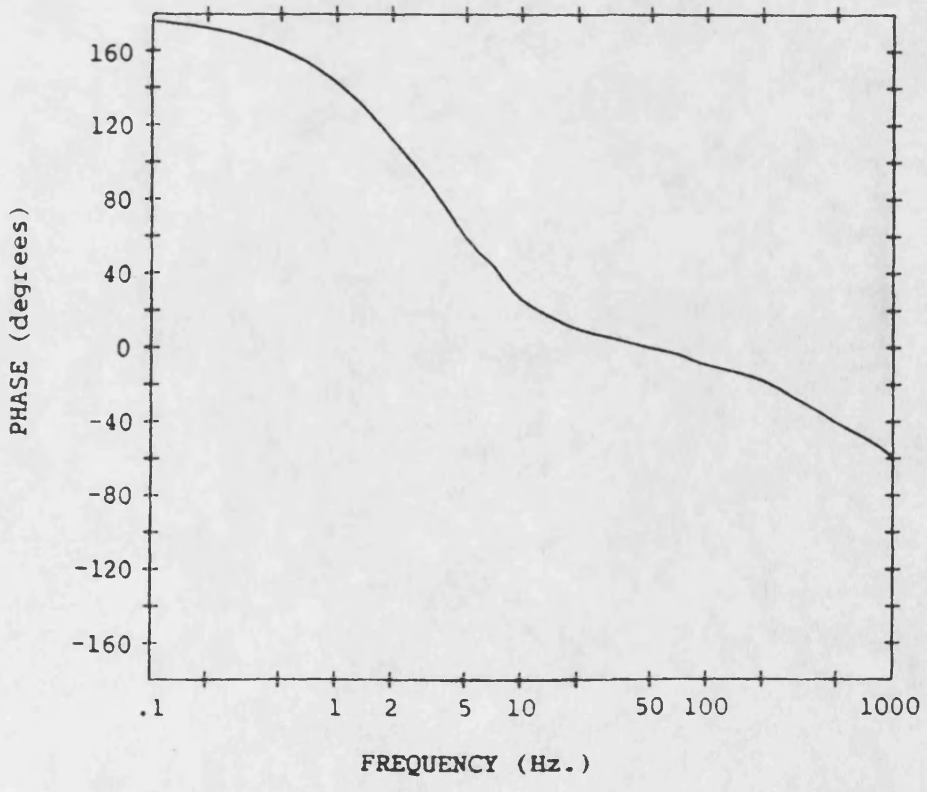

Fig 2.22 CT BURDEN CHARACTERISTICS

R/X = 1. 2. 5. 10. 20. 50.

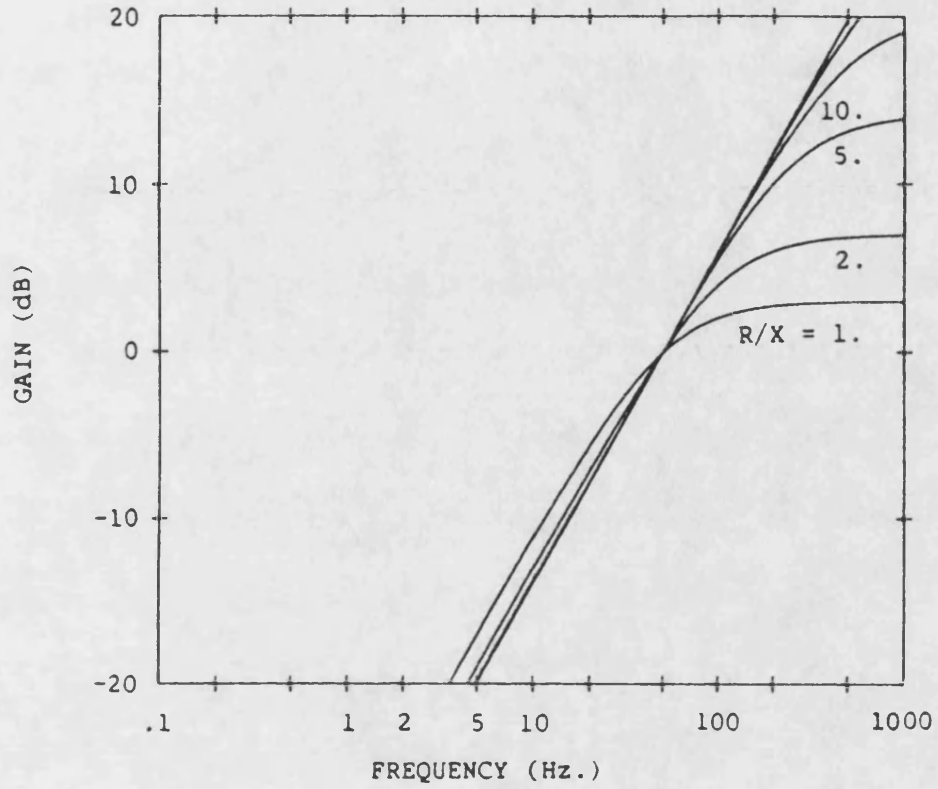

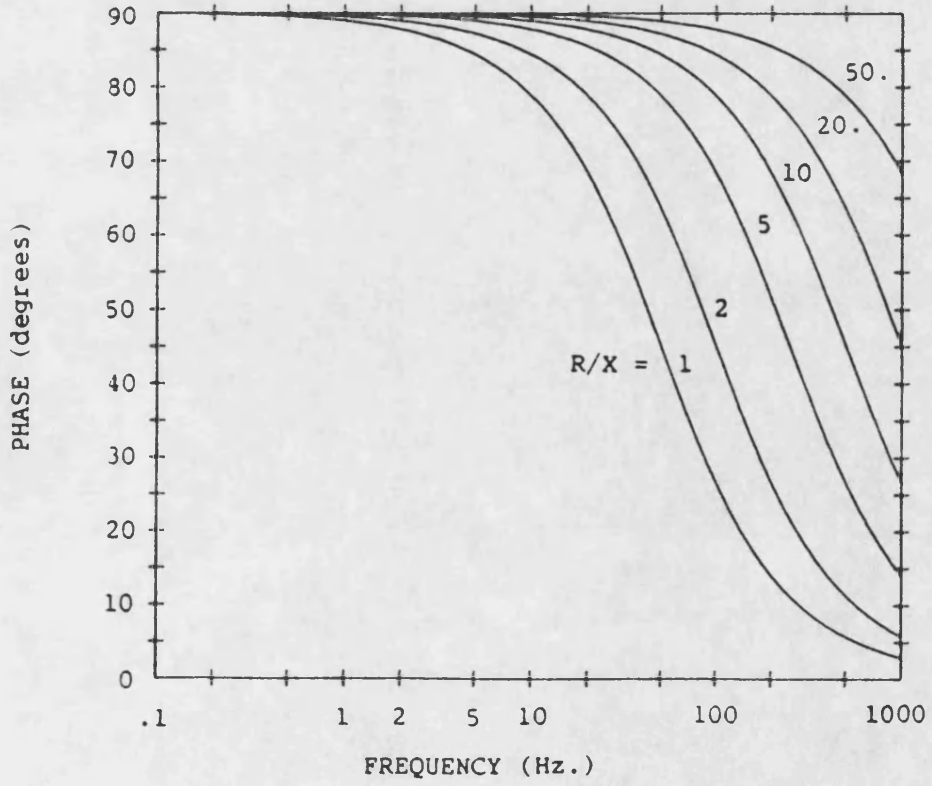

CHAPTER 3

DESIGN PROCESS

3.1 DISCUSSION

While it is desirable to include every possible phenomenon in simulations which are to test a final relay design, at earlier stages in the design process, a simpler system model may be used to advantage:

1) The initial design process inevitably involves much trial and error, in which trends rather than precise numbers are sought. It is often useful to simplify the signals which are presented to the relay, in order to gain an understanding of how it responds to the different components in isolation. Though different signal components may interact to degrade relay performance, it is usually fairly safe to assume that a design which doesn't work with simplified signals will not work in reality.

2) Simple programs require less computer time and memory and may be run on–line rather than as batch jobs. Hence the simulation turn–round time can be very fast and allow more 'design cycles' to be completed.

3) The effect on the impedance estimate of certain phenomena, such as current in–feed into fault resistance from the remote end of a feeder, or the lack of transposition between feeder conductors are not usually compensated for in relay algorithms.

It is anticipated that the algorithms used will not allow much freedom in specifying protection characteristic shape. Hence simulation of the phenomena mentioned in (3) may be postponed till a later design stage, as they are likely to reduce the application range rather than constrain design changes in the impedance estimating algorithm. The effects which cause problems in a relay design may be divided into three groups:

1) High frequency corruption; which is due to travelling waves and is maximum for voltage maximum faults.

2) Low frequency corruption, which is caused by CVT and CT transients for faults not occurring at a voltage maximum.

3) Fault resistance, which can cause the impedance presented to the relay to

differ greatly from the value were it not present. In an impedance measuring relay, the shape of the protection characteristic in the complex impedance plane may sometimes be designed to allow for this. Initially, however, the performance of each algorithm without protection characteristic modification will be studied, since even if such modification is possible, then there is often an operating time penalty and/or an increase in relay complexity.

The most obvious simplification is to omit the high frequency effects, which allows the use of lumped parameters for the transmission line, (which is assumed to be ideally transposed). It was decided to model a single end fed plain feeder despite the obvious limitations due to its simplicity. The fault distance, type and (linear) resistance may all be varied, and also the X/R and Z_0/Z_1 ratios of the source, which is represented as a reactance and resistance in series. (The formulation for the empirical source model (Fig 2.14) was also included.)

Concentration on low and power frequency terms may seem unrealistic in a relay which is supposed to react very quickly, but getting acceptable behaviour for these terms in isolation gives a good indication of overall viability. Note that since travelling waves are not simply related to a power frequency impedance, most relaying algorithms try to greatly attenuate them. The frequency responses of such filters naturally affect low frequency behaviour and are to be included in the model. It is more difficult to adequately filter low frequency terms (without unacceptably long group delays), hence the initial emphasis in this area.

The alternative to this approach is to build up a library of typical and worst case signals (containing all signal components), which may be used to test the relay algorithm. This has been done successfully in the past, but requires a large amount of disc storage for the waveform library.

3.2 POWER SYSTEM SIMULATION

The post–fault waveforms may be found by solving the network formed when either the sequence or modal (also called Clarke) component networks are interconnected.

For the source conditions used, i.e. equal positive and negative sequence sub–transient reactances, the latter choice would have the advantage of using real rather than complex arithmetic, but the network interconnections seem rather artificial e.g. for an a–e fault, one third of the mode 1 network is connected in series with half the mode 2 network and one sixth of the mode 3 network. Voltage sources also need to be inserted in each of the mode 2 and mode 3 networks, whereas the sequence network formulation requires only one (positive sequence) source.

Four sequence network interconnections are required to simulate all important types of fault, since (assuming ideal transposition), transposition of phases may be used to derive the three single phase to earth faults from an a–earth faulted network model, (Fig 3.1). Phase to phase fault simulations may similarly be derived from a b–c faulted network model, (Fig 3.2), and double phase to earth fault simulations from a b–c–e faulted network model, (Fig 3.3). A fourth interconnection is required for the balanced three phase fault, (Fig 3.4). It is possible to use the empirical source model: Fig 3.5 shows the changes needed for an a–e faulted network.

Since the networks are linear and complex arithmetic has to be used, there is great advantage in exciting the network by a complex exponential rather than a real signal. The response to a cosinusoidal (sinusoidal) excitation is then available as the real (imaginary) part of the complex time domain output.

The output to other point on wave excitations may then be found by forming a weighted sum of these outputs. This principle of deriving the output for any point on wave from two outputs in which that angle differs by 90 degrees, may be extended to the case where the output has been modified by a linear transducer model. Since such outputs are usually produced by time domain convolution of an input signal and an impulse response, the computational savings may be considerable.

The networks are solved using the Laplace Transform technique, with the following relations assumed (due mainly to ideal transposition):

$$R_1 = R_2, R_0 = 3R_1, R_{s1} = R_{s2}, L_1 = L_2, L_0 = 3L_1, L_{s1} = L_{s2}$$

Four classes of solution may be defined: depending on the number of current loops and

complexity of source model:

1) A single current loop and a simple source model, i.e. a–e, b–c and three phase faults. The currents and voltages in the Laplace domain may be determined by inspection.

2) Two current loops and a simple source model, i.e. double phase to earth faults. The roots of a complex quadratic equation must be found to solve the network.

3) A single current loop with empirical source model requires solution of a complex cubic equation.

4) Two current loops with empirical source model requires solution of a complex quartic equation.

Network solution is described more fully in Appendix 6.

3.3 TRANSDUCER AND ANALOGUE FILTERING SIMULATION

In the next section, the combined transducer and relay pre–filtering frequency (or impulse) response will be referred to as that of the transducer (for brevity). The technique to be described was originated by Barker [23], but since has been slightly refined. It generates superimposed components by subtracting a continuation of the pre–fault waveform from the input. One part of the output is formed by applying the power frequency gain and phase shift of the transducer to the continued pre–fault waveform, (which is a power frequency sinusoid). The other part of the output is zero until the fault time, after which, it is the convolution of the superimposed input signal and the impulse response of the transducer.

This has two main advantages compared with the process of convolving the input directly with the impulse response:

1) The transient arising from the sudden application of the steady state (i.e. pre–fault waveform) is eliminated.

2) The number of samples in the waveform which need to be convolved is reduced by the number of pre–fault samples.

The theoretical justification of the technique relies on the superimposed component prior to the disturbance being zero and hence contributing nothing to the pre–fault output. The

steady state component (which has an impulse spectrum) may therefore be multiplied by a power frequency gain in either the frequency or time domains, to give the required output. In the time domain the phase shift is produced by a delay.

The impulse (time domain) responses of the transducers $g(k)$ decay smoothly and hence the output signals may be approximated by discrete convolution:

$$y(k) = \sum_{i=0}^{i=k} g(i-k)x(k)$$

The sampling frequency of the discrete signals should be high relative to those features of their spectra for which accuracy is required.

The primary sampling rate is chosen to be 8 kHz., and the output rate is divided down to 4 kHz. or 2 kHz., whichever is required to test the relay simulations. No frequency band limiting is applied to the simulation signals before they are convolved, hence aliassing inevitably exists, but since it is only associated with the sharp waveform at fault incidence, the error is likely to be of the same form as the transducer impulse response and small in magnitude.

The phase shift may be applied to the input steady state waveform by taking a weighted average of the two samples which straddle the equivalent delay. i.e. 360 degrees phase shift at 50 Hz. corresponds to 20 ms., which corresponds to 160 samples at 8 kHz. sampling rate. It is important to take this much care over applying the exact amount of phase shift, rather than approximating the delay by an integer number of samples, since for many faults, the steady state and superimposed components will be of approximately the same magnitude but of opposite sign. A small phase shift error in the former will therefore give a much larger phase shift error in the sum.

The impulse response of a filter function may be found as the inverse Fourier Transform of its frequency response using the methods of Chapter 2. The impulse response is treated as a continuous function which is sampled to give a discrete time series. Discrete convolution is an approximation to convolving continuous functions (using the convolution integral) and then sampling the continuous output function.

The frequency response of a filter must be truncated at half the sampling frequency at which the signals are to be convolved, i.e. for 8 kHz. sampling, only the zero to 4 kHz. response must be included. The response at higher frequencies must be set to zero, since such frequencies cannot be correctly represented in the sampled waveform. Ringing of the time domain impulse response should not be a problem, since the low pass nature of the transducer frequency response (i.e. cut off frequency is less than 2 kHz.) should dominate high frequency behaviour, and make imposition of a frequency response windowing function unnecessary.

3.4 ANALOGUE INTERFACE

This consists of a second order Butterworth filter with its cut off frequency set (initially) at half the relay sampling frequency, to reduce aliassing produced when frequencies higher than this are sampled. Its frequency response is combined with that of the transducer to produce an impulse response so that only one convolution need be done for each signal.

The analogue voltage is scaled so that twice peak volts correspond to 9 volts secondary, and hard clipping is applied at a level of 10V. The phase current is scaled according to the application, e.g. for a 100 km. line with a 1200:1 current transformer, a gain of 0.589 V/A is used. Clipping is applied at 10 volts (positive or negative), corresponding to a maximum current of about 20 kA, or a fully offset waveform from a three phase fault at about 110 km. (with zero local source impedance). (The existence of clipping may be detected using analogue electronics). Separate current scaling is available for the directional and independent mode currents, since the criteria are different:

1) For the directional relay it is desirable that clipping does not occur for any reverse fault, since its occurrence extends the interval before measurement can recommence.

2) For the independent mode, the current must not clip for forward faults which are outside the protected zone.

Though the worse case results of imposing these criteria may coincide for a plain feeder, this may not be so in three ended applications: the directional relays will have to be set to have the same maximum sensitivity, but the lengths protected by the independent mode will depend on the distance to the Tee point. A 12 bit analogue to digital converter (11 bits plus sign, giving a range of –2047 to +2047 levels) is used to digitise the measurands.

Test parameters which may be specified are:

1) The amount of random noise added at various stages through the scaling and conversion process, (this has been set to zero in all the work in this thesis).

2) The gains of the current interfaces to the separate relays.

3) Whether filtering and/or transducer responses are to be included. (This is used mainly for program fault finding purposes).

4) Whether output is required at 2 kHz. or 4 kHz. relay sampling frequencies. (The appropriate analogue cut off frequency is automatically chosen, if applicable).

3.5 RELAY SIMULATIONS

The output from the analogue interface is used by both the directional and independent mode simulations. Each of these also require a set of parameters (algorithm type, time constants, gains and thresholds), which cannot sensibly be implemented as a series of nested loops, since two gains may need to be changed simultaneously, or the same input may mean different things in different algorithms.

Each different relay simulation therefore requires a complete set of relay parameters, though adjustment of the time constant parameters and thresholds (by a factor of 2) to cope with the two different relay sampling rates may be incorporated into the program. The output must show exactly what conditions prevailed for each test and how each part in the scheme behaved. The output possibilities for each part are given below:

1) Directional relay: For each of the 6 elements: (a–e), (b–e), (c–e), (b–c), (c–a), (a–b)

a) A flag indicating a forward or reverse decision or no operation.

b) The operating time (when applicable).

2) Long term clipping detector:

a) A flag indicating operation or not.

b) The operation time (when applicable).

3) Independent mode: For each of the 6 elements: (a–e),(b–e),(c–e),(b–c),(c–a),(a–b); there are four classes of output:

a) No operation of any element.

b) Minimum trip time of a specific element at a fixed reach setting.

c) Minimum setting for operation of a specific element (and trip time).

d) Minimum setting for operation of any element (and trip time).

The fourth class is a summary of the relay performance and useful for checking whether an encroachment has occurred, i.e. that an element has operated with a lower setting than the target element. The first directional element to operate is taken to decide the direction of the disturbance. If there is no operation or a reverse indication then neither of the other parts of the scheme will be triggered and hence their parameters are irrelevant. They are therefore set to zero in the printout.

The program is arranged to produce output in a format suitable for processing by the program described in Chapter 6. Whenever a set of results from the directional, extended clipping detector, or independent mode relays is available, it is output to a file (together with any test parameters which have changed since the previous output). If the program is run interactively, then the output is also directed to the terminal, but in an expanded form compared to that stored in the file, i.e. including words explaining what the numbers mean. A program was also written to read through the output file and expand it to the terminal, enabling the benefits of a reduced storage requirement and easy intelligibility to be combined.

3.6 DISCUSSION OF PROGRAM STRUCTURE

For any design of relay, it is necessary to investigate the performance for a range of fault types, distances and resistances, together with various source capacities and other parameters. This can be done most conveniently by arranging for the program to step through

the combinations of parameters and produce many sets of results for one program run. There are two ways of organising this:

1) By specifying the complete set of parameters required for each combination.

2) By specifying only the initial value, final value and step value of each parameter.

The latter choice has the advantage that large quantities of results, perhaps containing unforeseen details, may be easily generated. The former choice has the advantage that several unrelated onerous relaying conditions may be investigated, without having to step through all the permutations of the parameters, most of which will not present relaying difficulties. The advantages of both alternatives may be combined if supplementary complete sets of initial, final and step values for the parameters, may be used after the permutations of the first set have been exhausted. The first choice is equivalent to this, but with the restriction that for each parameter the initial and final values are equal.

To achieve this flexibility, the simulation program has to be structured so that the actual waveform generating code is surrounded by nested parameter varying loops. The order of these loops is not particularly critical, only affecting the order in which the power system parameters are permuted, but the innermost loop must implement fault point on wave variation since it operates on the time domain waveforms.

The program section which reads in the data will obviously appear before the parameter loops, and the program will branch back to this section after the outermost loop has been completed. Another set of parameters is then read in, waveforms generated and the process repeated, until the end of data is detected, and the program stops. The data reading section is coded such that, for the second and subsequent data sets, only changes from the preceding parameter specifications need be input.

The program structure may be outlined in pseudo–code as follows:

```
BEGIN DATA INPUT LOOP
    READ IN DATA UNTIL FLAG
    IF END OF DATA THEN STOP
    BEGIN POWER SYSTEM PARAMETER VARYING LOOPS
        GENERATE POWER SYSTEM WAVEFORMS FOR 2 POINTS ON WAVE
        CONVOLVE WITH TRANSDUCER IMPULSE RESPONSES
        BEGIN POINT ON WAVE LOOP
            FORM WEIGHTED SUM OF OUTPUTS
            REMAINDER OF ANALOGUE INTERFACE PROCESSING
            BEGIN RELAY PARAMETER VARYING LOOPS
                RELAY SIMULATION
                OUTPUT FORMATTING
            END RELAY LOOPS
        END POINT ON WAVE LOOP
    END POWER SYSTEM PARAMETER LOOPS
END DATA INPUT LOOP
```

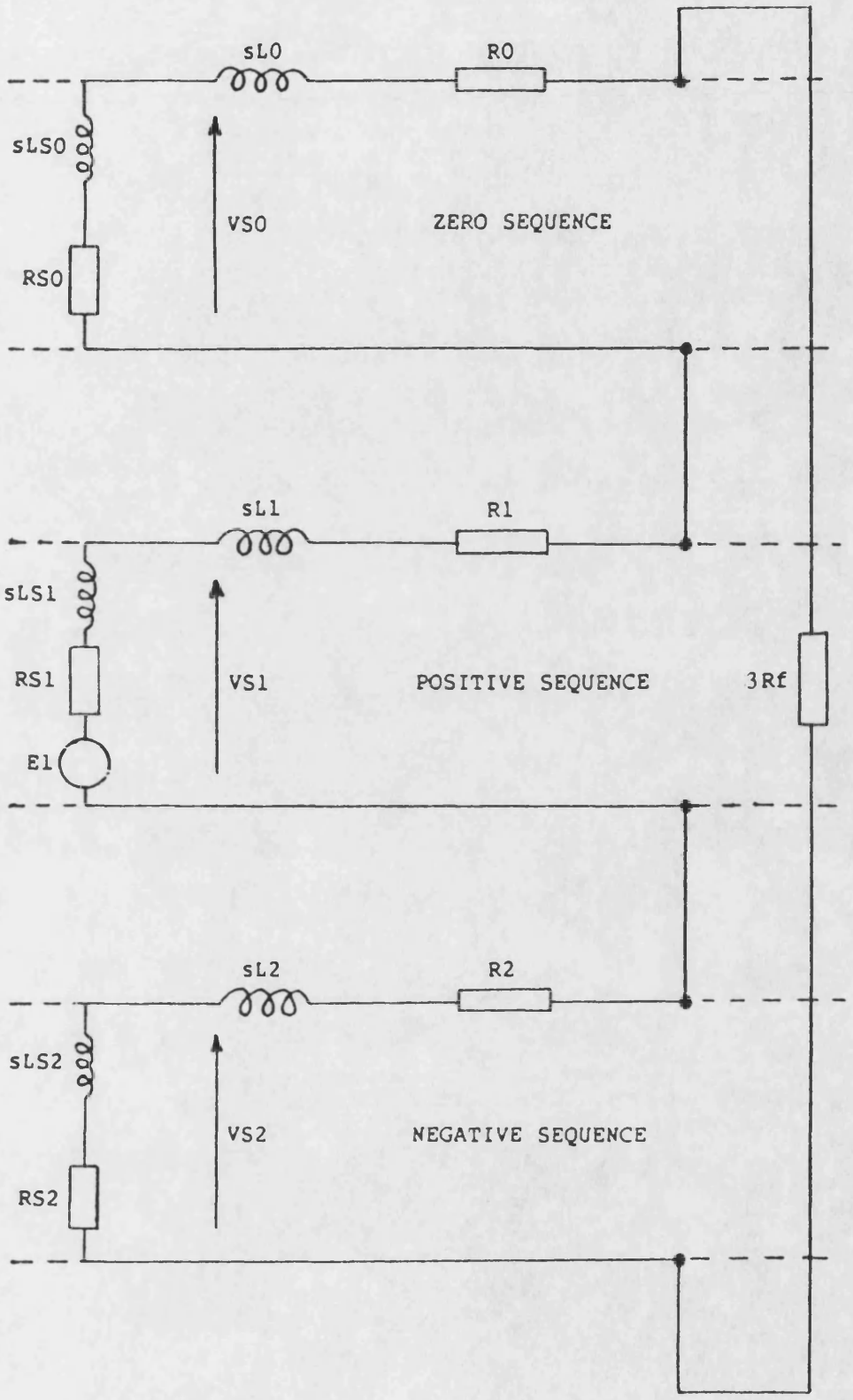

Fig 3.1 SEQUENCE NETWORK CONNEXION FOR AN A-E FAULT

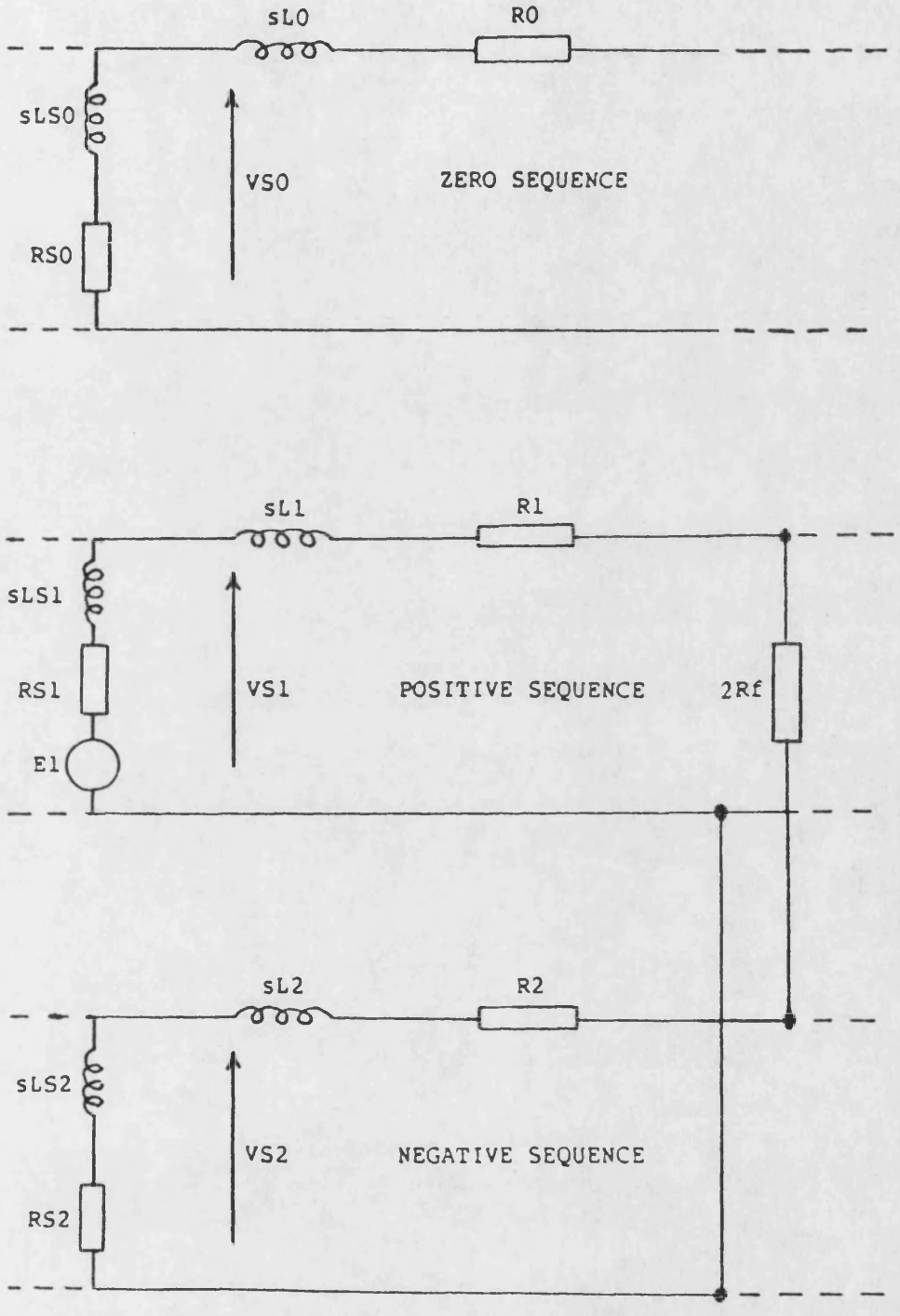

Fig 3.2 SEQUENCE NETWORK CONNEXION FOR A B-C FAULT

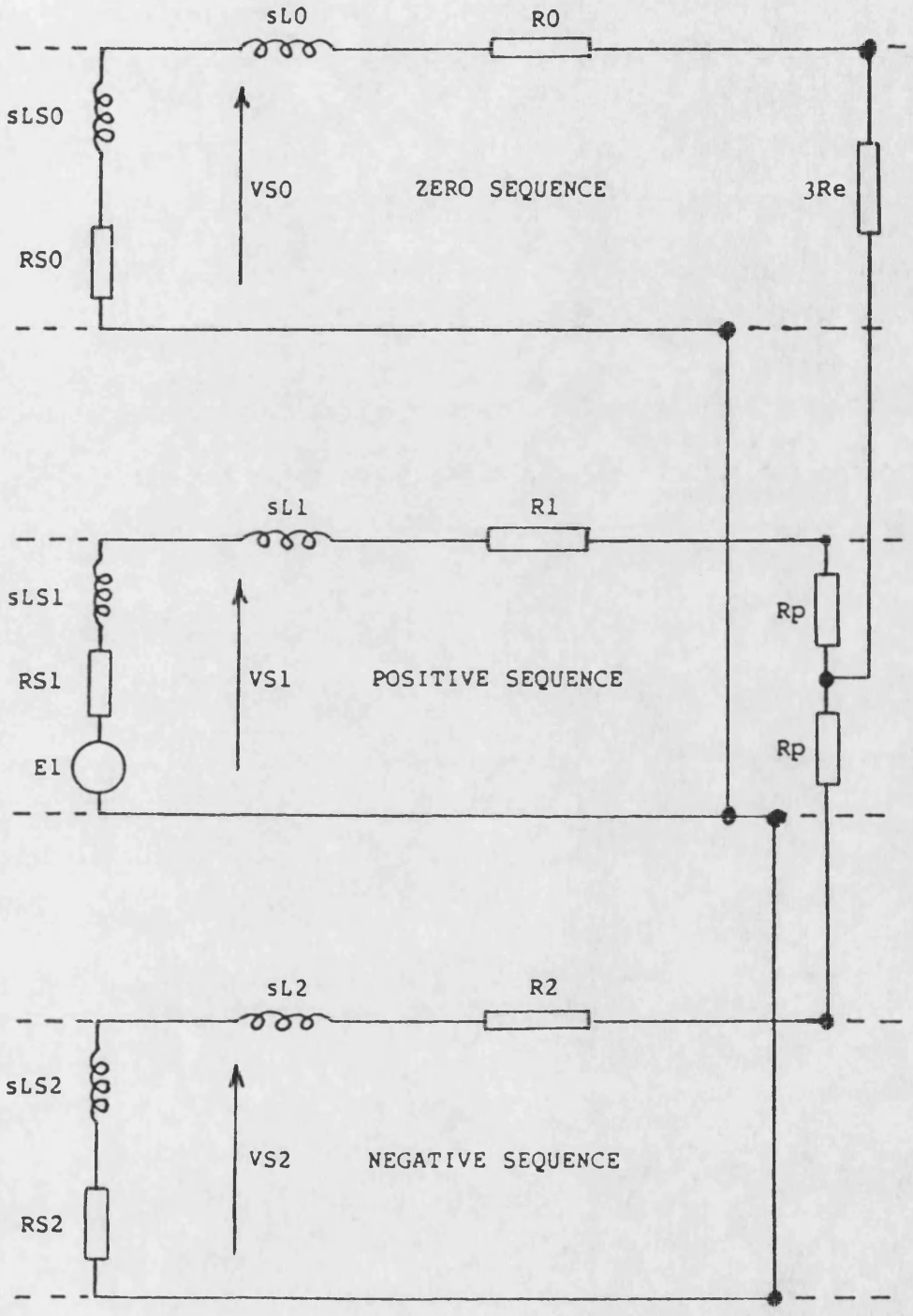

Fig 3.3 SEQUENCE NETWORK CONNEXION FOR A B-C-E FAULT

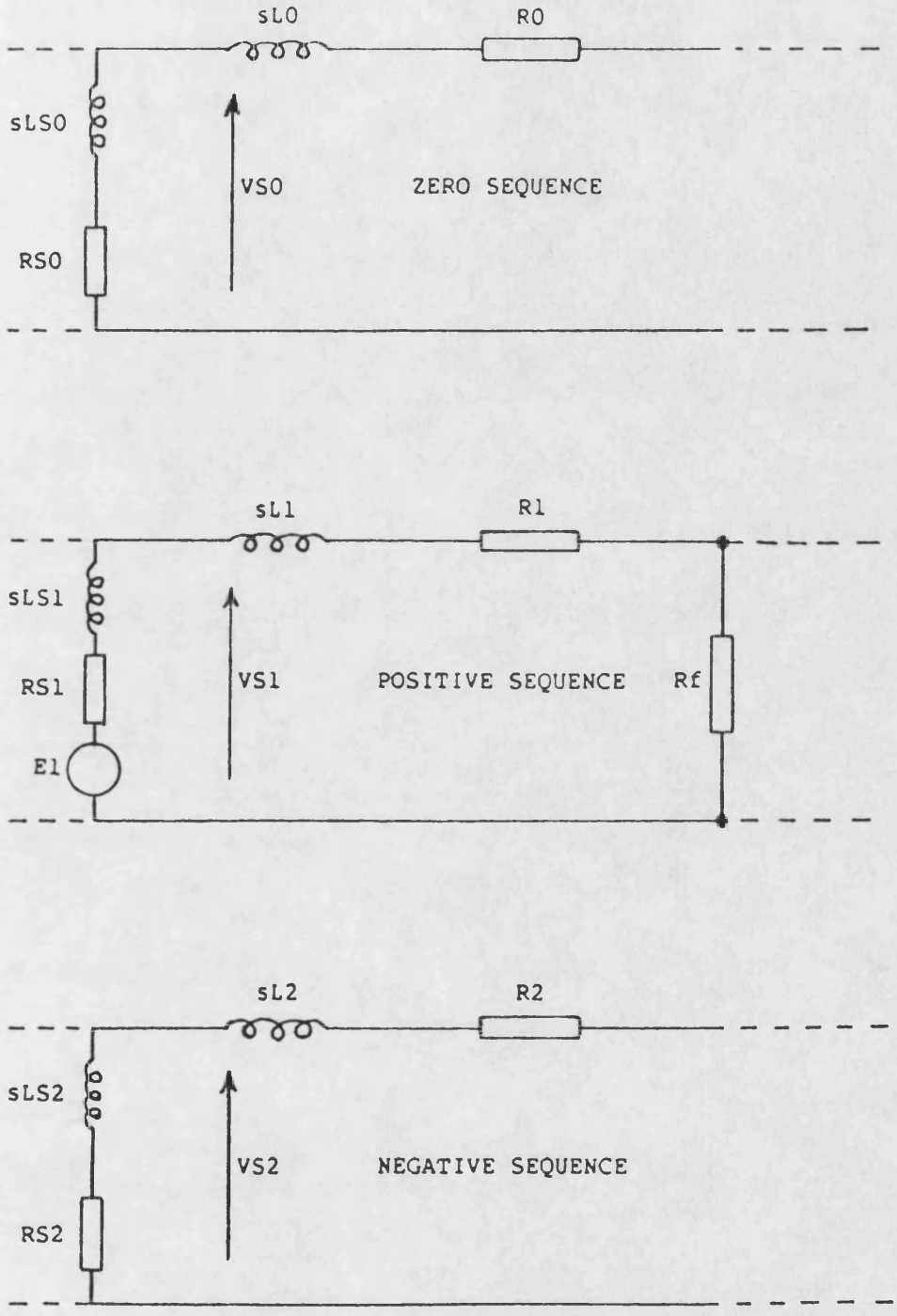

Fig 3.4

SEQUENCE NETWORK CONNEXION FOR A BALANCED THREE PHASE FAULT

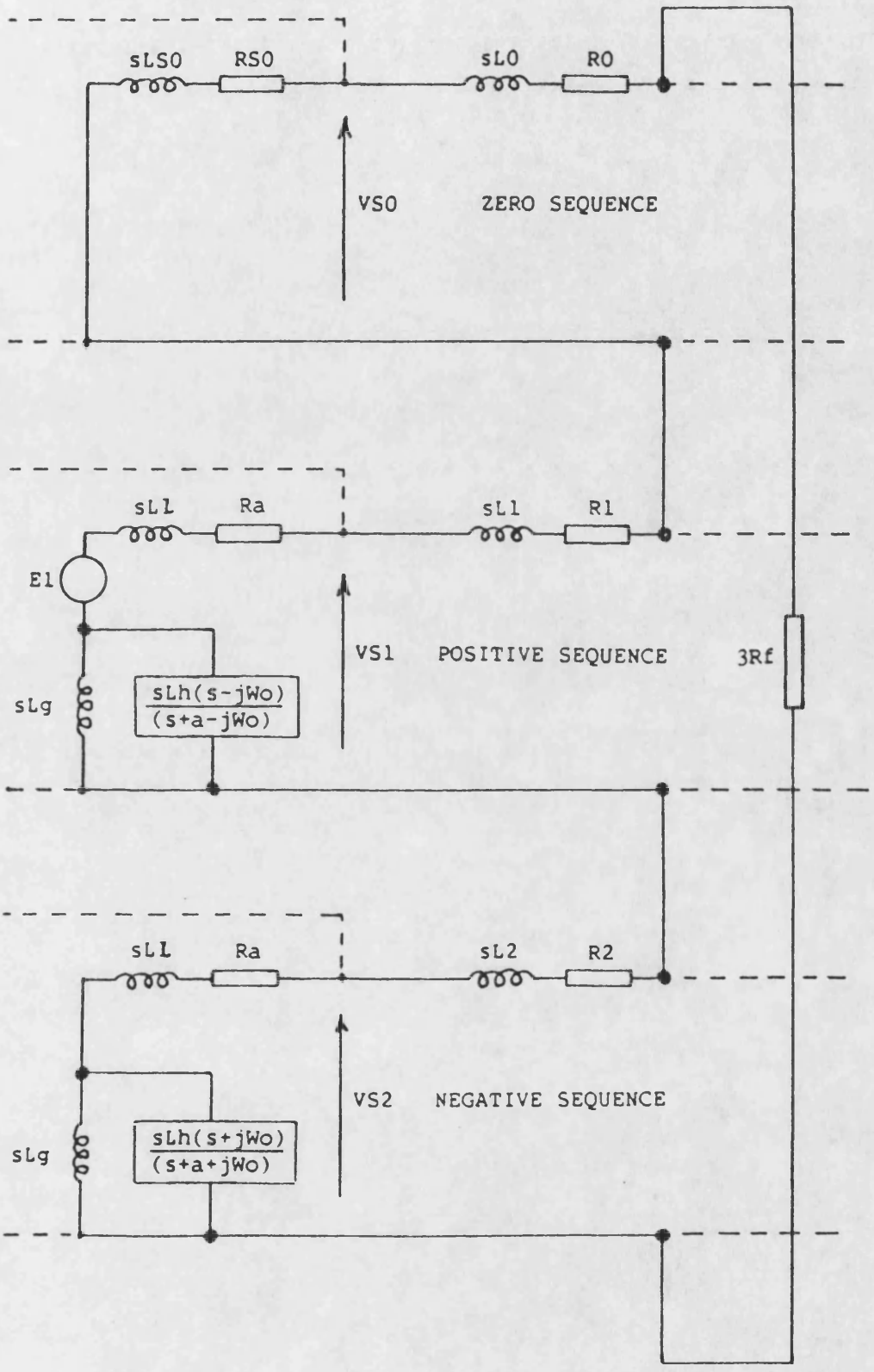

Fig 3.5 SEQUENCE NETWORK CONNEXION FOR AN A-E FAULT
(WITH EMPIRICAL SOURCE MODEL)

CHAPTER 4

TEED FEEDER PROTECTION SCHEME DESIGN

4.1 SCHEME DESIGN

The relaying scheme which will be used is now fairly common in the literature [2,13]. It consists of a directional relay (DR) blocking scheme with the addition of an independent mode relay (IMR) at each end. The IMR is designed to detect faults close to each relaying location without utilising information from other ends, hence it has a distance relay characteristic and inevitably makes use of the power system impedance between itself and the fault.

In a plain feeder application, the IMR is present solely to increase speed of operation for close–up faults, (and may be omitted if desired). In Teed feeder applications, its main purpose is to ensure that all the circuit breakers are tripped for an internal fault close to any of the busbars. In adverse circumstances such faults may cause fault current to flow out of the Tee preventing operation of the DR scheme.

The communication requirements are much greater for a Teed feeder application since intertrip channels must be provided to ensure that an IMR operation at one end causes trips at the other ends. Power line carrier communication (PLC) channels are adequate for the scheme, since decisions rather than relaying measurand data are to be exchanged. The communication channel delay is composed of two parts:

1) The actual time it takes for a signal to travel from the transmitter to the receiver. (For PLC, fibre optic link or microwave channels, this is small since the signals travel at or approaching the speed of light).

2) The duration of the message which is required for unambiguous interpretation of its meaning. This is a function of the channel bandwidth and the noise or interference which is present.

Wide bandwidth channels attain their greater speed by permitting shorter duration messages and could be used to implement the proposed scheme, but the benefit would probably be insufficient to justify the extra cost. Indeed, if a wide bandwidth channel were

present then current differential schemes (which would utilise it more efficiently) would probably be preferred.

The requirement for intertrip channels in a Teed feeder application does make the scheme less attractive commercially, since each extra PLC channel adds considerably to the scheme cost. However, the overall economics may still be favourable once the alternatives, i.e. extra capital expenditure on substations or transmission lines or a differential scheme using a wide bandwidth communication link, are considered.

In addition to the communication channels, several other scheme components are needed, which are usually considered as part of the relays:

1) Current clipping detector, (which is part of the analogue relay interface).

2) Frequency track unit, (which is necessary to ensure maximum relay sensitivity when the power system is not operating at nominal frequency).

3) Switch onto fault unit, (which detects whether a fault is present on the network when it is energised by closing a circuit breaker).

Designs for the last two units will not be developed in this thesis.

4.2 SCHEME PERFORMANCE

The logic needed to implement a relaying scheme can become quite complicated when several types of relay are used (Fig 4.1). Since the time between fault incidence and directional determination is variable, an allowance for this (and channel delay) has to be included. The various possible scheme operations and timing diagrams for a Teed feeder application are:

1) Remote external fault: Fig 4.2; In this case only the relay nearest to the fault comes to a directional decision, which since it is reverse does not cause a trip.

2) External fault: Fig 4.3; In this case the remote relays come to decisions that a forward fault exists, and would enable their associated IMRs to detect whether it was within their reach. They should not come to such a conclusion and tripping by the DRs should be prevented by the relay nearest to the fault detecting it as reverse.

3) External fault: Fig 4.4; This is much the same as the previous case except

the fault is seen as reverse by two DRs.

4) Internal fault: Fig 4.5; In this case fault current flows into the Tee at each end; each DR detects it as forward and hence after a co-ordination time trips its local circuit breaker. An IMR may also produce a trip signal if the fault is close enough to a busbar.

5) Internal fault: Fig 4.6; In this case the fault current flowing into one of the Teed feeders is insufficient to allow the relay measuring it to reach a directional decision. Though the DRs at the other locations will cause local trips, the circuit breaker at the low current location would have to be intertripped, unless sequential tripping (in response the DR responding to the signals produced by the other circuit breakers opening) was desired, (which is unlikely). A similar situation would exist if one of the circuit breakers was open before the fault, (except that there would then be no need to trip it).

6) Internal fault: Fig 4.7; In this case fault current flows out of the Tee at one busbar, hence the DRs are prevented from causing trips but the DR nearest the fault will have detected the fault as forward and have enabled the associated IMR. The fault will only be cleared if it is within the reach of the IMR.

The return of the scheme to 'normal' measurement is not shown but will be discussed in later sections.

4.3 RELAYING REQUIREMENTS

The scheme requirements may be loosely specified:

1) To enable faults to be cleared within one power frequency cycle over as much of the protected network as possible. This requires that the relay operating time be less than about 7ms [14].

2) To be able to protect as many Teed feeder configurations as possible. The application limits are ultimately determined by relay sensitivity. Superimposed component extraction allows a relay to have a much higher theoretical sensitivity than would otherwise be possible. However, immediately previous disturbances reduce a relay's ability to detect faults, i.e. the usable sensitivity.

3) To maximise fault resistance coverage.

4) To ensure that false trips do not occur.

a) Incorrect operation of the directional scheme may occur if an external fault is seen as forward by a remote relay, but the nearest relay does not reach a (reverse) directional decision. To prevent this happening the forward sensitivity of a relay is deliberately made less than its reverse sensitivity, but problems arise when the different usable sensitivities exist at the relaying locations. A solution can be obtained in plain feeder applications since the superimposed current should be the same at both ends for external faults. In Teed feeder applications this is not the case, and the implications are investigated in the next sections.

b) Incorrect interpretation of the relaying measurands causing a false IMR trip can arise in the following ways:

i) The power frequency components of the relaying measurands resulting from an external fault may correspond to an impedance which lies inside the protection area defined in the complex impedance plane. Solutions are to reduce the area or change the shape of the protection characteristic, but have the disadvantage of reducing the reach or fault resistance coverage of the IMR.

ii) The transient corruptions of the power frequency waveforms may cause errors in the impedance estimate. The solution is to increase the effectiveness of the relay filtering, but this is in conflict with requirements (1) and (2).

4.4 SEQUENTIAL DISTURBANCES

Although disturbances in rapid succession are not going to be studied, it is important to decide how the scheme would react to them. There are three areas of concern:

1) Effects due to scheme logic. If an external fault occurs immediately after an internal fault, then it is theoretically possible (assuming that the DRs have zero dead time following a directional decision) for the block resulting from the second disturbance to inhibit tripping.

2) Effects on the IMR.

3) Effects on the DR.

The last two topics are discussed in the following sections.

4.4.1 EFFECTS ON SCHEME LOGIC

Conventional distance relays either measure continuously or in a series of contiguous measurement periods. Under these circumstances, inclusion of the fault incidence transient (and some pre–fault information) is unavoidable and the design should accommodate this. However, when the time of fault is known, it is possible to exclude these undesirable parts of the waveform from the measurement algorithm, and obtain improved performance (under normal conditions), but a susceptibility to error when sequential disturbances occur.

In general an IMR algorithm using superimposed components could be greatly affected by a previous disturbance in either direction, whereas the effects on an total quantity algorithm would be less pronounced (due to the shorter impulse response of its filtering). Several courses of action are available depending on the magnitude and direction of the second disturbance:

1) If the second disturbance is not large enough to cause a second directional decision then no action can be taken. The algorithm must be designed to behave correctly for both forward and reverse faults occurring after measurement has commenced. This may imply a measure of directionality in the protection characteristic.

2) If the second disturbance is large enough to cause a second directional decision, then the first measurement must be terminated and a new one started (if the second disturbance was detected as forward).

4.4.2 EFFECTS ON THE DR

The principle of directional relaying (as discussed in the next Chapter) is comparison of superimposed component levels with thresholds. Even if the change in power system conditions produced by a fault could be represented by a step change in a power frequency sinusoid, the filters used to derive the superimposed components have non–negligible impulse response duration and, following a disturbance, the signals would be above the normal thresholds for at least that duration.

In practice, the situation is more complicated, with transient and sub–transient decays, power swings and excitation system transients existing in the post–fault waveforms. In addition, a fault on a power system is usually followed by other disturbances, i.e. circuit breaker trips and re–closures, which would extend the period before normal conditions are restored. Two design approaches are possible:

1) To adjust the thresholds according to background or past levels of superimposed components.

2) To use fixed thresholds, but disable operation for a certain time after a directional decision has been reached.

Fixed thresholds are simpler to implement, (though the choice of values may require data from field monitoring of actual transmission line waveforms), but suffer from the disadvantage that it is difficult to predict when the output from the relay superimposed extraction filter would have decayed to normal levels following a disturbance.

If fixed thresholds were used and the relay permitted to commence measurement while the signals were above the threshold levels, then there would be a risk of multiple decisions from the same disturbance. Therefore, after a disturbance, measurement must be suspended either:

1) For a fixed time, (which is problematic to specify), or

2) Until the signals have fallen below the threshold levels, which requires as much processing to implement as a variable threshold algorithm), and introduces the problem of how to ensure that all the relays begin measuring simultaneously (since different superimposed component levels will exist at each relaying location).

4.5 RELAY DIRECTIONAL SENSITIVITY RATIOS

As mentioned in the section on relaying requirements, the forward sensitivity of a DR will need to be made less than the reverse sensitivity, and since forward sensitivity ultimately limits the variety of configurations which may be protected, it is important that the constraints requiring relative sensitivities be examined.

For simplicity it may be assumed that the magnitudes of the superimposed voltages and currents at a relaying location will determine whether the DR reaches a directional decision. However, the superimposed extraction filter will produce an output for phase, frequency or amplitude modulations of the relaying signals. Some of these will actually be due to faults, but others may be the result of system switching operations or load fluctuations.

It will further be assumed that the relay thresholds will be automatically raised above the background superimposed component levels to allow detection of faults whenever possible. The superimposed voltage and current magnitudes at different relaying locations naturally do not bear the same ratio, and hence they should be assigned different forward/reverse sensitivity ratios, according to the application.

The most onerous cases are when disturbances occur in rapid succession, i.e. separated by less than the duration of the superimposed extraction filter impulse response. Such circumstances are not unlikely when system switching operations are considered, and it is essential that the scheme does not trip when presented with such a series of external disturbances. The following sections show the extreme values of sensitivity ratio which may have to be imposed to prevent this happening.

4.5.1 RATIOS NEEDED FOR PLAIN FEEDER APPLICATION

In this application, the superimposed current measured at each relay location should be the same for an external fault, and any forward/reverse current sensitivity less than unity should suffice. The superimposed voltage seen by the relay closest to the external fault will be greater than that at the other relaying location, and therefore there is no need to impose a sensitivity ratio. If sequential disturbances occur, then both relays will be desensitised, but it is no more likely that the forward looking relay detect the fault and the reverse relay not.

4.5.2 RATIOS NEEDED FOR TEED FEEDER APPLICATION

When feedround paths are absent, although equality of superimposed current at each relaying location cannot be guaranteed for an external disturbance, the largest superim-

posed current will be experienced by the (only) DR for which the disturbance is in the reverse direction. However, situations may be postulated where this favourable circumstance is overwhelmed by the effects of a previous disturbance, e.g. Fig 4.8.

The first disturbance behind busbar P produces superimposed relay currents in the ratios (P:Q:R): (–3.5:1:2.5). A second disturbance behind busbar R would produce superimposed currents in the ratio: (1:2:–3), requiring a forward to reverse sensitivity ratio of less than (2.5/3) to ensure that the second disturbance was identified as external by the scheme logic.

When feedrounds are present, far more extreme superimposed current distributions are possible. For faults on an external feedround, (e.g. Fig 4.9), fault current is fed out of the Tee through two busbars, giving superimposed current ratios at the relaying locations: (P:Q:R): (–1:–1:2). However, the effects of previous disturbances may compound the problem, e.g. a disturbance at busbar P produces superimposed relaying currents in the approximate ratio: (–11:9:2). Correct scheme logic operation therefore requires a forward to reverse sensitivity ratio of less than (1/9), which much reduces the ability of the DRs to detect internal faults.

The situation becomes much worse as the dissimilarity in the busbar source capacities and in the lengths of the feeders comprising the Tee is increased. Partial compensation for this can be obtained by making the forward current sensitivity a function of past values of superimposed voltage (in addition to past values of superimposed current) rather than a straight fraction of the reverse current sensitivity. In this way, DRs associated with low capacity local sources would suffer greater desensitisation while the effects of previous disturbances were present. This idea will be developed in the next Chapter.

4.6 FORWARD FAULT DETECTION REQUIREMENTS

4.6.1 PLAIN FEEDER APPLICATIONS

In these applications the following factors ease the implementation of a combined DR/IMR scheme:

1) The IMR function is non–critical, serving only to enhance performance.

2) The forward to reverse sensitivity ratio required is not extreme.

3) Identical relay setting may be used at each end. The reach setting of the IMR will obviously be as large as possible while ensuring that no trips can occur for faults past the remote busbar, (which will mainly be determined the the relay design).

4.6.2 TEED FEEDER APPLICATIONS

When feedrounds are present, none of the beneficial factors listed in the previous section apply. In particular, although the DR sensitivity at each end must be nominally equal, the reach of each IMR may only approach a fraction of the length of the feeder it protects. (Any attempt to set the reach past the Tee point could result in large reach errors due to current infeed into fault resistance.) However, the presence of intertrip channels will allow the (plain feeder) requirement that each DR detect an internal fault to be relaxed, (with the penalty of delayed tripping at the end(s) which didn't detect the internal fault).

The purpose of the IMR is to ensure that trips occur for configurations such as Fig 4.7, in which a sufficiently large fault current flows out of the Tee to cause the DR at R to reach a reverse directional decision. For the IMR at P to trip the circuit breakers, the following sequence must occur:

1) The DR at P must reach a forward directional decision (and enable its associated IMR). This is less likely if a low forward to reverse sensitivity ratio has had to be used.

2) The relaying measurands must correspond to an impedance within the IMR protected zone.

3) The IMR at P must be sensitive enough to interpret the measurands correctly. This task is made more difficult when the source capacity at Q is high and those at P,R are low.

The worst case occurs when the source capacities at P,R are zero: the DRs at those locations therefore see the same fault current, the magnitude of which decreases as the fault approaches the Tee point. Hence there is likely to be a range of fault positions for which

reverse directional decisions are produced by the DR at R, but no (forward) decision is reached by the DR at P (due to imposed sensitivity ratio).

If desired, the IMR could be enabled under such circumstances by making each DR produce two outputs for forward disturbances:

1) A decision using reduced forward sensitivity (for use in the directional part of the scheme).

2) A decision using maximum permissible (i.e. equal to reverse) sensitivity to enable the IMR.

In addition to the extra complexity, it is unlikely that a complete solution would be obtained due to the IMR almost certainly having a lower sensitivity than the DR, and the difficulty of protecting the region around the Tee point.

It must therefore be conceded that maloperations may occur under extreme operational conditions on some configurations and studies are needed to identify whether these constitute an unacceptable risk.

Fig 4.1 RELAY/SCHEME LOGIC BLOCK DIAGRAM

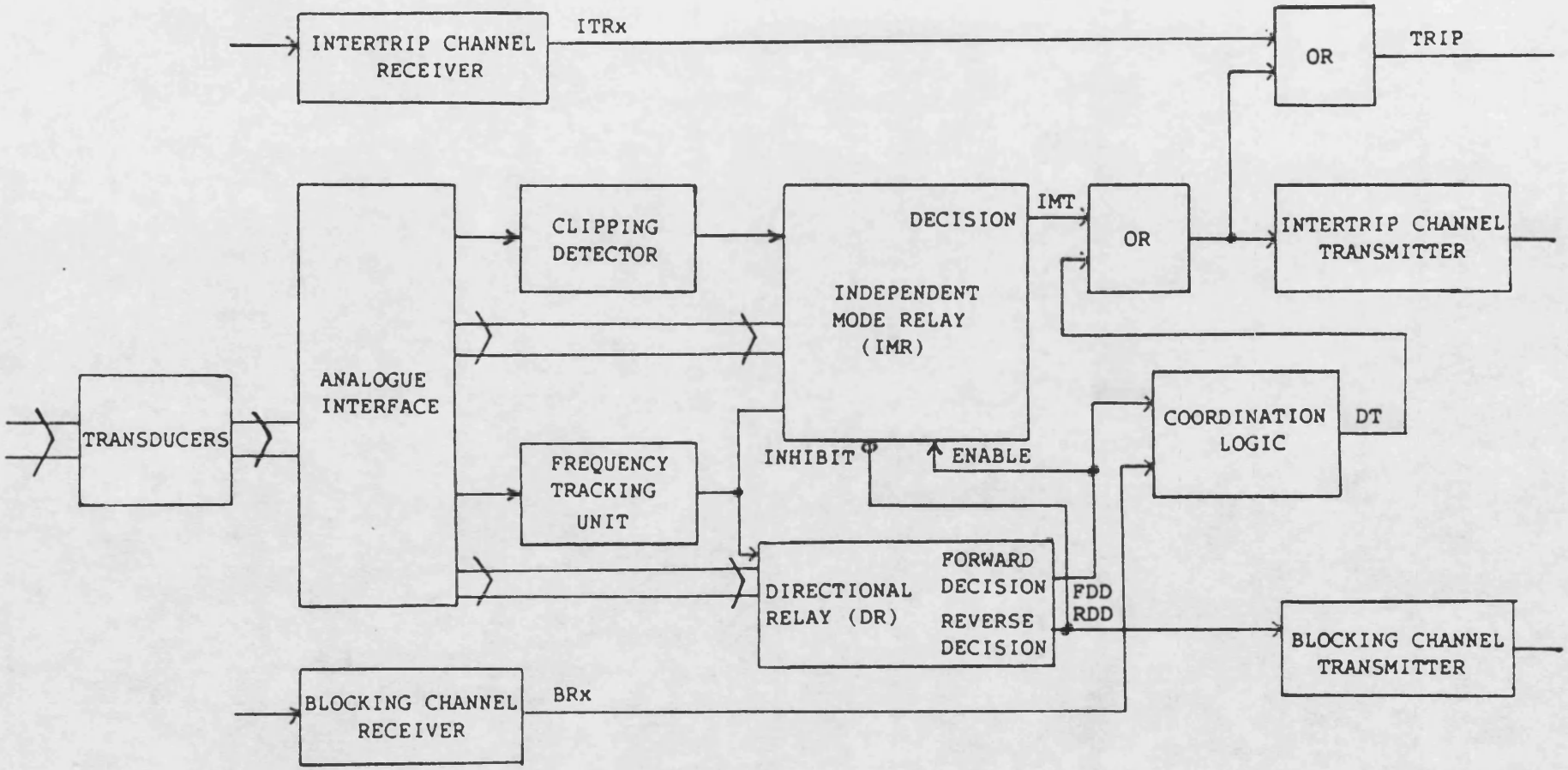

SCHEME LOGIC OPERATION

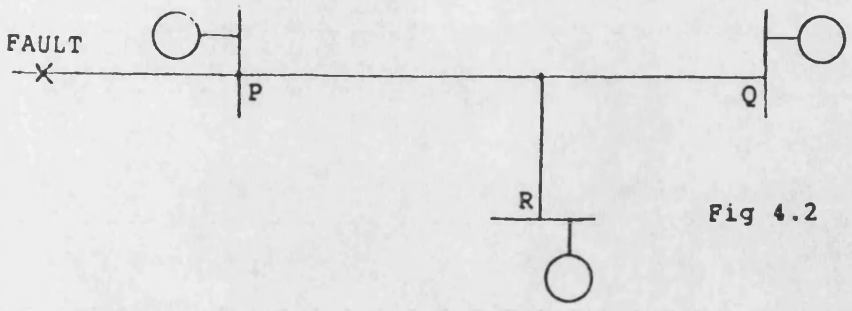

Fig 4.2

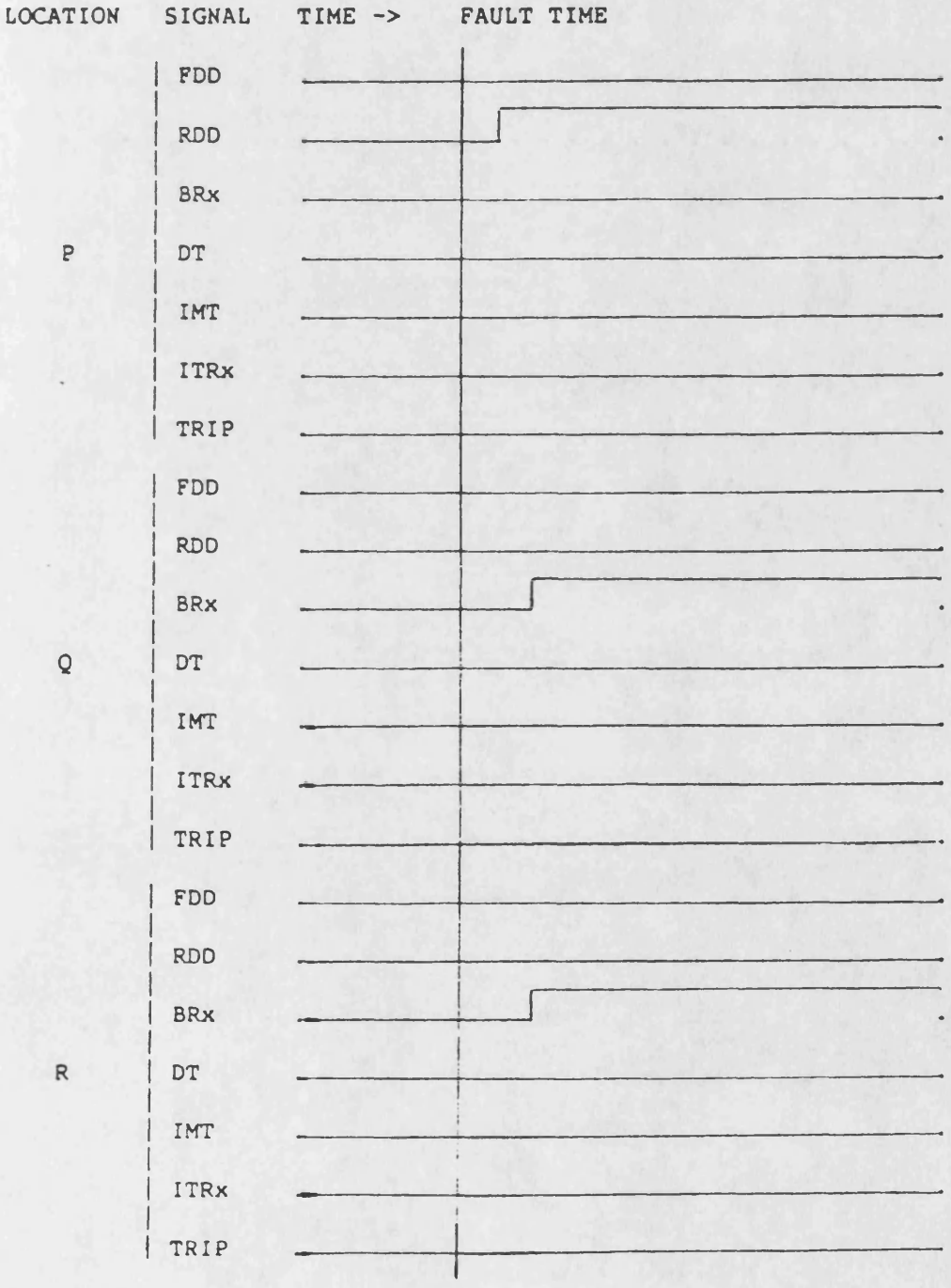

SCHEME LOGIC OPERATION

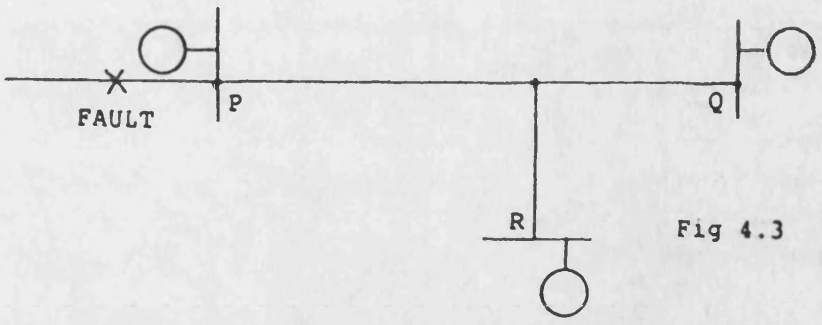

Fig 4.3

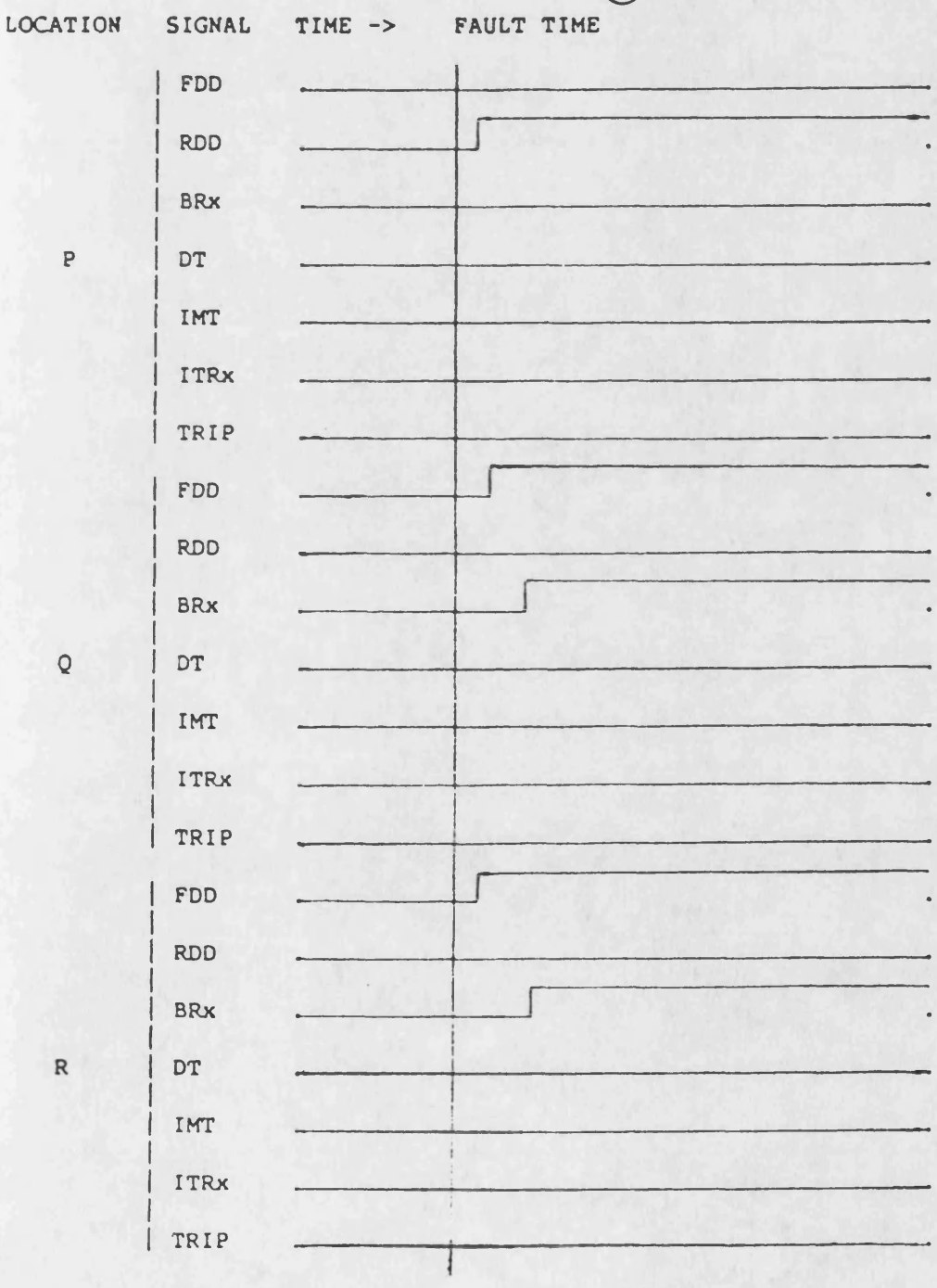

SCHEME LOGIC OPERATION

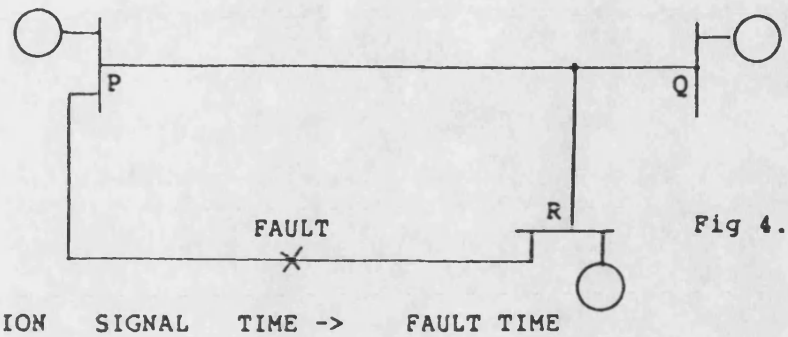

Fig 4.4

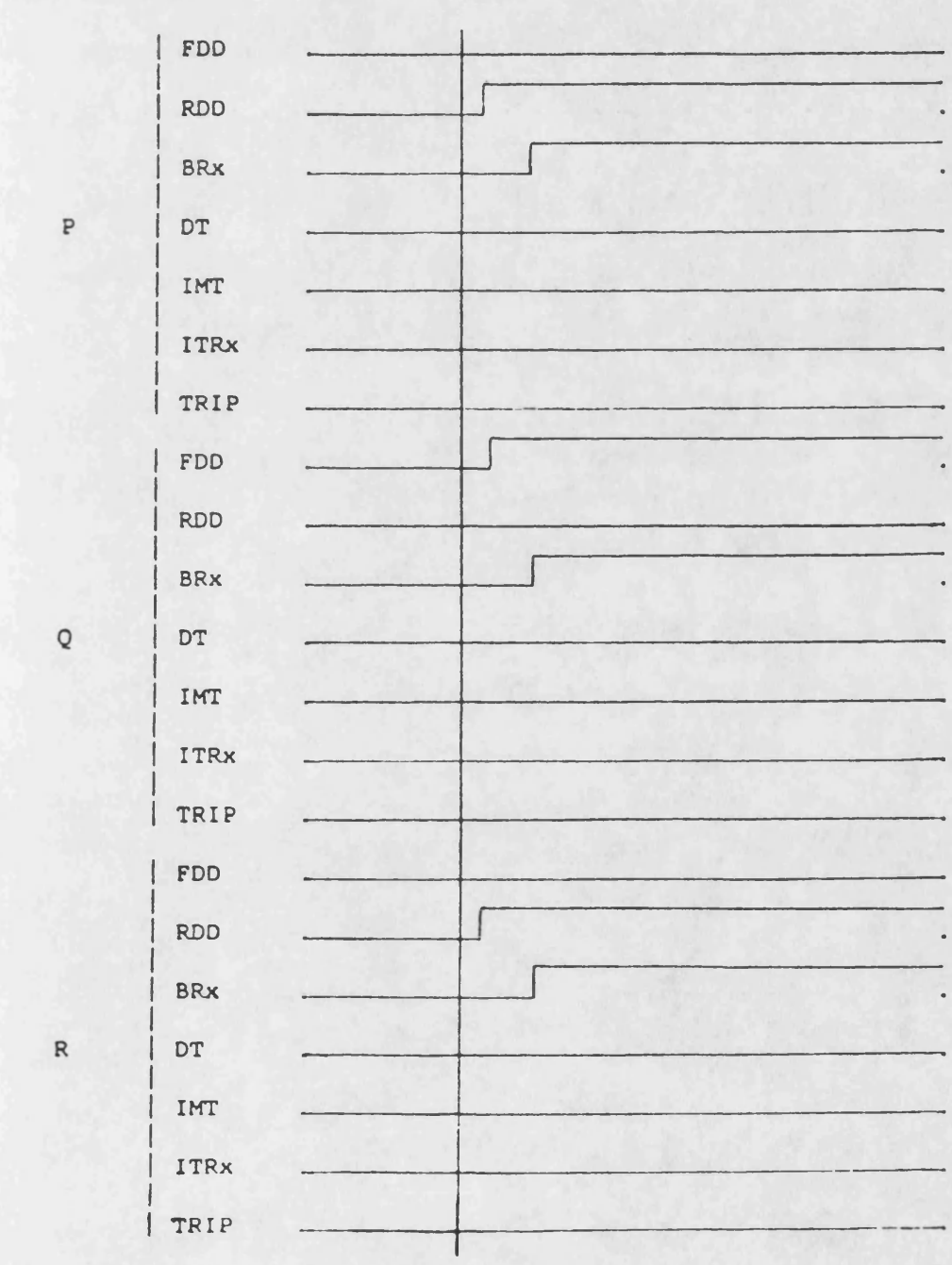

SCHEME LOGIC OPERATION

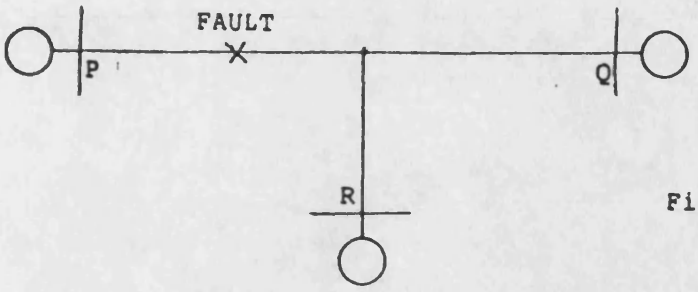

Fig 4.5

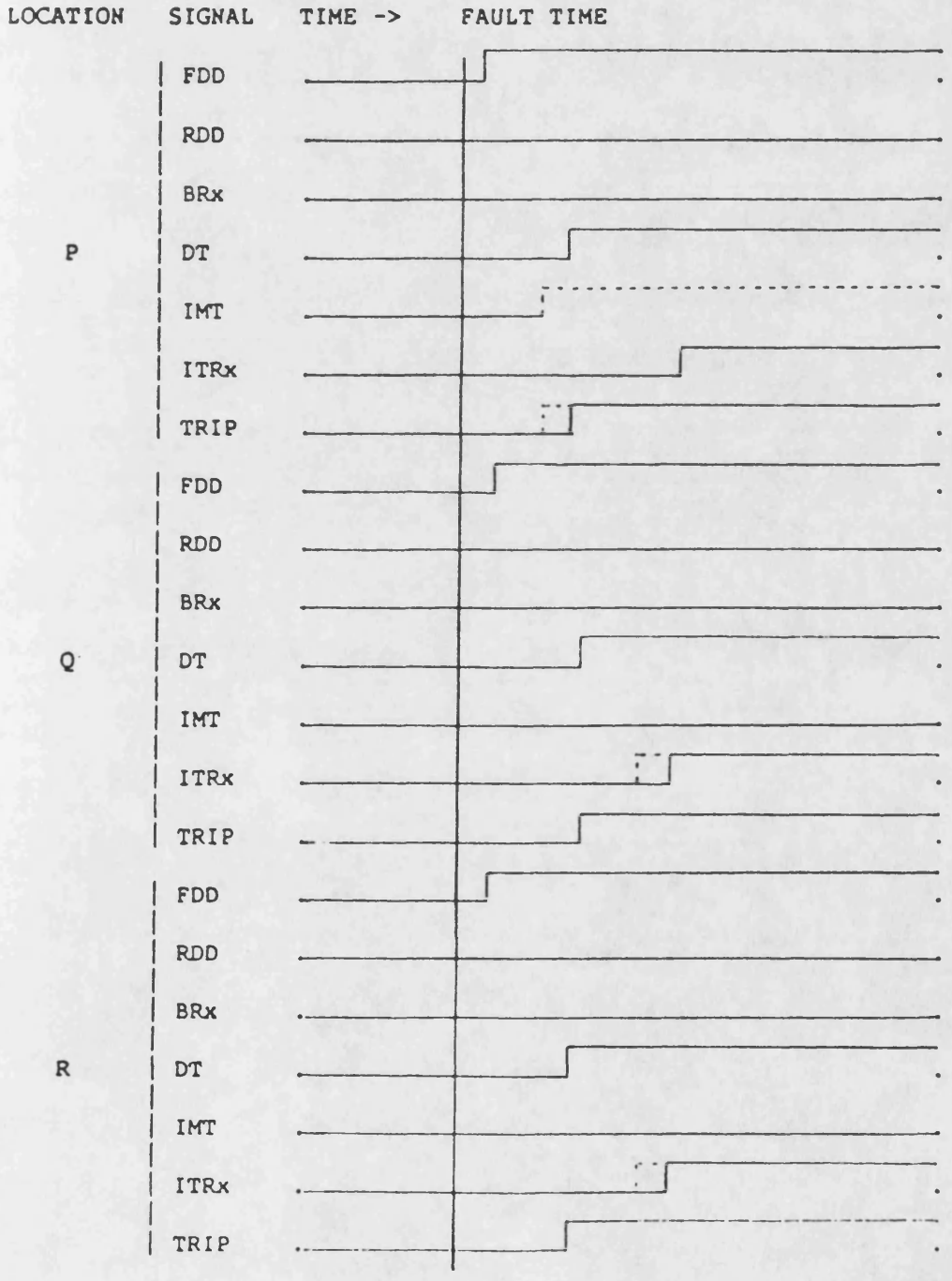

SCHEME LOGIC OPERATION

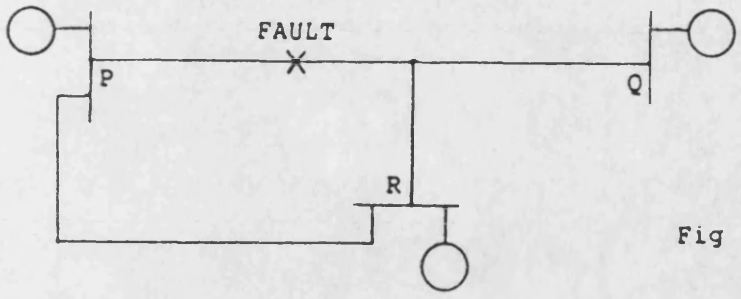

Fig 4.6

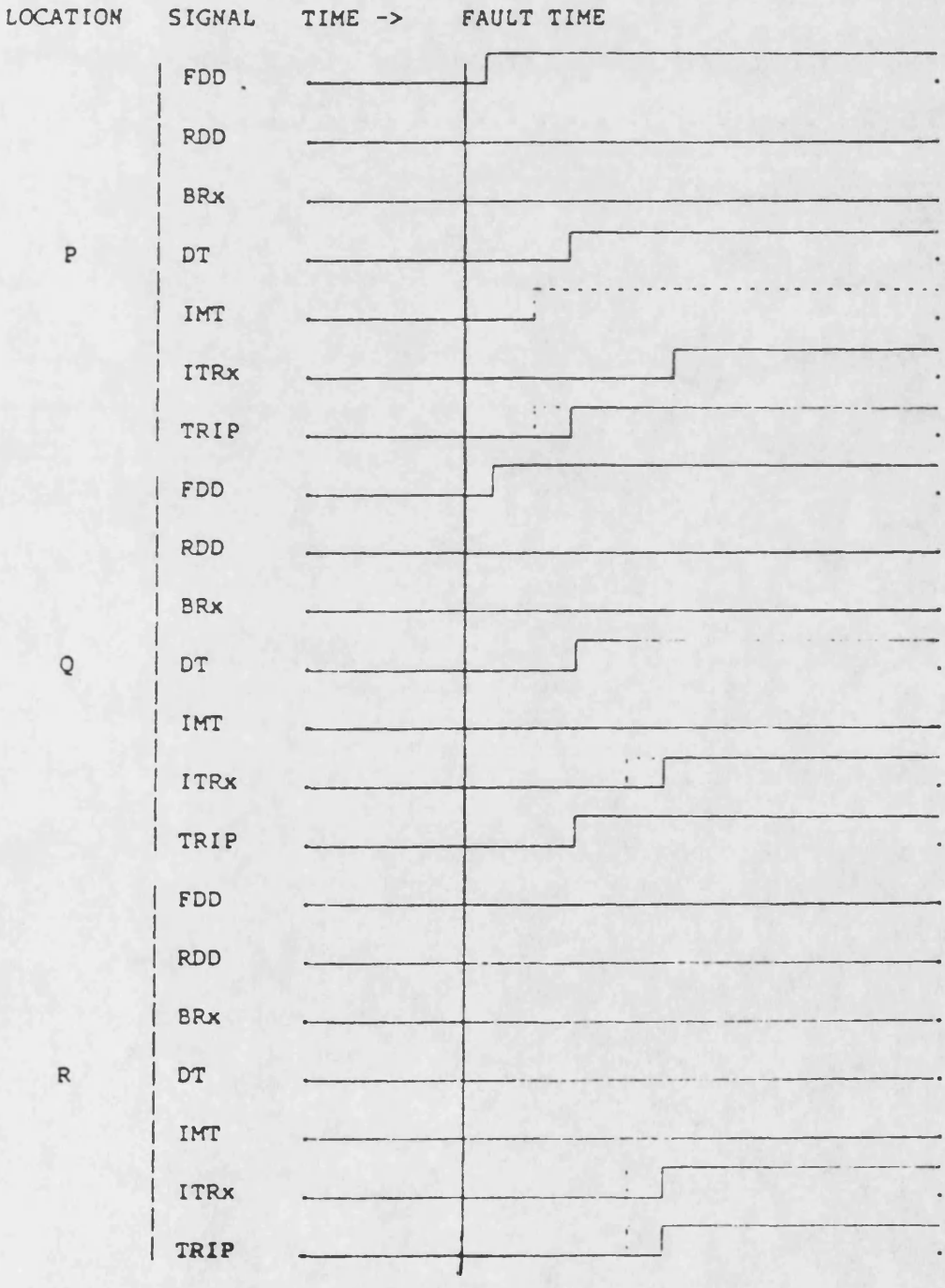

SCHEME LOGIC OPERATION

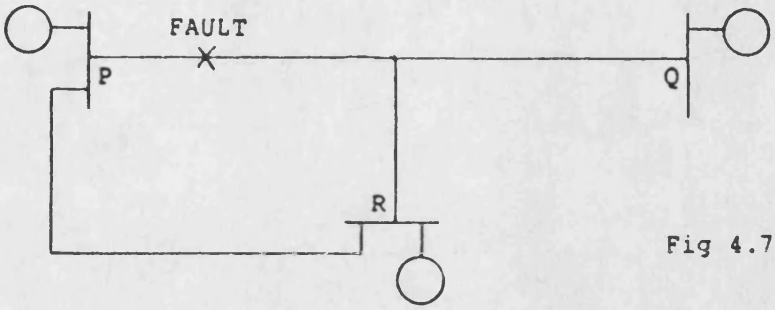

Fig 4.7

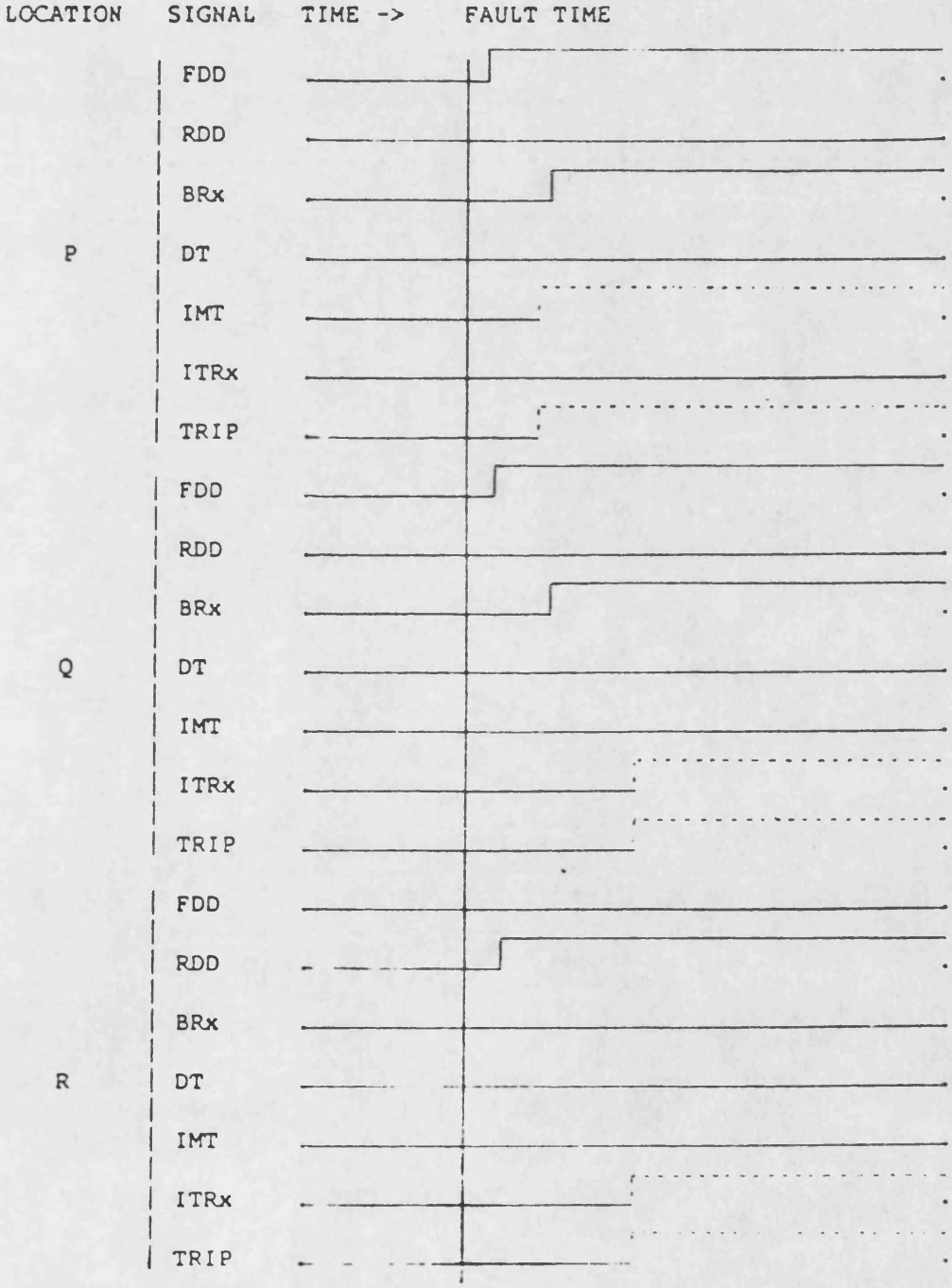

PROBLEMATIC TEED FEEDER CONFIGURATIONS

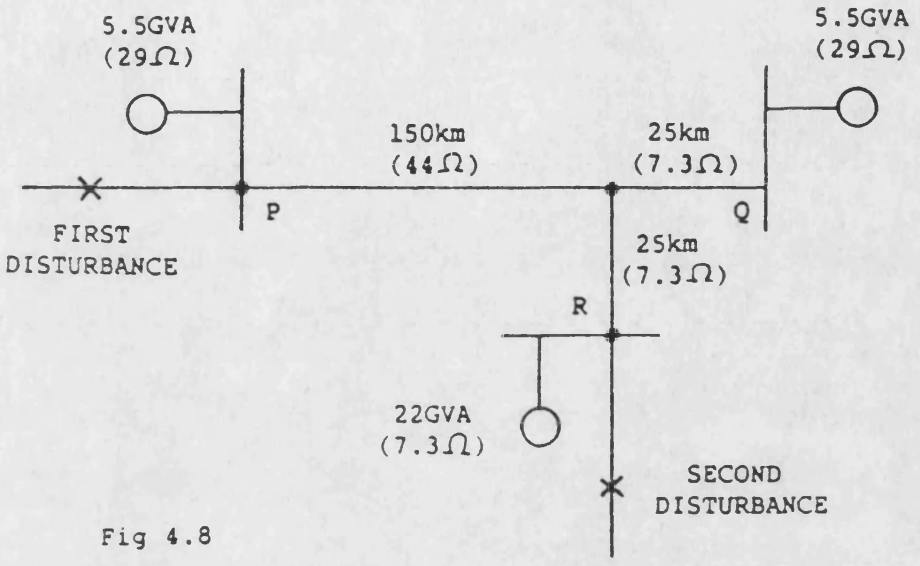

Fig 4.8

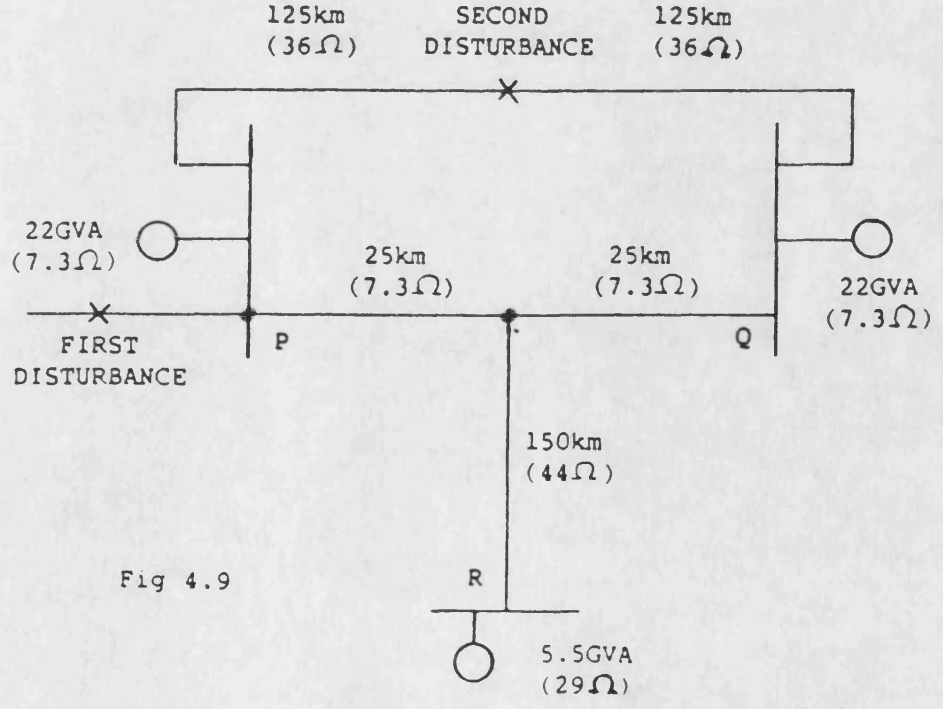

Fig 4.9

CHAPTER 5

RELAY DESIGN

5.1 DESIGN AIMS

The main aim of this project is to design an independent mode relay (IMR) to work in conjunction with a directional relay (DR).

An IMR, by definition, uses only measurands available at one relaying location and the design principle inevitably utilises the power frequency impedance between the relay location and fault point. Impedance measuring techniques have been exhaustively explored in connexion with distance relay design, and it may seem unlikely that anything new can be added. However, several features of a joint DR and IMR scheme may be exploited:

1) The IMR protection characteristic (described by an area in the complex impedance plane) need not discriminate between forward and reverse faults, since the relay will be enabled only for forward faults.

2) The start of measurement of an IMR can be triggered by the DR and the exclusion of pre–fault information guaranteed.

3) Some of the signals used in the DR and IMR may be identical or share a large part of their processing, allowing economies to be made in the processor workload.

4) An IMR (with different settings) could perhaps be used as a switch onto fault detector, which is an essential part of a relaying scheme. There would be an obvious saving in hardware.

5) Algorithms using superimposed components only would be immune from false trips caused by power swings and could, if desired, operate with the steady state load plus line impedance overlapping the protection characteristic in the complex impedance plane.

There is also work which needs to be done on DR design, in particular:

1) The co-ordination between relay sensitivities in the presence of power system disturbances needs to be considered. There are several aspects to this:

a) The filtering used to reject high and low frequency corruptions has an ef-

fect on the duration of superimposed components from previous disturbances.

b) The usable sensitivity must be identified as a function of the past and present superimposed components in the relay. It may then be possible to estimate the minimum usable sensitivity of other relays in the scheme and prevent false trips due to the effects of unequal fault current distribution between the relay locations.

2) The choice of relaying signals and the filtering used in DRs in the literature do not explicitly emphasise the importance of the frequencies close to power frequency. It is probable that variations in relay performance due to fault point on wave or type could be reduced once this is done.

3) Source dynamics need to be included in simulations to allow the behaviour of directional relays after (external) faults to be investigated.

5.2 SIGNAL CORRUPTIONS

Signal processing may be used to attenuate unwanted components in the measurands, which may be categorized as:

1) High frequency transients: travelling waves on the voltage and also on the current waveforms, (particularly if a mimic impedance has been used in the CT secondary). These have to be attenuated by low pass filtering, which generates exponentially decaying transients on the output for changes in input signal conditions.

2) Low frequency transients.

a) The CVT transient is proportional to the amplitude of the superimposed voltage and greatest for voltage minimum faults [68], when it may form the largest part of the voltage signal, and require an extra stage of filtering (with a zero at zero frequency).

b) Power system transients: A voltage transient is unlikely since high voltage power systems are usually homogeneous (i.e. the physical components have similar X/R ratios). However, even where this is not the case (e.g. when resistive grounding of transformers is used), the remedies necessary to cope with the CVT transient problems should deal with the similar effects.

3) CT saturation: This is a non–linearity which can seriously degrade relay performance, and its effects cannot be removed by linear signal processing. Special pre-

cautions have therefore to be taken:

a) Usually the CT ratios and dimensions will be such that saturation after a forward directional decision implies a fault within the protected zone. Limiting will be applied first in the analogue stages of the relay, hence an analogue saturation detector may be included in the scheme.

b) To attempt to make the relays operate before saturation occurs: It should certainly be possible for the local DR to reach a forward directional decision within the available time, but it may be more difficult for the IMR to reach a trip decision.

c) To ensure that IMRs operate correctly (or under–reach) when presented with clipped current signals.

d) To ensure that maloperation of the scheme does not occur when the relay(s) are recovering from the effects of clipped current signals.

The current transient and CT transient are serious problems and must be attenuated by high pass filtering or the use of a CT burden which mimics the X/R ratio of the local source. Mis–matches between these ratios and that of the transmission line are inevitable: the effects of the resulting transients will be investigated in the simulations.

5.3 COMPARISON OF ANALOGUE AND DIGITAL IMPLEMENTATIONS

The relays will be implemented using digitised signals and digital signal processing for the following reasons:

1) A large dynamic range is required to perform amplitude or magnitude comparisons between power system signals, and this is difficult to achieve using analogue electronics (due to noise and distortion).

2) Analogue noise pick–up should only occur before the analogue to digital converter stage. Once the signals have been digitised, algorithm behaviour may be accurately simulated using the same precision arithmetic as the target microprocessor.

3) The signal processing and filtering may be specified in software, which guarantees that the parameters will remain stable and reduces the amount of setting up needed on the actual hardware.

4) Some of the filter functions required do not have acceptable analogue

equivalents, e.g. delays are difficult to achieve.

5) Greater flexibility is possible in decision process and logic design.

On a 16 bit processor, if an attempt is made to generate integers outside the range –33768 to 33767, then an arithmetic overflow will occur causing the wrong answer to be produced. The problem usually occurs in the intermediate stages of a filter and the error may be disguised by subsequent stages. Computer simulations may not indicate when this has happened, and the subsequent behaviour of the mainframe computer may be different to that of a hardware implementation.

The signal scaling should allow as much of the integer range of the processor as possible to be used to reduce the significance of offsets introduced by the filtering. The use of higher precision (32 bit) arithmetic should be avoided if possible as it is significantly slower.

5.4 SAMPLING RATE

The rate at which each analogue variable is sampled, digitised and processed is one of the most critical parameters in a digital relay design. If it is too low, then the process delay, i.e. the period between samples, may become a significant proportion of the desired operating time and force undesirable compromises in algorithm design. For this reason, the minimum sampling rate is probably 1 kHz. giving a process delay of 1 ms. The maximum sampling rate is determined by:

1) The bandwidth of the digital filters in the algorithm.

2) The accuracy with which the sampled output is required to represent the continuous input.

3) The amount of time needed by the microprocessor to execute the relay algorithm. As the sampling rate is increased, the time available for this task decreases, resulting in either:

a) The need to increase processing power, i.e. more or faster microprocessors, which is expensive.

b) Pressure to simplify the algorithm (which must eventually be resisted).

The filter bandwidth is unlikely to be greater than 300 Hz., (which corresponds to the dominant travelling wave frequency on a 250 km. transmission line), hence a frequency much above ten times this value would seem excessive.

The sampling frequency is therefore chosen to be 2 kHz. Once this rate is specified, the anti–aliassing analogue pre–filter can be designed. The cut–off frequency can be chosen anywhere between say 300Hz. and half the sampling rate. Though the choice is unlikely to be critical, certain guide-lines may be suggested:

1) If only superimposed components are to be extracted from the signal, then the frequency should be as low as possible and replace part of the low pass filtering which would otherwise have to be implemented digitally. This course will also reduce digitisation noise.

2) If total quantities are to be derived, then a low cut off frequency may cause pre–fault information to persist longer in the post fault signals (due to the longer duration of the filter impulse response). Hence starting to measure (and filter digitally) only once the fault has been detected gives better results if the maximum permissible pre–filter cut off frequency is used.

A technique which offers many of the advantages of sampling at 4 kHz., i.e. simpler anti–aliassing filter design and better rejection of travelling wave frequencies close to 4 kHz, is to digitise analogue signals at a 4 kHz rate, then average consecutive samples and perform the rest of the processing at a sampling frequency of 2 kHz.

5.5 FREQUENCY TRACKING

The performance of the frequency tracking unit will determine, to some extent, the amount of superimposed component extraction filtering that is necessary in a DR. Certain difficulties are likely to present themselves in connexion with this device:

1) The choice of measurands (from which the frequency is to be determined) is difficult in three phase systems.

2) The step change in phase angle of the measurands which may accompany fault incidence may cause the algorithm to produce an erroneous pulse in the measured

frequency signal.

3) Long time constants are necessary to produce low steady state frequency errors, but they also give large transient errors when the frequency is changing quickly, e.g. in power swings.

It is most important than the rate of change of measured frequency output from the unit is kept low and does not initiate directional decisions. Hence a relatively large transient frequency error is possible and the filtering and the decision process in the relay should be designed to cope with it.

5.6 FILTERING

5.6.1 GROUP DELAY

The group delay T is a measure of the delay introduced by a filter. It is defined by analogy with a unity gain constant delay stage, which has the following transfer function $G(\omega)$ and phase function $\Theta(\omega)$:

$$G(\omega) = \exp(-j\omega T) \qquad \Theta(\omega) = -\omega T \qquad T = -\frac{d\Theta(\omega)}{d\omega}$$

The phase and delay functions are more complicated functions of angular frequency in actual filters, and it is only correct to define a group delay at a certain frequency if the transfer function is constant around that frequency. This condition is met for low pass filters below their cut–off frequency.

5.6.2 SUPERIMPOSED EXTRACTION FILTERS

Digital superimposed component extraction filters achieve a sharp notch in the frequency response by adding or subtracting delayed versions of the input signal. If k is the current sample, $x(k)$, $y(k)$ are the input and output, and n is the number of samples per millisecond, i.e. $n = 2$ for 2 kHz sampling, $n = 4$ for 4 kHz sampling, then the simplest filter implementations are:

1) Half cycle extraction.

$$y(k) = x(k) + x(k - 10n)$$

If a power frequency sinusoid (Fig 5.1a) is suddenly applied to such an extraction filter,

then the output produced is drawn in Fig 5.1b. The output is equal to the theoretical superimposed component for 10 ms., after which it is zero. This should be long enough for a DR to operate, but might restrict IMR performance towards the reach boundary. However, the major disadvantage of the filter is that the frequency response peaks at zero frequency and even power frequency harmonics, which prevents its use unless it is cascaded having a filter having zeros at these locations.

2) Full cycle extraction.

$$y(k) = x(k) + x(k - 20n)$$

This has an ideal frequency response with zeros at zero frequency, power frequency and all harmonics. The response to an applied power frequency sinusoid lasts for 20 ms. and is drawn in Fig 5.1c.

It has been assumed that the sampling frequency is an integer multiple of power frequency, making the notch of the extraction filter coincide exactly with the steady state pre–fault frequency, but this may not be achieved during power swings (for reasons discussed in Section 5.5). It is therefore desirable that the filter output is minimised for small deviations of system frequency. This may be achieved by cascading stages of superimposed component extraction filtering as described by Barker [23].

The output resulting from a discrepancy between the notch angular frequency $W_0+\Delta$ and power frequency W_0 is easily found for the full cycle extraction filter with a power frequency cosinusoidal input:

$$x(k) = \cos\left(\frac{kW_0}{1000n}\right) \qquad y(k) \approx \frac{2\pi\Delta}{W_0 + \Delta}\sin\left(\frac{kW_0}{1000n}\right) \approx 0.02\Delta$$

This is too large to ignore. However, two stages of extraction can be cascaded to reduce the steady state error. The combination of half and full cycle extraction filters gives:

$$y(k) = x(k) + x(k - 10n) - x(k - 20n) - x(k - 30n)$$

$$\approx -\frac{1}{2}\left(\frac{2\pi\Delta}{W_0 + \Delta}\right)^2 \cos\left(\frac{kW_0}{1000n}\right)$$

This has the disadvantage that the response to an applied power frequency sinusoid (Fig 5.2b) is more complicated than that of a single stage filter and makes the post–fault assessment of the usable sensitivity more difficult. A different compromise cascades two stages of full cycle extraction:

$$y(k) = x(k) - 2x(k-20n) + x(k-40n)$$

$$\approx -\left(\frac{2\pi\Delta}{W_0+\Delta}\right)^2 \cos\left(\frac{kW_0}{1000n}\right)$$

The response to the application of a power frequency sinusoid is drawn in Fig 5.2c, and shows that although the response has a longer duration, it is better behaved than in the previous example. On the other hand, the output for a steady state frequency deviation is twice the previous value.

It is possible to slightly stagger the notches of the cascaded filters to broaden the notch, but this cannot give acceptable performance for really severe steady state frequency deviations. The expedient of further increasing the number of stages of superimposed extraction will reduce the steady state output, but at the price of a long duration badly behaved impulse response.

5.6.3 LOW PASS FILTERING

There are two main types of low pass filter which may be implemented on a microprocessor:

1) Running average (finite impulse response).

2) Recursive (infinite impulse response).

The power frequency parameters and (z domain) frequency response formulae are given in Appendix 7. The choice between them depends partly on the suitability of the frequency (and impulse) response and partly on the efficiency of the filter algorithm, since the available time window (and hence number of microprocessor operations) will inevitably be limited.

5.6.3.1 RUNNING AVERAGE FILTER

A running average filter requires m memory locations containing the present sample and $m-1$ past samples. The output is the sum of these, usually scaled by a factor $1/m$. Division and multiplication in microprocessors is very time consuming, unless m is chosen to equal an integer power of 2, when scaling may be accomplished by merely shifting the binary number a number of places to the right in the accumulator, Other choices for m usually mean that the stage gain cannot be made unity and require the signal to be attenuated before processing, (which is undesirable).

$$y(k) = \frac{1}{m}\sum_{i=0}^{m-1} x(k-i) = y(k-1) + \frac{x(k) - x(k-m)}{m}$$

The filter frequency response for $m=8$ at 2 kHz sampling rate is drawn in Fig 5.3. This filter has no precise analogy in analogue electronics, but its its properties are essentially characterised by the zeros in the numerator of the transfer function expression, i.e. for 2 kHz sampling there are zeros at $2000/m$ Hz and its harmonics.

5.6.3.2 RECURSIVE FILTER

The recursive filter is an analogy of a single pole analogue filter, and may be implemented using the following algorithm:

$$y(k) == y(k-1) + \frac{x(k) - y(k-1)}{m}$$

The constant m is usually chosen to equal an integer power of 2 (for efficient microprocessor implementation), though this does restrict the values of corner frequency which may be used. The filter frequency response for $m=4$ at 2 kHz sampling rate is drawn in Fig 5.4.

5.6.3.3 COMPARISON OF FILTER IMPLEMENTATIONS

The frequency responses of a running average filter $m=8$ and a recursive filter $m=4$ show a very similar frequency response, but the former has a higher power frequency gain and greater high frequency attenuation. On the other hand it is more laborious to implement and has a higher group delay. If two running average filters are to be cascaded then it is

desirable to make their zeros interleave rather than coincide, i.e. a cascaded filter in which m takes values *7,9* will in general perform better than one in which m takes values *8,8*. The reduction in usable dynamic range is negligible in this case.

In a microprocessor implementation, the requirement for storing $m-1$ previous samples may be satisfied by allocating 256 memory locations and addressing them by the 8 lower bits of a 16 bit binary number. In this way the memory address is incremented for each new sample, but returns to the first location for the 257th, 513th, etc. allowing the filter algorithm to run continuously. Despite the elegance of this technique, these manipulations are often awkward to implement on conventional microprocessors, e.g. 68000. The filter does have the advantage of a finite impulse response: there being no contribution from events not represented in the m memory locations.

If a recursive filter is used immediately after the waveforms have been digitised, then it is quite possible for the output to be near the positive limit and the input to suddenly switch to the negative limit (e.g. due to travelling waves). The difference would then exceed the allowable range even though the difference divided by m did not. The solution is obviously to rewrite the equation:

$$y(k) = y(k-1) + \frac{x(k)}{m} - \frac{y(k-1)}{m}$$

This is more laborious to implement, but allows the signal levels to be doubled safely. This filter has the disadvantage that a positive or negative output offset of up to $m-1$ digitisation levels may exist due to the division operation. If the input is known to be of only one polarity (i.e. positive) then the filter may be biassed to remove the offset. The modified algorithm is:

$$y(k) = y(k-1) + \frac{x(k) - y(k-1) - (m-1)}{m}$$

5.6.4 HIGH PASS FILTERING

The critical parameters of the filters described are the power frequency gain (and phase) and the maximum gain (which will occur at a higher frequency). If the ratio between these gains is too large then step changes in the input will produce large transients (relative to

steady state power frequency output), which are undesirable. The filter constants have been chosen to avoid this. The power frequency parameters and z domain frequency response formulae are given in Appendix 7.

5.6.4.1 DIFFERENCING OVER AN INTERVAL

The filtering considered will be of a very simple kind: essentially forming the difference of the input over a number of samples (m), which tends to reduce low frequency components more than those at higher frequencies.

$$y(k) = x(k) - x(k-m)$$

This process differs from analogue differentiation in that:

1) There is an interval (of m samples) during which a change at the input is passed straight to the output.

2) The frequency response of the two techniques is different.

Analogue differentiation: $G(z)$ = constant * log(z)

Finite differencing: $G(z) = 1 - (1/z)^m$

The filter frequency response for m=7 at 2 kHz sampling rate is drawn in Fig 5.5.

5.6.4.2 DIFFERENCING USING A RECURSIVE FILTER

Another way of high pass filtering is to subtract a low pass filtered version of the signal from the signal itself. At certain frequencies low pass filtering introduces a phase shift without significantly reducing the magnitude. The main advantages of differencing with a filtered instead of a delayed version of a signal are that:

1) The maximum gain is reduced from 2 to about unity.

2) Only one previous value of a variable needs to be retained.

The algorithm uses an internal variable $a(k)$, which is initially set to zero. The following equations are evaluated once per sample in the order given:

$$y(k) = x(k) - a(k-1) \qquad a(k) = a(k-1) + \frac{y(k)}{m}$$

From the z transform it can be seen that the gain is equivalent to differencing over an interval of one sample i.e. the numerator, together with recursive low pass filtering and a gain

of $2m-2$, (the denominator). The filter frequency response for $m=4$ at 2 kHz sampling rate is drawn in Fig 5.6.

5.6.4.3 DIFFERENCING USING TWO RECURSIVE FILTERS

Yet another way of obtaining a differenced output is to subtract a version of the input filtered by one value of m from a version filtered with a different value of m. The advantage is a reduction in high frequency gain compared to the previous technique, and less offset error than the cascading of simpler filters. The filter frequency response for $m=2,m=8$ at 2 kHz sampling rate is drawn in Fig 5.7.

5.6.4.4 TRANSVERSAL FILTER

A general finite impulse response filter may be designed by forming the sum of the present and past samples of the input signal multiplied by weighting coefficients, $b(i)$:

$$y(k) = \sum_{i=0}^{m} b(i)x(k-i)$$

The coefficients generally all have the same sign in low pass filters, but for high pass filters (with a zero at zero frequency), the sum of the coefficients must be zero:

$$\sum_{i=0}^{m} b(i) = 0$$

For efficient implementation on a microprocessor, the filter algorithm should have the following properties:

1) The coefficients should be integers or fractions which allow the multiplications (or divisions) to be effected easily, i.e. ideally they should have values which equal integer powers of 2 (or their reciprocals).

2) The algorithm should be recursive, i.e. the output for the next sample may be efficiently generated using the last value of the output.

In the simplest form of high pass response, all the weighting coefficients have the same modulus, but half of them are positive and half are negative, (this response may be generated by cascading a delay differencing stage and a running average low pass filter stage. A better response is obtained if the coefficients obey the following linear relationship:

$$b(i) = \frac{m-2i}{m}$$

The coefficients take convenient values if m equals an integer power of 2. The algorithm may be implemented recursively if the output from a running average filter $u(k)$ is available:

$$u(k) = \frac{1}{m}\sum_{i=0}^{m-1} x(k-i) \qquad y(k+1) = y(k) + x(k+1) + x(k-m) - 2u(k)$$

The frequency response for $m=8$ at 2 kHz sampling is plotted in Fig 5.8. The zeros occur at approximately 319.2 Hz, 548.8 Hz and 774.9 Hz. Note that the phase difference between the outputs $u(k)$ and $y(k)$ is 90^0.

5.7 POINT ON WAVE EFFECTS

5.7.1 ANALOGUE FILTERS

Consider a power frequency sinusoid $x(t,\phi)$ suddenly applied to a single pole analogue filter, (time constant: T):

$$x(t,\phi) = \sin(W_0 t + \phi)$$

$$Y(s,\phi) = G(s)X(s,\phi) = \frac{X(s,\phi)}{1+sT}$$

Hence,

$$y(t,\phi) = \frac{1}{\sqrt{1+W_0^2T^2}}\left(\sin(W_0 t + \psi) - \exp\left(\frac{-t}{T}\right)\sin(\psi)\right)$$

$$\psi = \phi - \arctan(W_0 t)$$

At an instant t, the phase angle ϕ which produces the maximum modulus of the output can be found by solving the equation:

$$\frac{dy(t,\phi)}{d\phi} = \cos(W_0 t + \psi) - \exp\left(\frac{-t}{T}\right)\cos(\psi) = 0 \qquad 0 \le \phi < \pi$$

The value of ϕ satisfying this equation is obviously a function of the measuring time t, and will be termed the critical phase angle $\rho(t)$. Substituting this value into the expression

for the output, the maximum instantaneous value or envelope $\varepsilon(t)$ of the output may be found.

$$\varepsilon(t) = \sqrt{(y(t,\phi))^2 + \left(y\left(t,\phi+\frac{\pi}{2}\right)\right)^2}$$

The graphs of normalised envelope and critical phase angles against time are drawn for filter time constants of 1.73ms. and 3.4ms. in Fig 5.9. Several conclusions may be drawn from these graphs:

1) The critical phase angle is approximately a linear function of time, but the slope decreases as the filter time constant increases, i.e. the measurement time to cover a certain angular range is increased.

2) The envelope is approximately constant after a time equal to the filter time constant has elapsed.

3) If a constant, rather than time varying envelope were used as a comparison threshold, then the 'reach' of an IMR or DR would be very dependent on fault point on wave, particularly if the measurement time did not allow the critical phase angle to pass through a range of 180^0.

4) Attempting to reduce the measurement time by doubling the number of comparators would require that filters with markedly different characteristics, i.e. a high or band pass function, be used, so that the critical phase angle would vary over a different range.

5.7.2 CASCADED FILTERS

In actual practice, several stages of digital and analogue filtering are likely to be used, and a closed form expression of the output quickly becomes unwieldy. The envelope may be calculated from the time domain outputs for the zero and ninety degree fault points on wave as shown in the previous section. The critical phase angle is given by:

$$\varrho(t) = \arctan\left[\frac{y\left(t,\frac{\pi}{2}\right)}{y(t,0)}\right]$$

Graphs showing the characteristics of a running average filter $m=8$ cascaded with a recursive low pass filter $m=4$ for a 2 kHz. sampling rate are drawn in Fig 5.10.

5.7.3 HIGH PASS FILTERS

The transient response of filters having a zero at zero frequency is critical. An initial assessment main be made by comparing the power frequency gain with the maximum excursion in the time domain step response. If the latter is much larger, e.g. when the difference is taken over a small number of samples, then that filter design will be unsuitable.

The smoothness of the step response is also important, since abrupt transitions may cause similar effects in the critical phase angle characteristic, making it more difficult to treat each fault point on wave equally. These considerations narrow the choice to:

1) A filter which takes the difference of the input signal and a version of itself delayed by a number of samples. The behaviour of this filter with $m=7$ and followed by a recursive filter $m=4$ at 2kHz sampling is shown in Fig 5.11.

2) A filter which forms the difference of the input signal and a low pass filtered version of itself. The behaviour of this filter using a recursive low pass filter $m=4$ followed by a recursive filtering stage $m=4$ at 2kHz sampling rate is shown in Fig 5.12.

3) A filter which forms the difference of two recursive low pass filtered signals, e.g. the behaviour of a filter with $m,4m=2,8$ and 2 kHz. sampling rate is shown in Fig 5.13.

4) A transversal filter. To make a fair comparison, this must be cascaded with a stage of recursive lag filtering. The filter behaviour with $m=8$ for the transversal stage, and $m=4$ for the second stage is shown in Fig 5.14.

The filters have remarkably similar responses; but there are differences in high frequency response and impulse response duration which favour the transversal filter, which will henceforth be used whenever band pass or high pass functions are required. The output waveforms from a high pass filter (scaled by a factor 0.5) cascaded with a low pass filter when unit amplitude sinusoids and cosinusoids are applied are shown in Fig 5.15. The filter constants are those used in Figs 5.10 and 5.14 respectively.

5.8 DIRECTIONAL RELAY DESIGN

5.8.1 INTRODUCTION

The changes in currents and voltages which occur when a power system is faulted can be represented (assuming linearity) as the response of the un–energised post–fault network to the application of a voltage generator in the fault path (Fig 1.2). Since most of the energy of the superimposed generator is concentrated about power frequency, (and the relay filtering will attempt to reject high and low frequency transients), the power system components may for our purposes be represented by their lumped parameters (evaluated at power frequency).

The voltages and currents may be found by constructing sequence component networks for each fault type (e.g. Figs 3.1 to 3.4). However, since superimposed conditions are being considered, the voltage generators exist at the fault point rather than the source locations: the cases for each of the principal fault types are drawn in Figs 5.16, 5.17, 5.18, 5.19.

Given a suitable choice of relaying measurands, (which is discussed in Section 5.6), the three phase fault networks may be reduced to an equivalent single phase network as drawn in Fig 5.20a. Two relays protecting feeders connected to the same busbar would see the same superimposed voltage (V) but approximately anti–phase superimposed currents, assuming that the fault was in a forward direction from one relay and in the reverse direction from the other. (Note the phase relation only applies to power frequency components). Referring to Fig 5.20a:

$$E = (sL_x + R_x)I_f + V \tag{1}$$

$$V = (sL_g + R_g)(I_f + I_r) \tag{2}$$

$$V = -(sL_r + R_r)I_r \tag{3}$$

Hence:

$$V\left(1 + \frac{sL_g + R_g}{sL_r + R_r}\right) = (sL_g + R_g)I_f$$

If one of the following conditions is met:

$$\frac{L_r}{R_r} \approx \frac{L_g}{R_g} \qquad L_g^2 + R_g^2 \ll L_r^2 + R_r^2$$

The following approximation may be made:

$$V = K(sL_g + R_g)I_f \tag{4}$$

Where K is a real constant.

If the current I is passed through a mimic impedance to form a mimic voltage V_m:

$$V_m = (sL_m + R_m)I \tag{5}$$

Then assuming:

$$\frac{L_r}{R_r} \approx \frac{L_g}{R_g} \approx \frac{L_m}{R_m}$$

Directional determination may be obtained by comparing the polarities of V, V_m in the time domain:

1) If the relaying current I can be identified with the current I_f in equation (4), then a forward fault exists.

2) If the relaying current I can be identified with the current I_r in equation (5), then an external fault exists.

It is necessary to make several determinations over a small time period to outweigh erroneous decisions produced by noise or phase shift imbalances. Barker [23] used a counter, which was incremented for a forward determination and decremented for a reverse determination. A directional decision was output when a count threshold was crossed.

The minimum counting time must be greater than the maximum period for which phase shift may cause the discriminant signals to violate the directional criterion. For a power system, the ratio of inductive reactance to resistance X/R may vary between values of approximately 5 to greater than 30. However, the phase shift error caused by assuming a wrong value is not large, i.e. $\arctan(5) = 78.7^0$, $\arctan(30) = 88.1^0$, and 10^0 at power frequency corresponds to about 0.56 ms. Minimum counting times of greater than twice this figure still allow fast directional determination.

5.8.2 BASIC DESIGN CONSIDERATIONS

DRs have used magnitude comparisons between signals formed according to the rule:

$$v_f = V - kI \qquad\qquad v_b = V + kI$$

This is equivalent to the comparison of the polarities of V, kI. A comparison of the magnitudes of V, kI against thresholds also needs to be made to guarantee that they are large enough to make any polarity conclusion meaningful. If it is, then a counter will be either incremented (for a forward determination) or decremented (for a reverse determination), until a certain positive or negative count is reached, which is taken as a decision that the fault is forward or reverse. Further counting which would cause the count to exceed these levels is inhibited.

Comparing (filtered) signal levels with thresholds inevitably leads to a dependence of operation time and/or sensitivity with fault point on wave, as discussed in 5.7.

In previous work [23], in order to determine whether the comparison was significant, the instantaneous amplitudes of v_f, v_b were compared against a single threshold (derived from past values of the larger of V, kI. In this design, V, kI will be compared against separate thresholds, since it is unnecessarily pessimistic to assume that the background levels for these two signals are the same. If V, is derived from the line voltage and kI from the current, then the ratio of background noise on the signals (excluding that arising in the relay) is likely to reflect the relative magnitudes of the p.u. current mimic and source impedances. The latter may vary over wide limits depending on the system and how many generators are in service.

Once a disturbance is over, the directional determination counter will need to be reset to prevent any influence on subsequent decisions. However, it is not easy to define when this occurs. Barker [23] chose to reset the counter if the count had not changed during a certain time interval. To assess the relative merits of this and alternative strategies, it is desirable to clarify the function of the decision process, particularly when sequential faults occur. As the signals exceed the decision process thresholds, it is likely that there

will be a burst of directional determinations. The time at which this occurs will be dependent on the fault point on wave and filter characteristics.

5.8.3 PHASE SENSITIVE RECTIFICATION

Conventional full wave rectification inverts negative half cycles of the input: i.e. the output is equal to the input multiplied by the sign of the input. Phase sensitive rectification is here defined as multiplying one signal by the sign of the second. If the magnitude of the second signal is zero, then the output is also zero. In the case of two sinusoids having the same frequency (ω) but different phase angles, this would have the effect of producing a constant level equal to the magnitude of the first signal multiplied by the cosine of the phase shift between them, together with an alternating signal containing frequencies 2ω and higher harmonics. It is the constant level which is of interest.

5.8.4 CHOICE OF DISCRIMINANTS

One of the most fundamental design considerations for a DR is the number of directional detectors. Two were used by Barker[23] (corresponding to transmission line aerial modes), but cases can be devised where directional decisions would disagree. An obvious solution to this problem is to have only one detector. This may be designed using the fact that the superimposed current outflow along the sound phase(s) will always be less than the current inflow on the faulted phase(s). A suitable discriminant is therefore the sum of three sign adjusted superimposed current signals.

Zero sequence compensated phase currents were used initially. The sign of each term is adjusted by multiplying by the sign of the associated phase voltage and an extra negative sign is included to make the discriminant C positive for forward disturbances:

$$C = -(C_{ae}\mathrm{sgn}(V_{ae}) + C_{be}\mathrm{sgn}(V_{be}) + C_{ce}\mathrm{sgn}(V_{ce}))$$

The magnitude of this discriminant can readily be compared with a threshold to determine its significance.

A problem with using zero sequence compensated phase currents to construct the directional discriminant becomes apparent for earth faults close to the busbar. If current clipping occurred, each sound phase would contribute a reverse polarity current to the discri-

minant, and their sum could outweigh the faulted phase contribution. For faults very close to a busbar, the counter might not reach the forward decision threshold before reverse counting leading to a reverse directional decision began. In view of this effect, delta current and voltage quantities are considered more suitable candidates, and the discriminant C is constructed as follows:

$$C = -(C_{bc}\text{sgn}(V_{bc}) + C_{ca}\text{sgn}(V_{ca}) + C_{ab}\text{sgn}(V_{ab}))$$

The discriminant may therefore be defined as the negated sum of the three delta currents each phase sensitively rectified (c.f. 5.8.3) with respect to its corresponding delta voltage. Summing three quantities (which are limitted to the same range of values) implies an increase in the range of the sum. This may be allowed, which would require 32 bit arithmetic, or prevented, by reducing the range of the inputs, i.e. by pre–dividing by 4. The latter option will be used as the ultimate sensitivity of the relay is not reduced, since the range of the output is still greater than that of the analogue to digital converter. A block diagram of this process is shown in Fig 5.21, with the processing for voltage signal significance described in 5.8.8.

5.8.5 VARIABLE LEVEL THRESHOLD

This facility is required to maximise relay sensitivity during periods when the superimposed components are above the levels that would be expected under normal operating conditions. The requirements are:

1) The algorithm should mediate a smooth sensitivity decrease during and a smooth increase after a disturbance.

2) A threshold should be the product of the magnitude of the (delayed) superimposed component and a safety factor.

3) The rise in thresholds should not occur until the relay has had time to reach a directional decision. After that time the thresholds should rise and prevent further counting (in the absence of a subsequent more powerful disturbance).

It is desirable that maximum sensitivity be restored as quickly as possible after a disturbance, but the performance will largely depend on the choice of superimposed extraction

filtering: if one full cycle stage is used then full sensitivity will be restored more quickly, but sensitivity during prolonged power swings would be lower than that available if two full cycle stages had been used. The latter consideration is judged more important and two full cycle stages are used in the design.

The are two alternative ways of deriving a threshold signal T_{ir} for the current discriminant C:

1) To use delayed values of C.

2) To use combinations of superimposed delta currents:

$$T_{ir} = k(|C_{bc}| + |C_{ca}| + |C_{ab}|)$$

The latter option is clearly preferable as C is zero when the voltage signals are not significant.

5.8.6 DISCUSSION ON THRESHOLDS

It may readily be appreciated that discriminants need to be compared against thresholds to determine whether a decision may safely be taken. In a directional protection scheme, the threshold should reflect not only whether a discriminant is significant (i.e. above background noise) at the local end, but whether the local discriminant is significant given the conditions at the other end(s). Unfortunately, in the case of Teed feeders, conditions at the other ends are not known and have to be inferred using assumptions as to source capacities.

If the current discriminant C were to indicate a fault in the reverse direction, then there would be no need to consider the conditions at the other ends, hence C may initially be compared with the lowest threshold compatible with local conditions. If this results in a reverse decision then a block signal will be issued. If the current discriminant C were to indicate a fault in the forward direction, then, assuming the fault external to the Tee, a forward decision may only be allowed to be reached if a relay at one of the other ends be capable of detecting it as reverse. Hence C needs to be tested against another threshold (termed the forward current threshold) which represents the worst case condition at the other ends. There are three alternative ways of generating this:

1) To use a simple multiple of local current. This is the simplest option, but insensitive to fault direction and local source capacity.

2) To use the sum of the scaled modulus of local superimposed voltage and current. This introduces a local source capacity dependency, but requires a more complex algorithm.

3) To use the modulus of the scaled sum of local superimposed voltage and current. This requires the most complex algorithm, since the three phases of the assumed current at a remote end have to be generated from local voltage and current signals. However, there is great benefit in having the forward threshold dependent on the direction of the previous disturbance.

In the event none of these alternatives can cope with the wide range of conditions which are met. A new forward current discriminant C_f needs to be defined which will be compared against the forward current threshold. (This will only occur if the current discriminant C indicates a fault in the forward direction). The forward current threshold may then be generated from the constituents of C_f in the same way that T_{ir} was generated from the constituents of C, but with a larger (usually much larger) numerical scaling factor.

5.8.7 DERIVATION OF FORWARD CURRENT DISCRIMINANT

If there is a fault external to a Teed feeder for which the line lengths and source capacities are known, then, given the superimposed voltage and current at one end, the superimposed currents at each of the other ends may be estimated. All of the superimposed currents are proportional to the superimposed voltage at the Tee point, and this is the best quantity from which to construct the forward current discriminant. The delta Tee point voltages may be constructed by summing the local superimposed voltage and (negated) superimposed current scaled by the line impedance to the Tee point (referred to relay units). Directional information is lost in forming this discriminant, so taking the modulus of the signals is most appropriate:

$$C_f = (|V_{tbc}| + |V_{tca}| + |V_{tab}|)$$

A block diagram of this process is shown in Fig 5.21. Omission of a term when the corresponding relaying point superimposed voltage is non–significant is also shown.

One of the advantages of using this discriminant is that no assumption is necessary about the local source capacity, however, in order to set the ratio by which the forward threshold exceeds the discriminant, assumptions about the source capacities at the other ends are necessary as shown in section 5.8.10.

5.8.8 VOLTAGE DISCRIMINANT

A single threshold for the voltage signals may be derived from the superimposed delta voltages:

$$T_{vr} = |V_{bc}| + |V_{ca}| + |V_{ab}|$$

Signal delay and perhaps scaling would also be included. There are three ways which the information on the significance of the voltage signals may be used:

1) By comparing the magnitude of each superimposed delta voltage with this threshold: if the threshold is not exceeded, then the associated phase rectified current term would be omitted from the current discriminant sum C.

2) By comparing a voltage discriminant (constructed in the same way as the threshold but with the delay omitted) with the threshold could be used to enable (or disable) comparison of the current discriminant with its threshold.

3) To omit assessement of voltage significance altogether. This would place a much heavier responsibility on the reverse current threshold algorithm preventing incorrect decisions being made. However, an incorrect reverse decision is unlikely to be disasterous, whereas an incorrect forward decision certainly would be. It will have been noted that the forward current discriminant and threshold are formed using superimposed voltage and therefore apply a check similar to that desired (for forward directional decisions).

If considerations of random errors in voltage and current signals are excluded, then the last option is satisfactory. However, greater security will be achieved if voltage significance is monitored, and in particular, if only correlated current and voltage disturbances

(on a phase or delta quantity basis) are used in a discriminant. Hence the first option will be employed. There is a slight difficulty in that like is not being compared with like, i.e. a magnitude is being compared with the sum of three magnitudes, but scaling of 1/4 for the sum and 1/2 for the delta quantity will give satisfactory results. The threshold will be derived in the same way as the current and forward current thresholds, and the significance processing for the voltage signals is shown in Fig 5.21. The comparator outputs a 'high' when the threshold magnitude is greater than the magnitude of the other input and the gate outputs zero when it receives this signal; otherwise its output equals its input.

5.8.9 IMPLEMENTATION OF VARIABLE LEVEL THRESHOLD ALGORITHM

The ideal shape for the variable level threshold algorithm (VLTA) output would be a steep rising edge followed by a flat top and then a reducing level which always exceeded the associated discriminant amplitude. The steep initial slope is particularly important: the situation where the discriminant and threshold levels cross several times makes it difficult to distinguish between single and multiple disturbances. The flat top is important for much the same reason: once the threshold has exceeded the discriminant, it should stay there until the superimposed signals produced by the disturbance have disappeared. Attempting to make the peaks in the threshold level occur at the same time as the peaks in the discriminant is an alternative, but riskier option.

It has been found necessary to use 32 bit arithmetic in the production of a threshold signal to avoid rounding error. Five stages in the production of a threshold:

1) A signal (which may range over the whole 16 bit integer range) is rectified and added to the two other (similarly treated) phase signals. The summed signal is then added to a similarly treated phase shifted signal sum. There are two possible ways of generating sets of signals phase shifted by 0^0 and 90^0:

a) By using different filtering i.e. low pass and band pass filtering. This implementation (Fig 5.22) involves a large processor workload since transversal filters are required to generate the 90^0 phase shifted signals.

b) By using a quarter power frequency cycle delay to generate the 90^0 phase shifted signals. As can be seen in the block diagram (Fig 5.23), there is a consequent sav-

ing in complexity and processor workload. An alternative way of generating the desired threshold is shown in Fig 5.24: the digital nature of the signals is exploited by selecting the maximum of the present value or the value delayed by 3.5, 8.5 or 13.5 ms. This tends to make the threshold stay high for an excessively long duration when signals which have been processed through two stages of superimposed component extraction filtering are used. A way of reducing this time is to similarly process a set of signals which have only undergone one stage of superimposed component extraction filtering (denoted by the prime), and select the lower of the thresholds produced. Both thresholds are valid, but the single stage threshold would be higher under normal conditions c.f. 5.6.2.

2) Scaling (multiplication by an integer and fractional scaling factor) is described in 5.9.10.

3) A stage of low pass recursive filtering is then used to smooth the output. Initially a recursive filter was used, but a running average filter (m=8) was substituted, to avoid the exponentially decaying tail the former produces.

4) Introduction of a delay, so there is sufficient time for a direction decision to be made before the thresholds rise (preventing further directional determinations for the original disturbance).

5) Division of signal by an integer power of 2 to remove factors accumulated in processing and reduce output within range of a 16 bit integer.

The outputs from the first two implementations to voltage minimum and maximum single phase to earth faults are shown in Fig 5.25 and Fig 5.26. It can be seen that the first implementation gives a far steeper initial rise in threshold level, and the threshold also returns to quiescent level more quickly. The former is preferable despite considerable extra complexity. The combination of one full and one half cycle superimposed component extraction stages produces an unsatisfactory threshold waveform as can be seen in Fig 5.27. The implementation shown in Fig 5.24, will actually be used as it has better behaviour than either of the other implementations. Typical waveforms will be shown in chapter 6.

5.8.10 CALCULATION OF FORWARD CURRENT THRESHOLD

Assuming an external forward fault, the superimposed voltage at the Tee point can be found from the local superimposed current and voltage. Then assuming a realistic source capacity on the shorter of the remote arms, an upper bound to the larger of the remote fault currents can be found. The forward current threshold is set to mimic this bound as a function of the local superimposed voltages and currents.

For the configuration of Fig 4.9, the superimposed current amplitudes for a disturbance behind that busbar may be expressed in terms of the superimposed Tee point voltage V_t, (assuming the source capacities shown):

$$I_p = 5.5\frac{V_t}{73} \qquad I_q = 4.5\frac{V_t}{73} \qquad I_r = \frac{V_t}{73}$$

A disturbance at the mid–point of the feed round would cause superimposed current amplitudes related by the following equation:

$$2I_p = 2I_q = I_r = \frac{V_t}{73}$$

Hence for the same conditions at relay R, a range of currents of 11:1 is possible at relay P. To prevent maloperation if the two disturbances were to occur in close succession, the forward decision current discriminant C_f and threshold T_{if} at relay R should obey the following formulae:

$$C_f = \frac{V_t}{73} \qquad T_{if} > \frac{11\ V_t}{73}$$

The 'greater than' condition arises from the presence of a safety factor between the (reverse) current discriminant and threshold at a remote relay. The conditions for relays P and Q for these conditions are not nearly so stringent:

$$C_f = 4.5\frac{V_t}{73} \qquad T_{if} > \frac{5.5\ V_t}{73}$$

However, the ratio between the threshold and discriminant would normally have a minimum value of two to allow for changes in system topology (i.e. feed round connections).

5.8.11 CURRENT CLIPPING

If an external fault causes current clipping to occur at a directional relay in a Teed feeder application, then the following problems arise:

1) Ensuring that there are not erroneous directional determinations at the relay where clipping occurred.

2) Ensuring correct operation at the other relays requires that their forward current thresholds be raised until the sensitivity is less than the reverse sensitivity of the affected relay.

Clipping depends on total current and may persist for several power frequency cycles, whereas the superimposed signals which are used to construct discriminants and thresholds are only valid for 20 ms. Even if a threshold algorithm were devised which could ensure correct operation for local current clipping, co–ordination of sensitivities would require the estimation of total current conditions and modelling of the threshold behaviour by relays at remote ends for periods of say 60 ms. Given the high factor which is necessary between the forward discriminant and threshold for linear conditions in some Teed feeder conditions, the improvement in scheme performance gained by attempting to measure when the effects of clipping are present is likely to be small.

In order to disable the DR scheme while the effects of clipping are present, the following functions need to be present:

1) A means of detecting whether the current input signals are clipped. This may be done in the analogue stages by comparing the signals with levels.

2) A method of determining when the effects of clipping have disappeared. Since the relay filtering has a finite impulse response duration, this time may be assigned using a delayed version of the 'clipping present on input' signal.

3) A means of communicating that local current clipping has been detected. This may effectively be done by transmitting a block signal until the effects of clipping have disappeared.

4) A method of reducing relay sensitivity. Initially this was done by raising thresholds to maximum, but a better way is simply to inhibit counting (and reset counters

to zero). The thresholds then have locally determined values at the resumption of measurement.

If possible, the relay current gain should be set to avoid current clipping for external faults. For forward faults causing clipping, a block signal would not be transmitted locally, but if the fault were external then another (more affected) relay in the scheme would do so. Tripping would be expected to occur for internal faults (whether clipping occurred or not), making co–ordination of post–disturbance sensitivities unnecessary in such cases.

5.8.12 DECISION PROCESS

It is important that a fault in one direction closely following one in the opposite direction should be quickly detected, as the IMR algorithm may be non–directional. The behaviour of a simple counter scheme is less than ideal in this respect as the time to detect the second fault is at least twice the minimum operating time, since the count has to change from one limit to the other. This limitation may be overcome by using two counters, each having the same inputs, but one counting positively for forward fault determinations: (the count would be constrained to lie between zero and the decision level N). The reverse decision counter count would be constrained to lie between zero and $-N$ and counting would be in the negative direction (for a reverse fault determination). In each counter, a directional determination opposite to the desired direction would cause counting in the opposite direction.

There are also advantages in reducing the count (modulus) when a non–significant directional determination occurs:

1) The counter will be reset automatically.

2) The decision criterion is well matched to the form the determinations would be expected to take following a single disturbance, i.e. a continuous burst.

The decrement for a non–significant determination should be less than the increment for a significant one. If a minimum decision time of 3 samples is chosen, then N could be chosen as 12, with an increment of plus or minus 4 for significant determinations, and

a decrement of 1 otherwise. A further refinement is to 'hold' any directional decision until its counter has decremented to zero. This would avoid temporary decrementation and then incrementation back to the decision level being treated as a separate disturbance.

5.8.13 DESIGN SUMMARY

The design may be conveniently divided into two parts:

1) Analogue signal processing. A block diagram is shown in Fig 5.28. The impose limits blocks prevent signals exceeding the input range of the analogue to digital converters. As mentioned in 5.4, sampling and digitisation of waveforms occurs at 4 kHz, but the rest of the processing is carried out at 2 kHz. This is achieved by averaging the values of two 4 kHz samples.

2) Digital signal processing. This may be divided into four categories:

a) Digital filtering. The digital filtering required for the b–c detector is shown in Fig 5.29. The filtering used consists of two stages of running average filters (m=2,m=4) for current signals, and (m=4,m=4) for voltage signals. An initial gain of 8 multiplies the output from the analog to digital converter (–2047 to +2047 levels) for the voltage signal, but a gain of 7 was the maximum that could be used before arithmetic overflow occurred with severely clipped current signals. The difference in filtering produces about a ten degree phase shift, almost eliminating the phase offset between current and voltage signals. Two stages of full cycle superimposed component extraction filtering as discussed in 5.8.5 are used, though the output after one stage is made available for the VLTA algorithm as discussed in 5.8.9.

b) Generation of forward and reverse fault determinations. The block diagram of this process is shown in Fig 5.30. The construction of discriminants and thresholds was discussed in Sections 5.8.4, 5.8.5 and 5.8.7, though the use of single stage superimposed component extraction filtered signals as additional inputs to the VLTA has not been drawn in Fig 5.30. The VLTA was discussed in 5.8.9, and the implementation shown in Fig 5.24. The action of the reverse current comparator is to output a NON SIG(R) indication if the upper input magnitude is less than the lower and the inputs have the same polarity. If the inputs have opposite polarity then a NON SIG(R) indication will be output

if the upper input magnitude is less than twice the lower. Otherwise the reverse current comparator will produce a REV or a FWD indication for same and opposite polarity inputs respectively. The forward current comparator produces a FWD indication only if its upper input is more positive than its lower and the reverse current comparator has indicated a forward disturbance. Otherwise a NON SIG indication is output.

c) Processing when clipping is detected. The block diagram of this is shown in Fig 5.31, and was discussed in 5.8.11. The implementation compares the analogue values of phase currents with positive and negative limits (MAX and –MAX). If one or more of these comparisons is true, i.e. the current magnitude exceeds the limit, then a counter is set to have the value NMAX. In the absence of further clipping indications, the count is decremented each sampling interval until it reaches zero, (further decrementation is prevented). This condition is detected by the digital comparator and its output then goes to zero. Hence the output of the digital comparator will be 'high' from the start of clipping until a period (determined by NMAX) has elapsed since the last clipping indication. A delay is introduced to allow time for a directional decision to be reached

d) Decision process. The block diagram of this is shown in Fig 5.32 and was discussed in 5.8.12. If the CLIPPING EFFECTS PRESENT input is 'high' then the forward counter is reset to zero. The comparators produce a 'high' output if the signal at the upper input is greater than that at the lower. The timers inhibit counting for a period of 12.5 ms. once a directional decision has been reached. This was found to be the shortest time after which it could be guaranteed that the threshold level would exceed the discriminant level.

5.9 INDEPENDENT MODE ALGORITHM

5.9.1 PRINCIPLES

The IMR is to have distance protection characteristics: only operating for faults within a certain reach, which implies impedance measurement. The conventional formulation relates the relay voltage and current (in Fig 5.20b) by an equation such as:

$$V = ZI = (sL_x + R_x)I \qquad (6)$$

The voltage calculated using the above equation (and values of L_x, R_x corresponding to the reach point) can be compared with the measured quantity to determine whether a fault exists in the protected zone. Since the superimposed and pre–fault components of the measurands can be derived, the determination may use alternative pairs of quantities. Many principles are possible, but consideration of the following three outline the essential features:

Total quantities: $$V = V_{ss} + V_{sup} = ZI = Z(I_{ss} + I_{sup}) \quad (7)$$

Construction of fault point voltage: $$V_{ss} - ZI_{ss} = -V_{sup} + ZI_{sup} \quad (8)$$

Construction of relaying point voltage: $$V_{ss} = -V_{sup} + ZI_{sup} + ZI_{ss} \quad (9)$$

Initially, the magnitudes of the two sides of the equation will be compared: with a trip deemed necessary if the right hand side exceeds the left hand side. If the phase of the discriminants is also considered, then a circular 'mho' protection characteristic is obtained, but fault resistance coverage would be increased by not doing so.

The construction of the fault point voltage magnitudes at various points on the transmission line for a faulted (single phase) circuit when pre–fault power flow is present is shown in Fig 5.33 (not to scale). It is assumed that the vectors represent power frequency sinusoids and the (zero resistance fault is at the reach point). The complex value of Z is determined by the reach setting and the transactor phase shift. (Additional phase shifts may be introduced by filtering or using delayed signals, but these are refinements.) The relaying location voltage corresponds to point P, and the fault point to point F. The post–fault estimate of the voltage OB is constructed from the superimposed voltage at the relay (OD) plus the superimposed current scaled by the reach setting.

5.9.2 PRE–FAULT CURRENT

Taking a term from one side of the equation to the other can have a marked affect on behaviour of any algorithm. The most difficult term to deal with is that due to the pre–fault current, since this determines the assumed pre–fault fault point voltage according to the following equation:

$$|V_{ss} - ZI_{ss}| = \sqrt{|V_{ss}|^2 + |ZI_{ss}|^2 - 2|V_{ss}||ZI_{ss}|\cos(\theta)} \qquad ,\theta = \arg\left(\frac{ZI_{ss}}{V_{ss}}\right)$$

In particular, for typical choices of θ, the magnitude of fault point voltage may exhibit quadratic behaviour with respect to fault distance, i.e. initially decreasing as the magnitude of ZI_{ss} increases from zero, reaching a minimum, and then increasing. For weak sources, the rate of increase in fault point voltage with fault distance may exceed that of ZI_{sup}. For algorithm (8), this means that assuming a fault distance larger than the actual one may not give a clearer and quicker trip decision (as would be hoped), but in some cases, a failure to trip. This behaviour will not happen if magnitudes are compared using either of the other two principles.

The behaviour of algorithm (8) may be illustrated with reference to Fig 5.34. The fault is again at F, but the relay is set for approximately twice the fault distance. Hence the point B corresponds to the left hand side of equation (8) and point E corresponds to the right hand side. It can be seen that point B lies outside the circle defined by radius OE, and hence the magnitude criterion is not satisfied, and a trip would not be issued. This behaviour will only occur at weak sources where the superimposed voltage magnitude is almost as large as the pre–fault voltage magnitude.

Assuming initially that the relay has three earth fault and three phase fault elements, the prevention of encroachment between elements is a major consideration. In this respect, principles in which V_{ss} and ZI_{ss} appear on the same side of the equation have a definite advantage where large pre–fault power flows are present. Consider a case Fig 5.35 where the fault point voltage is rotated 60^0 relative to the steady state relaying voltage vector V_{ss} and an a–e earth fault occurs. The vector OG represents ZI_{ss}, which will be the same for all earth fault detectors, (as will be discussed in 5.9.3), and the vector FG represents V_{sup} for the a–phase. (V_{sup} for the sound phases are shown as zero in the diagram; using actual values would exacerbate the case demonstrated).

If reach point voltage estimates are constructed, then the right hand sides of the equation for the three fault detectors correspond to Ha, Hb, Hc, and the left to Pa, Pb, Pc (the busbar

voltages for the a, b and c phases). In one of the sound phase elements, (the b–e element for an a–e fault) the ZI_{ss} term has the same magnitude as V_{ss} and approximately the same direction as ZI_{sup} and $-V_{sup}$. This element is therefore likely to trip at a lower reach setting than the a–e fault detector since the ratio of magnitudes of Hb:Pb is greater than that of Ha:Pa. In either the total quantities or construction of relaying point voltage principles, this would be sufficient to cause overreaching, but such behaviour is absent when algorithm (8) is used.

However, the pre–fault current will cause problems for all principles in the following instances:

1) When the magnitude of the superimposed voltage increases with fault distance from relaying point (even over a small part of the line), there is the possibility of the relay over–reaching: e.g. if the fault was actually at F in Fig 5.36, a setting of 0 km would probably be sufficient for tripping to occur, i.e. |OP| = |OD|. In fact underreaching is likely for faults more distant than point B, (BE is parallel to FD and OE perpendicular to PD).

2) When the magnitude of the line voltage is zero at some point within the protection zone (due to large power swings).

If either of these circumstances is detected then tripping needs to be restrained.

The algorithm which constructs two estimates of the fault point voltage seems to be the most attractive option as it is least likely to suffer from encroachments. Non–operation when the reach setting greatly exceeds the actual fault distance will need to be investigated since many Teed feeder IMR applications feature low capacity sources (which exacerbate the problem).

5.9.3 PROCESSING OF EARTH FAULT MEASURANDS

In conventional distance relaying, three sets of earth fault measurands each comprise a phase voltage and a zero sequence compensated phase current. The compensated current e.g. for an a–e fault, I_a', is formed such that (assuming ideal transposition):

$$V_a = Z_1 I_a' \qquad I_a' = I_a + \left(\frac{Z_0}{Z_1} + 1\right) I_0 \qquad I_0 = \frac{I_a + I_b + I_c}{3}$$

The ratio of zero sequence to positive sequence impedance Z_0/Z_1 relates solely to the line: it is known to be a complex number, but may be approximated (at power frequency) by a real constant (equal to 3). It is not possible to specify this ratio with great precision, since it will vary with soil resistivity which itself depends on the amount of moisture present.

The zero sequence compensation uniquely provides both the pre–fault current I_{ss} and the superimposed zero sequence current $5I_0$ if the faulted phase corresponds to the fault element, or a superimposed zero sequence current $2I_0$ if it does not. However, the formula also produces a non–zero superimposed current when phase to phase faults occur, which can lead to problems of encroachment by earth fault detectors. The ability to separate the pre–fault and superimposed components and process them differently allows other compensation regimes to be employed. One which is particularly attractive is to make the superimposed current component $5I_0$ for all earth fault elements. This should prevent earth fault detector encroachment for phase to phase faults, but at the cost of making encroachment by say the b–e detector for an a–e fault more likely. However, the latter problem is more amenable to solution.

5.9.4 VALIDITY CHECKS

If the following condition is satisfied, then the superimposed voltage does not increase with fault distance:

$$-\frac{\pi}{2} < \arg\left(\frac{ZI_{ss} + ZI_{sup}}{V_{sup} - ZI_{sup}}\right) < \frac{\pi}{2} \tag{10}$$

Although it is assumed that the IMR will be triggered only for forward faults, the following condition (which essentially checks that the superimposed voltage and current are consistent with a forward fault) is useful to prevent encroachments:

$$-\frac{\pi}{2} < \arg\left(\frac{ZI_{sup}}{V_{sup} - ZI_{sup}}\right) < \frac{\pi}{2} \tag{11}$$

The requirement that the line voltage magnitude does not go through zero within the protected zone is equivalent to the following condition:

$$-\frac{\pi}{2} < \arg\left(\frac{V_{ss}}{V_{sup} - ZI_{sup}}\right) < \frac{\pi}{2} \tag{12}$$

This condition will have the side effect of preventing tripping when the difference between the phase angles of the pre–fault voltage at the relaying and fault points exceeds 90^0. However, this is unlikely to be a severe practical restriction.

5.9.5 FILTERING

The implementation of the relay algorithm and validity checks require comparison of magnitudes of signals which have been described in terms of power frequency phasors rather than time domain signals. It is important to distinguish between the cases for which this is valid, i.e. where the signals actually are pure sinusoids, and those for which the signals contain power system and filtering transients. The pre–fault components of voltage and current comprise the first case, provided that the filter input is not gated, i.e. constrained to be zero until a triggering signal is received (either from the DR or from within the IMR). Substantial transients will be present on superimposed signals (c.f. Section 5.7), whether filter input signals are gated or not. Similarly gating of pre–fault signal filtering will introduce transients dependent on the phase angle of the input sinusoid at the triggering instant.

5.9.6 MAGNITUDE COMPARISON

A simple realisation of a magnitude comparator consists of an instantaneous amplitude comparator followed by a counter, which would be incremented if the rectified signal applied to one input were greater than that applied to the second and decremented otherwise, (but prevented from having a negative count). A trip signal would be issued if a count threshold were exceeded.

The operation of such a scheme is shown in Fig 5.37, where the comparator inputs (before rectification) were equal amplitude sinusoids with a phase difference of 45^0 (not the worse case). Tripping should not occur in this case, requiring a high count threshold to

prevent false trips on counter excursions, which would slow relay operation when tripping were desired.

A possible improvement is to use additional delayed versions of the time domain signals to make comparison of time domain signals less dependent on the relative phase angle of the signals. Consider two time domain signals:

$$x(t) = \cos(W_0 t) \qquad y(t) = \cos(W_0 t + \phi)$$

And their delayed versions:

$$x'(t) = x\left(t - \frac{\pi}{2W_0}\right) = \sin\left(W_0 t - \frac{\pi}{2}\right) = -\cos(W_0 t)$$

$$y(t) = y'\left(t - \frac{\pi}{2W_0}\right) = \cos\left(W_0 t + \phi - \frac{\pi}{2}\right) = \sin(W_0 t + \phi)$$

Applying $u(t)$, $v(t)$, where:

$$u(t) = |x(t)| + |x'(t)| \qquad v(t) = |y(t)| + |y'(t)|$$

to the inputs of an instantaneous comparator gives much less oscillatory counter behaviour than applying $/x(t)/$, $/y(t)/$, as Fig 5.38 shows. Hence the counter threshold may be set lower and faster operation obtained. The process is akin to multi–phase rectification; the 'ripple frequency' of the rectified signal increases as the number of components used to form the comparator signals. The higher this frequency, the easier it is to remove and the shorter the time necessary to estimate the signal magnitude.

Pairs of signals in which the power frequency component is phase shifted by different amounts may be generated by passing each signal through a filter with a different frequency responses rather than by delaying one of them. However, it is difficult to achieve sufficient phase shift between the signals with this method.

Better smoothing of rectified signals may be achieved by adding a delayed version of the rectified signal to itself before amplitude comparison were undertaken. Unfortunately this actually introduces additional fault point on wave dependence into the results, since the same transient is present in both signals.

5.9.7 CONSTRUCTION OF SIGNAL PAIRS

Point on wave dependence may be overcome by ensuring that in the 'delayed' signal not only is the power frequency component delayed by 5ms, but the transient corresponds to application of the signal at that delayed time. A block diagram of an implementation for superimposed signals is shown in Fig 5.39. It can be seen that two sets of filters are needed, with associated gating and delay functions. No output would be available until 5 ms. after the IMR has been triggered, which may seem too large a price to pay. However valid pre–fault signals are available for times prior to IMR triggering time, and the implementation shown in Fig 5.40 can be used.

The technique of generating signal pairs can be used to reduce the ripple on phase sensitively rectified signals. When the phase difference between the two input sinusoids approaches 90^0, the constant component of the output is zero, and the alternating component will have the same amplitude as the input. Low pass filtering will have some effect in reducing the alternating component, but a more effective technique (for pre–fault signals) is to generate a second set of signals for both inputs and phase sensitively rectify them. Adding the outputs will result in a large reduction in output ripple.

5.9.8 IMPLEMENTATION OF REACH ALGORITHM

Gating is required for all signals to ensure that transients introduced by relay filtering originate at the same time. The following options are available for treating equation (8):

1) Simple rectification of left and right hand sides. This would have the advantage that the transient present in each comparator signal would be identical if the estimates of fault point voltage were in phase, but that performance would be similar to that shown in Fig 5.37 if they weren't.

2) Rectification of signal pairs constructed as in 5.9.7 for the left hand side (pre–fault quantities) and simple rectification of right hand side. This option will give a less accurate comparison than the previous one when the estimates of fault point voltage are in phase, but the reduction in ripple in one of the comparator inputs should allow a

lower count threshold.

3) Construction and rectification of signal pairs for both sides.

All these alternatives were tried but the latter was easily the best. Though counting cannot start until 5 ms after a DR forward signal is received, a lower count threshold is possible and the discriminants show much less fault point on wave dependency.

5.9.9 IMPLEMENTATION OF CHECKS

In terms of time domain signals, the checks require that the constant component of phase rectified output of the numerator with respect to the denominator be greater than zero. Since measurement cannot start until 5 ms. after a DR forward decision has been received, it is advantageous to use signal pairs (cf 5.9.7), particularly for the check described by equation (10), as the phase difference between the pre–fault current and the superimposed fault point voltage estimate is likely to be close to 90^0.

The phase rectified outputs of superimposed current, pre–fault voltage and pre–fault current are all generated with respect to the superimposed fault point voltage estimate. Equation (10) may be implemented by utilising the output available from the implementation of equation (11).

5.9.10 SIGNAL SCALING

The processing stage at which signals are combined and scaled affects the following:

1) The amount of processing which has to be done.

2) The behaviour of the relay when current clipping occurs.

The voltage signals for both the DR and IMR are easily dealt with. Since over–voltages on the power system are high frequency phenomena, the maximum voltage which may be expected after passing through the VT and anti–aliassing filter stages is likely to be little greater than 1 p.u. Hence the three phase voltages may be scaled, digitised and filtered before the relaying quantities are formed.

There are advantages in applying current scaling in the analogue stages of an IMR, since digital scaling involves multiplication which consumes processor time and may reduce the dynamic range. However, digital scaling will be included and modelled since setting

the reach in software is a distinct advantage. There are two stages in the implementation:

a) The required digital current gain is resolved into an integer power of 2 times a (proper) fractional part.

b) The voltage signal is then divided by the integer part of the gain, and the current signal multiplied (as a series of additions, subtractions and divisions by 2) by the fractional part of the gain. Clearly there is little point in having full 16 bit accuracy in the fractional gain; the number of bits used may be specified in the data. (Generally 5 bits are used, giving approximately 3% error. This procedure is also used in the DR to scale the thresholds and form the forward current signals.)

5.9.11 ZERO SEQUENCE COMPENSATION

A zero sequence current could be formed in the analogue stages and then digitised, but summation of digitised signals will be modelled, even though this involves a digital multiplication. The following sequence of digital operations approximates that process fairly accurately, while preventing arithmetic overflow:

$$I_e = \frac{I_a}{4} + \frac{I_b}{4} + \frac{I_c}{4} \qquad I_{ex} = I_e + \frac{I_e}{4} + \frac{I_e}{16}$$

For conventional compensation: limit I_{ex} to the range $-16384 < I_{ex} < 16384$

$$I_{ae} = \frac{I_a}{2} + I_{ex}$$

For compensation as used in this design: limit I_{ex} to the range $-6553 < I_{ex} < 6553$ and then multiply by 5. The overall factor multiplying the zero sequence current is then 1.641 compared to the desired value 1.667.

The effective digital multiplication may be combined with the range setting multiplication detailed in the next section if I_e is derived before the latter is applied. Different ratios of the superimposed components of the zero sequence and phase current may be used as described in 5.9.3.

5.9.12 DESIGN SUMMARY

A block diagram of the analogue stage of the IMR for a–phase quantities is shown in Fig 5.41. Processing for the other phase quantities is identical to that shown for the a–phase.

A block diagram of the derivation of superimposed and pre–fault components of voltage is shown in Fig 5.42. Scaling for the voltage signals would consist of binary shifting, i.e. division by 2 or 4 if necessary, but usually not even that. Only a single stage of running average filtering is used as band pass filtering is applied to the signals at a later stage. A block diagram of the derivation of superimposed and pre–fault components of current is shown in Fig 5.43. The single sample delay introduced into the signal path of the steady state currents is to correct the phase angle. The processing is similar to that used for the voltage signals except that scaling involves digital multiplication as discussed in 5.9.10, and the processing for the superimposed earth fault detector signals is as discussed in 5.9.3 and 5.9.11.

A block diagram of the processing of the superimposed and pre–fault components of voltage and current for one fault detector element is shown in Fig 5.44. The transversal filters have filter constant $m=16$ and pre–divide their input signals by 64 to prevent overflow and numerical rounding errors in filter calculations. The quantities required to evaluate the validity checks (discussed in 5.9.4 and 5.9.9) are produced at outputs A, B, C and the quantities for the reach point algorithm (discussed in 5.9.1) at outputs D, E. The phase sensitive rectification stages (discussed in 5.8.3) have two inputs: the input without the arrow is rectified with respect to the input with the arrow. All phase sensitive rectification is done with respect to the pre–fault voltage at the fault point.

Different processing for superimposed and pre–fault quantities is used (as discussed in 5.9.9). The gate functions ensure that the input to the transversal filters is zero until 5 ms after a DR forward decision is received at which time the gate is opened. (The gate would close 20 ms after this and the rest of the relay would be reset, since both sets of superimposed and pre–fault signals would no longer be (theoretically) valid.) The LP FILTER elements are running filters with $m=8$.

A block diagram of the evaluation of the checks and reach point algorithm determination is shown in Fig 5.45. The comparators produce a 'high' output when the value at the upper input is larger than that at the lower. Checks (10, 11) in 5.9.4 may be combined by comparing the phase rectified output of ZI_{sup} with respect to $V_{sup} - ZI_{sup}$ with the maximum of either zero (check (11)) or the negative of the phase rectified output of ZI_{ss} with respect to $V_{sup} - ZI_{sup}$ (check (10)). If any of the checks produce a 'high' output then counting is inhibited. The counter will increment if its other input is 'high' and decrement if it is not, but decrementation below a count of zero is prevented.

5.10 COMMONALITY BETWEEN IMR AND DR DESIGNS

If digital scaling of current signals in the IMR is adopted, the analogue stages of both relays can be made identical. Much of the digital filtering (before combination of signals into delta and earth fault quantities) is the same, with the exception of the initial digital gain. Since the difference is due to the presence of transversal filters, commonality would be improved if the gain factor (7/8) were added immediately before them rather than at the first digital stage.

SUPERIMPOSED COMPONENT EXTRACTION FILTER WAVEFORMS

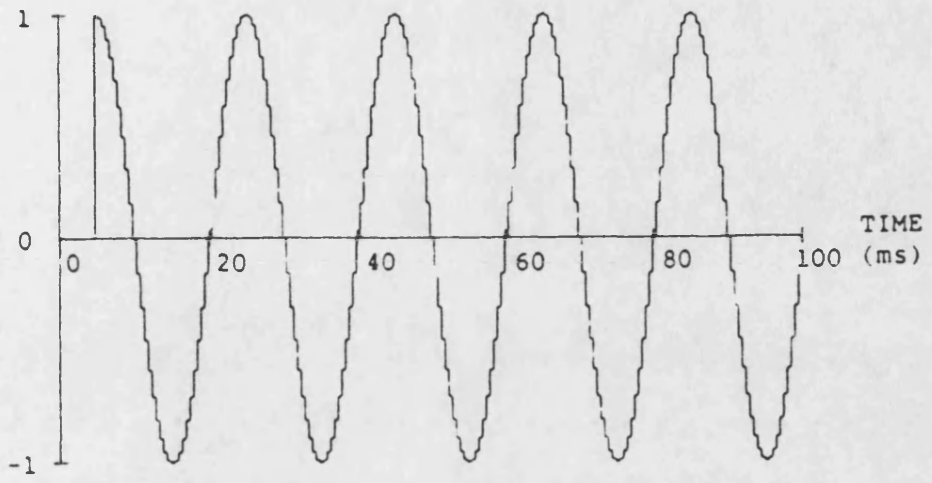

Fig 5.1a INPUT

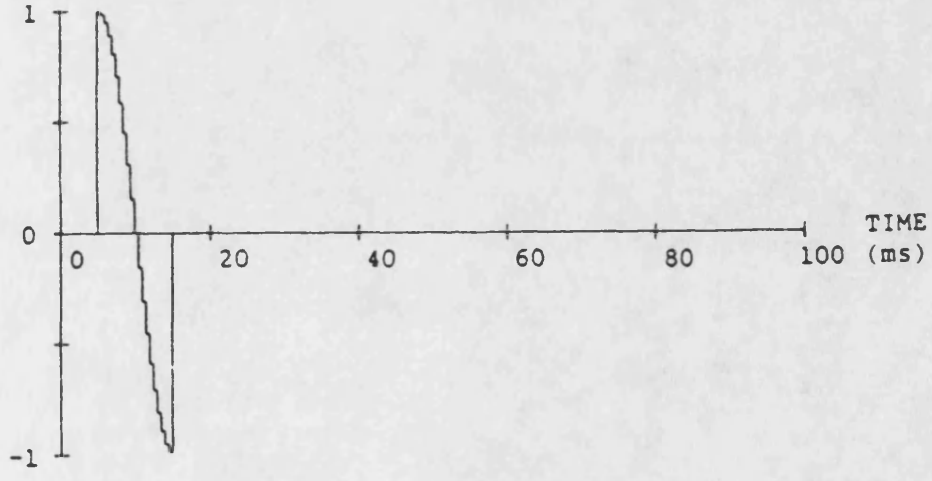

Fig 5.1b HALF CYCLE STAGE OUTPUT

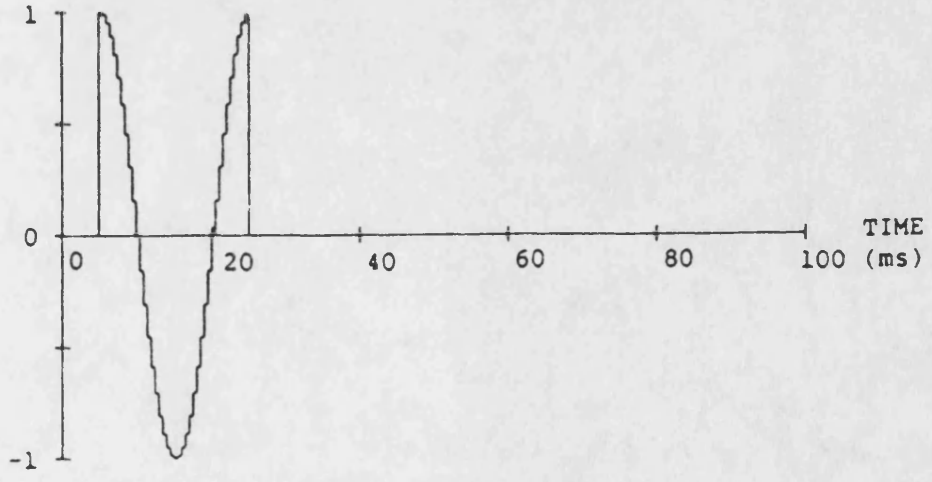

Fig 5.1c FULL CYCLE STAGE OUTPUT

SUPERIMPOSED COMPONENT EXTRACTION FILTER WAVEFORMS

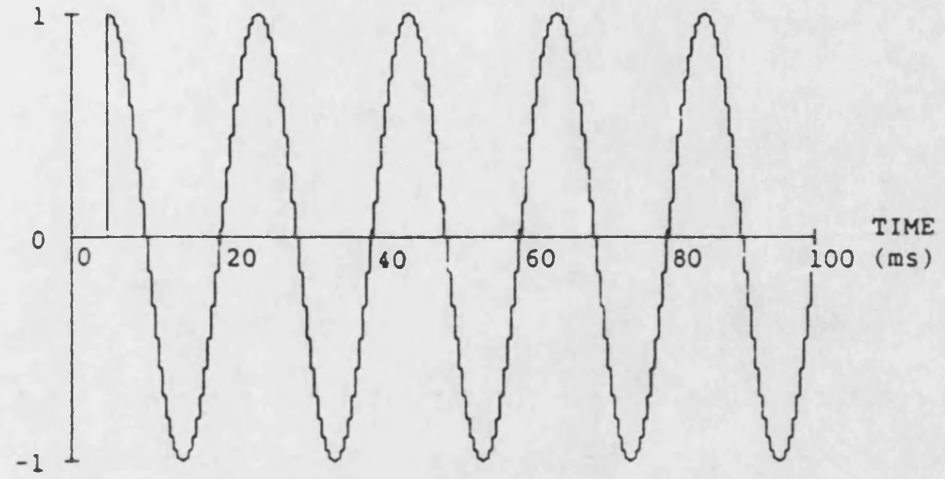

Fig 5.2a INPUT

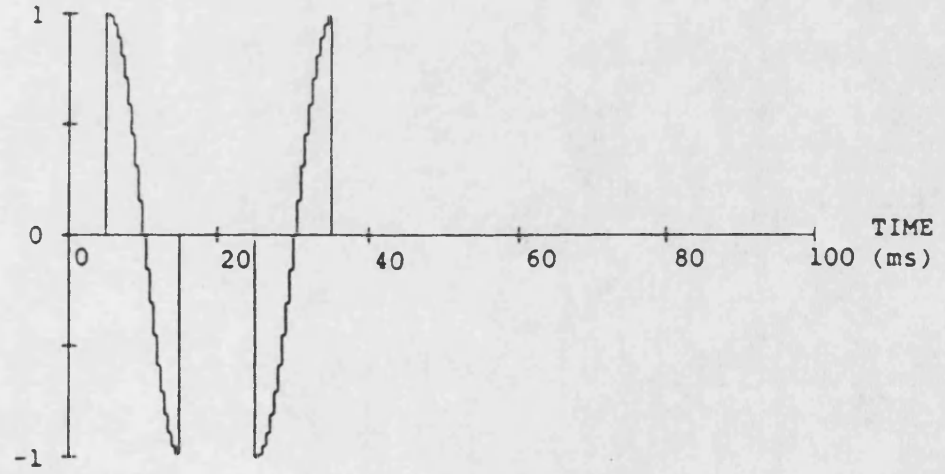

Fig 5.2b OUTPUT FROM CASCADED HALF AND FULL CYCLE STAGES

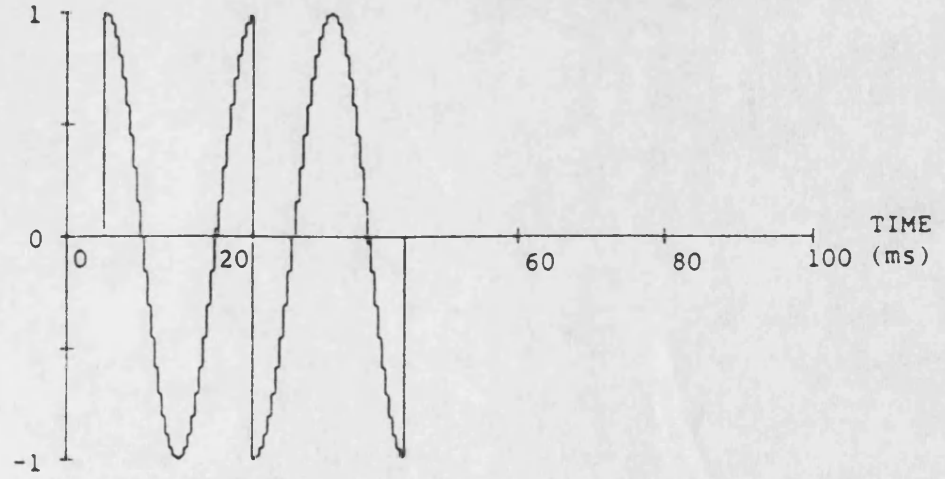

Fig 5.2c OUTPUT FROM TWO CASCADED FULL CYCLE STAGES

Fig 5.3 RUNNING AVERAGE FILTER FREQUENCY RESPONSE

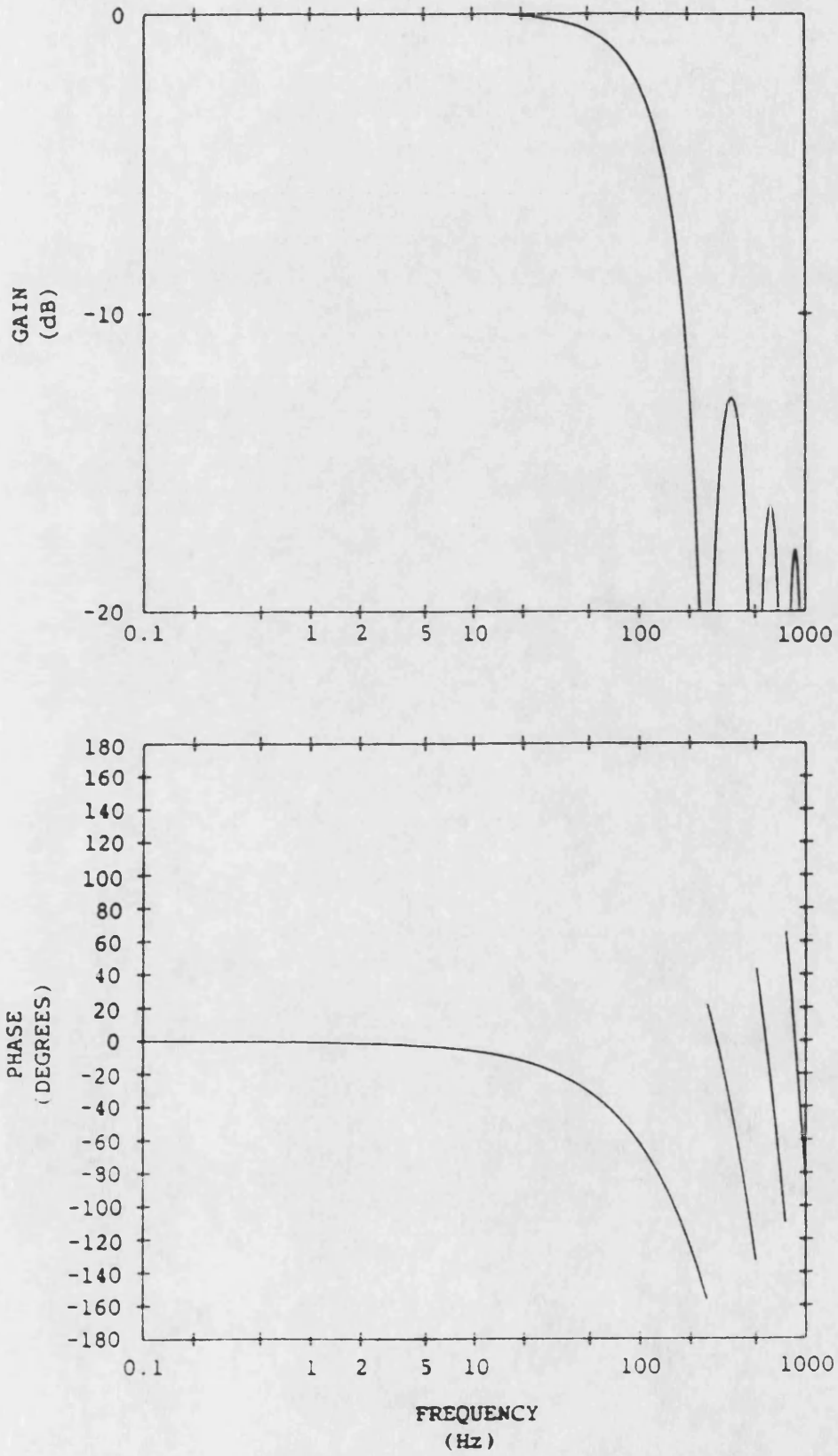

Fig 5.4 RECURSIVE LOW PASS FILTER FREQUENCY RESPONSE

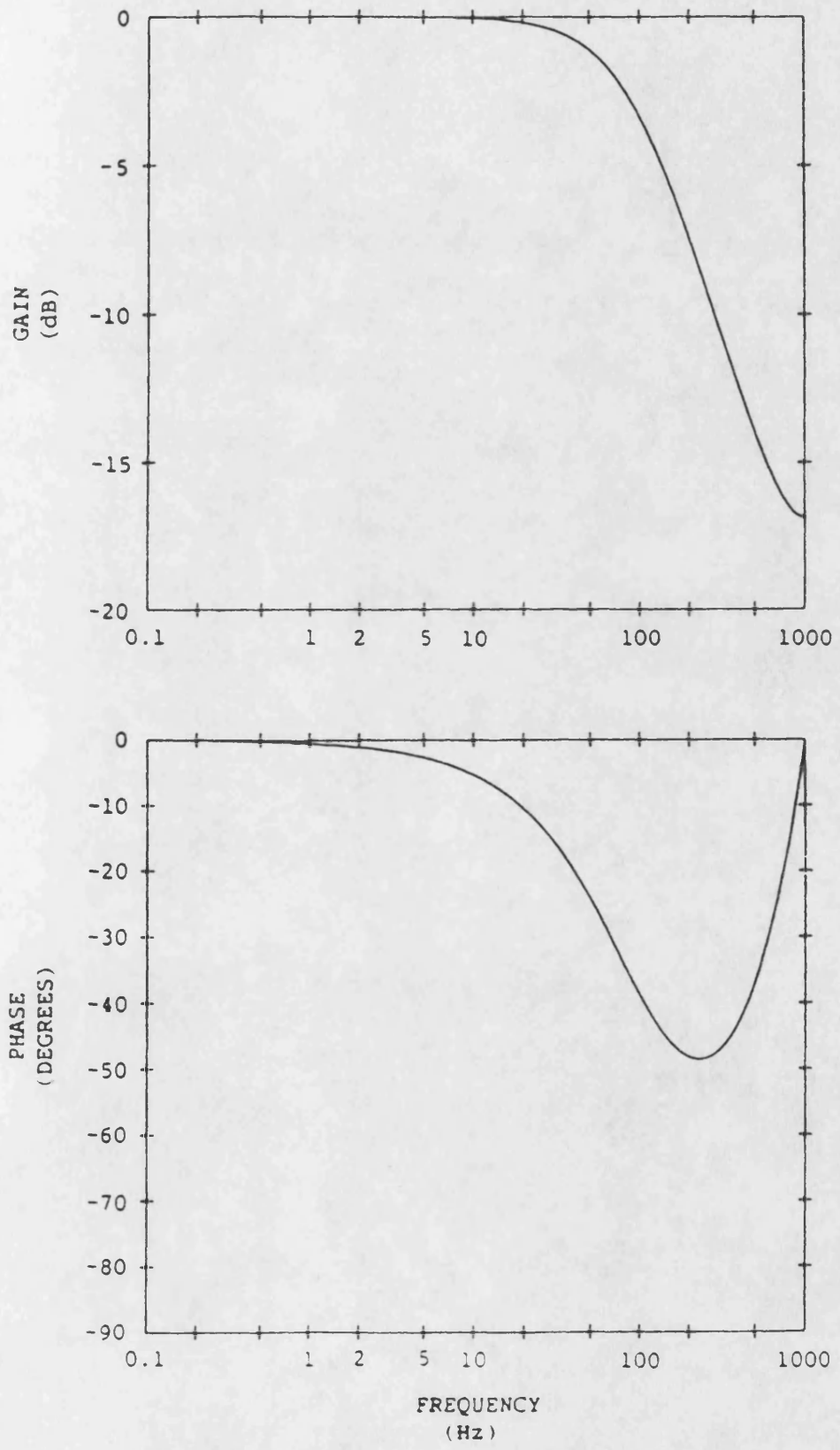

Fig 5.5 DIFFERENCING (OVER 7 SAMPLES) FREQUENCY RESPONSE

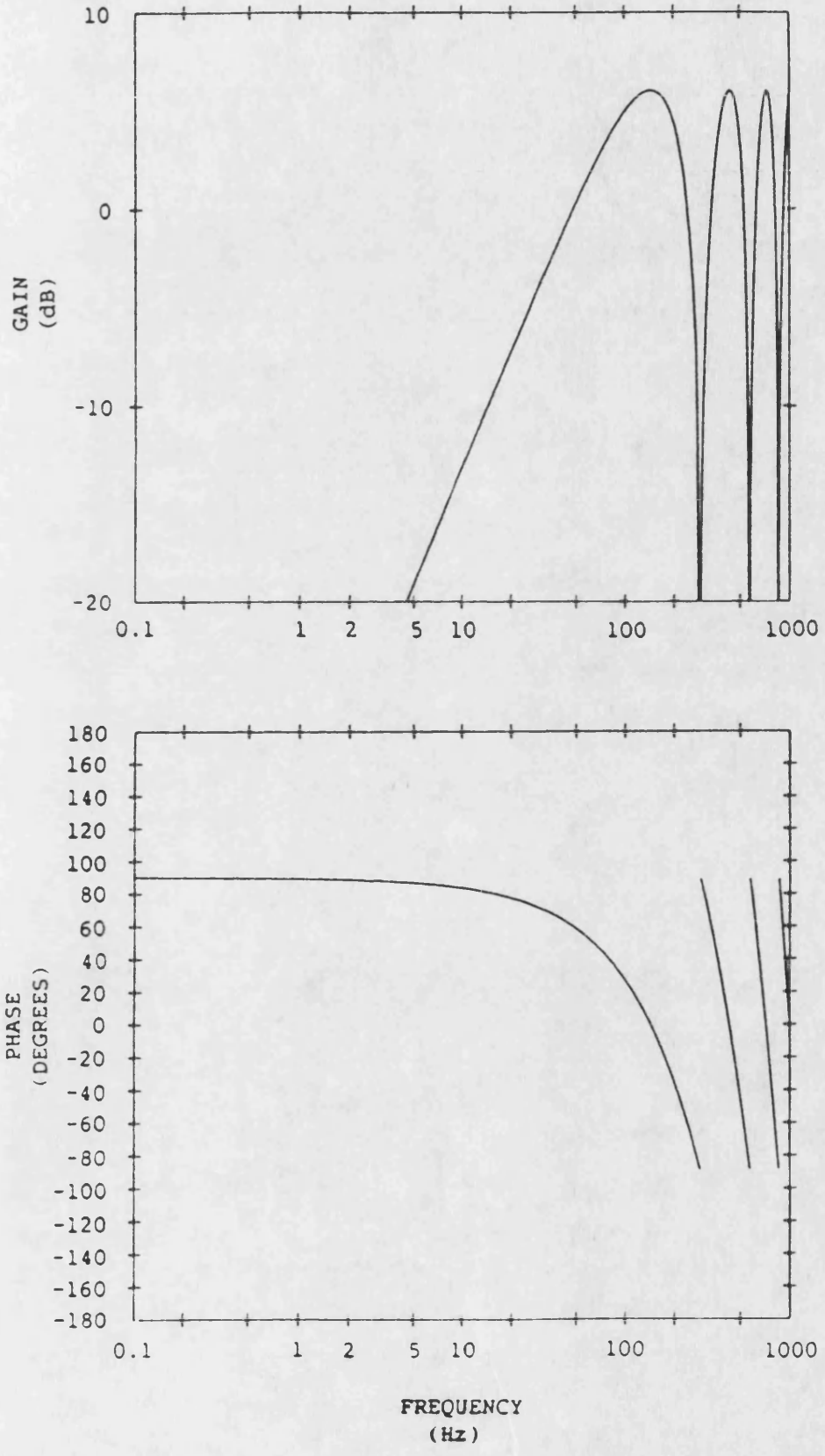

Fig 5.6 DIFFERENCING (USING A LP FILTER) FREQUENCY RESPONSE

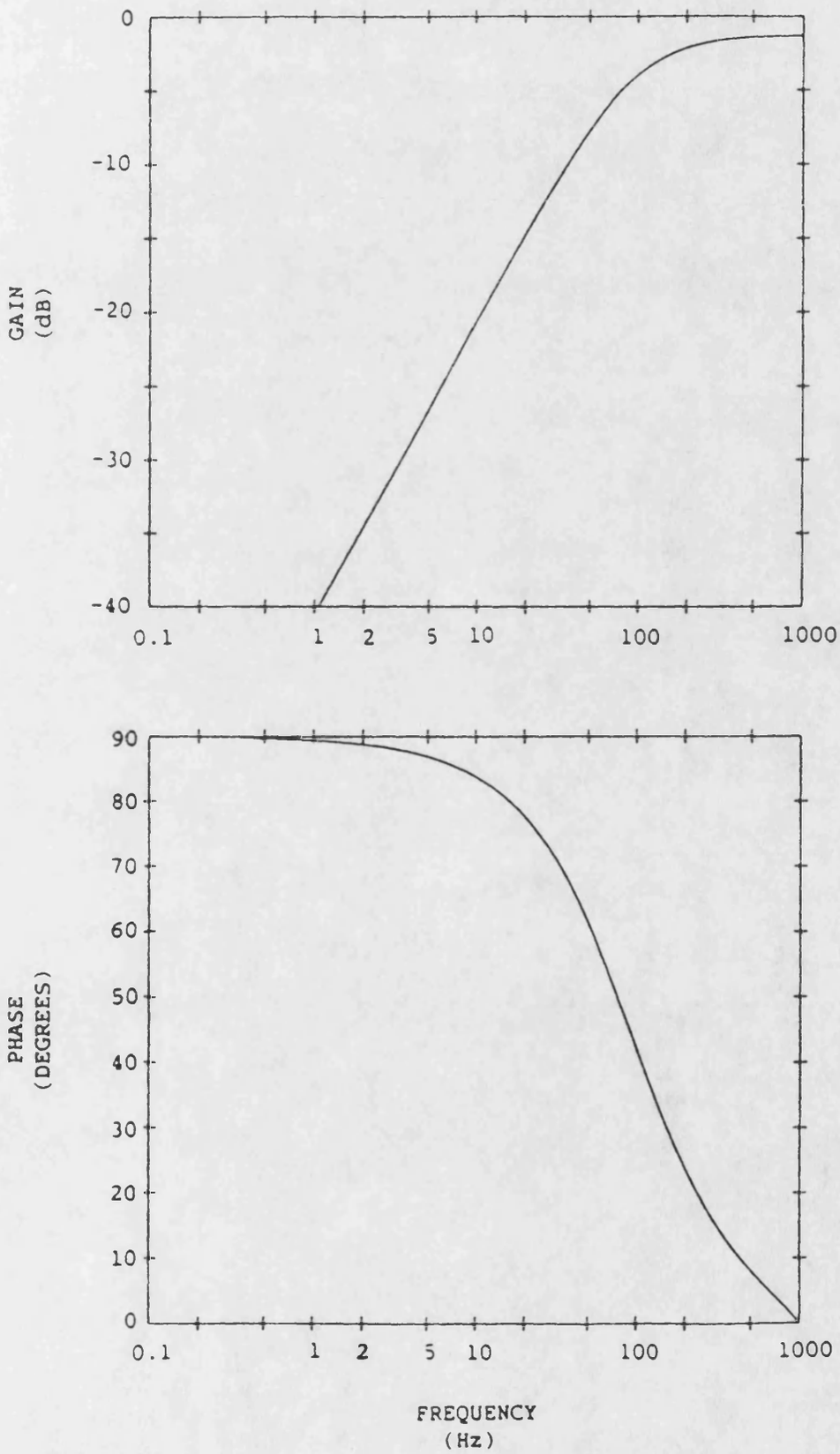

Fig 5.7 DIFFERENCING (USING 2 LP FILTERS) FREQUENCY RESPONSE

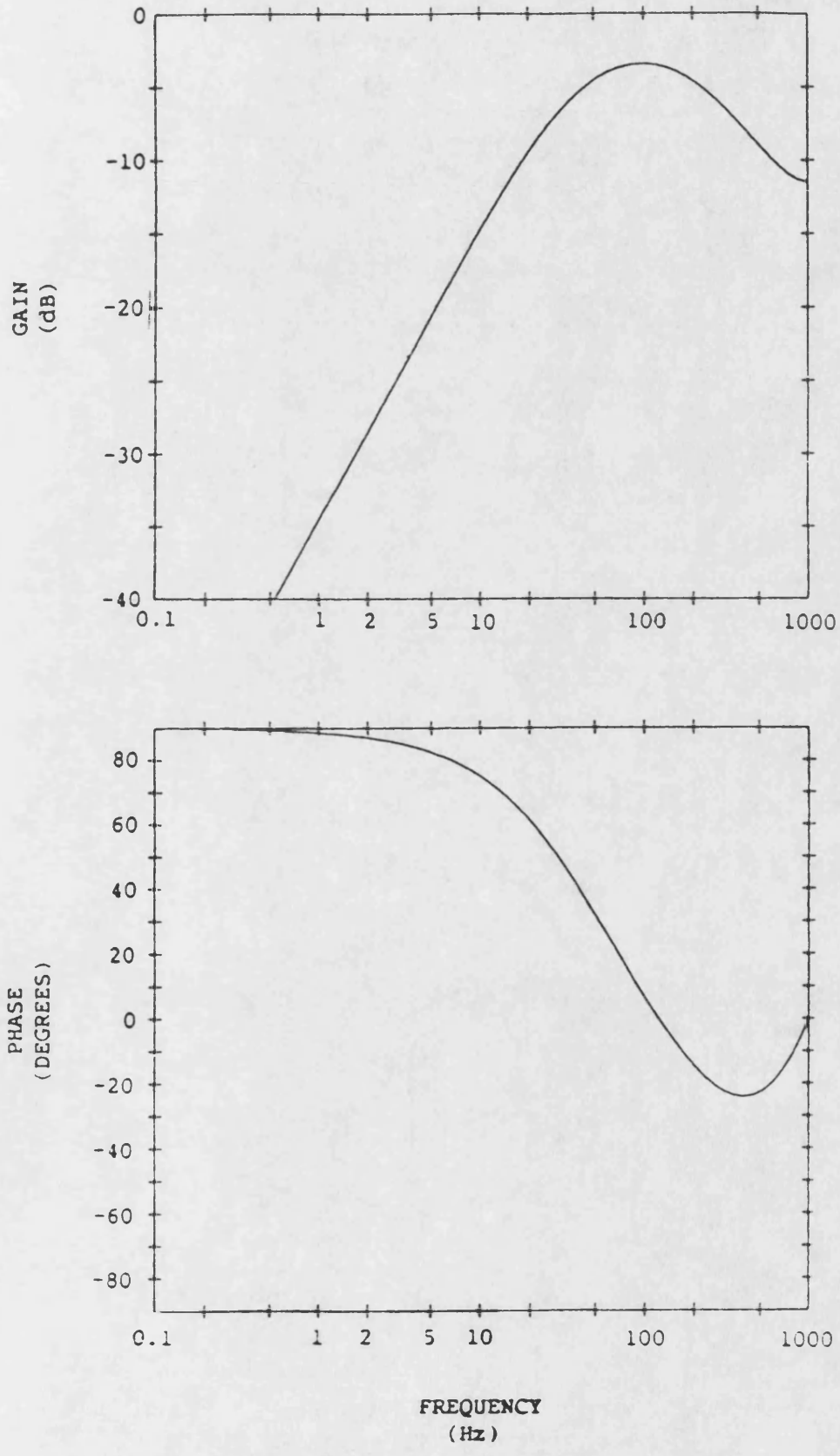

Fig 5.8 TRANSVERSAL FILTER FREQUENCY RESPONSE

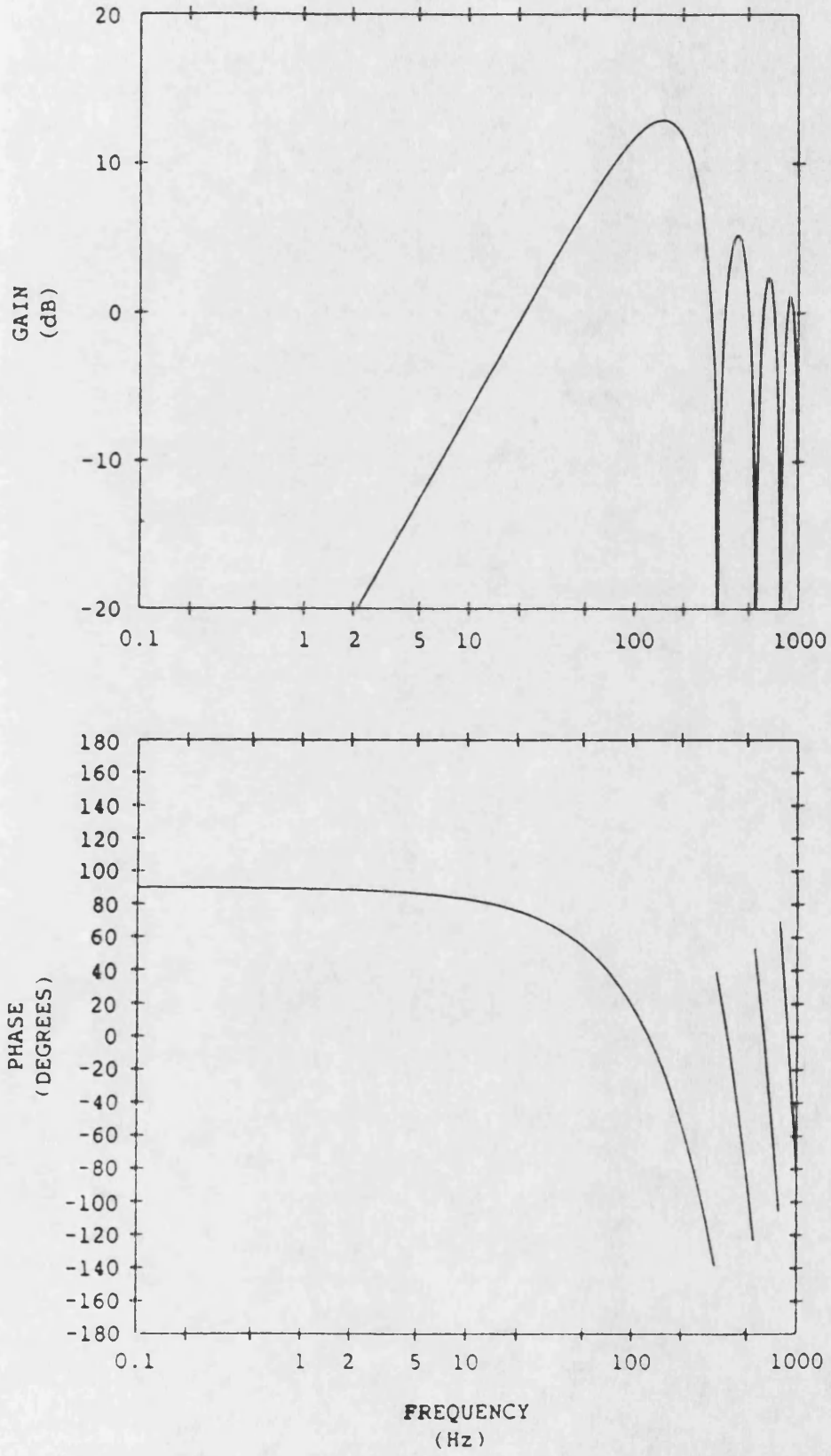

Fig 5.9 ANALOGUE FILTER CHARACTERISTICS

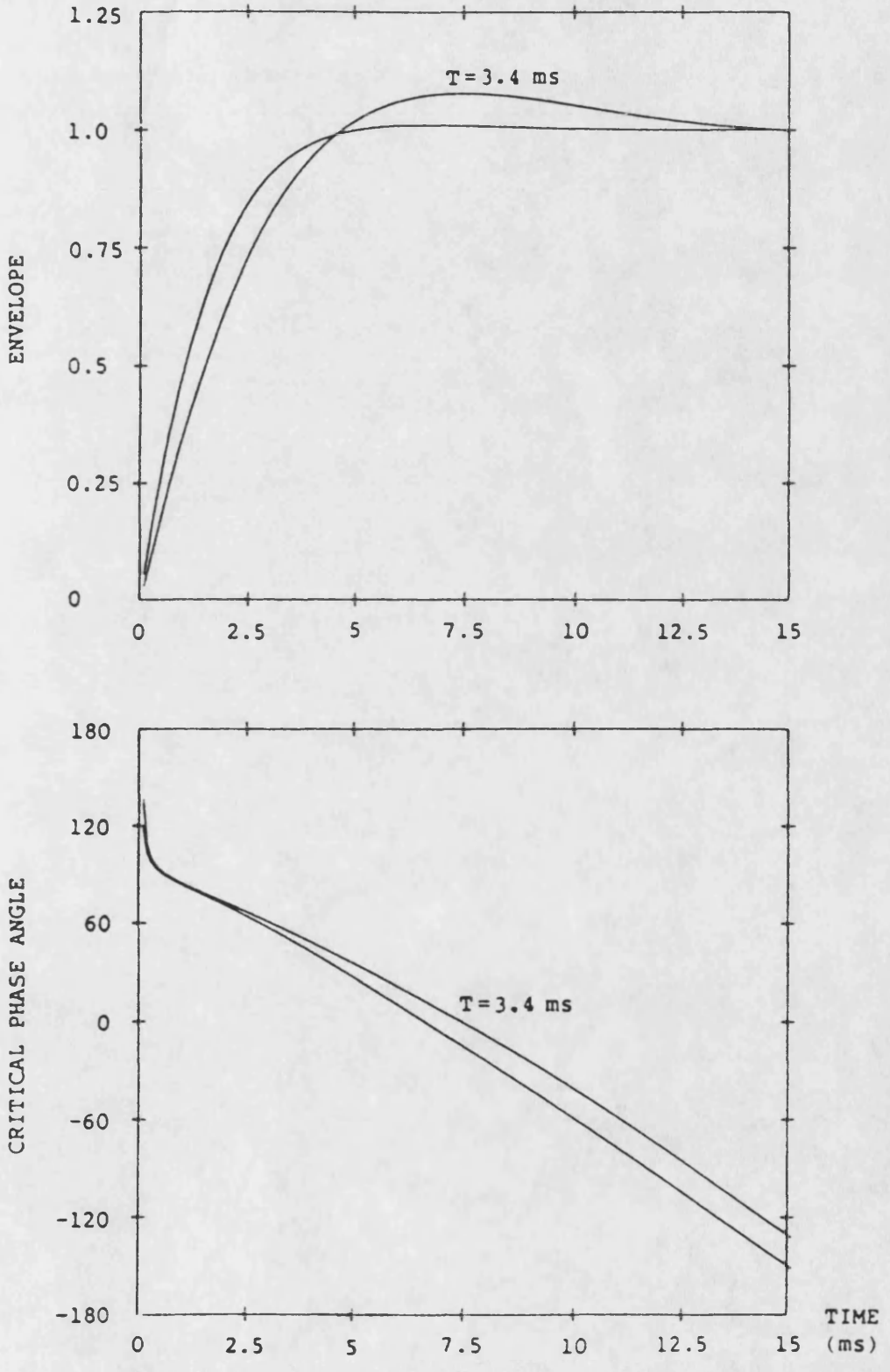

Fig 5.10 CASCADED LOW PASS DIGITAL FILTER CHARACTERISTIC

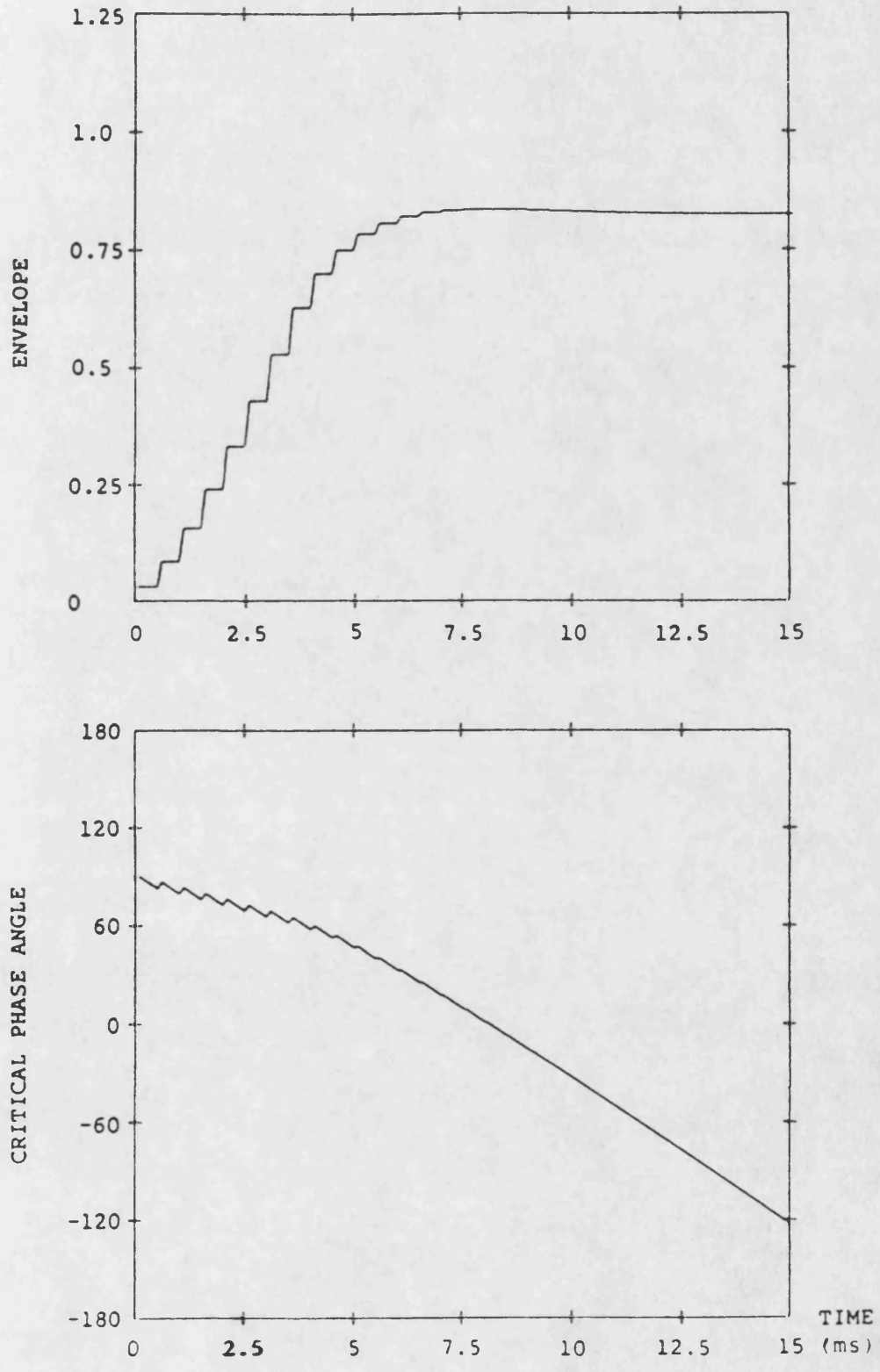

Fig 5.11 DIGITAL HIGH PASS FILTER CHARACTERISTIC
(DIFFERENCE OVER 7 SAMPLES)

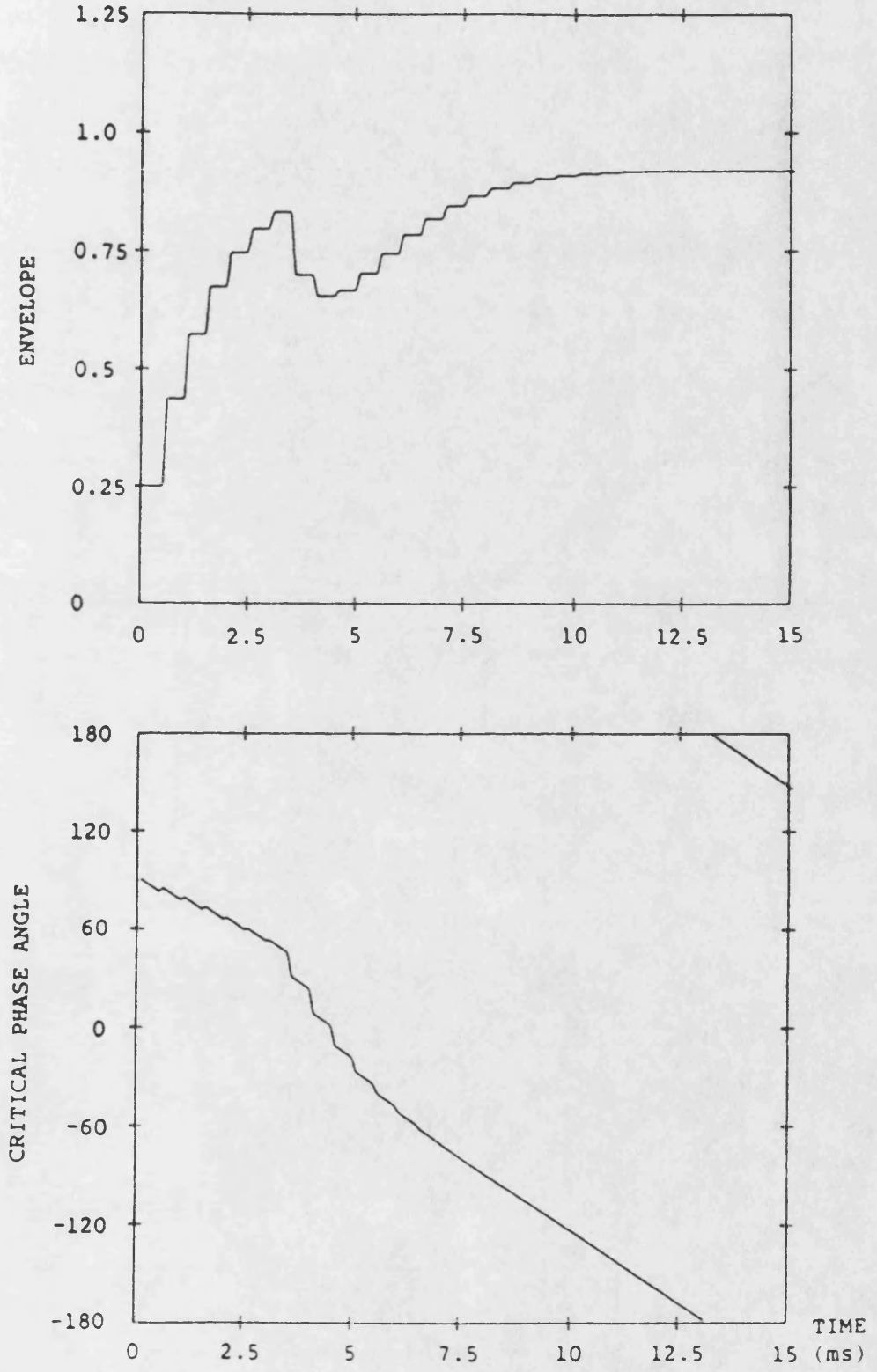

Fig 5.12 DIGITAL HIGH PASS FILTER CHARACTERISTICS

(USING AN LP FILTER)

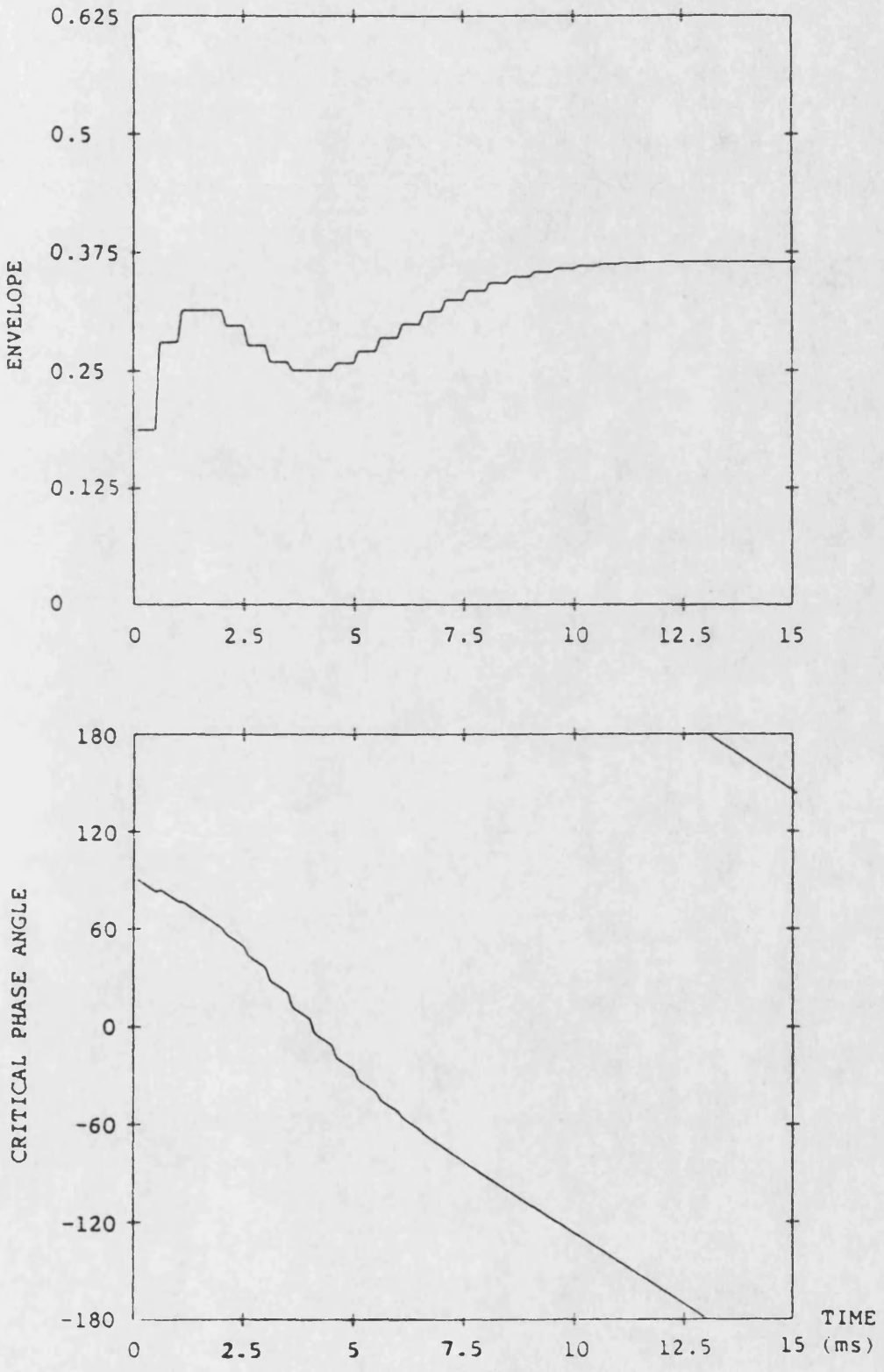

Fig 5.13 DIGITAL HIGH PASS FILTER CHARACTERISTICS
(DIFFERENCE USING 2 LP FILTERS)

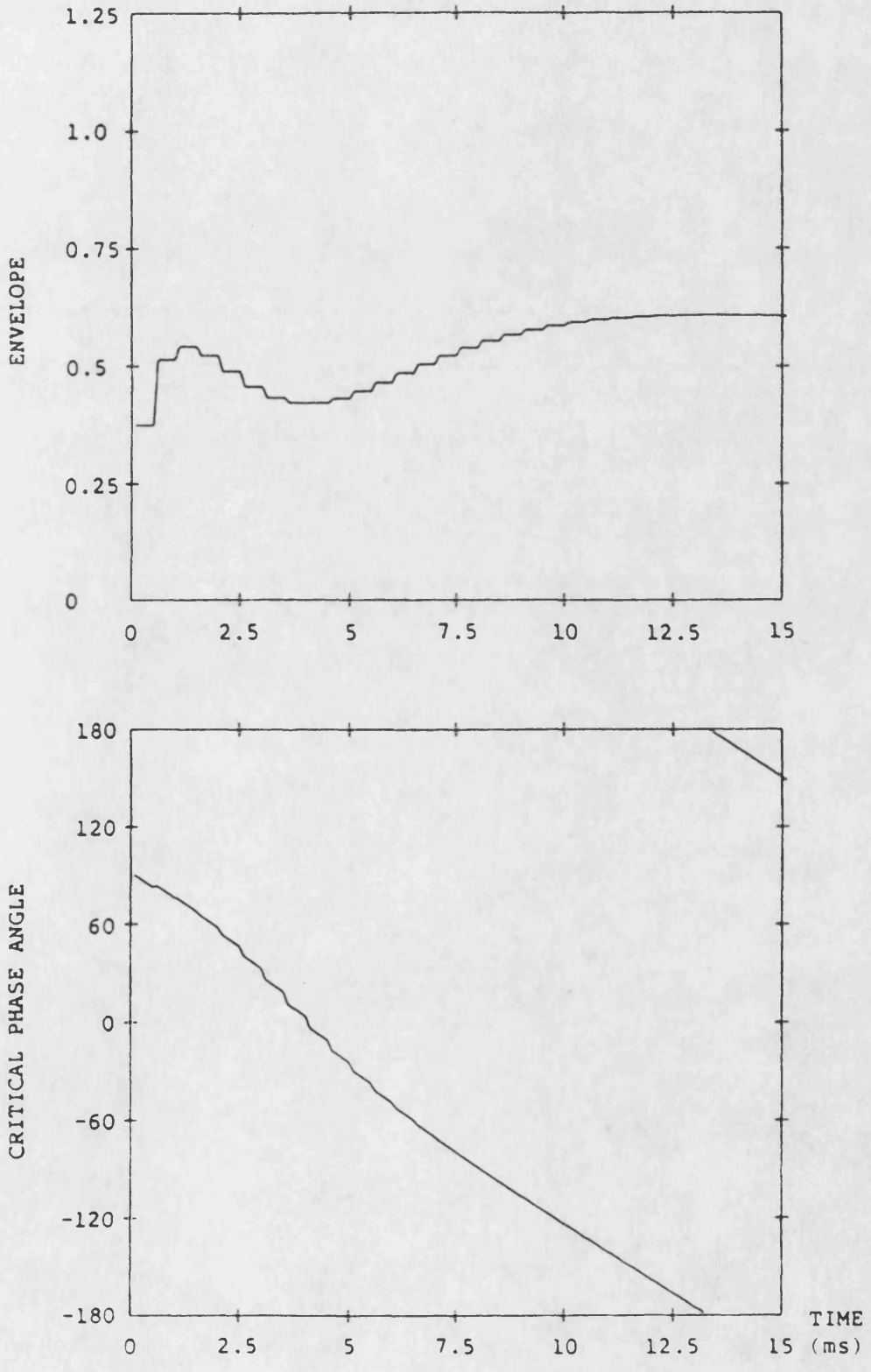

Fig 5.14 DIGITAL HIGH PASS FILTER (TRANSVERSAL) CHARACTERISTICS

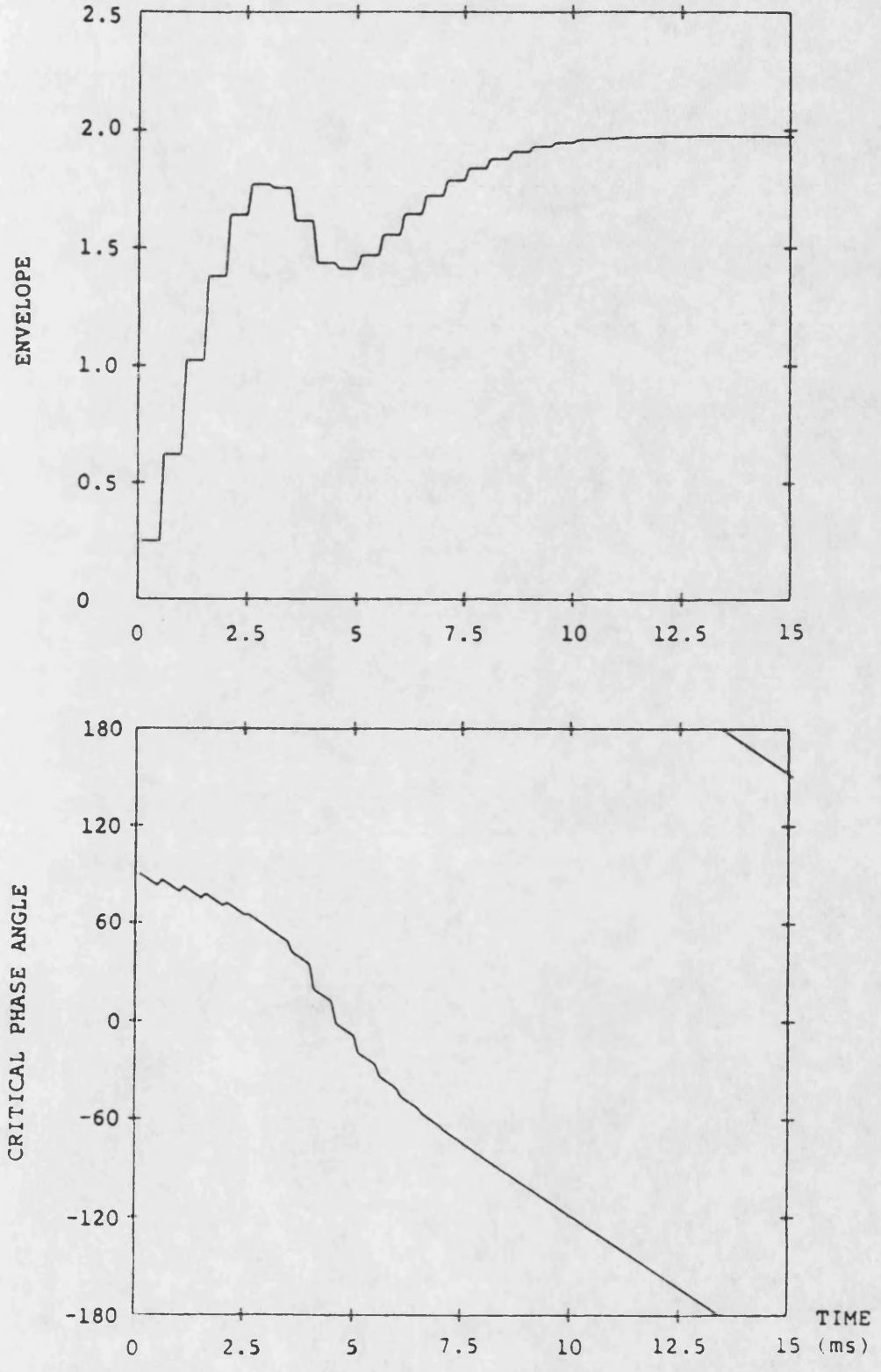

COMPARISON OF LOW AND (SCALED) HIGH PASS FILTER OUTPUTS

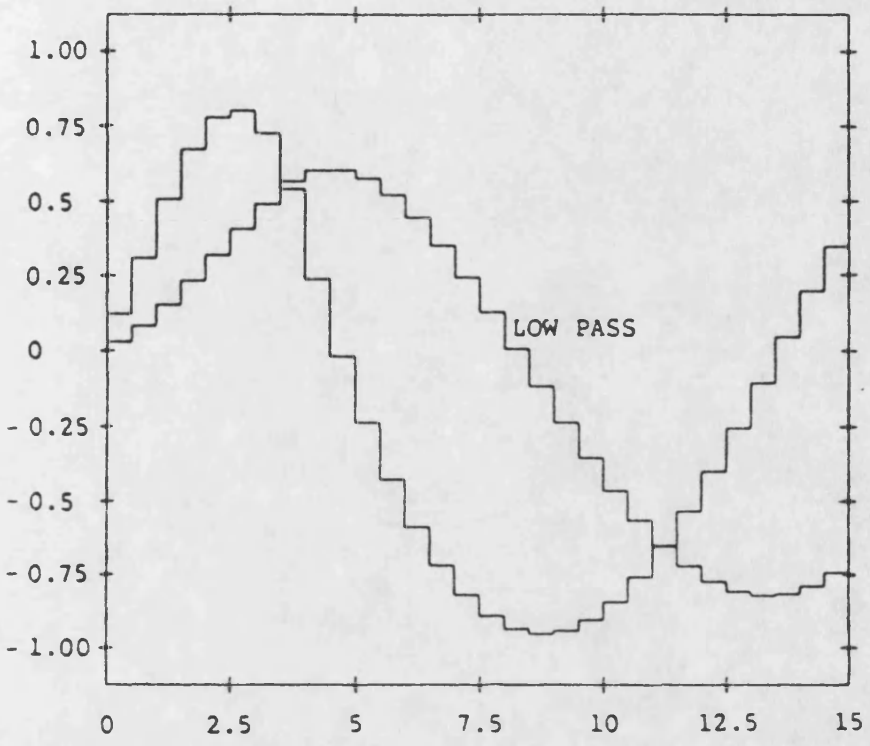

Fig 5.15a COSINUSOIDAL INPUT

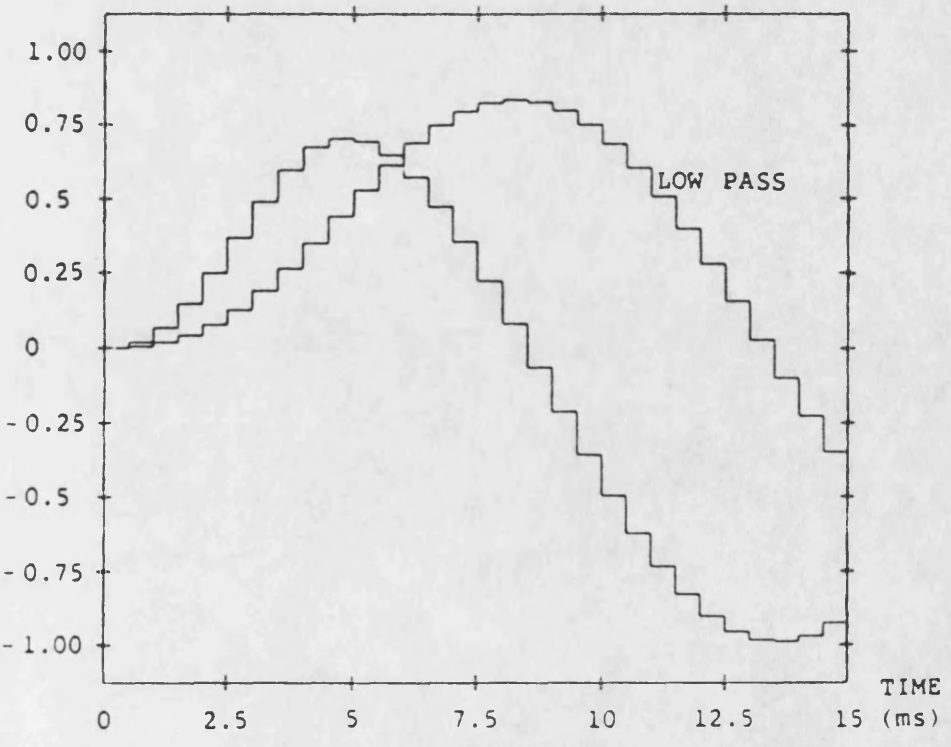

Fig 5.15b SINUSOIDAL INPUT

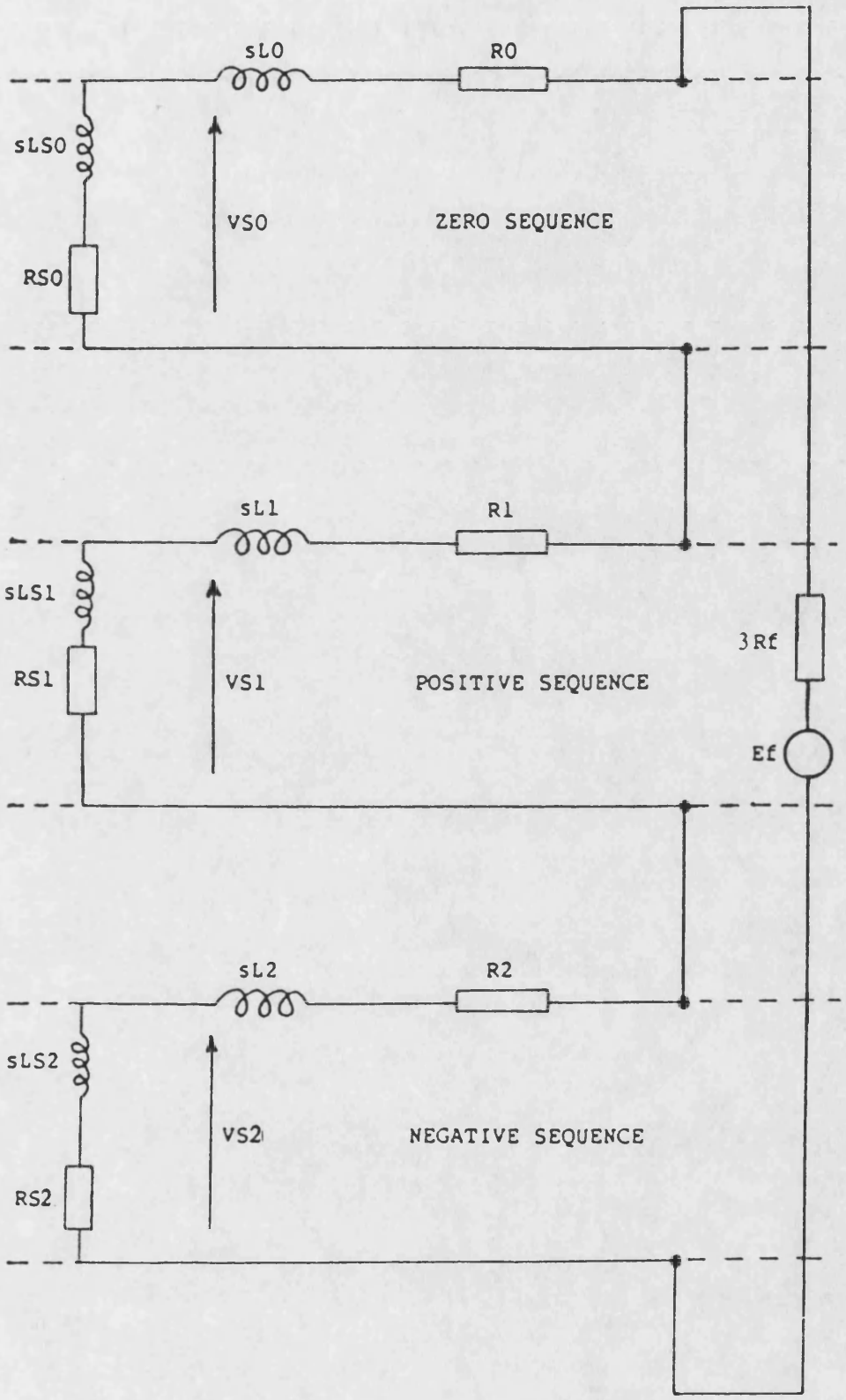

Fig 5.16 SEQUENCE NETWORK CONNEXION FOR AN A-E FAULT

(SUPERIMPOSED COMPONENT)

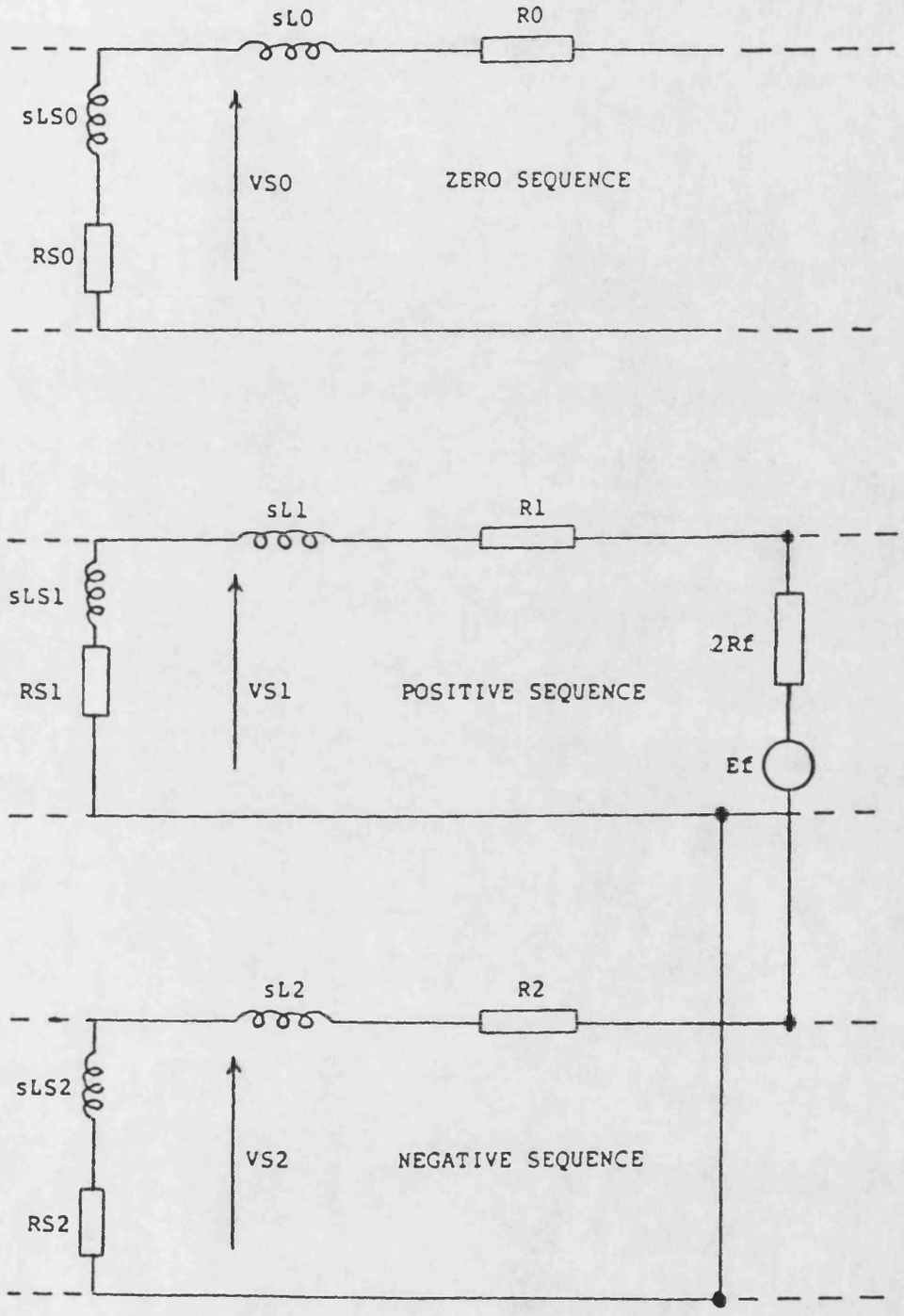

Fig 5.17 SEQUENCE NETWORK CONNEXION FOR A B-C FAULT

(SUPERIMPOSED COMPONENT)

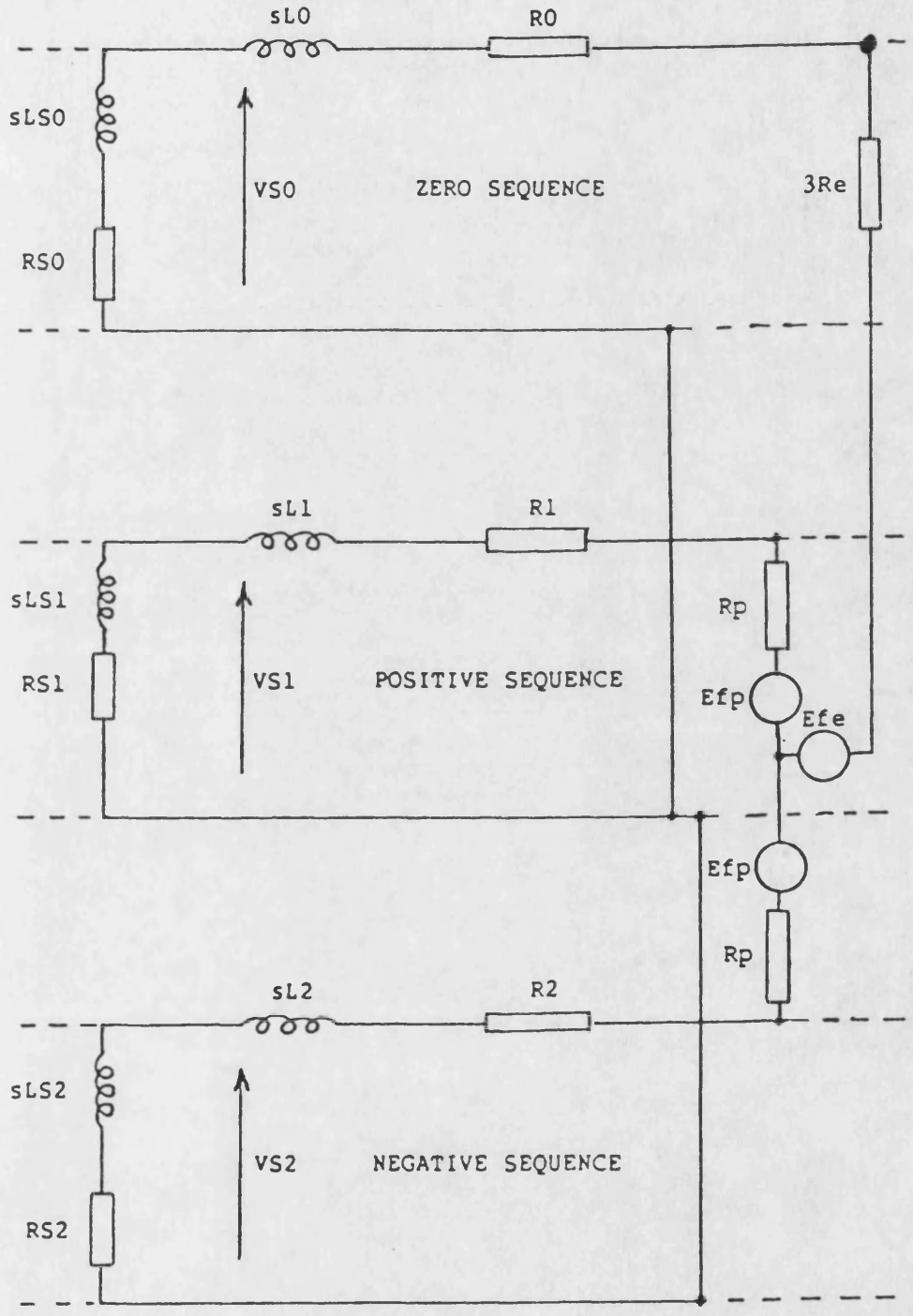

Fig 5.18 SEQUENCE NETWORK CONNEXION FOR A B-C-E FAULT

(SUPERIMPOSED COMPONENT)

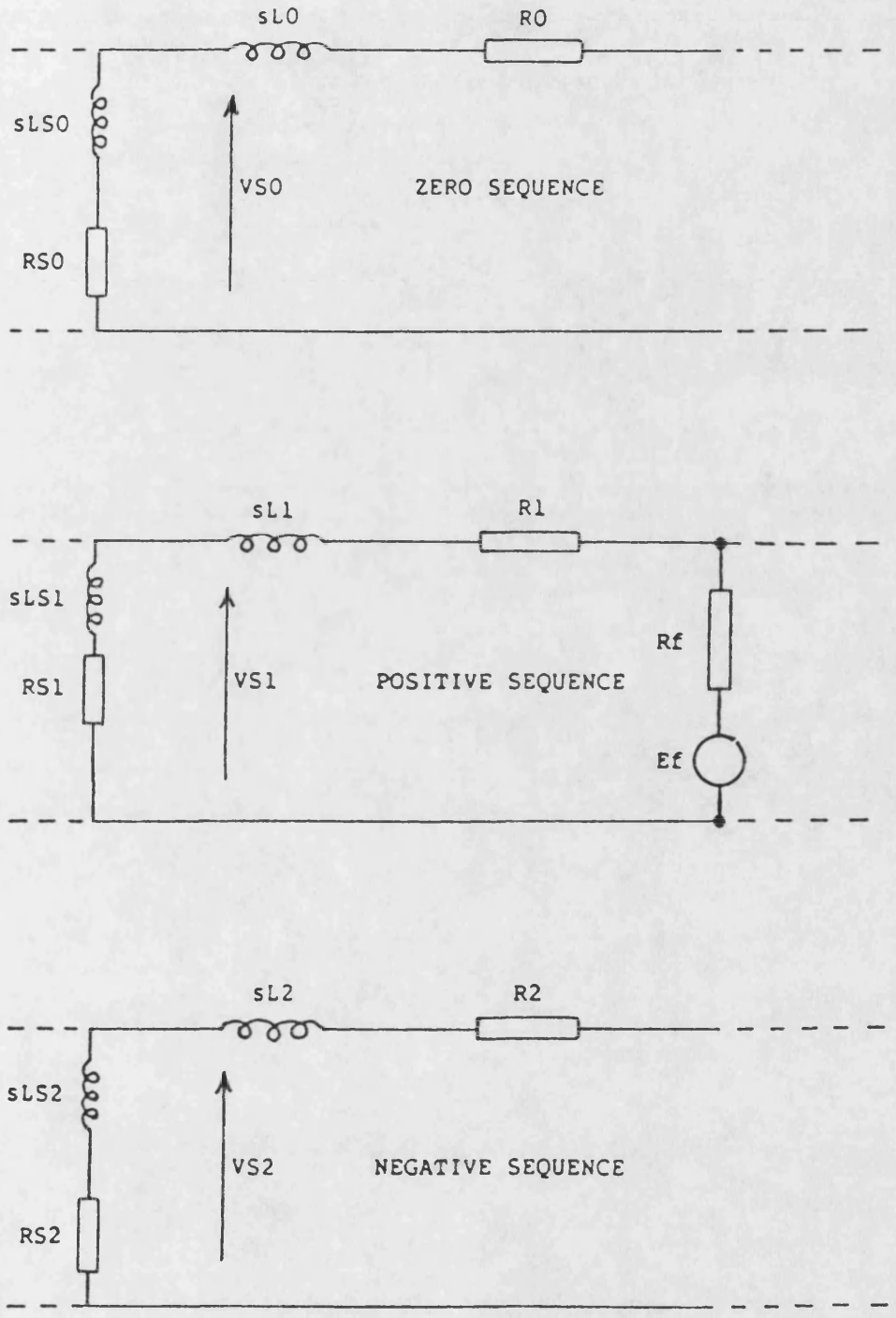

Fig 5.19

SEQUENCE NETWORK CONNEXION FOR A BALANCED THREE PHASE FAULT

(SUPERIMPOSED COMPONENT)

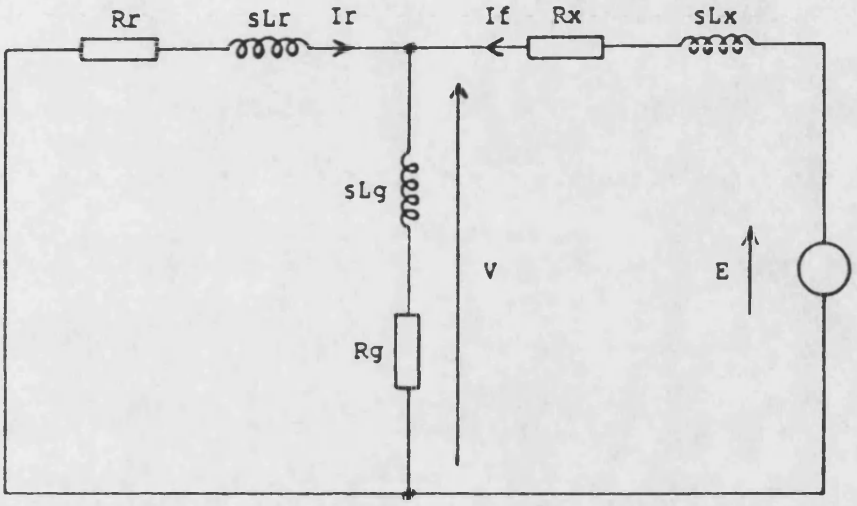

Fig 5.20a SUPERIMPOSED QUANTITY PRINCIPLE

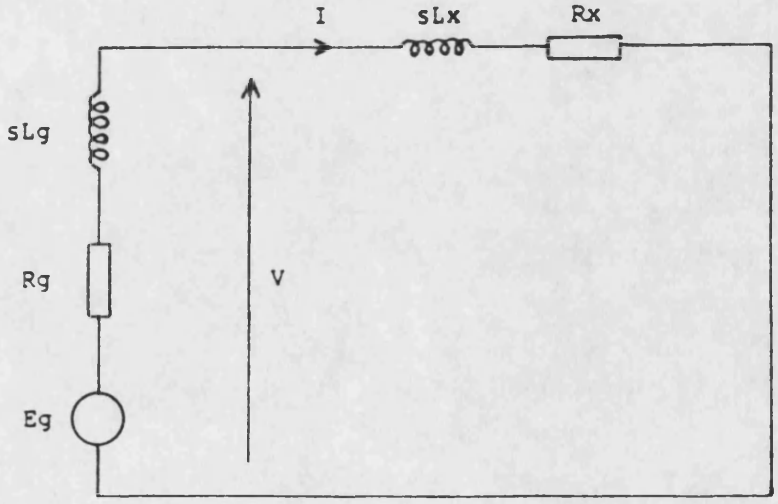

Fig 5.20b TOTAL QUANTITY PRINCIPLE

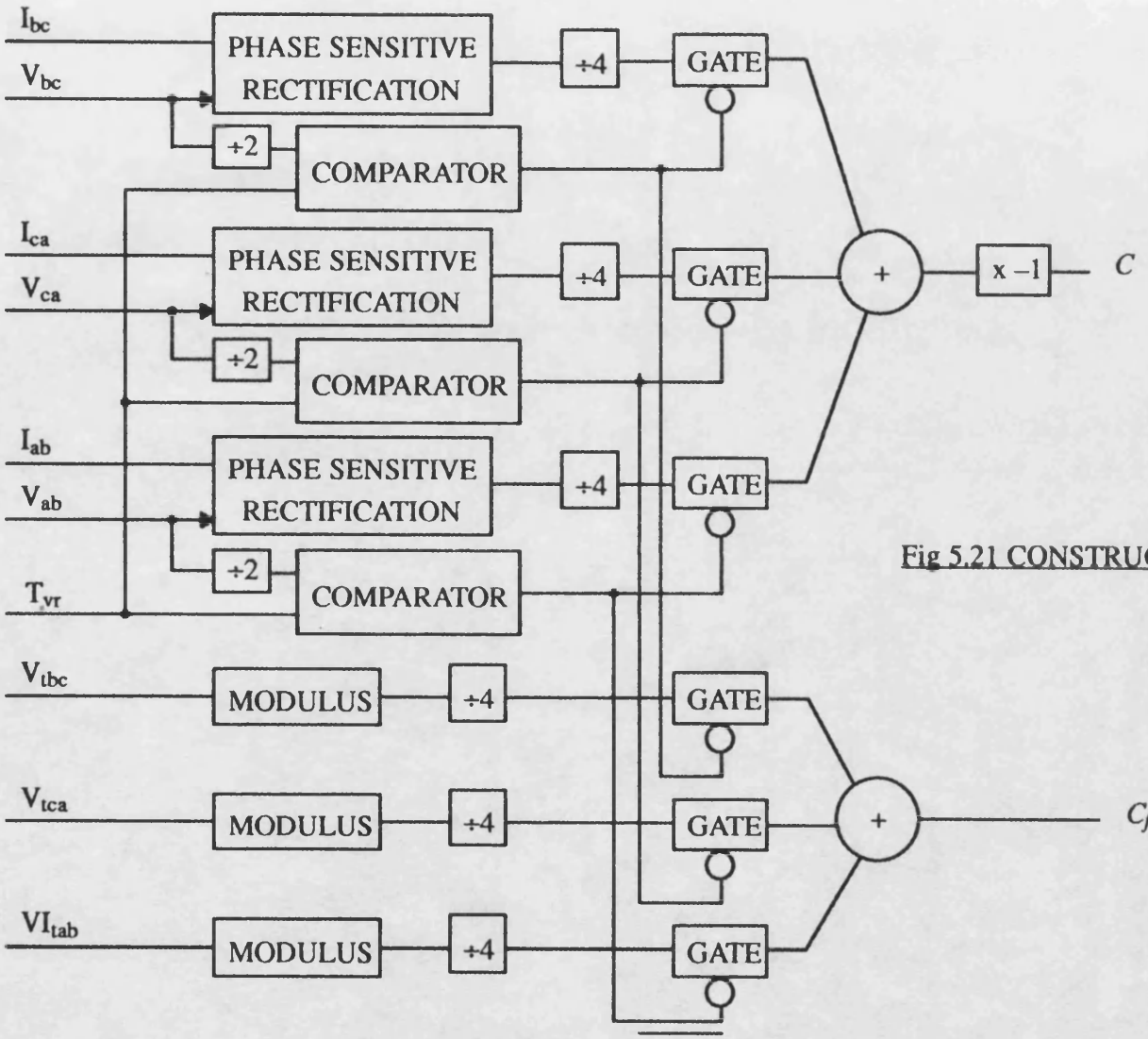

Fig 5.21 CONSTRUCTION OF CURRENT DISCRIMINANTS

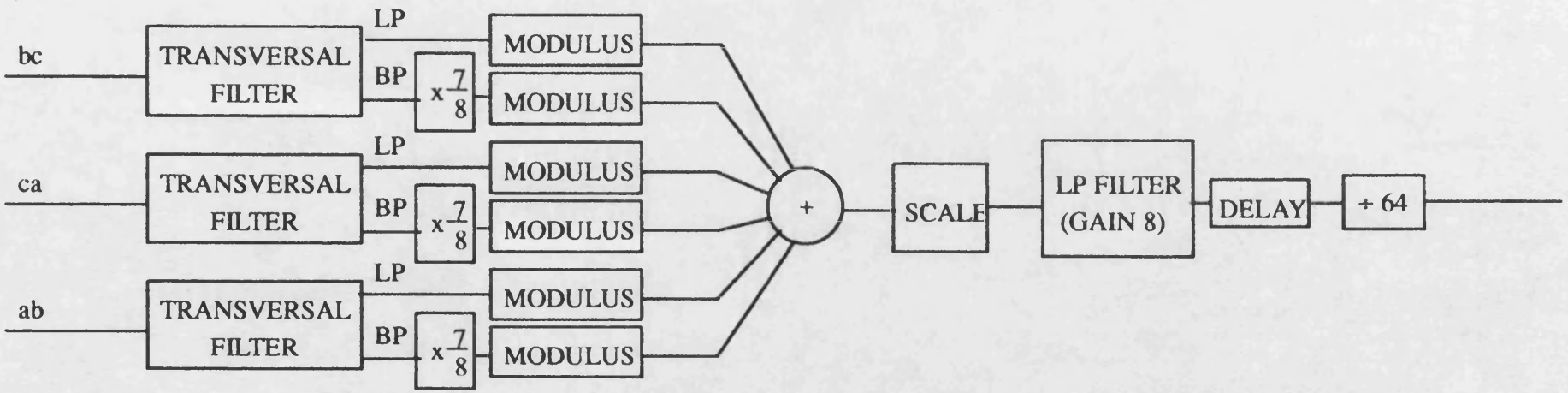

Fig 5.22 PHASE SHIFT OBTAINED BY FILTERING

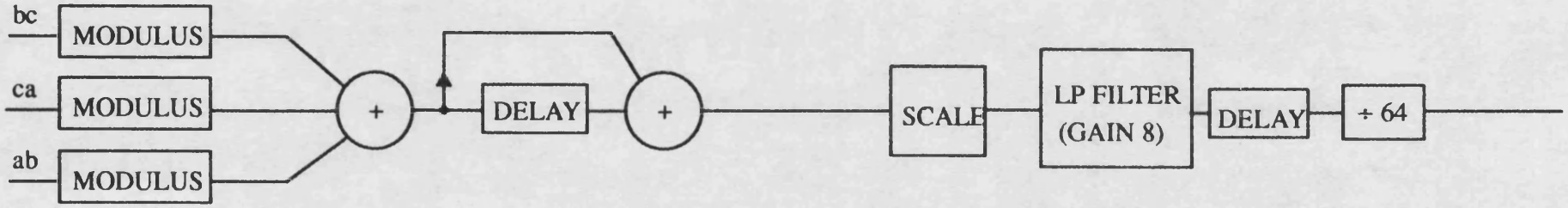

Fig 5.23 PHASE SHIFT OBTAINED BY TIME DELAY

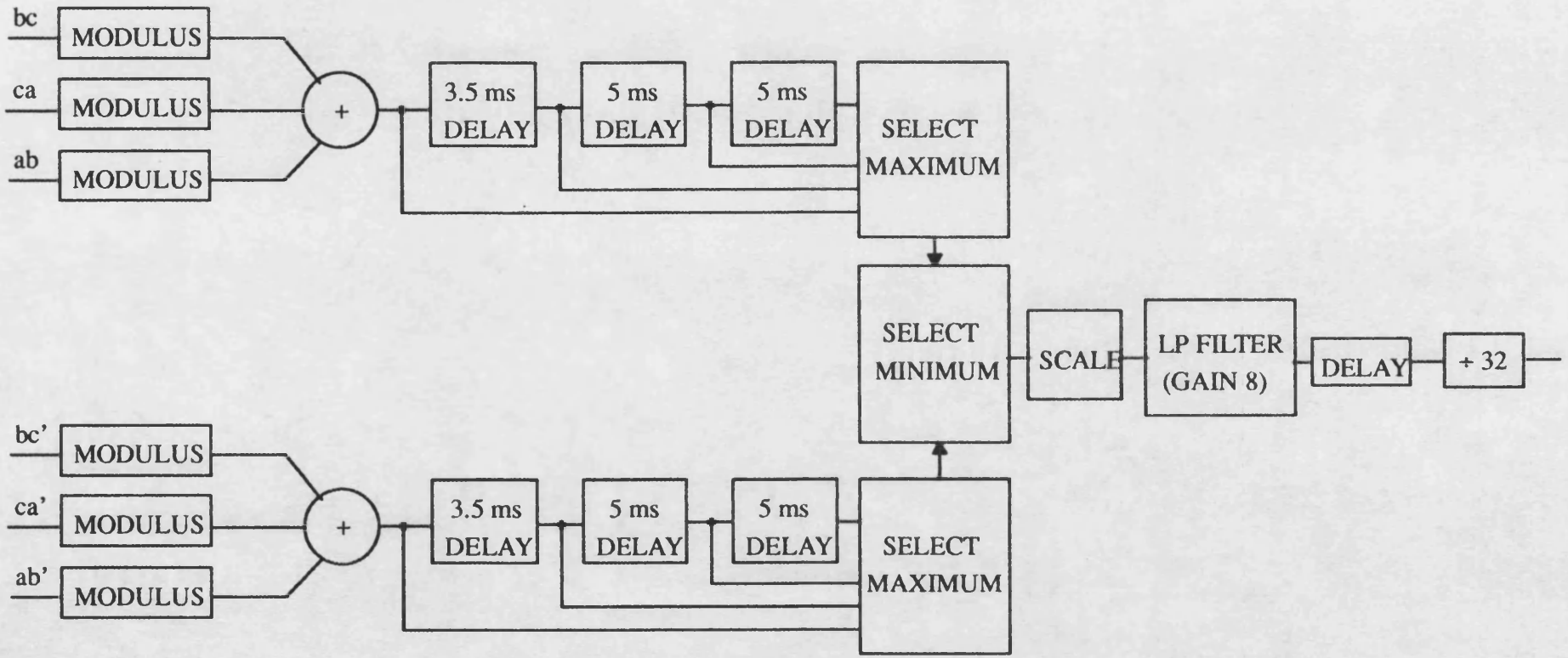

Fig 5.24 IMPLEMENTATION USING SIGNALS WHICH HAVE UNDERGONE A DIFFERENT NUMBER OF STAGES OF SUPERIMPOSED COMPONENT EXTRACTION FILTERING

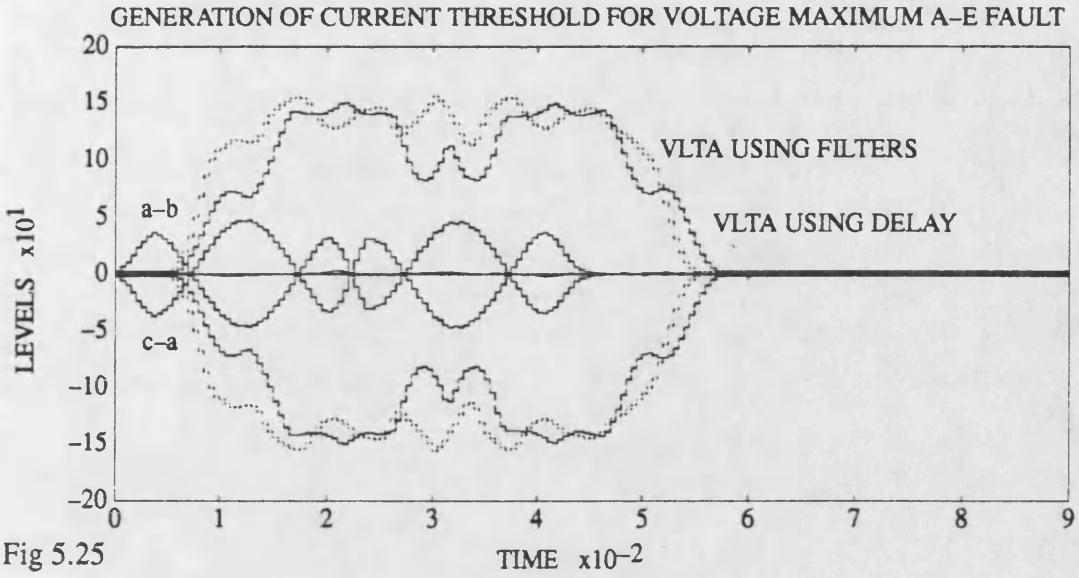

Fig 5.25

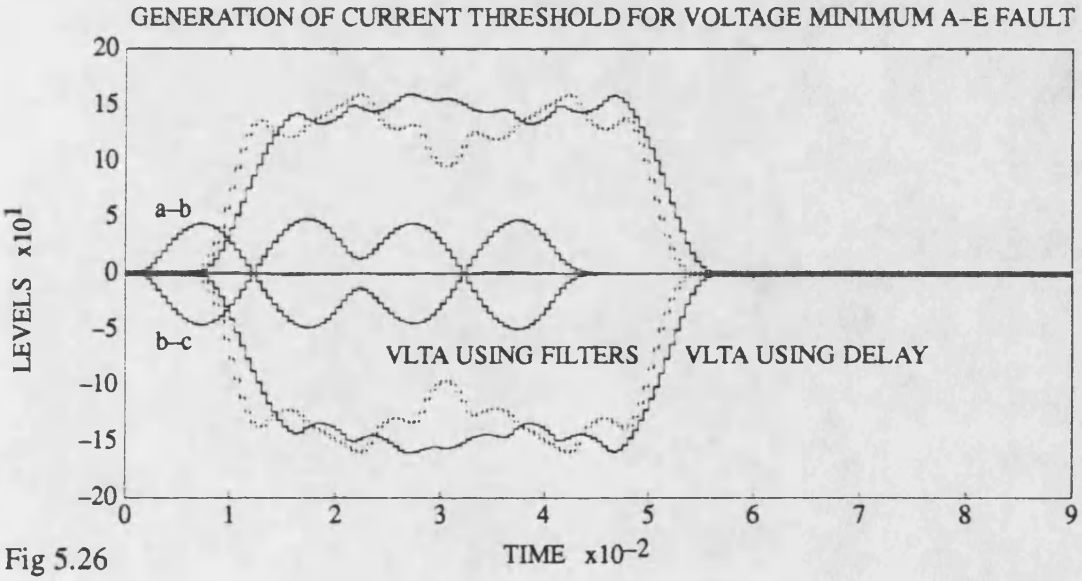

Fig 5.26

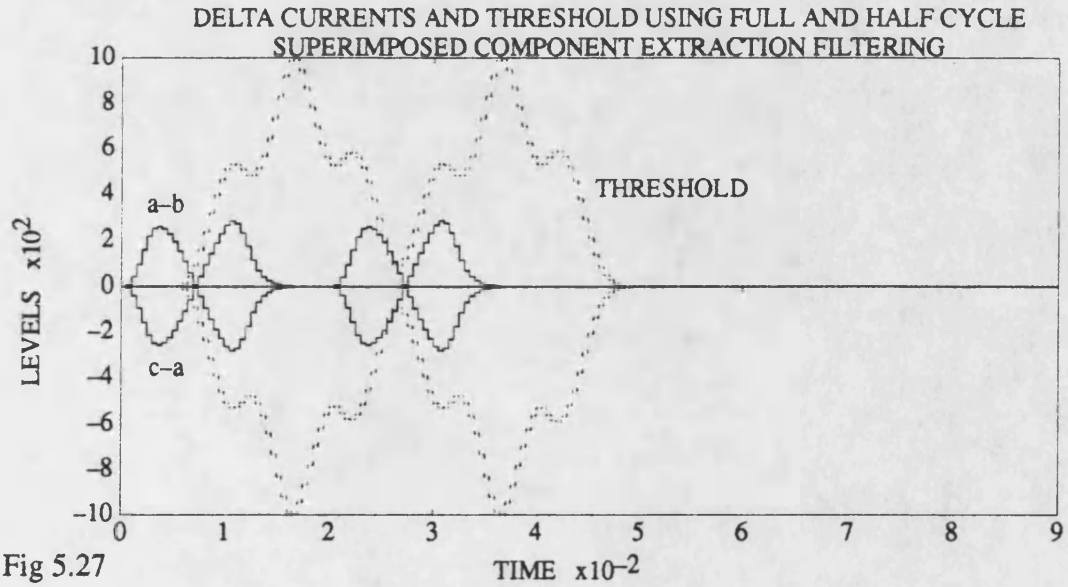

Fig 5.27

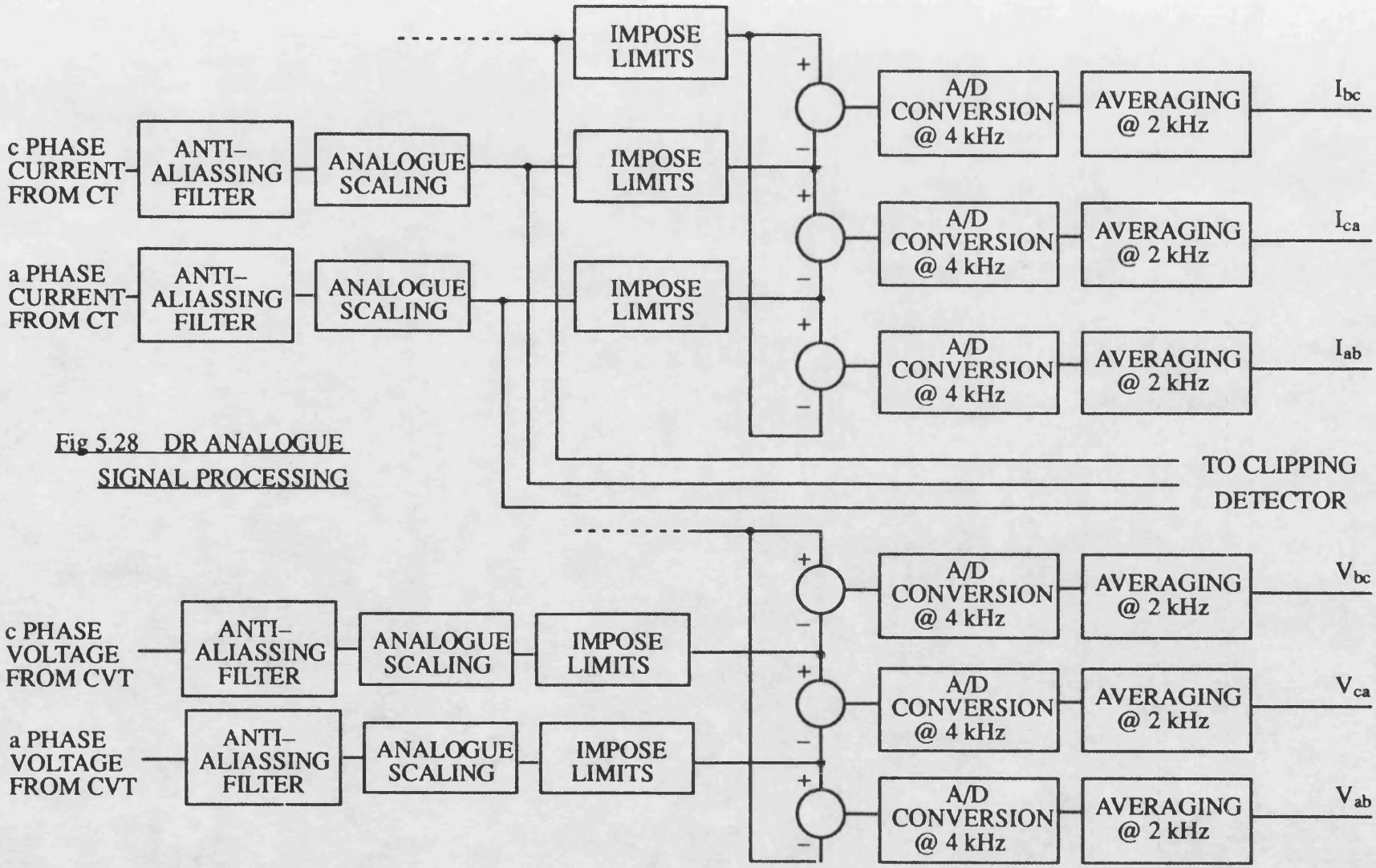

Fig 5.28 DR ANALOGUE SIGNAL PROCESSING

Fig 5.29 DIRECTIONAL RELAY FILTERING

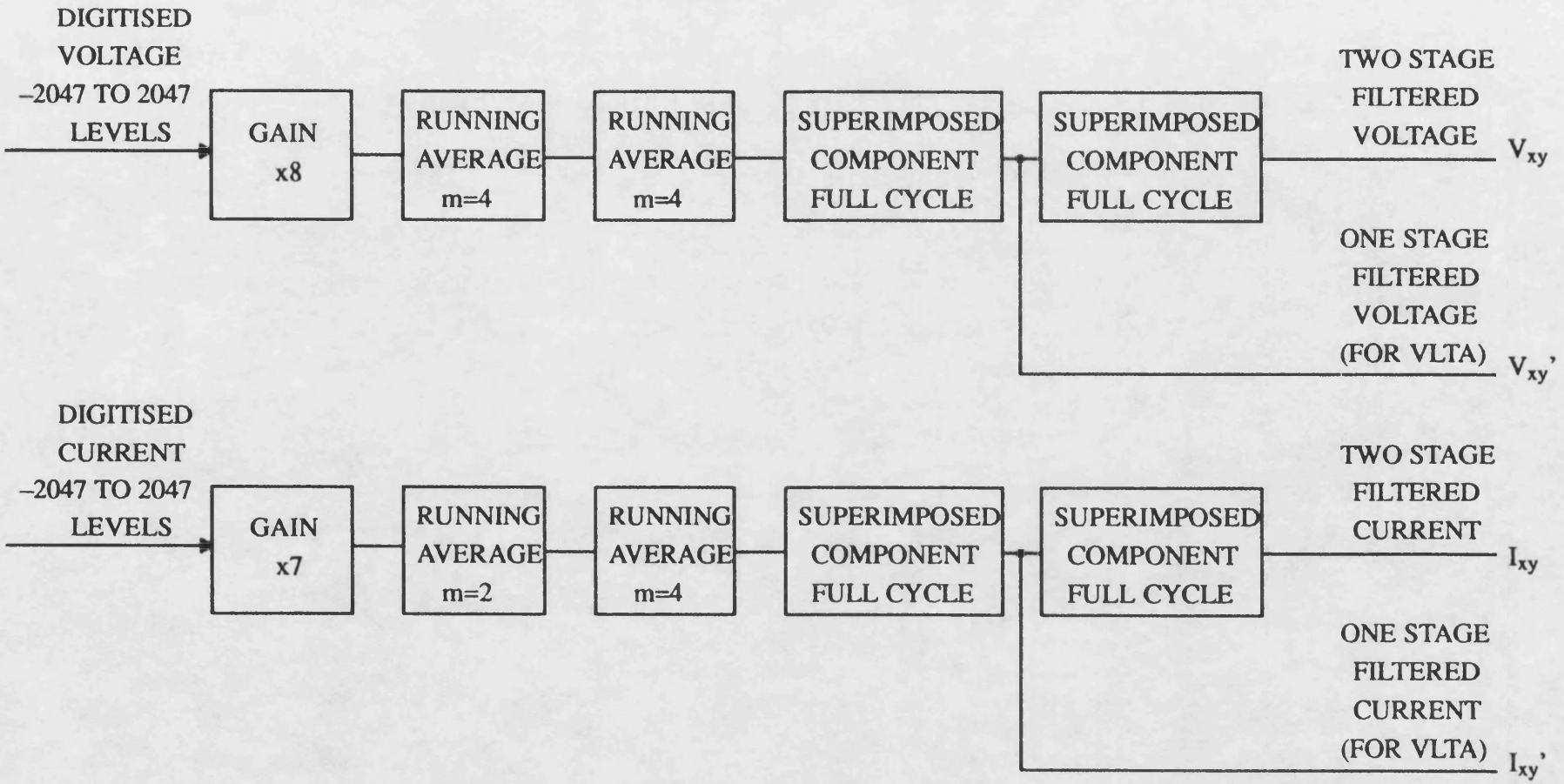

Fig 5.30 DIRECTIONAL RELAY BLOCK DIAGRAM

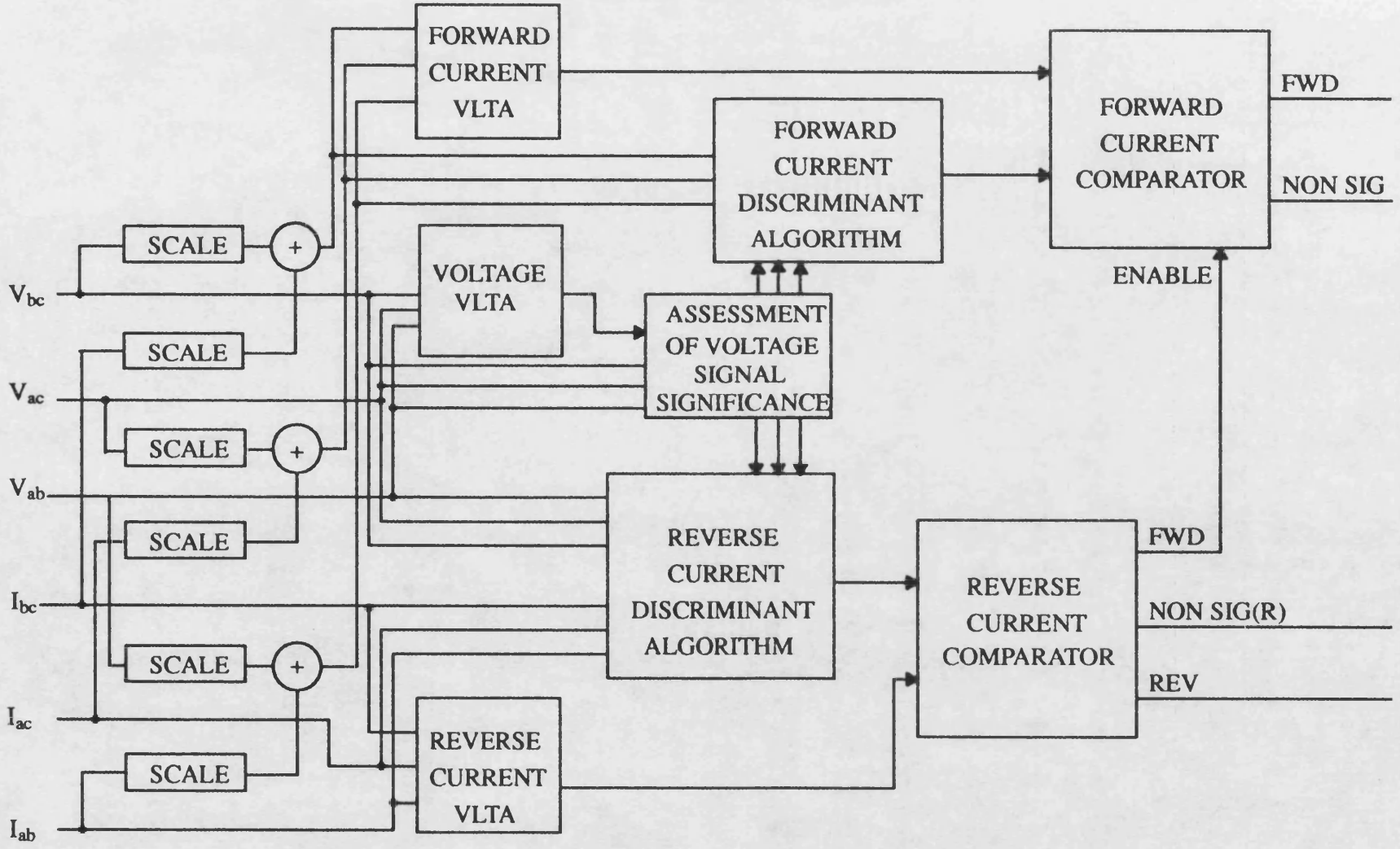

Fig 5.31 CLIPPING DETECTOR

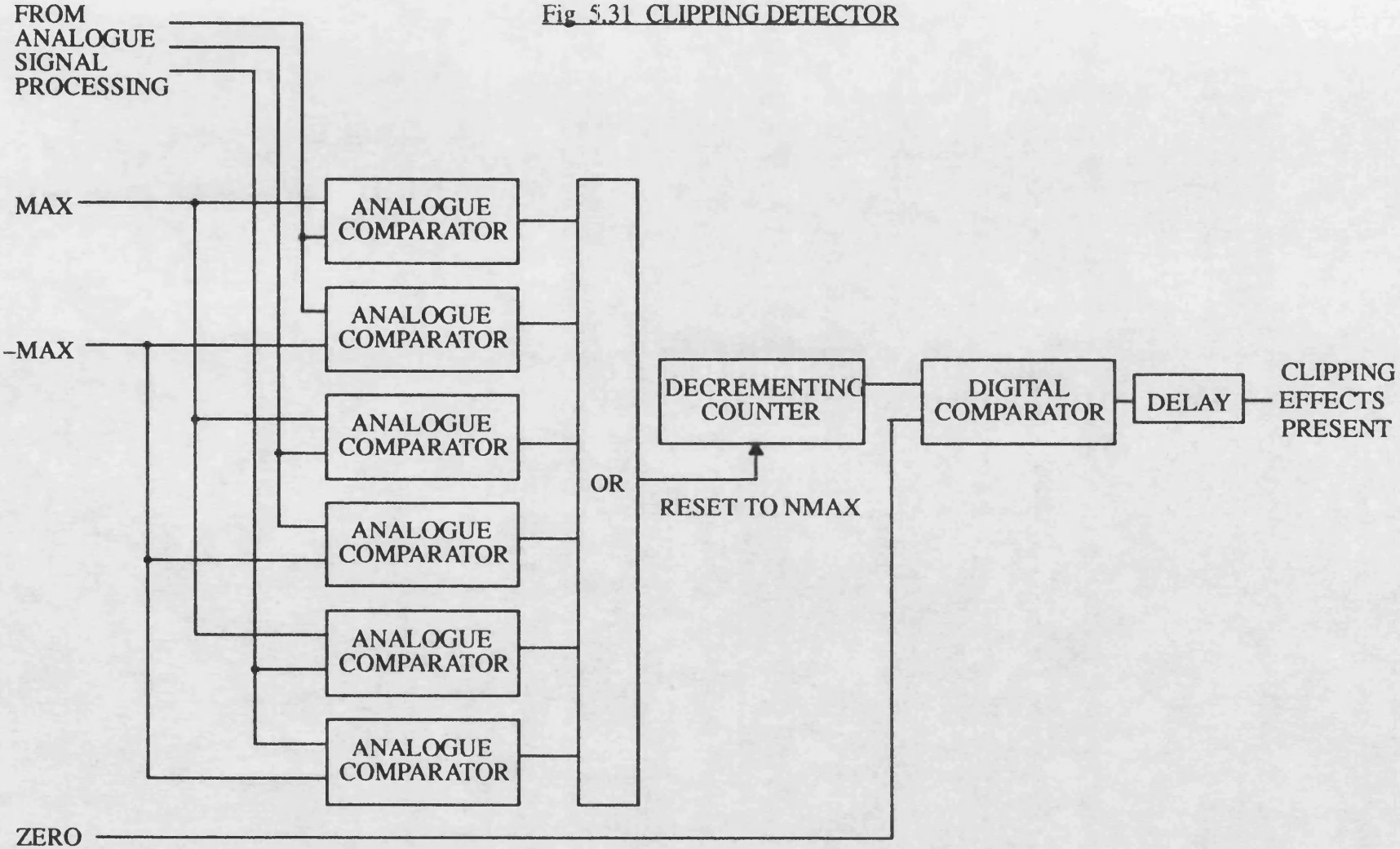

Fig 5.32 DIRECTIONAL RELAY DECISION PROCESS

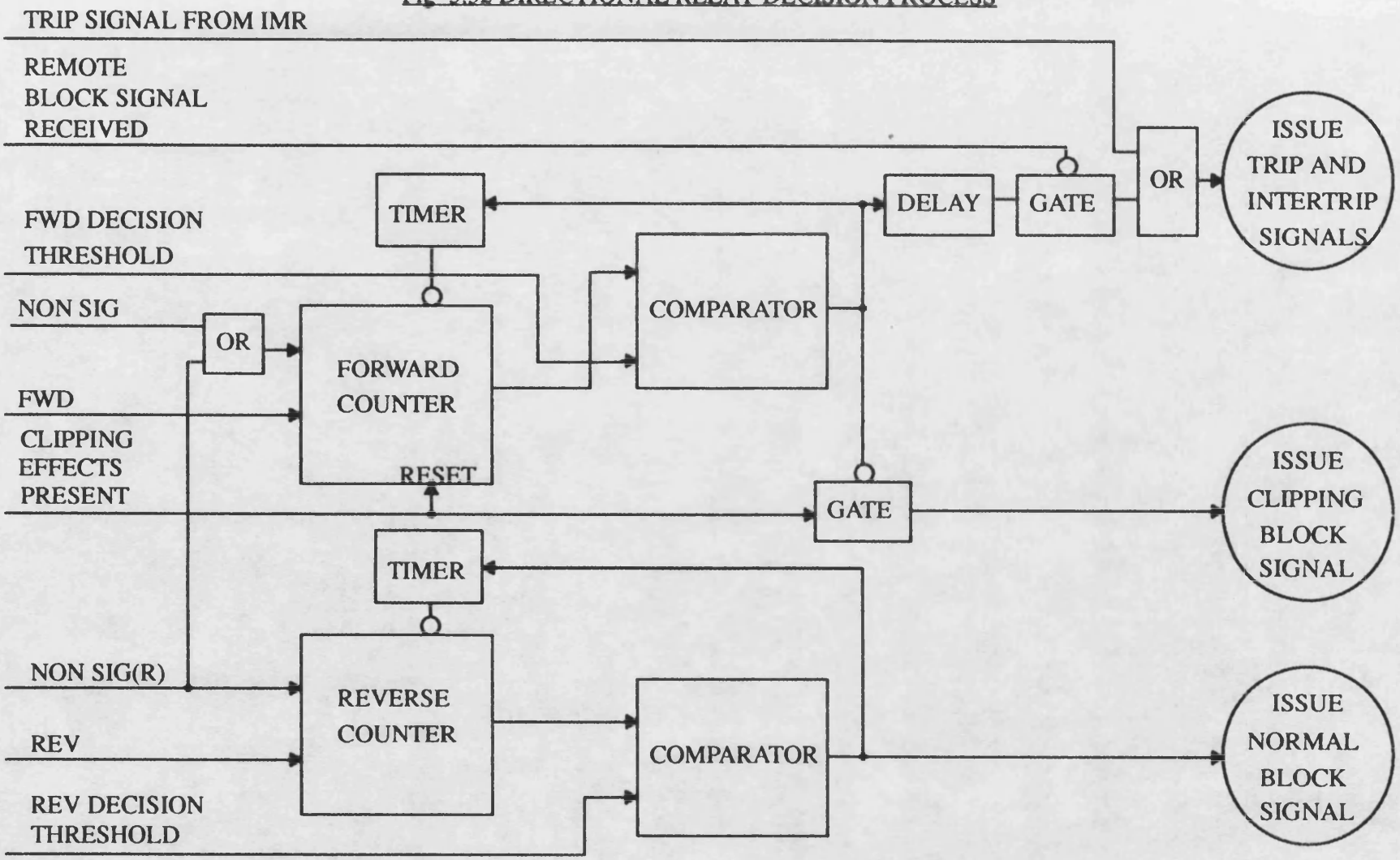

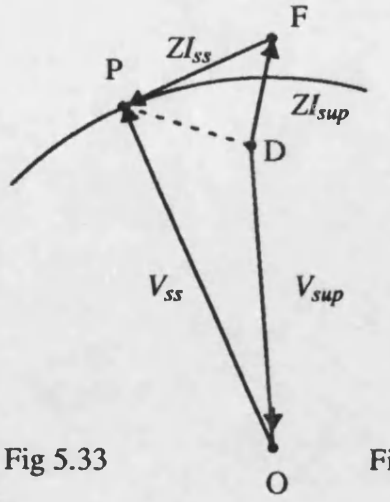

Fig 5.33

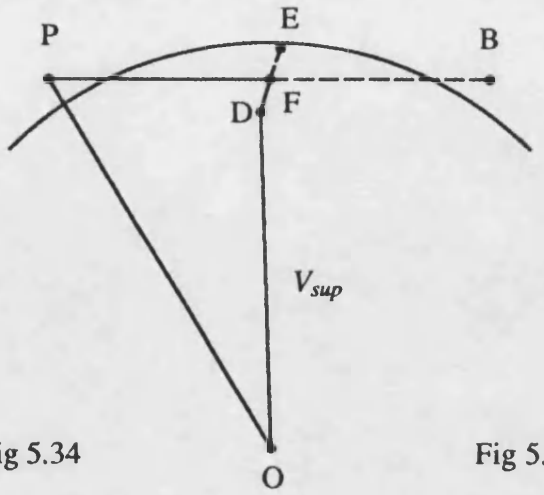

Fig 5.34

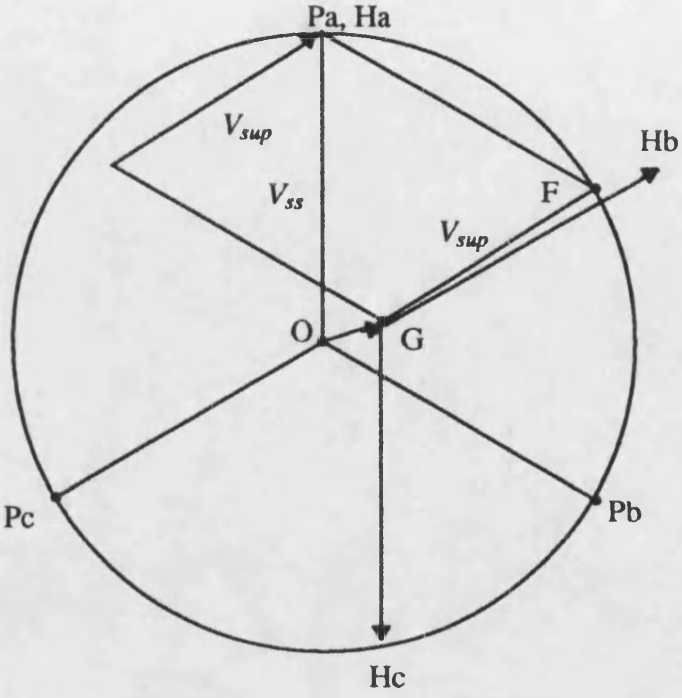

Fig 5.35

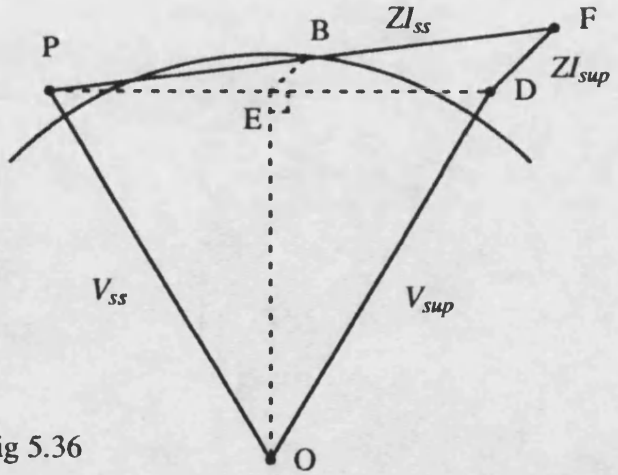

Fig 5.36

Fig 5.37 SIMPLE COMPARATOR SCHEME

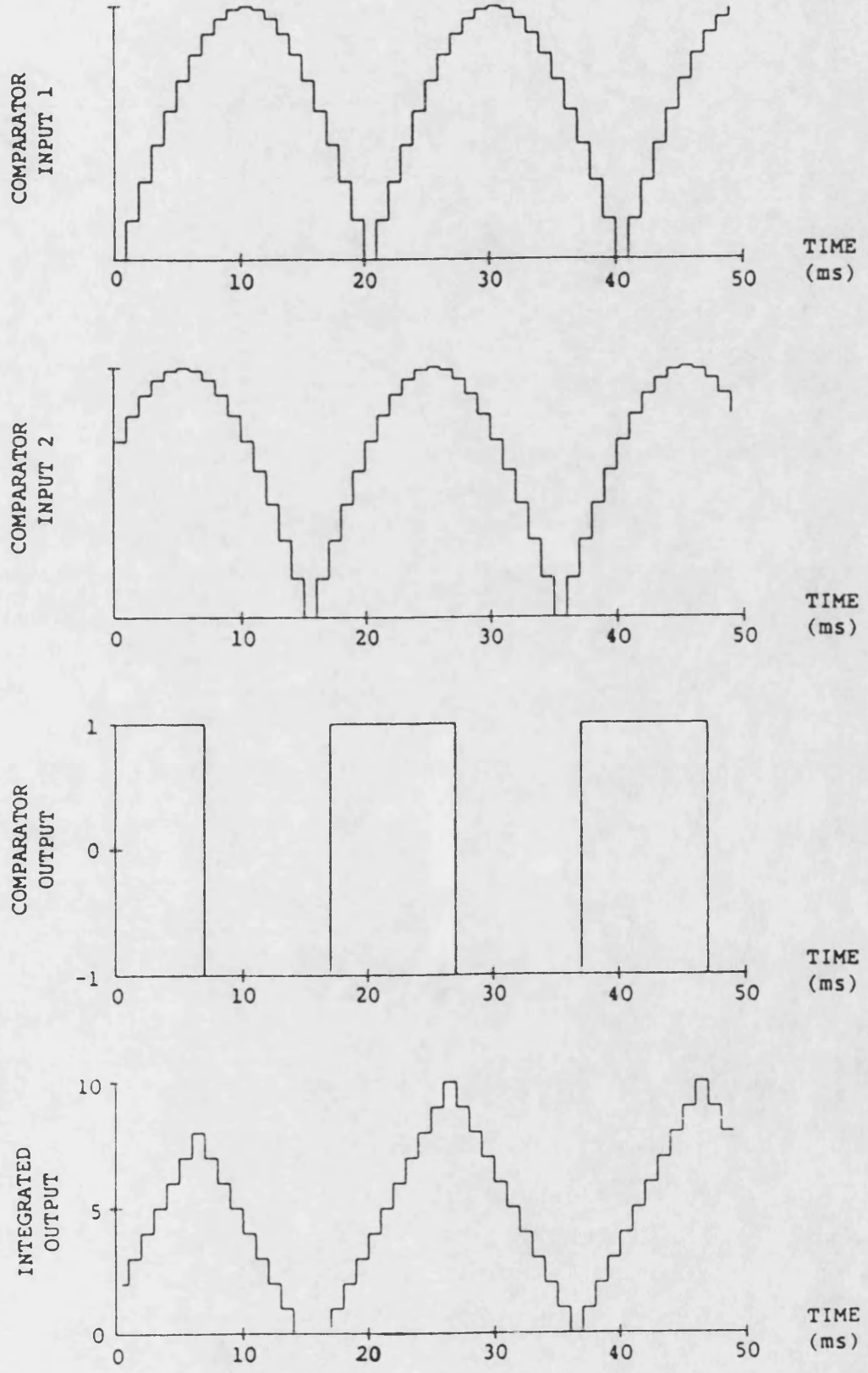

Fig 5.38 MODIFIED COMPARATOR SCHEME

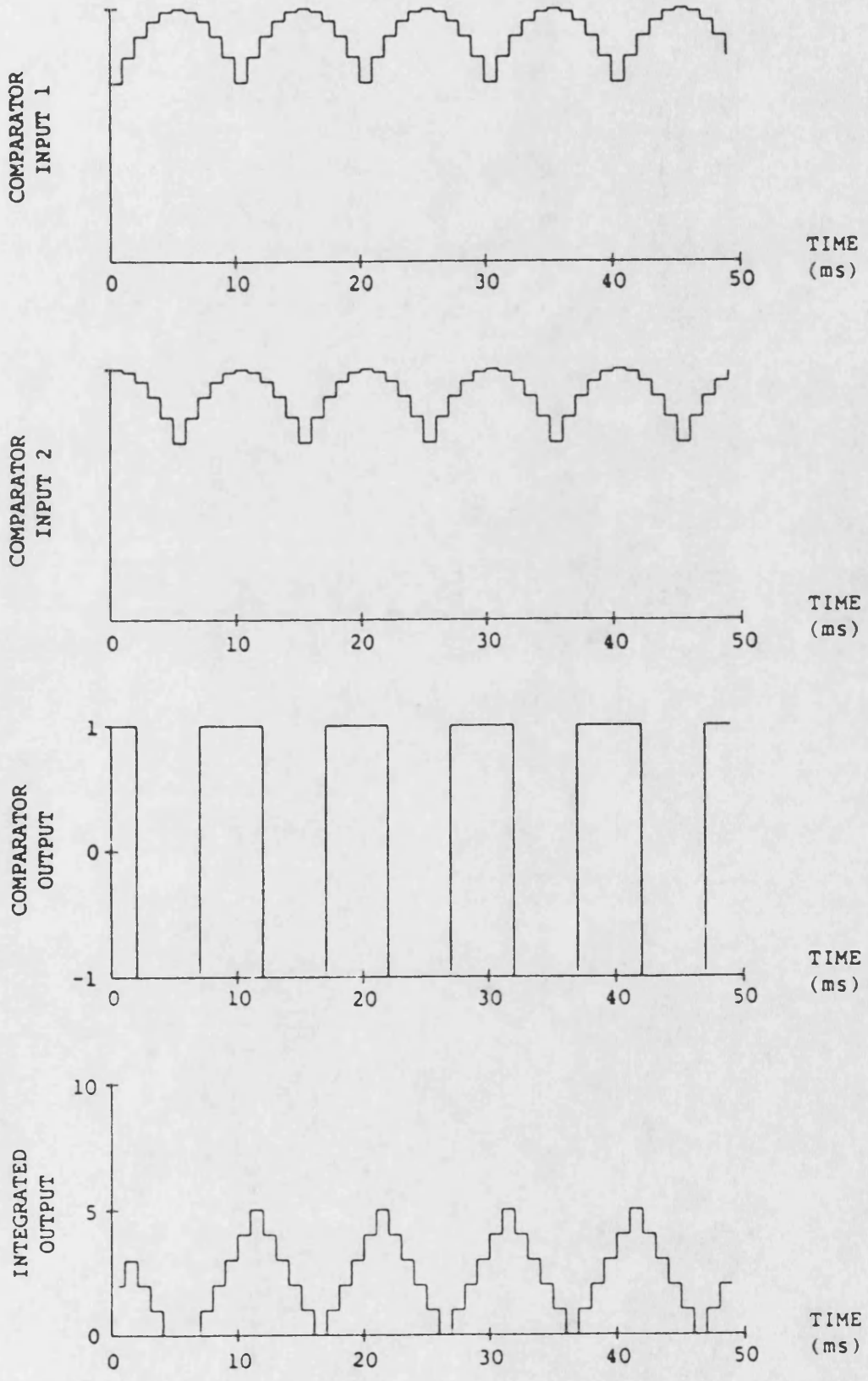

CONSTRUCTION OF SIGNAL PAIRS

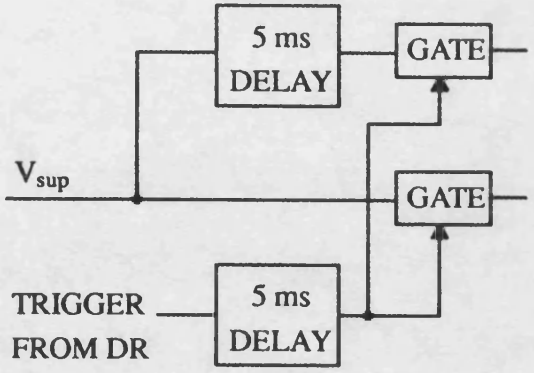

Fig 5.39 SUPERIMPOSED COMPONENT SIGNALS

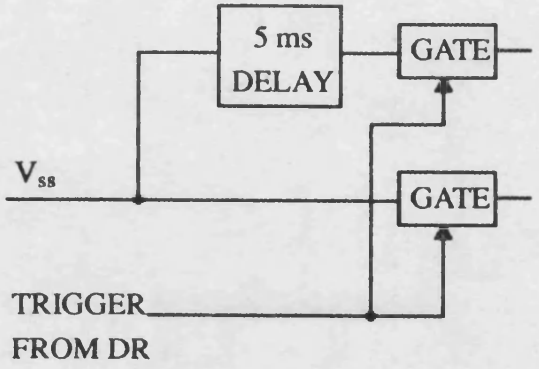

Fig 5.40 PRE–FAULT SIGNALS

IMR ANALOGUE SIGNAL PROCESSING

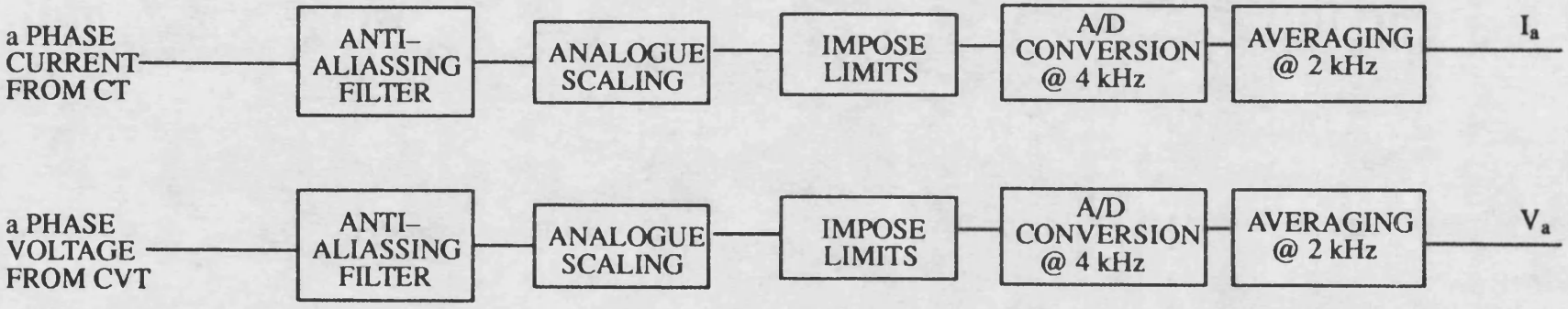

Fig 5.41 a–PHASE QUANTITIES

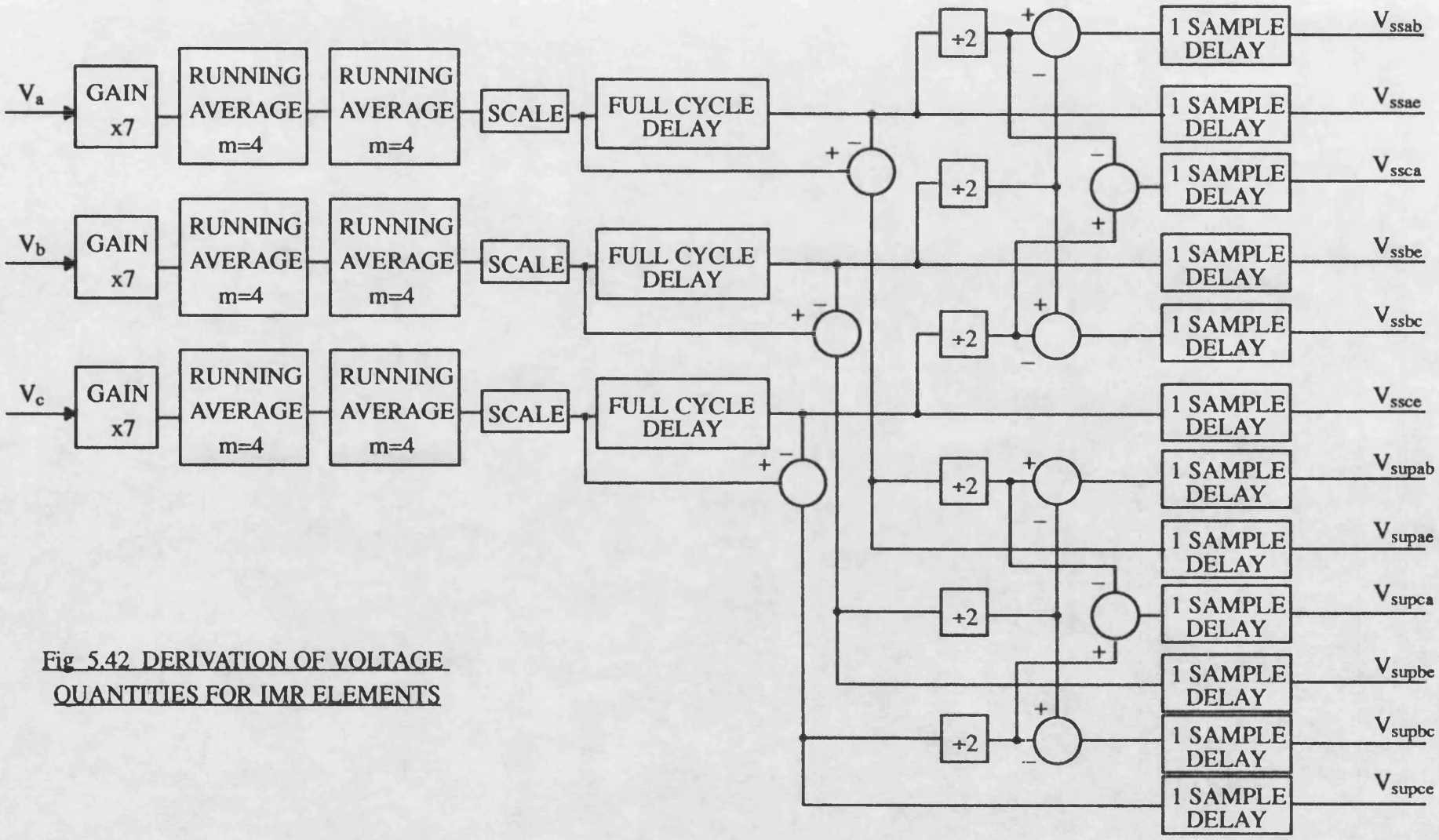

Fig 5.42 DERIVATION OF VOLTAGE QUANTITIES FOR IMR ELEMENTS

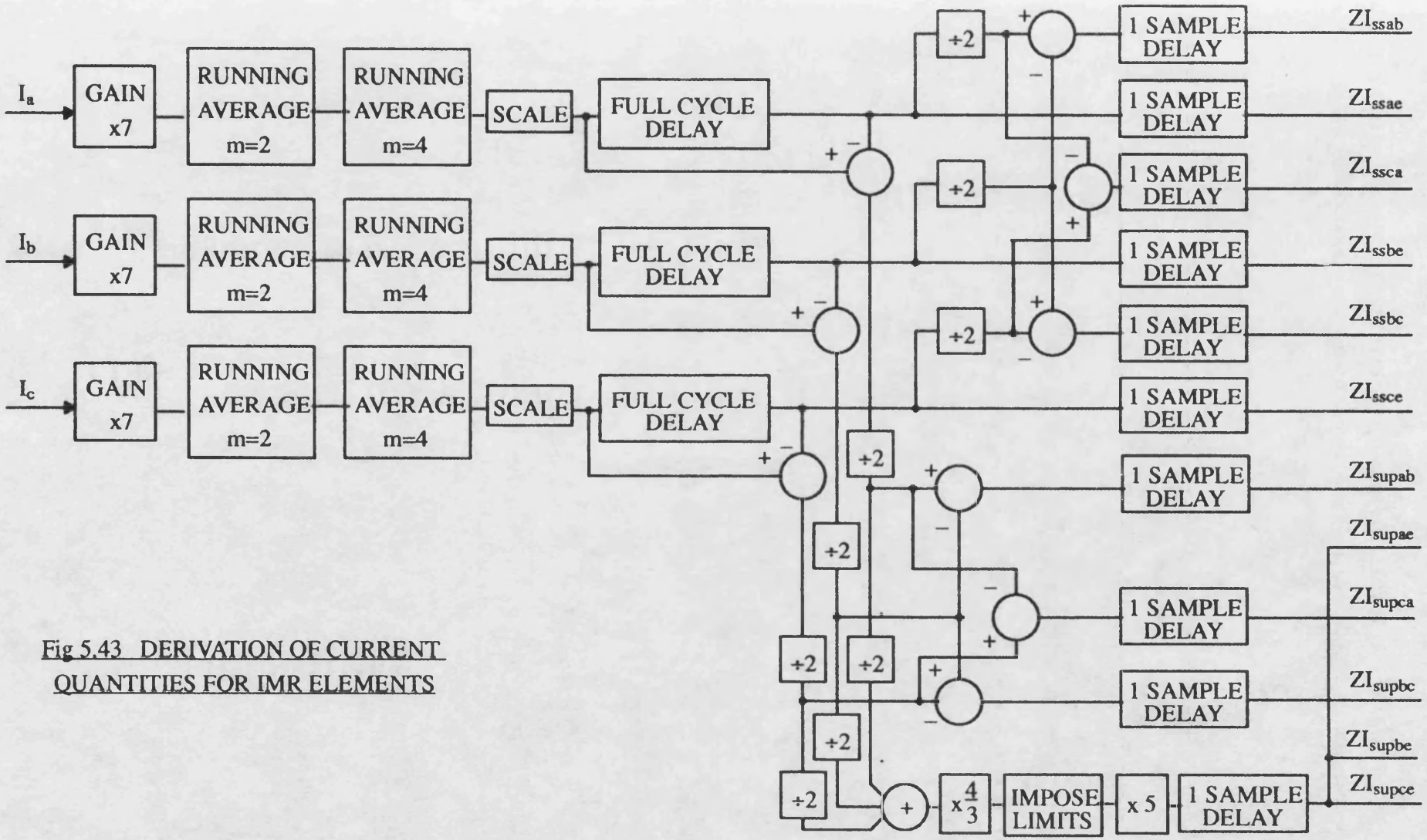

Fig 5.43 DERIVATION OF CURRENT QUANTITIES FOR IMR ELEMENTS

Fig 5.44 IMR DIGITAL SIGNAL PROCESSING (PER ELEMENT)

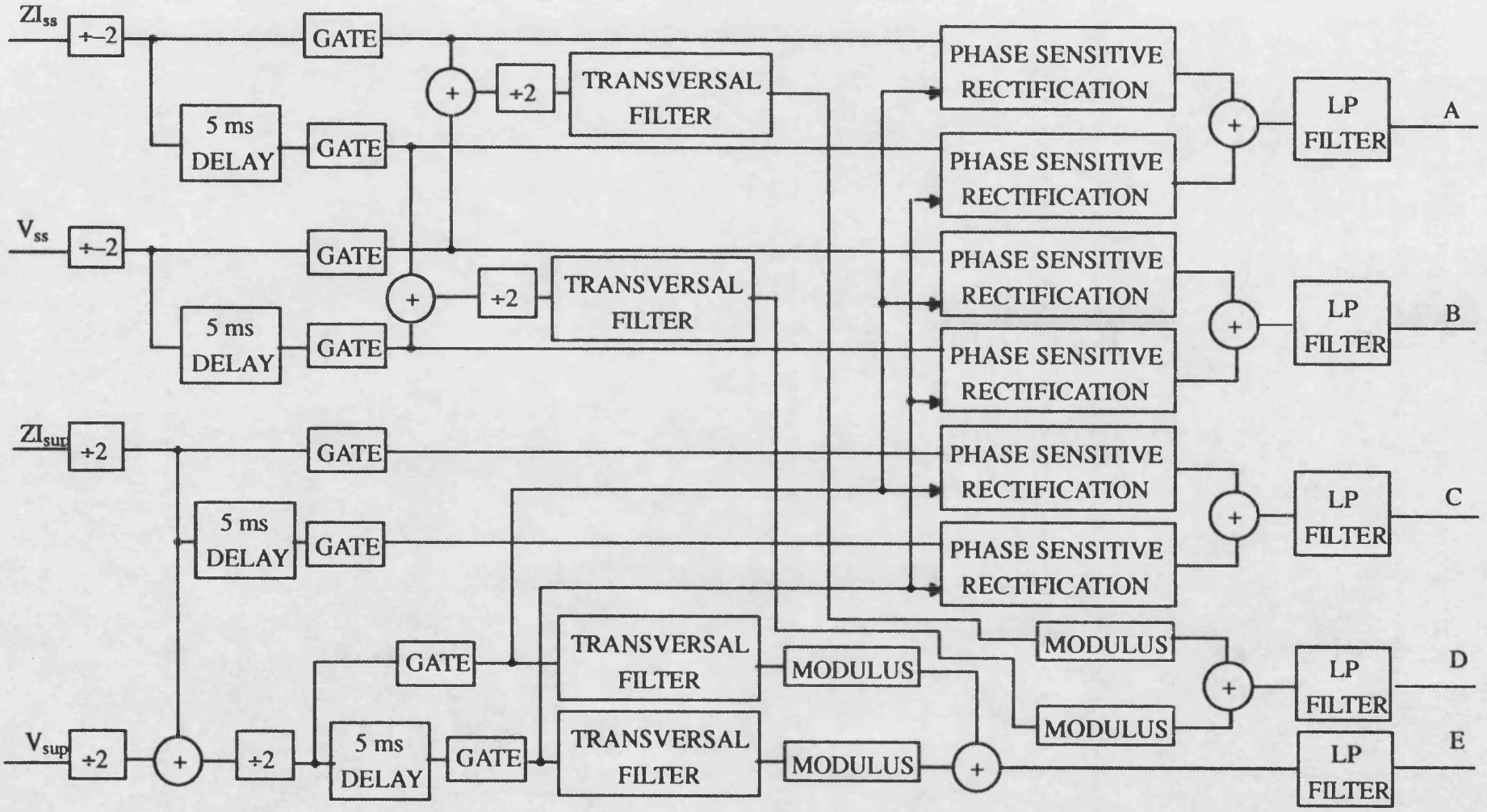

Fig 5.45 IMR REACH POINT AND CHECK PROCESSING (PER ELEMENT)

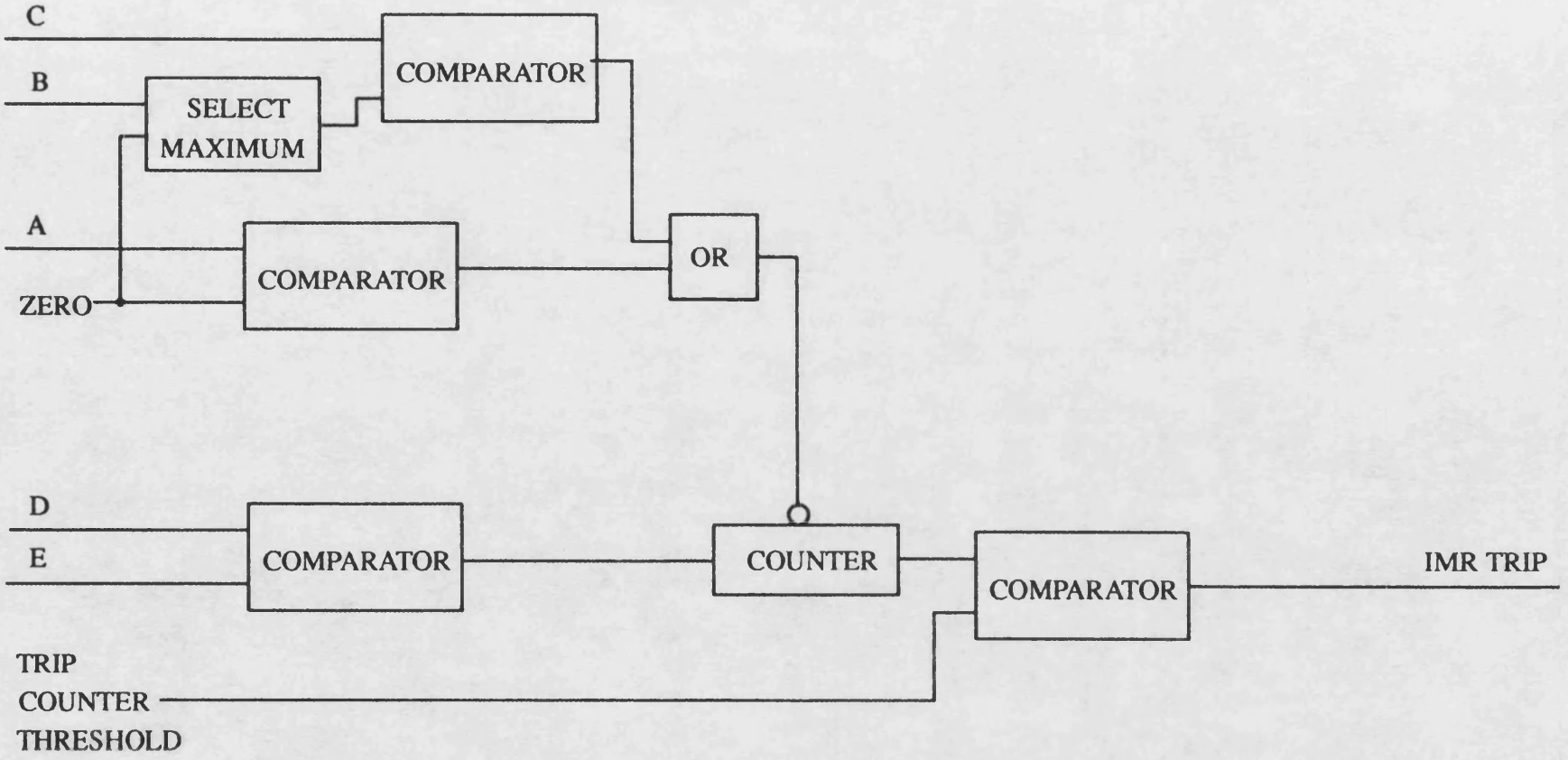

CHAPTER 6

6.1 PROGRAM VALIDATION

6.1.1 METHOD

The program formulation finds the time domain equivalent of a spectrum by integrating the product of the spectrum and a complex exponential. The accuracy of the results may be judged by repeating the calculation with a refined integration interval. There are several stages at which this process is necessary:

1) Primary power system waveforms. The current waveform (ideally unfiltered, but in practice with some low pass filtering) is required when current clipping by the CT occurs.

2) Waveforms produced by including linear transducer model frequency response in simulation program:

a) Using simple (sub–transient reactance) generator model.

b) Using more complete generator model (featuring transient and synchronous reactances.

c) Using frequency variant generator model.

3) Comparing output of primary current waveform convolved with CT impulse response and that produced by above single step method.

6.1.2 WAVEFORM CONSTITUENTS

The total output waveform is the sum of several constituents:

1) The steady state pre–fault waveform.

2) The steady state quantities resulting from the superimposed sources applied at the fault point.

3) The transient quantities resulting from the subtraction of item (2) from the spectrum generated by the fault excitation and network and transducer frequency responses.

It has been found possible to eliminate the correction term made necessary by the truncation of the frequency spectrum of item(2) by treating the latter as a sinusoid passed

through 2 single pole filters, for which the spectrum rolls off much more quickly. Additional exponential decay terms in the time domain are required to match the change in the spectrum. These can be calculated by finding the inverse Laplace Transform of the filtered spectrum. A low pass filter corner frequency of 100 Hz is used.

The spectrum of item (3) is divided into segments covering a defined frequency range with equally spaced sampling points. The end point frequency of one segment is the start point frequency of the next segment, but the number of points an frequency interval between points will differ in adjoining segments. Evaluation of time domain contribution from a segment depends on the frequency range covered and two approaches are needed.

6.1.2.1 EVALUATION OF NARROW FREQUENCY BAND SEGMENTS

In narrow frequency band segments, it is worthwhile to shift the spectrum so that it is centred about zero frequency and use the DFT to evaluate the time domain contribution. Interpolation between DFT output data points can then be done before the frequency shift is restored, reducing the number of DFT calculations required. The factor by which the number of DFT points is less than the number of FFT points (for the high frequency segment(s)) will be termed the interpolation factor.

6.1.2.2 EVALUATION OF WIDE FREQUENCY BAND SEGMENTS

In wide frequency band segments, the time domain contribution is evaluated using the FFT, and the number of integration points is constrained to be an integer power of 2. For validation purposes, the simple expedient of redoubling the number of integration points until repeatability is achieved is acceptable, but the frequency interval required near spectrum peaks makes the use of the FFT alone hopelessly inefficient.

6.1.2.3 LOCAL ERROR REDUCTION

A way of reducing error in localised regions is to perform additional integrations, using smaller integration sub–intervals. Each interval which requires refinement would have a number of extra points equally spaced between its two existing (end) points. The difference between the new data points and the spectrum assumed in the coarse integration (i.e. a linear interpolation between end point values), would then be evaluated using the DFT.

This an efficient way of increasing integration accuracy in localised regions, but requires information on error magnitude distribution. A measure of error magnitude in an interval may be derived by finding the difference between an estimate of the spectrum formed using linear interpolation and one formed using a higher order interpolation rule.

If four data points are (x_0, x_1, x_2, x_3), then the difference between the two estimates of the value at $(x_1 + x_2)/2$ is proportional to $(y_1 + y_2 - y_3 - y_0)$. If this error is squared and added to the error generated in a similar way for the other two phases, then a list of error magnitudes for each interval for a particular output (e.g. voltage at busbar P) may be generated. An ordered list of the intervals in which the *n* largest errors occur is then found using a binary sorting algorithm. The lists of all desired outputs are then combined by taking an entry from each list in turn and discarding all duplicate references to intervals. There is quite a high degree of commonality in the lists, except in the case of 3 phase faults.

The number of extra points in these additional overlaid segments, and the number of segments can be specified such that say the 10 intervals with the highest error have a certain sub–interval, the next 10 a larger sub–interval and so on, such that unnecessary refinement does not occur in every selected interval.

6.1.3 APPLICATION STUDY

The best way to show how the various parameters are set is by an example. On a 125km plain feeder (Fig 2.12), a voltage maximum a–e fault, 32km from P, with source capacities of 6 GVA at P and 0.6 GVA at Q, will show many features. Initially the sources will be modelled as subtransient reactances with X/R = 30 and $X_0/X_1 = 1$.

6.1.3.1 SPECTRUM SEGMENTATION

The spectrum in the frequency range .001–100 Hz is divided into a number of narrow band segments as detailed below:

1) Low frequency point: 0.001 Hz. No interpolation needed.

2) First segment: .001 Hz to 49.001 Hz. 98 spectrum points used. Interpolation ratio specified at 16 for 8 kHz sampling, i.e. at 2 kHz sampling only one quarter of the time domain points would be found using the DFT; the others would be derived by

interpolation.

3) Second segment: 49.001 Hz to 49.961 Hz. 48 spectrum points used. Interpolation ratio: 64.

4) Third segment: 49.961 Hz. to 50.04 Hz. 79 spectrum points used. Interpolation ratio: 64.

5) Fourth segment: 50.04 Hz. to 51 Hz. 48 spectrum points used. Interpolation ratio: 64.

6) Fifth segment: 51 Hz. to 100 Hz. 98 spectrum points used. Interpolation ratio: 16.

7) Sixth segment: 100 Hz to 8.1 kHz. 8192 spectrum points found. FFT algorithm used generates time domain output at 8 kHz rate. Every fourth sample is therefore used to give 2 kHz. output. It would be more efficient to split this range into 4 segments and generate output directly at 2 kHz using the FFT algorithm.

6.1.3.2 UNFILTERED WAVEFORMS

The primary system a–phase voltage spectrum amplitude and phase are shown in Figs 6.1 and 6.2 and the time domain waveforms in Fig 6.3. The current waveform is scaled by a resistive load corresponding to the positive sequence impedance of the line between the relaying location and the fault. The simulation is repeated but with 1024 points in the sixth segment in Fig 6.4, and again with 1024 points in the sixth segment, but with 40 extra segments each containing 7 points. The few extra points result in considerable convergence towards the 8192 point results. A measure of the small residual difference is shown in Fig 6.5.

6.1.3.3 WAVEFORMS SUITABLE FOR TIME DOMAIN CONVOLUTION

If the simulation output is to be processed through a time domain simulation of a transducer, then the frequency spectrum of both the primary system signals and that used to generate the impulse response of the transducer must both be truncated at the Nyquist frequency. Both integrations suffer serious error due to truncation and require that the sampling frequency be doubled.

The transducer simulation consists of the CT model followed by a 1 kHz 2 stage Butterworth relay input filter. The impulse response is shown in Fig 6.6, and was generated at a sampling rate of 16 kHz using 8192 FFT points. The error may be assessed by convolving a sinusoid with the impulse response and comparing the result with a sinusoid modified by the steady state gain and phase of the filtering. The amplitude error is approximately +.2%, and the phase error is –1 degree, (at 8 kHz sampling the errors are +.87% and –2 degrees respectively).

6.1.4 TEED FEEDER CONFIGURATIONS USED

A feeder configuration in which an internal fault can produce a reverse DR directional decision is shown in Fig 6.7. Fig 6.8 is used in calculated of the analogue current gain. All the sources have a Z_0/Z_1 ratio of 1. and an X/R ratio of 30, unless otherwise specified.

6.1.4.1 WAVEFORMS PROCESSED THROUGH TRANSDUCERS

When convolution is used to process power system signals, comparability with results generated directly from a frequency domain simulation (in which the transducer response was included) may be achieved by sampling at double the rate, i.e. 16 kHz instead of 8 kHz and using twice the number of points, of which approximately half are set to zero. A solid a–e fault 50 km from P using the configuration of Fig 6.7 is simulated using these parameters. The primary system current waveform at P (scaled by a resistance corresponding to 50 km line impedance) is shown in Fig 6.9 together with the voltage waveform with the CVT frequency response included.

6.1.4.2 COMPARISON OF CURRENT WAVEFORMS

When current clipping occurs, it is not valid to model the clipping occurring solely after the CT, particularly as the inductive burden causes the phase of the output signal to differ from the primary current. Fig 6.10 shows the result of convolving the primary output current (Fig 6.9) with the CT impulse response (Fig 6.6) (dotted line) compared with the output when the CT frequency response is included in the frequency domain simulation. The output is compared after digitisation in the DR. Fig 6.11 (which is an enlargement of Fig

6.19) shows that there are differences between the two current waveforms, which become apparent when the superimposed components are extracted.

6.1.5 FAULT POINT ON WAVE AND POWER FLOW CHARACTERISTICS

It is useful to display results as both these parameters are varied, since there can be considerable interdependence of the characteristics. Although a different steady state solution is required for each power flow case, for variations in point on wave and pre–fault power flow, for single phase to earth or pure phase faults, only two transient solutions (at different fault points on wave) are required to generate all cases.

The variation in the magnitude of the pre–fault voltage at the fault point on the a–phase as the power angle between busbars P and Q is varied is shown in Fig 6.12. (Busbar R has the same angle as busbar P and the positive sequence voltage at each busbar is 1. p.u. As mentioned in Chapter 2, the pre–fault voltages may also contain zero and negative sequence components).

6.2 DIRECTIONAL RELAY

6.2.1 INTRODUCTION

The complete testing of a DR design would include the following topics:

1) Definition of internal fault region(s) for which the scheme transmits a blocking signal.

2) Evaluation of forward directional decision time, in order to determine when the associated IMR would be triggered, or to determine the time for a DR scheme trip.

3) Assessment of relay sensitivity for all types of fault and various values of fault resistance at various fault points on wave.

4) Confirmation that the relay sensitivities at the Teed feeder ends remain co–ordinated.

5) Confirmation that the scheme behaves acceptably in the presence of current clipping due to an external fault.

Results will not be presented for topics (4) and (5), though consideration has been given to them in the relay design.

6.2.2 RELAY SETTING DETAILS

The DRs at each end of the Teed feeder need to have the following settings:

1) Ratio of (reverse) current threshold to discriminant.

2) Safety factor multiplying voltage threshold.

3) Analogue current gain.

4) Voltage and current ratios used to construct Tee point voltage signal.

5) Ratio of forward current threshold to discriminant.

All these except the last two are the same for each relay.

The value of (1) that is needed has been found by experiment to be 2.25. This may seem high, but it is necessary to ensure that the threshold traverses the discriminant level then stays above it (particularly in the period just after the threshold starts to rise). The safety factor multiplying the voltage threshold has been set to 1. A higher value would be used in practice, (and would mask problems with the current thresholds). The analogue current gain is set to 0.428 Volts per Amp, which corresponds to current clipping just starting for a three phase solid fault at P (with an infinite busbar at Q) in Fig 6.8.

Using the analogue current gain, the ratios of current to voltage needed to construct an analogue of the Tee point superimposed voltage can be found: the equivalent impedance of 1 km of feeder is 0.01245 voltage levels / current levels. The forward current ratio required may be worked out for a relay at end P using the method of 5.8.10, (assuming faults at Q and R). The value (which is the same for relay R) is 3.55 must then be multiplied by the reverse current threshold ratio. The results are summarised in the following table:

	COMBINATION RATIOS		$C_f : C$
DR LOCATION	V : I (exact)	V : I (integer)	RATIO
P	1 : 0.996	1 : 1	8
Q	1 : 0.062	15 : 1	9/4
R	1 : 0.996	1 : 1	8

6.2.3 DEFINITION OF REGIONS WHERE DR SCHEME FAILS

The behaviour of the DRs when a fault occurs at various distances from the busbar P is summarised in the following table:

	FAULT DISTANCE FROM P (km)		
DR LOCATION	0 to 51	51 to 55	> 55
P	FWD	FWD	FWD
Q	FWD	FWD	FWD
R	REV	NO–OP	FWD
SCHEME	FAIL	INTERTRIP	TRIP

The precise fault distance at which the transition in behaviour for the DR at R occurs does vary slightly (±2 km) with fault conditions. It is assumed that the IMR is present but does not operate. For faults in the range 51 to 55 km from P, the DRs at P and Q produce local trip signals which are propagated by the intertrip channel. If intertripping were not provided then sequential tripping i.e. relay R detecting the opening of circuit breakers at P or Q would have to suffice.

The relay behaviour at R is characterised by a superimposed current null for a range of fault positions, but the superimposed voltage is always significant. The application limits determined by superimposed voltage, e.g. when long lines and high source capacities are present, will not be investigated.

The effect of fault resistance on DR application limits is of interest for the cases where internal faults cause reverse decisions at relay R. Assuming an IMR reach setting of 80 km, the most optimistic estimate for IMR fault resistance coverage would be 80x0.29 or 23 Ohms, and the DR at R is likely to produce a reverse decision for fault resistances above that value. For faults less than 51 km from P, up to four regimes may be defined as the fault resistance is increased.

	FAULT RESISTANCE R (Ohms)			
DR LOCATION	$0 \leq R < x$	$x \leq R < y$	$y \leq R \leq z$	$R > z$
P	FWD	FWD	FWD	NO–OP
Q	FWD	FWD	NO–OP	NO–OP

	FAULT RESISTANCE R (Ohms)			
R	REV	REV	NO–OP	NO–OP
IMR AT P	TRIP	NO–OP	NO–OP	NO–OP
SCHEME	INTERTRIP	FAIL	INTERTRIP	FAIL

The values x, y, z will vary with fault position, and the regime $y \leq R \leq z$ may not be present if high forward current threshold to discriminant ratios are used at the relay at P. It is also possible that the relay at Q could produce a forward decision for fault distance (< 51 km) and resistance combinations where the relay at P does not operate.

6.2.4 TYPICAL WAVEFORMS AT R

6.2.4.1 EARTH FAULT

The waveforms for the relay at R for a solid voltage maximum a–e fault 50 km from P in the configuration of Fig 6.7 are shown in the following sections. Internal waveforms for the voltage and forward current VLTAs at the selection of minimum level stage show the delta quantities and the level formed by the algorithm. The delta quantities have been processed through two stages of superimposed component extraction filtering in all cases and divided by a factor of 4 for the currents and 2 for the voltages.

The delta quantities and level generated using two stage filtered signals for voltage are shown in Fig 6.13. The trace of the threshold has had the delay stage which occurs at the VLTA output incorporated (for easier comparison). It can be seen that the current signals are both very distorted and close to the minimum threshold level, but the voltage signals are much cleaner and larger, as would be anticipated from the discussion in the previous section.

The fall in threshold level occurs approximately 20 ms after the fall in signal magnitude, which is undesirable as the scheme would be unnecessarily desensitised for that period. The current discriminant and level generated using single stage filtered signals are shown in Fig 6.14. The fall in threshold level now matches the fall in signal magnitude fairly closely. The misalignment between the peaks of the threshold and signals is corrected when the threshold is filtered. Fig 6.15 shows the threshold at the output of the voltage

VLTA and the delta voltages, which exceed the threshold for several short discrete periods after the threshold has risen.

The delta quantities and intermediate threshold level generated using two stage filtered signals for (reverse) current are shown in Fig 6.16. Fig 6.17 shows the intermediate threshold level generated using single stage filtered signals together with the delta current signals combined to form a discriminant but assuming that the voltage signals are always significant. Fig 6.18 shows the forward current signals at the same stage as the current signals in Fig 6.17.

The benefits of monitoring voltage significance for current and forward current signals can be seen in Fig 6.19 and Fig 6.20, which show the threshold, the discriminant constructed assuming voltage signals are always significant, and the discriminant constructed using the voltage significance information shown in Fig 6.15. The latter construction is zero outside those short periods when a delta voltage rises above the voltage threshold, and even in those cases its value is less than that of the other construction. The sign of the current discriminant shows that the fault is in the reverse direction, (the forward current discriminant does not contain any directional information). Note that in some cases the discriminant assuming the voltages are always significant is less than when their significance is considered.

The current thresholds at the VLTA output are obviously smoother and higher than at the intermediate stage, and in the case shown, the associated discriminant does not re–cross the threshold once they have crossed, even when the voltage significance is not considered. The behaviour of the decision counters is shown in Fig 6.21: the forward decision counter remains at zero throughout, but the reverse one reaches its decision threshold in 3 ms. from the time of fault incidence. The count is held for 12.5 ms and then decrementation is allowed to start (the discriminant will definitely be less than the threshold after that time.

Fig 6.22 shows the current discriminant and threshold for a similar fault occurring at a voltage minimum. The decision counter reaches a reverse decision in 4.5 ms.

6.2.4.2 THREE PHASE FAULT

A solid three phase fault at 55 km from P was simulated for the configuration of Fig 6.7, for points on wave of 0^0 and 90^0 relative to the a–phase voltage. A section of the pre–fault and post–fault simulated a phase power system voltage (but including CVT frequency response) is shown for the relay at R in Fig 6.23. The phase current (scaled by a resistance corresponding to 55 km of transmission line impedance) is shown on the same graph but is hardly visible.

Fig 6.24 shows the current threshold and the discriminant (two traces depending whether voltage significance was considered). Comparison with the a–e fault previously considered shows the threshold does not settle to its quiescent level as quickly after the fault. This is due to the travelling wave distortion apparent in Fig 6.23, which also causes the DR to reach a reverse decision, when the sign of the discriminant indicates that over a longer time span the fault would be considered to be in the forward direction. The counter behaviour is shown in Fig 6.25.

For a fault at 90^0 point on wave (where the travelling wave components are smaller), the relay does reach a forward directional decision as shown in Figs 6.26, 6.27 and 6.28.

6.2.5 FAULT POINT ON WAVE AND POWER FLOW CHARACTERISTICS

A surface plot of the DR operating time of the relay at P for a solid a–e fault 50 km from P is shown in Fig 6.29. The operating time varies from 2 ms. to 5.5 ms, with maximum operating typical operating time of 4 ms. occurring at 160^0 point on wave. The relay always detects the fault as forward, even at extreme power angles when the magnitude of the pre–fault fault point voltage is much reduced (c.f. Fig 6.12).

The situation for the DR at R, as shown in Fig 6.30, is not so clear cut: reverse operation does not occur at extreme power angles, and the maximum operating time is increased to 8.5 ms. The typical reverse decision time is 3.5 ms. rising to 7 ms. at 160^0 point on wave.

The characteristic when the fault resistance is increased to 5Ω is shown in Fig 6.31. There is a marginal increase in operating time in a few cases and no operation occurs in a few more, but overall there is very little change from the previous figure.

6.3 INDEPENDENT MODE RELAY

6.3.1 INTRODUCTION

The complete testing of an IMR design would address the following topics:

1) Checking that over–reach past remote busbars, perhaps caused by encroachment between detectors, does not occur for practical reach settings.

2) Evaluation of operating time for practical settings.

3) Determination of fault resistance coverage.

4) Checking that maloperation will not occur if the IMR is triggered while atypical system conditions prevail, i.e. during power swings.

5) Checking that tripping still occurs for close up faults where the current signal is very much distorted by clipping.

The Teed feeder configuration shown in Fig 6.7 will be used for the studies in this section, as it presents particular problems for the IMR as well as the DR. One of the second order effects of feed–rounds in Teed feeders is that the effective value of source impedance can depend on fault position, since the ratio of superimposed current in the feed round to superimposed relaying current is fault position dependent. The effective source capacity (at P) for a fault at the Tee point can therefore be half that for a local close up fault.

6.3.2 TYPICAL WAVEFORMS

6.3.2.1 A–E ELEMENT

A solid a–e fault 50 km from P on the configuration shown in Fig 6.7 will be studied, and the waveforms presented are those for the IMR relay at P, since this needs to operate for the scheme to trip when the DR at R detects this fault as external. Reach settings of 50 km are used and the time the DR at P takes to detect the fault as forward is 2 ms. for a voltage maximum fault and 2.5 ms for a voltage minimum fault.

Fig 6.32 shows the superimposed and pre–fault signals as occurring on the right hand edge of Fig 5.43 for a voltage maximum fault, and Fig 6.33 shows the same quantities for a voltage minimum fault. The pre–fault power flow was zero and hence the steady–state current I_{ss} in the first 20 ms after the fault consists only of line charging current. The slow decay of the CVT transient can be seen in the voltage minimum fault V_{sup} trace (Fig 6.33). The fault occurs at zero time: the waveforms are delayed by the several stages of filtering and the delay deliberately introduced.

The results of combining but not filtering quantities are shown for voltage maximum and voltage minimum faults in Figs 6.34, 6.35. The approximate equality of the quantities which will form the reach discriminants, i.e. $V_{ss} - ZI_{ss}$ and $ZI_{sup} - V_{sup}$ can be seen for times in the range 5 to 20 ms after the fault, but there is an offset in the case of the voltage minimum fault, which requires the signals to be band pass filtered as shown in Fig 5.44.

Since there is zero pre–fault power flow, both the pre–fault voltage V_{ss} and superimposed current ZI_{sup} are in phase with the constructed superimposed reach point voltage $ZI_{sup} - V_{sup}$, and phase sensitive rectification approximates simple rectification. The waveforms of the check quantities (before low pass filtering) for voltage maximum and voltage minimum faults are shown in Figs 6.36, 6.37. All the signals are zero until 5 ms after the associated DR issues a forward decision, and the pre–fault current signal is also zero during the measuring period. The pre–fault voltage and superimposed current waveforms correspond to simple rectification of the corresponding traces in Figs 6.34, 6.35, plus addition of the rectified signal delayed by 5 ms (as shown in the block diagram Fig 5.44). Both traces are clearly positive for all of the measuring period.

The waveforms for the reach discriminant before low pass filtering are shown for voltage maximum and minimum fault cases in Figs 6.38 and 6.39. It can be seen that the relationship between the two discriminants is maintained for the whole of the measuring time, i.e. 20 ms. after triggering and that the absolute peak value attained by one waveform in Fig 6.38 very nearly equals its equivalent in Fig 6.39. These figures do not include the versions of the signals delayed by 5ms, when these are added the results are shown in Figs

6.40, 6.41. The addition makes the discriminants (even before low pass filtering) more nearly monotonic.

The low pass filtered check waveforms for the two fault points on wave are shown in Figs 6.42 and 6.43. The steady state current waveform is shown after the stage (in Fig 5.45) where a minimum value of zero is imposed. Both the checks are satisfied: i.e. the phase rectified pre–fault voltage is greater than zero and the phase rectified superimposed current is greater than the pre–fault current check signal, hence counting is not inhibited.

The low pass filtered reach point discriminant waveforms are shown in Figs 6.44, 6.45. In both cases, the pre–fault constructed fault point voltage always exceeds the superimposed quantity estimate and counting does not occur. This is acceptable behaviour since the relay would obviously operate at a slightly higher setting, as only the discriminant containing the superimposed current would be larger. The minimum setting required for tripping is 59 km for both voltage minimum and maximum faults with a counter threshold of 6.

6.3.2.2 B–E ELEMENT

The fault details used are the same as in the previous section, but only waveforms for a voltage maximum a–e fault are shown. The unfiltered check signals for the b–e element are shown in Fig 6.46. The effect of phase rectifying the pre–fault b–e voltage with respect to the constructed superimposed b–e fault point voltage is to produce a steady negative level (corresponding to the 120^0 phase difference) plus an oscillating component. The latter would have been much larger if a second signal (delayed by 5 ms.) had not been added. The superimposed current trace is identical to the corresponding trace for the a–e element (Fig 6.36). The filtered check waveforms in Fig 6.47 show that the pre–fault voltage check is negative for all of the measurement period and counting would be inhibited.

The reach point discriminants before low pass filtering are shown in Fig 6.48, and after filtering in Fig 6.49. They clearly show that no counting would take place (even if it were not inhibited by the checks). This would not have been so if the discriminants had consisted of rectified quantities without the addition of delayed versions.

6.3.2.3 A–B ELEMENT

The a–b element check waveforms before filtering for the fault used in the previous section are shown in Fig 6.50 and the a–b reach discriminants in Fig 6.51. The corresponding filtered waveforms are shown in Figs 6.52, 6.53. The phase difference between the pre–fault a–b voltage and the constructed superimposed a–b fault point voltage is only 30^0, so the pre–fault voltage check does not prevent counting, but, as in the case of the b–e element, the reach discriminants do not indicate that counting should occur. If a higher reach setting were used, counting and attainment of the trip threshold would be more likely in the a–e element, as required.

6.3.2.4 A–E ELEMENT WITH PRE–FAULT POWER FLOW

Waveforms will be shown for a voltage maximum a–e fault. Fault and configuration details are identical to those of 6.3.2.1 , but the pre–fault angle of the voltages at busbar Q leads those at busbars P,R by 60^0, causing large pre–fault currents to flow. The effect of the fault is apparently to change the a phase current magnitude very little, as shown in Fig 6.54. However, the signals inside the relay are very different as the relaying and fault point voltages are no longer the same.

Fig 6.55 shows the pre–fault and superimposed quantities for the a–e element for a setting of 50 km. As would be hoped, the pre–fault and superimposed quantity constructions of fault point voltage are similar to each other for a large portion of the measuring period.

The waveforms of the checks before filtering are shown in Fig 6.56. The superimposed current trace is the same shape as the zero pre–fault power case, though the magnitude is reduced (due to the reduced superimposed voltage at the fault point). The phase angle between the pre–fault relaying voltage and the superimposed fault point voltage causes the pre–fault voltage check to be less positive than in Fig 6.36. In Fig 6.57 the unfiltered reach discriminants which show greater discrepancy than in the zero pre–fault power case. The filtered check and discriminant waveforms are shown in Figs 6.58, 6.59. The pre–fault voltage check is positive for the whole measurement period, as is the superimposed current trace, but the latter is exceeded by the pre–fault current trace for the initial

3 ms. during which time counting would be prevented. The filtered reach discriminants are unfortunately most nearly equal during this period, and greater under–reaching occurs: the minimum setting for operation is 65 km.

6.3.2.5 PRE–FAULT POWER FLOW FOR 80 KM SETTING

Fig 6.60 shows the reach point discriminants for the a–e element for the fault described in the previous sub–section, but with a reach setting of 80 km. The superimposed reach discriminant is larger than the pre–fault one, but a phase shift now exists between them which makes comparison more difficult. Fig 6.61 shows the filtered check waveforms, which is very similar to Fig 6.58, except that both current waveforms are larger. Fig 6.62 shows the filtered reach point discriminants and Fig 6.63 shows the resulting counter behaviour.

The discrepancy between the results in cases where only the pre–fault power flow differs is due to magnitude and phase error in the value of Z, by which the current is multiplied. This topic is discussed at length in section 6.3.5, as it has been found that a common value of Z cannot be used for all relay elements.

6.3.2.6 FAULT RESISTANCE CHARACTERISTIC

The case considered is a 50 km 5Ω resistance a–e fault with zero pre–fault power flow. Unfiltered constructions of fault point voltage using pre–fault and superimposed component quantities are shown for voltage maximum and voltage minimum fault point on wave angles in Figs 6.64, 6.65. The result of producing signal pairs from each discriminant, filtering, rectifying and adding them is shown for the two cases in Figs 6.66, 6.67. The result of low pass filtering the previous signals can be seen in Figs 6.68, 6.69.

The superimposed component discriminants are markedly different for the two cases and this may be related to the presence on a slowly decaying offset in the case of the voltage minimum fault, which reduces the likelihood of tripping. The minimum relay settings to trip for this fault are 62 km and 73 km. The presence of the offset would make tripping more likely if a measurement time greater than 20 ms. had been used, as can be seen in Fig 6.67.

The situation becomes even more extreme as the fault resistance is increased: Fig 6.70 shows the pre–fault and superimposed quantities for the a–e fault detector element with a setting of 80 km. The fault simulated is a 20 km 20 Ω a–e voltage minimum fault with zero pre–fault power flow. The superimposed fault point voltage estimate has a very definite offset. At first sight this is strange, since the CT and transactor should remove any offset from the current signal, and an increase in fault resistance would make any offset decay more quickly. However, the offset in Fig 6.70 arises from the rate of decay of the current and hence increases with fault resistance.

The band pass filtering used in forming the discriminants is ineffective in removing the offset as may be seen in Fig 6.71, and an additional stage of transversal filtering (with m=8) was introduced with results as may be seen in Fig 6.72. The effect on the filtered discriminants is shown in Fig 6.73 (original filtering) and Fig 6.74 (extra filtering): the extra filtering makes the performance worse not better.

An unexpected feature of relay behaviour is that fault resistance coverage is better when a large pre–fault current exists. This may be illustrated for the previous fault, but with a power angle of 80^0 between the pre–fault voltages at busbar Q and those at P and R. Fig 6.75 shows the pre–fault and superimposed quantities and Fig 6.76 shows the discriminants. It can be seen that the superimposed voltage estimate peaks before the pre–fault estimate, which makes tripping more likely, and in Fig 6.75 the offset on the superimposed fault point voltage estimate adds to rather that diminishes the first peak. Comparison of the filtered discriminants (Fig 6.77) shows that tripping will occur 11 ms after the fault for this relay setting (80 km). The minimum setting for operation is 45 km, which is much less than the theoretical value of 72 km for a circular impedance characteristic centred at complex zero. However, the minimum reach setting for operation exceeds 20 km under all fault point on wave and pre–fault power flow conditions.

The behaviour may be attributed to the decay of the current transient: when there is no pre–fault power flow it causes a component in the filtered current which diminishes the first peak of the superimposed voltage estimate, but for large pre–fault power flows (both leading and lagging) it increases it. The effect occurs at all fault points on wave.

6.3.3 FAULT POINT ON WAVE AND POWER FLOW CHARACTERISTICS

Fig 6.78 shows the minimum reach setting required to trip a solid a–e fault 50 km from P. The regions where the relay does not operate occur when either the setting required is greater than 80 km, or the checks prevent tripping within 20 ms. It can be seen that no over–reach occurs, with the smallest trip setting being 51 km. The increase in setting required with increasing power angle will be discussed in 6.3.5.

The operating time of the IMR at P for a setting of 80 km and the same fault is shown in Fig 6.79. The view shown here is from a different viewpoint to show limits of operation at positive power angles. There is a central plateau in which the operating time is 11 ms, but this rises to a maximum (21 ms.) as the power angle increases or decreases from zero and the fault type approaches voltage minimum.

Fig 6.80 shows the minimum reach for operation when the fault resistance is increased to 5Ω. The main effects are an increase in the reach setting required to trip and a reduction in range of power angle for which the minimum trip setting is less than 80 km. These effects are distinct for negative power angles at the edge of the operation characteristic. The presence of fault resistance does not cause encroachment or overreach in this case.

Fig 6.81 shows the operating time for a relay setting of 80 km for the above fault. The minimum operating time has increased to 12 ms. and the plateau in the middle has shrunk.

The minimum reach setting for operation for a 20 km fault with 20Ω fault resistance is shown in Figs 6.82 and 6.83. Two views are used as the extent of the region where operation does not occur for a setting of 80 km or less is difficult to represent otherwise. The operation time for a setting of 80 km is shown in Fig 6.84.

6.3.4 EFFECT OF SOURCE PARAMETERS

The effect of varying source capacity, Z_0/Z_1 and X/R ratios for the source at P for a 50 km solid a–e fault will be described in this sub–section. Fig 6.85 shows the minimum reach for operation characteristic when the Z_0/Z_1 ratio is increased to 3 (from 1). (The source capacity and X/R values remain at the previous values of 2 GVA and 30.) Comparing this figure with Fig 6.78, shows an overall reduction in reach setting required to trip

for the 50 km fault and 2 km over–reach for a few cases around 50^0 point on wave and -120^0 power angle. Operation also occurs at higher positive power angles than in the case $Z_0/Z_1=1$.

Fig 6.86 shows the operation time for a relay setting of 80 km. The effect of the increase in DR operating time around 160^0 point on wave may be seen, as well as the conditions for which tripping occurs relatively quickly i.e. in 11 ms. The effect of increasing Z_0/Z_1 at this source capacity is to greatly increase the fault loop impedance and change the proportions of the superimposed fault point voltage estimate due to voltage and current. When $Z_0/Z_1 = 1$, the proportions are approximately equal, but the voltage contribution predominates when $Z_0/Z_1 = 3$, and reach errors become more likely (as the reach setting will depend on the difference between two large quantities). This case will be discussed further in 6.3.5.

Studies were also done with a very large source capacity (35 GVA) at P to check the behaviour of the relay when the superimposed voltage is very small. The ratios of Z_0/Z_1 and X/R were 3 and 30. Fig 6.87 shows the minimum reach for operation and Fig 6.88 shows the operation time for a reach setting of 80 km. The operating time characteristics for the three cases, i.e 2 GVA source capacity; Fig 6.79: $Z_0/Z_1=1$, Fig 6.86: $Z_0/Z_1=3$, and 35 GVA source capacity Fig 6.88 are reasonably similar, but the high source capacity case shows the largest area of minimum operation time (11 or 11.5 ms). The corresponding minimum reach setting for operation show the same trends, with IMR operations occurring for slightly more high positive power angle cases (and slightly fewer high negative angle cases) with a 35 GVA source than for the corresponding 2 GVA source case.

In the 35 GVA source study there are a very few cases of encroachment by the c–e element which operates more quickly than the a–e element at the minimum setting for operation, e.g in 12 ms compared to 14 ms for a setting of 65 km at 100^0 point on wave and 80^0 power angle. This is a consequence of the high ratio of the superimposed current to voltage which effectively makes the superimposed voltage estimate for each earth fault element the same. The checks would not prevent counting for any earth fault element since they use this voltage estimate as a phase reference. As discussed in 6.3.5, the magnitude of

pre–fault fault point voltage may not be identical for each of the three phases and the element for which it is least may produce the trip signal rather than the desired element. However, although this is not the desired behaviour, it is not catastrophic either, since potential over–reach will be limited to the percentage difference between pre–fault phase voltages.

Studies were also done with the ratio of source reactance to resistance (X/R) changed from 30 to 10 for the two previous source capacities and ratios of Z_0/Z_1, but there was very little change in the results. The the relay operated for slightly more cases at high positive power angles, but slightly fewer cases at high negative power angles when X/R = 30.

6.3.5 EFFECT OF UNTRANSPOSED POWER LINE CONDUCTORS

In the relay design it has been assumed that the line impedance between the relay and the fault was approximately 0.29 Ω/km at a phase angle of approximately 80^0. What was not realised was the serious effects that actual deviations from this value can have in comparison of constructed pre–fault and superimposed voltages. Using the configuration in Fig 6.7 (with Z_0/Z_1=1. for each source), the impedance of 50 km of line was measured by dividing the difference of the relay point and fault point pre–fault voltage by the pre–fault current at P. This is done for each of the phases and also for the three delta quantities.

In the relay design (Fig 5.44), phase current (without zero sequence compensation) is used to calculate the pre–fault fault point voltage estimate. This is incorrect, since zero sequence currents do exist even before the fault, and should be properly treated, i.e. by using the conventional compensation formula. The phase calculation is repeated using zero sequence compensated phase current to quantify that source of error.

	PHASE			SEQUENCE		
	a	b	c	0	1	2
VOLTAGE AT P (kV)	306.7	334.2	342.6	18.6	326.6	26.2
VOLTAGE AT F (kV)	237.0	260.0	257.7	6.4	251.5	8.8
CURRENT PF (kA)	16.1	16.5	16.3	0.2	16.3	0.3

	|Z| Ω	θ^0		|Z| Ω	θ^0		|Z| Ω	θ^0
a	15.23	78.09	b	13.64	90.38	c	14.31	91.36
a–e	15.35	76.56	b–e	13.83	91.57	c–e	13.93	91.64
b–c	13.9	91.67	c–a	15.72	85.60	a–b	13.51	82.13

Comparison of the phase calculation using compensated quantities (second row of data) with the first row of data shows only a slight change: this is to be expected as the ratio of the zero sequence to positive sequence component of pre–fault current at P is only .014. However, a wide spread of both magnitude and phase exists, and it is the phase variation which causes most error (principally in the pre–fault fault point voltage estimate). When large pre–fault currents are flowing, V_{ss} and $-ZI_{ss}$ usually are approximately 90^0 out of phase, and their sum is very sensitive to phase error in Z. Magnitude error in the value of Z will tend to alter the phase of the pre–fault reach point discriminant, but a phase error in ZI_{ss} will cause a significant change in the magnitude of $V_{ss} - ZI_{ss}$. The superimposed quantity discriminant is much less affected since $-V_{sup}$ and ZI_{sup} are almost in phase for a fault at the reach point.

If phase error in the current scaling factor Z produces an over–estimate of pre–fault fault point voltage for positive power angles, then an under–estimate would be produced for negative power angles. A trend of this form is clearly visible in the results presented for a–e faults, but the difference between Figs 6.78 and 6.85 shows that pre–fault considerations cannot totally account for the effects observed.

Signals may be relatively easily phase shifted by delaying them by an integer number of samples, and in the case of the pre–fault current, valid information is available from the time before the relay is triggered by the DR. At a 2 kHz sampling rate, increments of 9^0 are available and may be assigned to the elements as follows:

	a–e	b–e	c–e	b–c	c–a	a–b
samples delay	2	0	0	0	1	1

These delays may be implemented by changing the 1 sample delay added to the pre–fault

currents (at the right hand side of Fig 5.43) to the above delay appropriate to the element. The results presented for the a–e fault have included this correction: the remaining trend corresponds to an error magnitude $< 9^0$, which cannot be removed by a simple delay. Corrections have not been applied to superimposed current, though it would have been consistent to do so.

If the same magnitude of Z is used for all superimposed and pre–fault currents then certain elements are likely to over–reach and others to under–reach. Since the current quantities are already digitally scaled, (but only in the relatively coarse steps provided by the digital current scaling technique (5.9.10)), a relatively small design change would be required to scale them individually to compensate for lack of transposition. This is most likely to be necessary when the superimposed voltage is small, i.e. for the important cases of relays close to large capacity sources. However, this design change has not be implemented.

The nature of the source in the simulation will also have an effect on the apparent impedance of a section of line, since the proportions of sequence components in the pre–fault current and voltage would be affected. This would particularly affect the earth fault detectors since zero sequence compensation is not exact.

6.3.6 RESULTS FOR DIFFERENT FAULT TYPES

The practical effects of these changes may be judged by the results for solid faults of other types at 50 km from P. Fig 6.89 shows the minimum reach for operation and Fig 6.90 shows the operating time for an 80 km relay setting for a b–e solid fault with 2 GVA source capacity at P. The view is from a different direction to that used for the a–e fault, and the trend of minimum reach to trip against power angle is opposite to that for the a–e fault, indicating that the phase error is of opposite sign.

The equivalent results for a b–c fault are shown in Figs 6.91, 6.92

6.4 IMR BEHAVIOUR WHEN CLIPPING OCCURS

The configuration used in the simulation is that of Fig 6.7, but with a source capacity at P of 35 GVA and a 3 phase solid fault 1 km from P with zero pre–fault power flow. The fault point on wave is 30^0 with respect to the a phase voltage minimum. The a–b primary

voltage (including CVT frequency response) and current (scaled by a resistance of 0.29Ω) is shown in Fig 6.93. The result of clipping in the CT model and relay produce considerable distortion of the current waveform as shown in Fig 6.94.

6.4.1 DR WAVEFORMS

The waveforms of the reverse current discriminant (generated with and without voltage significance information) are shown in Fig 6.95. Despite the distortion, the directional information is valid and indicates a forward disturbance. The corresponding waveforms of the forward current discriminant are shown in Fig 6.96 and a forward decision is issued in 1.5 or 2 ms for all fault points on wave.

6.4.2 IMR WAVEFORMS

The pre–fault and superimposed components for the a–b fault detector with a reach setting of 80 km are shown in Fig 6.97. The superimposed fault point estimate exceeds the pre–fault estimate for all the measuring time as shown in Figs 6.98 and 6.99, and the relay trips in the minimum operating time for all points on wave. Any of the phase elements would have shown a similar picture, and some of the earth fault elements may also operate since the sum of three clipped currents does not always equal zero. The minimum reach for the phase elements to operate is 3 or 6 km (depending on point on wave). (The granularity of the increment is due to the coarseness of the digital reach multiplication).

6.5 NEW SOURCE MODEL

6.5.1 INTRODUCTION

In order to compare the results from the new source model with those from the old, the first parameter which needs to be set is the source capacity. However, if the source capacity in the new model is set so that the total voltages and currents look similar to those for the simple model, then the superimposed voltage at the new model is much higher and the superimposed current much lower than previously (implying that the source capacity is too low). If the source capacity is raised, then it is possible to get approximate comparability of either the superimposed voltage or current, but the total quantities waveforms

are then very different. In the cases shown, it is attempted to equate the superimposed relay current.

6.5.2 PARAMETERS

The modelling of the generator mutual inductance is described in Chapter 2 (2.4.6) with the parameters (K = 2.56, S = 0.5). A field winding with (reactance X_{fd} and series resistance R_{fd}) is modelled in parallel with the mutual inductance, and leakage reactance and transformer reactance are lumped together as X_l which is in series with the armature resistance R_a. The zero sequence impedance is modelled as a reactance (which includes transformer reactance) X_0 in series with a resistance R_0. The p.u. values of these parameters are tabulated below.

R_a	X_l	X_d	R_{fd}	X_{fd}	R_0	X_0
.00365	.34	.9	.0824	.321	.011	.34

Zero and positive sequence quantities will be referred to the same base of 0.55 GVA.

6.5.3 WAVEFORMS

Fault details are the same as described in 6.3.2.1 , i.e. an a–e fault 50 km from P. The a phase digitised voltages at P for the new and simple source models are shown in Fig 6.100 and the currents in Fig 6.101. The obvious points to note are the presence of travelling wave signals and decay of signal magnitude on both the current and voltage signals in the new source model. Both post–fault current and voltage signals are larger than for the simple model, which would normally imply a larger source capacity.

The superimposed delta voltages and threshold in the DR are also greater in the new model as shown in Fig 6.102. The current discriminant and threshold are shown in Fig 6.103 and the forward current discriminant in Fig 6.104. The very close similarity in the two models between the delta currents when the phase currents differ, reflects the differing proportions and phases of positive, negative and zero sequence components in the

two models' outputs. As would be expected, both the voltage and current thresholds take longer to decay back to quiescent level with the new model.

The pre–fault and superimposed quantities for the a–e element in the IMR with a reach setting of 50 km are shown in Fig 6.105 and the check and discriminant quantities in Fig 6.106. Although the superimposed quantities differ significantly from those produced using the simple model c.f. Figs 6.32, 6.34, the discriminants are much more nearly equal as can be seen in Fig 6.107 and after low pass filtering in Fig 6.108. This should improve reach accuracy.

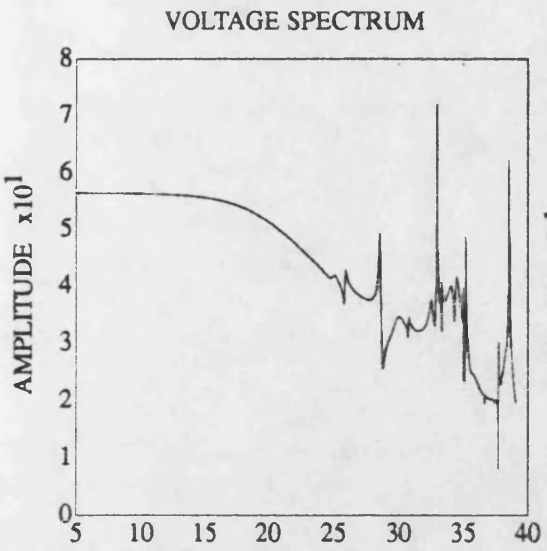

Fig. 6.1

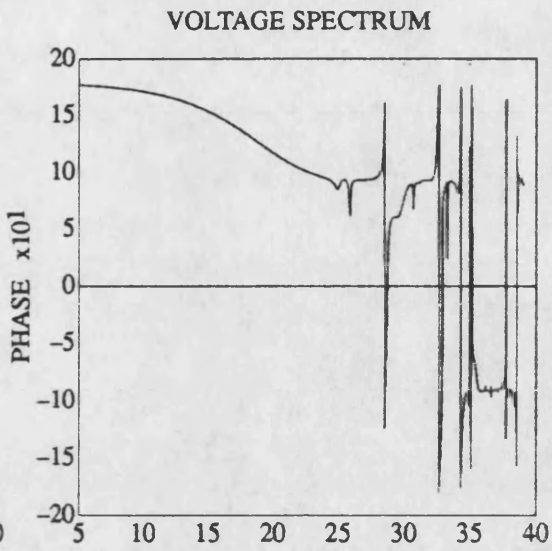

Fig. 6.2

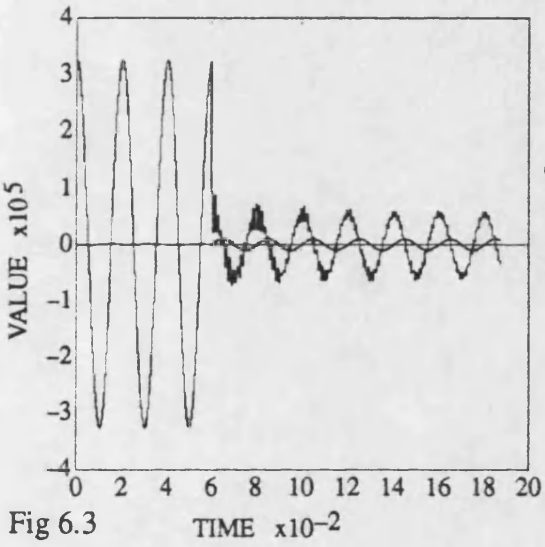

Fig 6.3

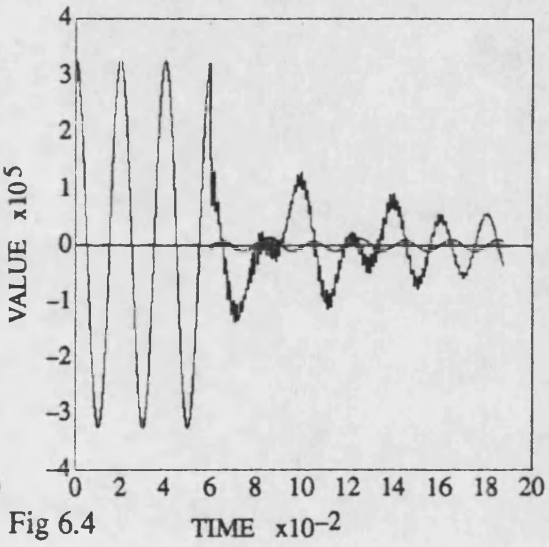

Fig 6.4

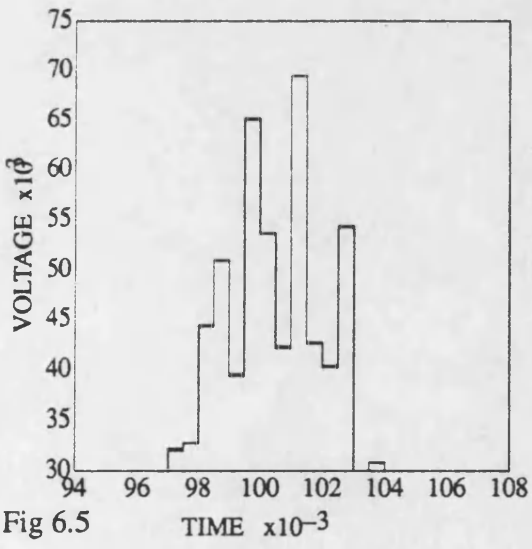

Fig 6.5

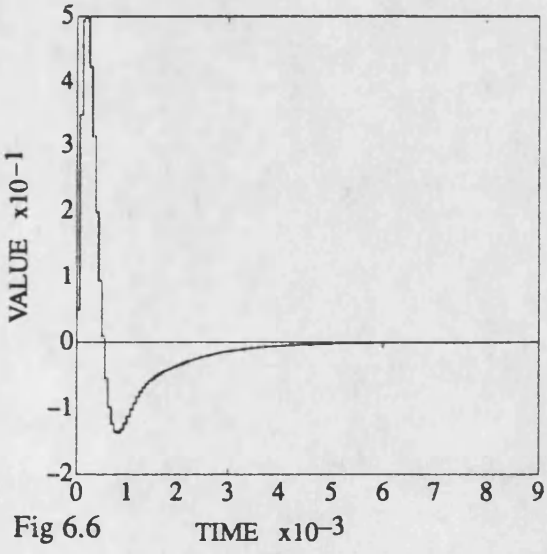

Fig 6.6

INTERNAL FAULT CONFIGURATION

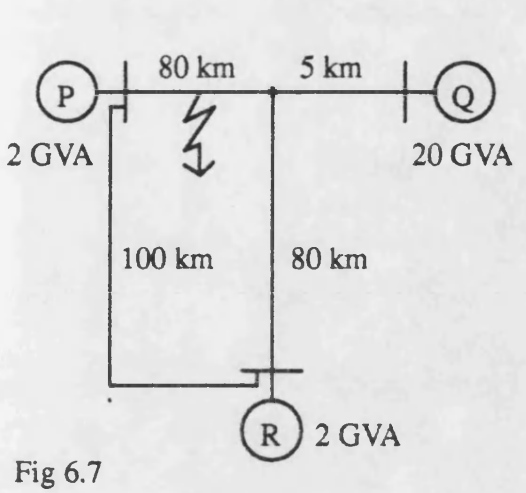

Fig 6.7

EXTERNAL FAULT CONFIGURATION

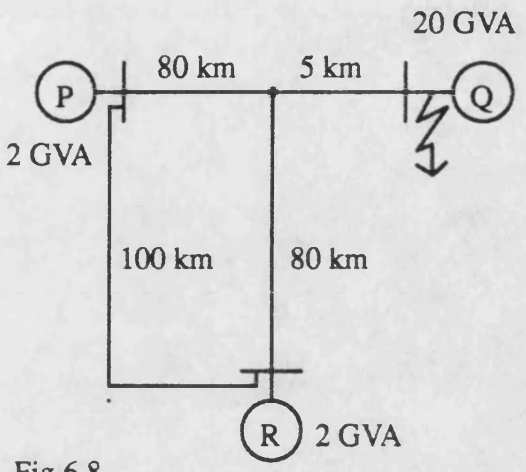

Fig 6.8

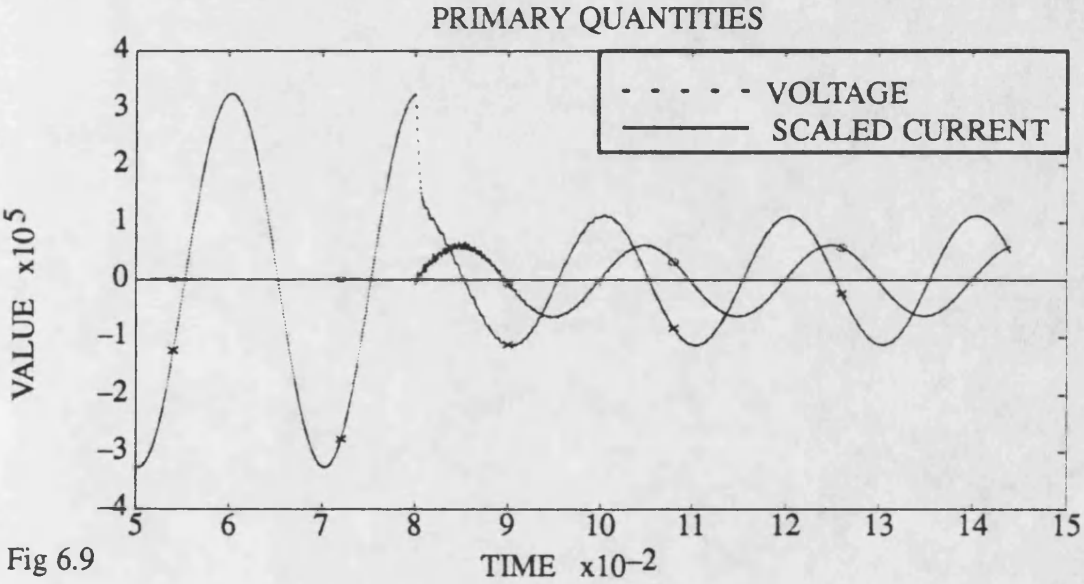

Fig 6.9

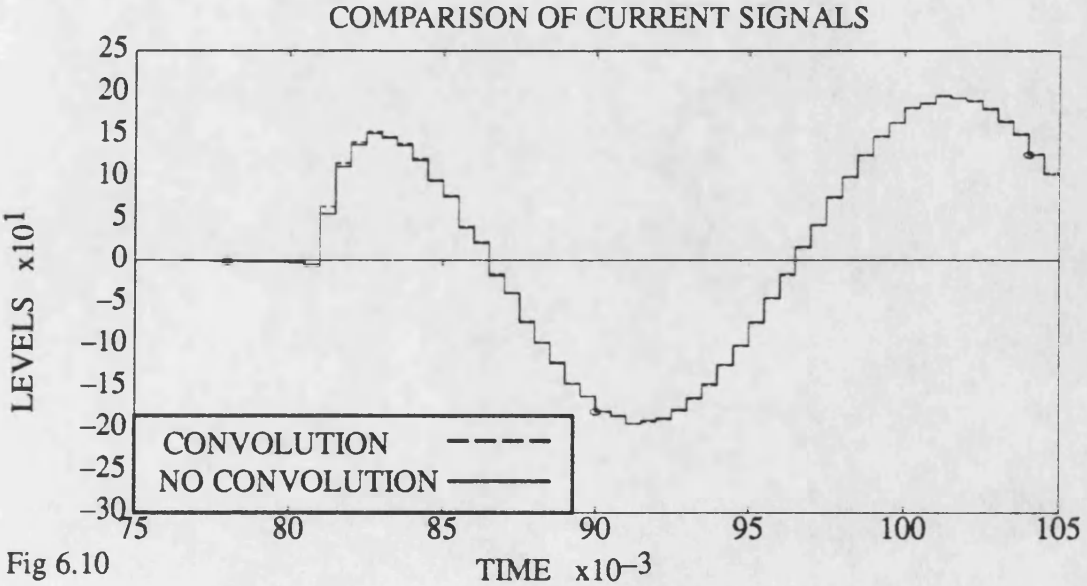

Fig 6.10

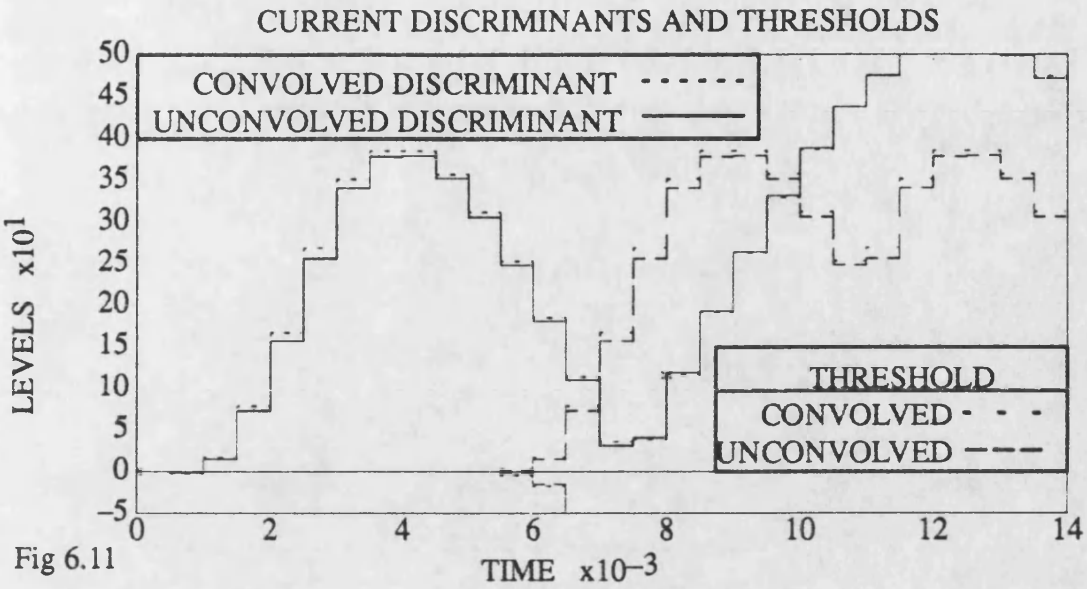

Fig 6.11

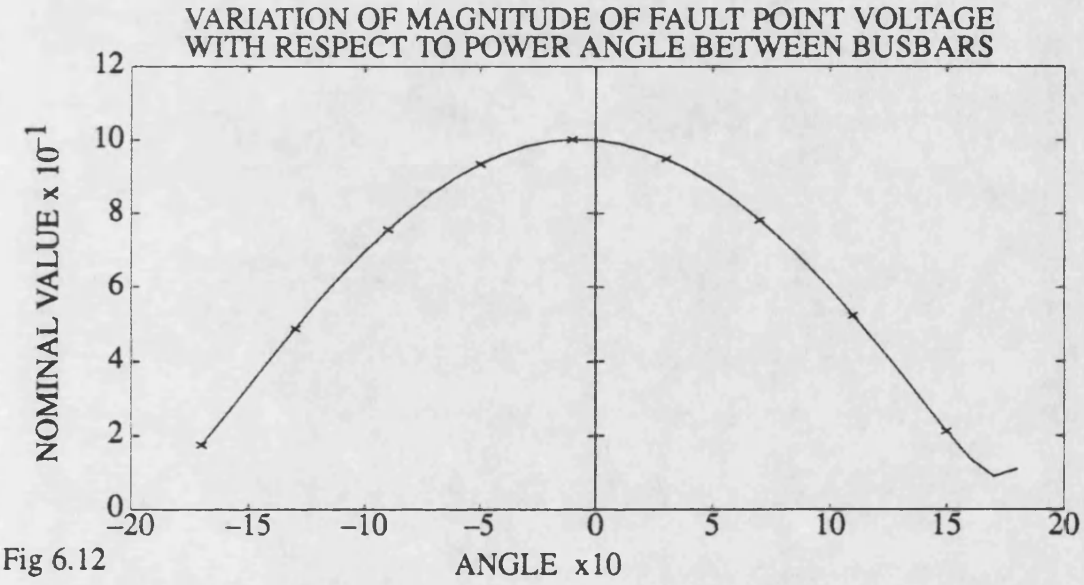

Fig 6.12

DELTA VOLTAGES AND 2 STAGE FILTERED INTERMEDIATE THRESHOLD

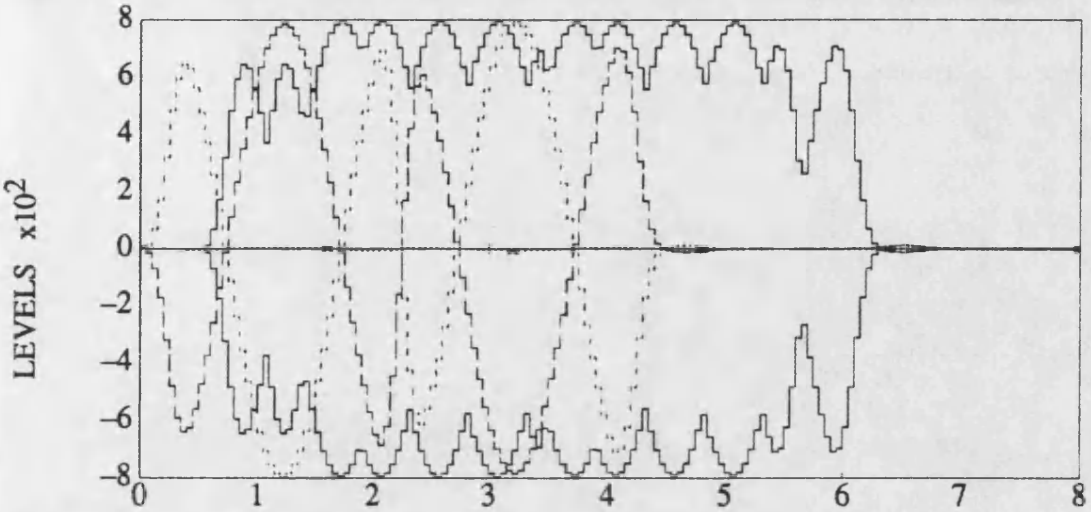

Fig 6.13

DELTA VOLTAGES AND 1 STAGE FILTERED INTERMEDIATE THRESHOLD

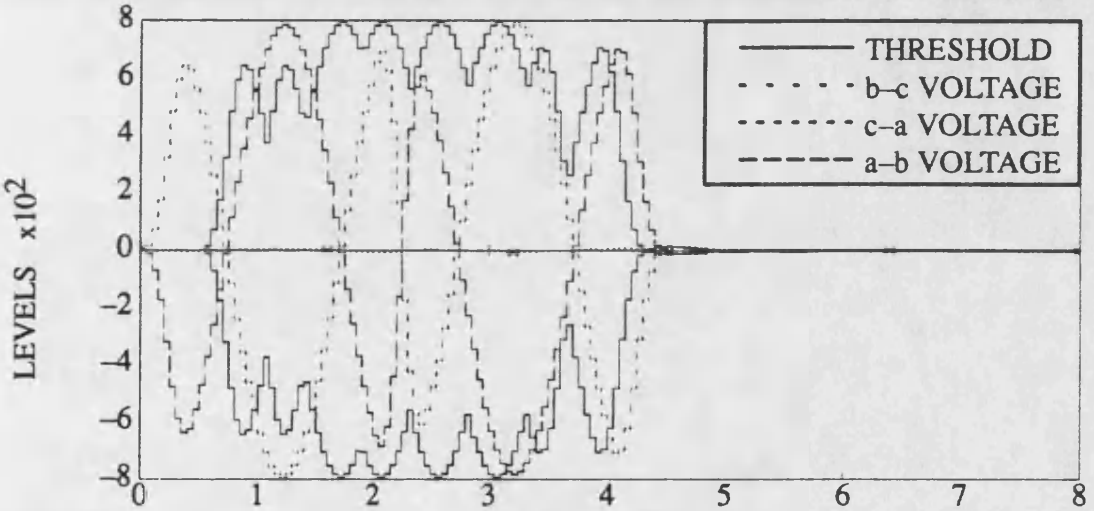

Fig 6.14

DELTA VOLTAGES AND THRESHOLD AT VLTA OUTPUT

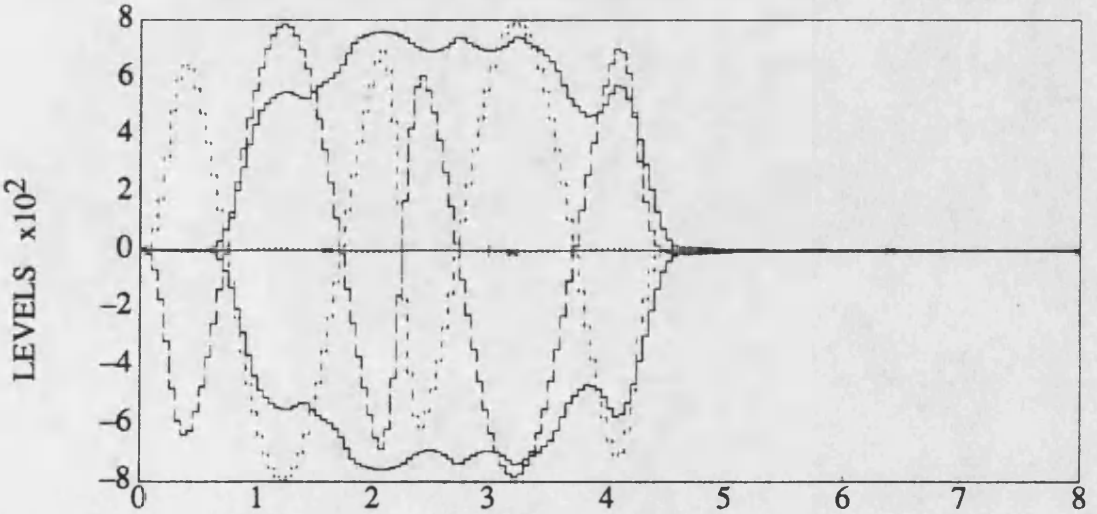

Fig 6.15

DELTA CURRENTS AND 2 STAGE FILTERED INTERMEDIATE THRESHOLD

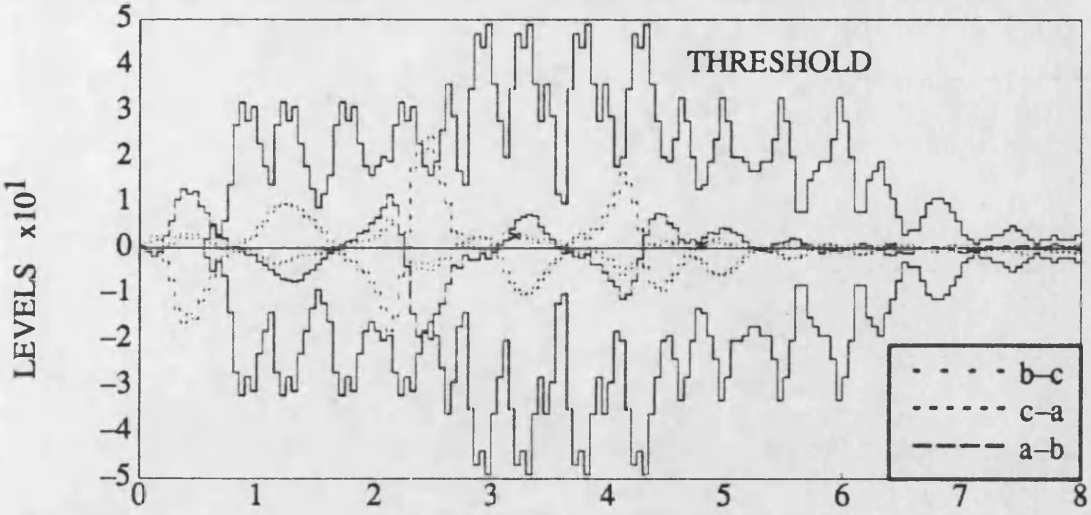

Fig 6.16

DISCRIMINANT AND 1 STAGE FILTERED INTERMEDIATE THRESHOLD

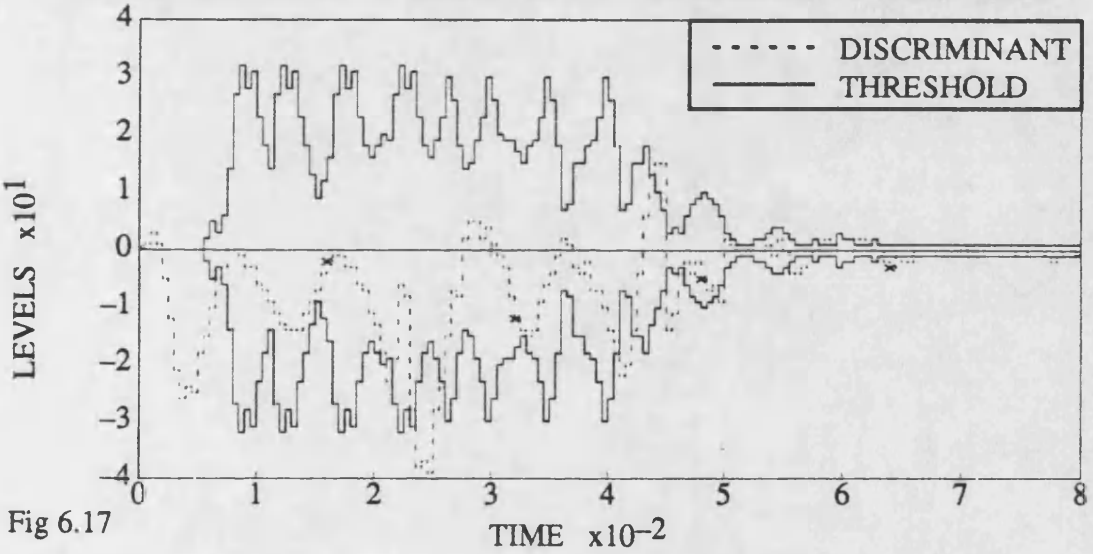

Fig 6.17

FORWARD CURRENT DISCRIMINANT AND INTERMEDIATE THRESHOLD

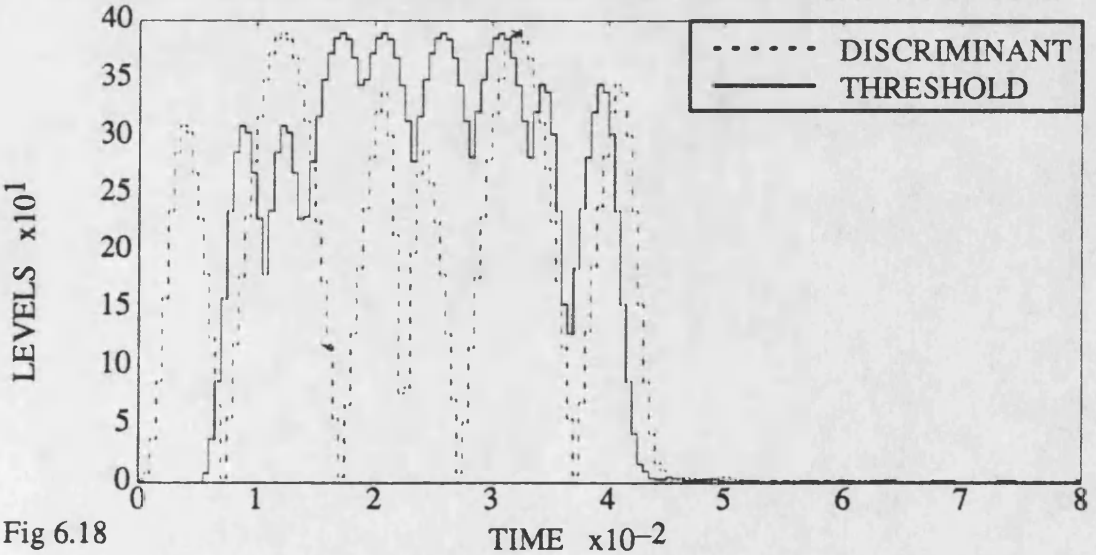

Fig 6.18

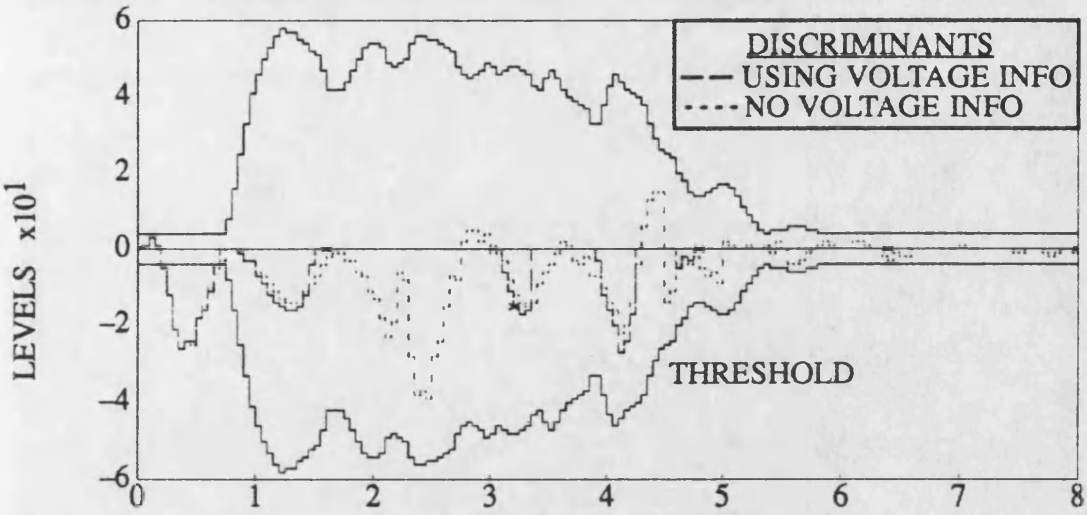

Fig 6.19

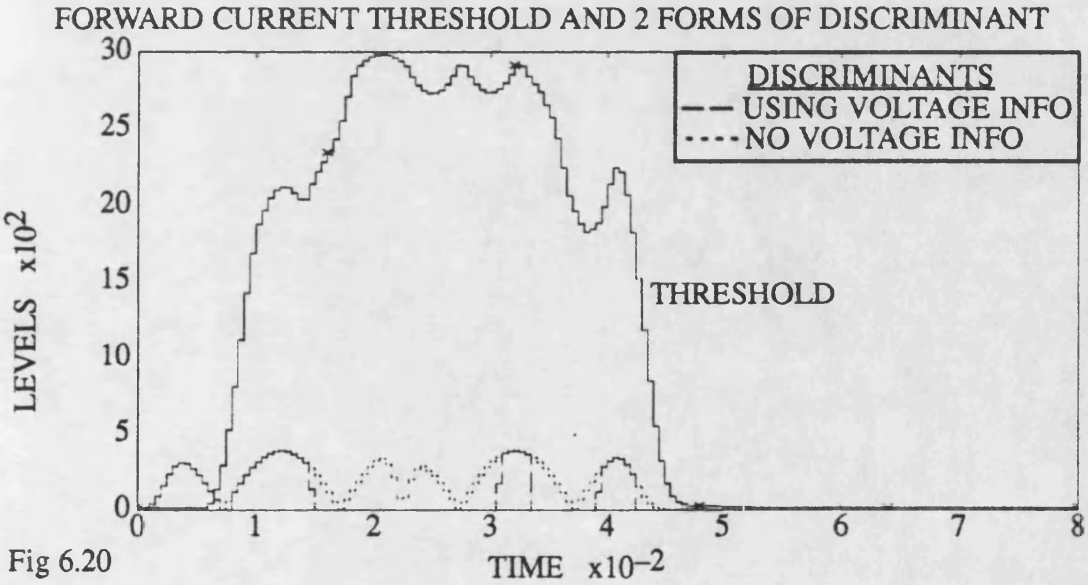

Fig 6.20

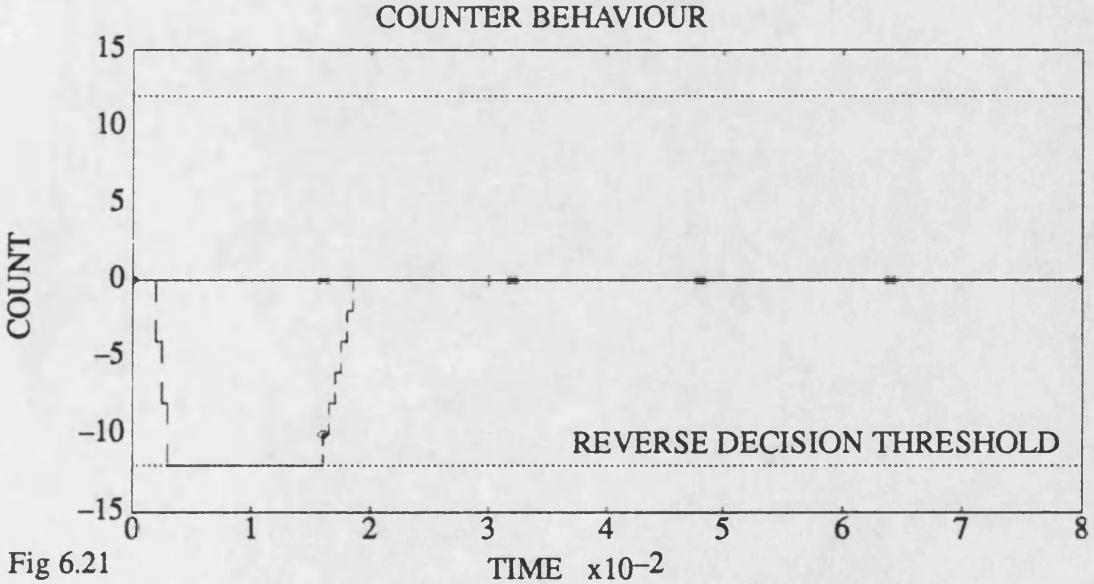

Fig 6.21

VOLTAGE MINIMUM FAULT: CURRENT DISCRIMINANT AND THRESHOLD

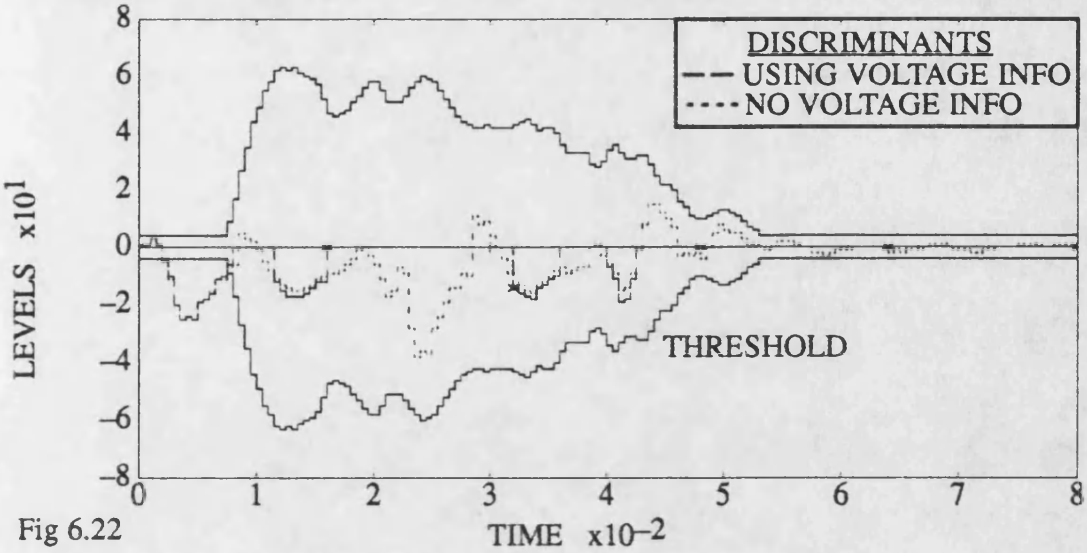

Fig 6.22

3 PHASE FAULT: A–E VOLTAGE

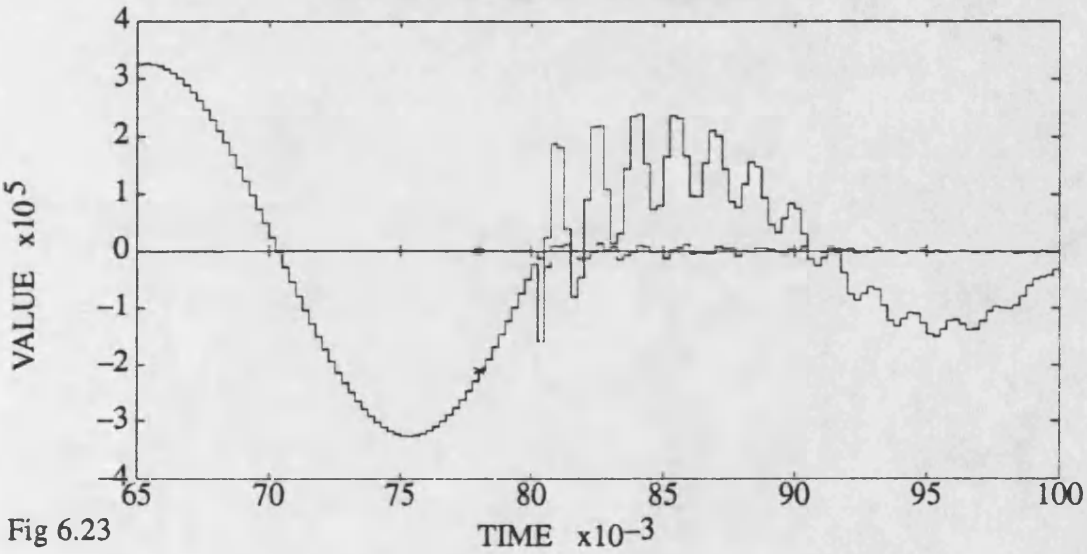

Fig 6.23

CURRENT THRESHOLD AND DISCRIMINANT

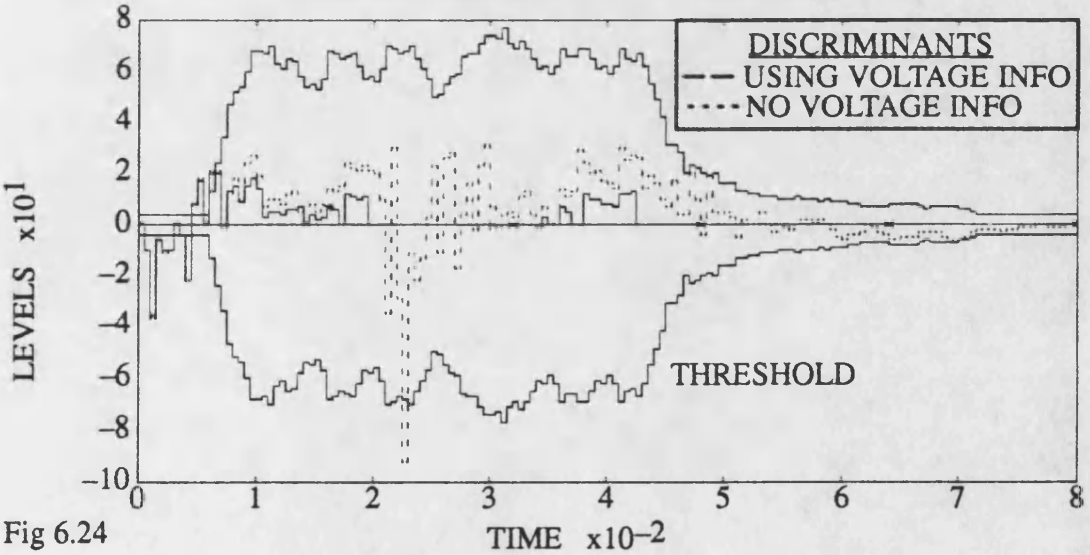

Fig 6.24

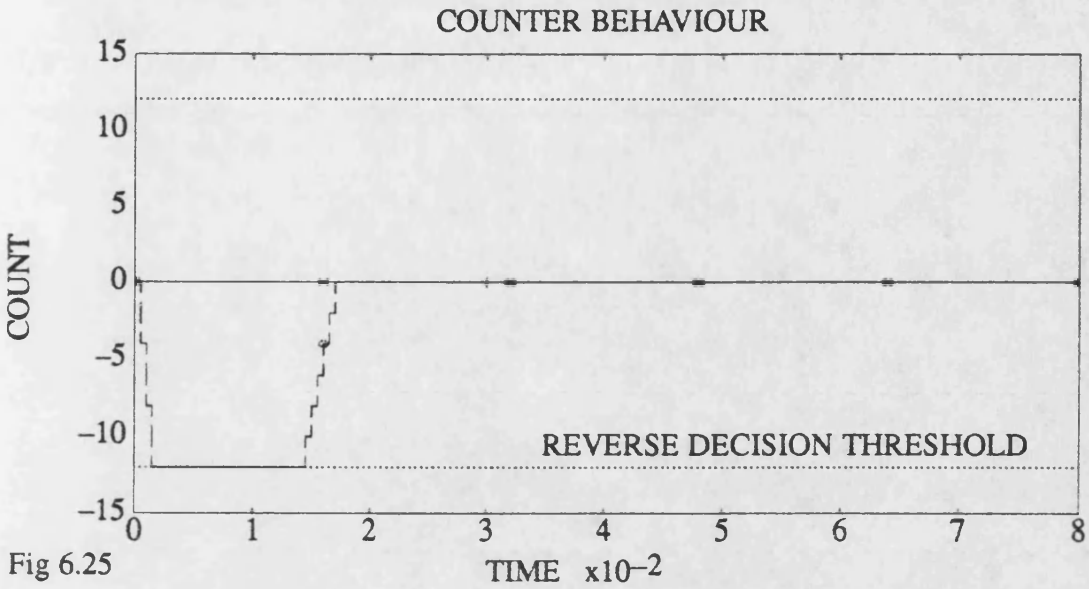

Fig 6.25

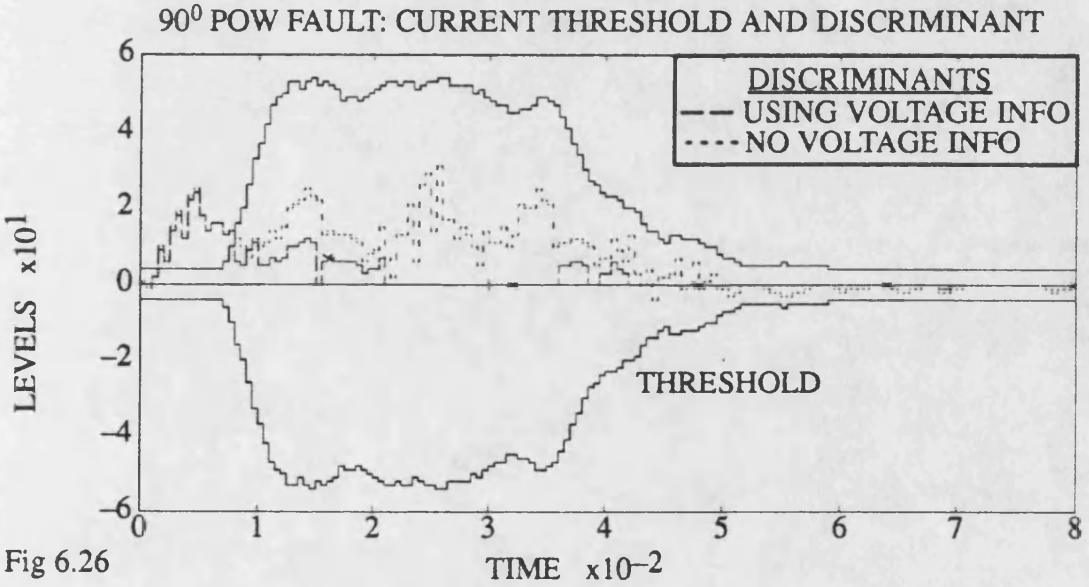

Fig 6.26

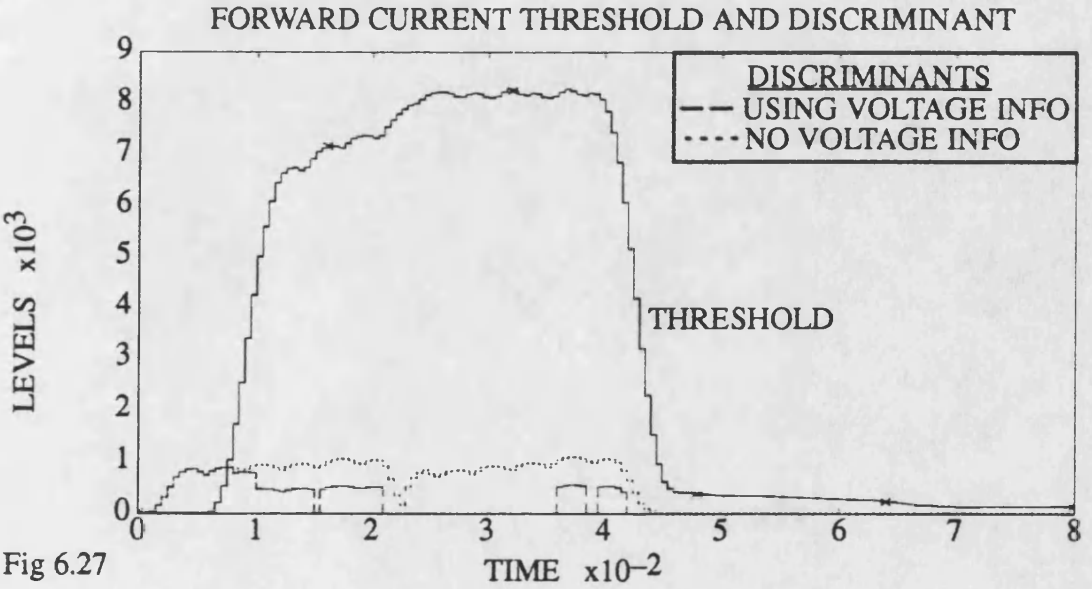

Fig 6.27

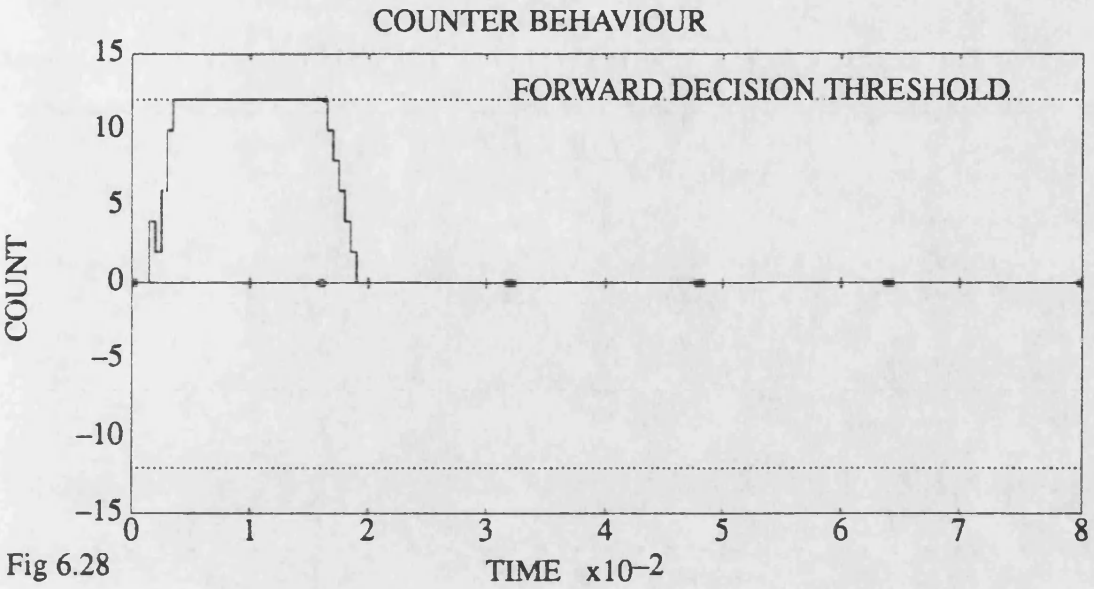
COUNTER BEHAVIOUR
FORWARD DECISION THRESHOLD
COUNT
15
10
5
0
−5
−10
−15
0
1
2
3
4
5
6
7
8
TIME x10−2
Fig 6.28

Fig 6.29 OPERATION TIME FOR DR AT BUSBAR P

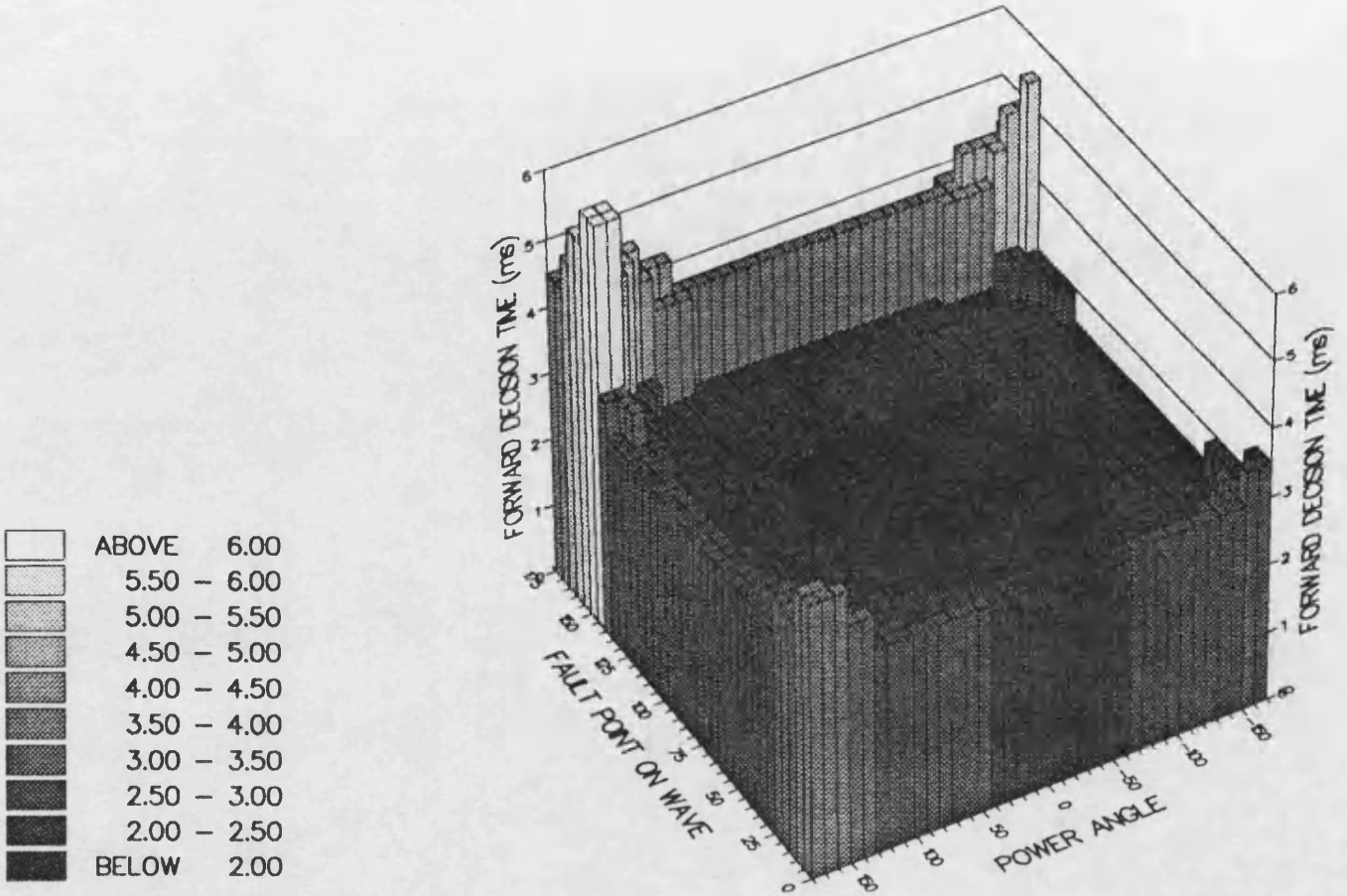

Fig 6.30 OPERATION TIME FOR DR AT R: SOLID FAULT

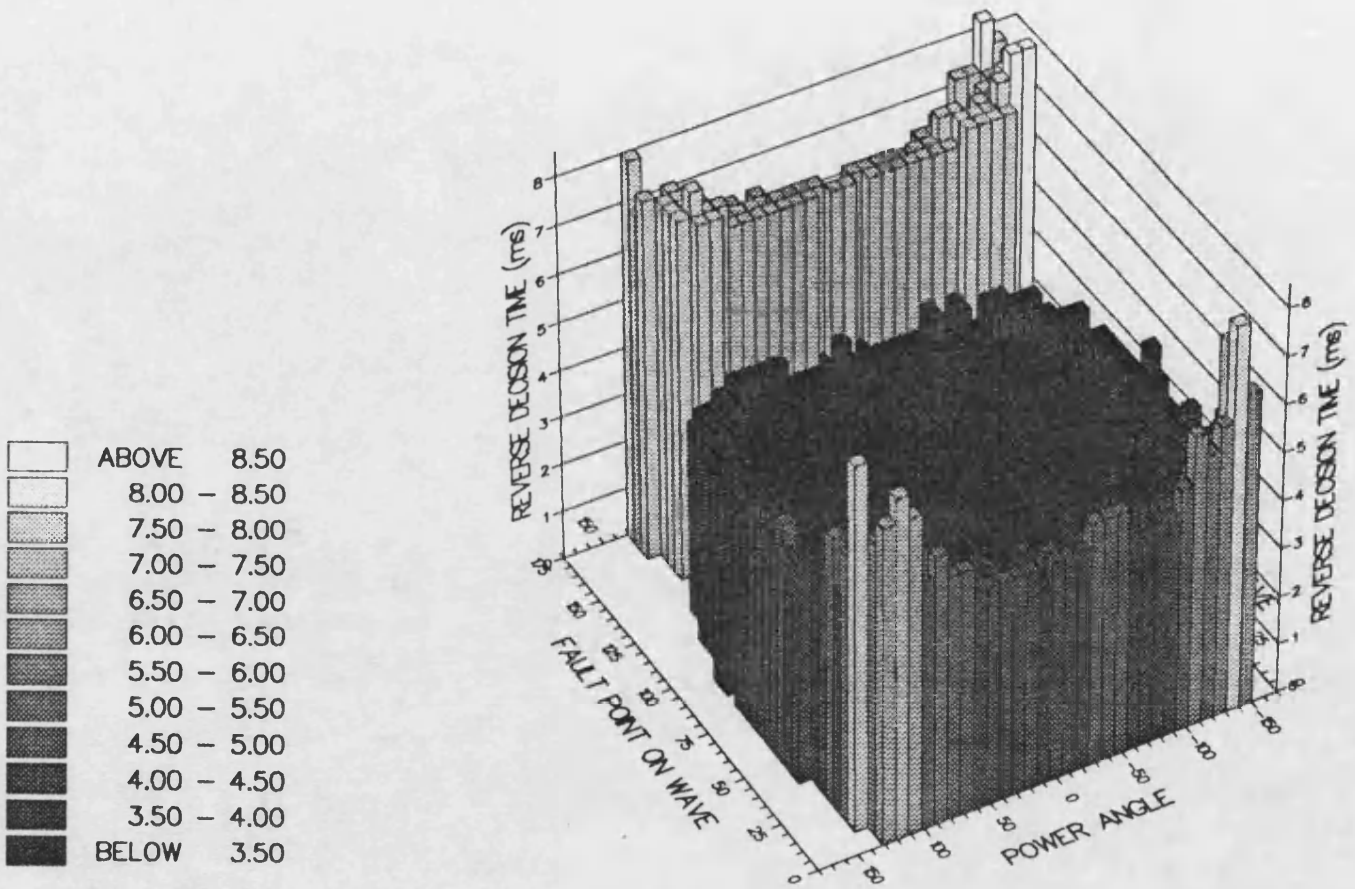

Fig 6.31 OPERATION TIME FOR DR AT R: 5Ω A–E FAULT

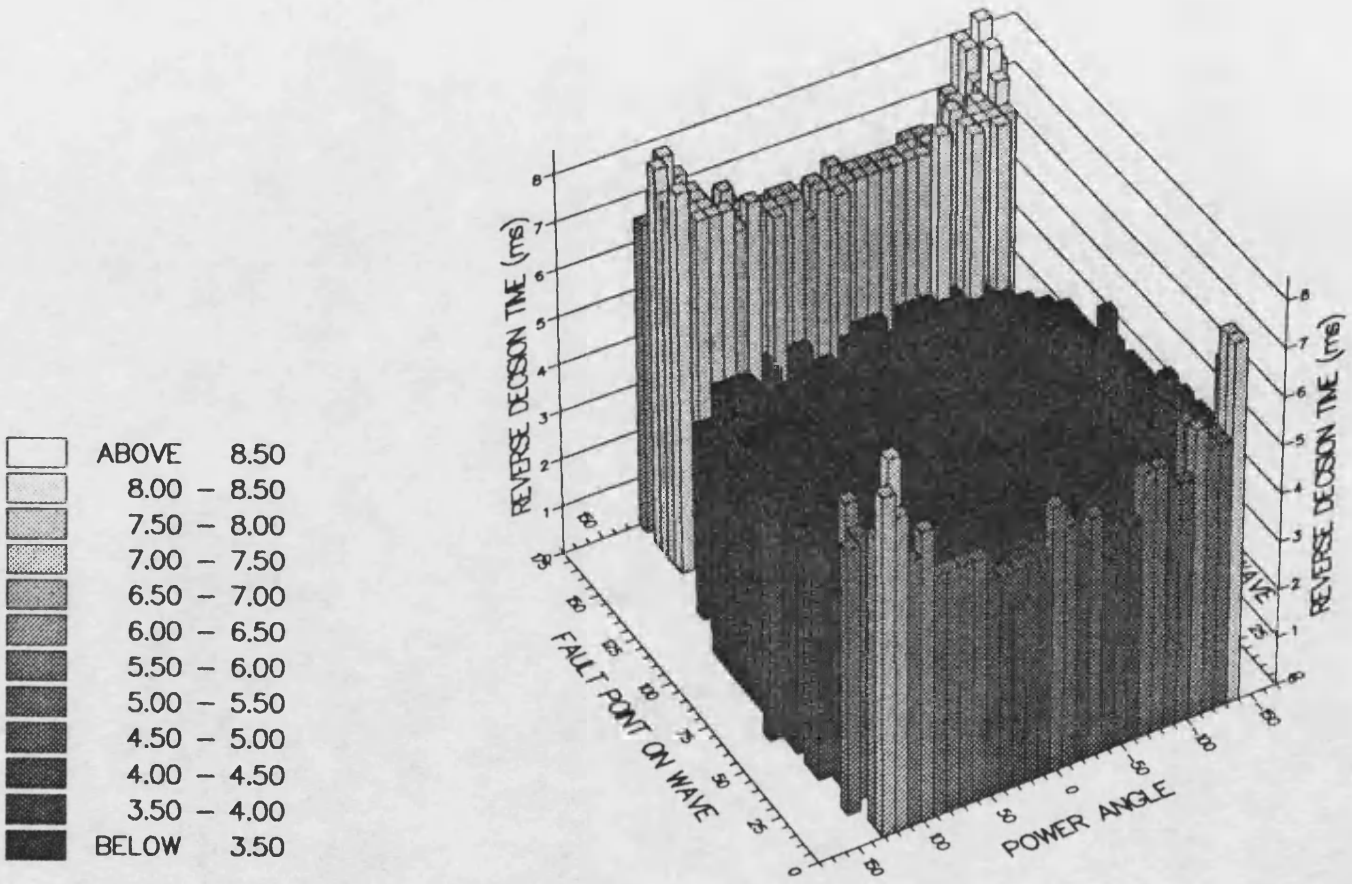

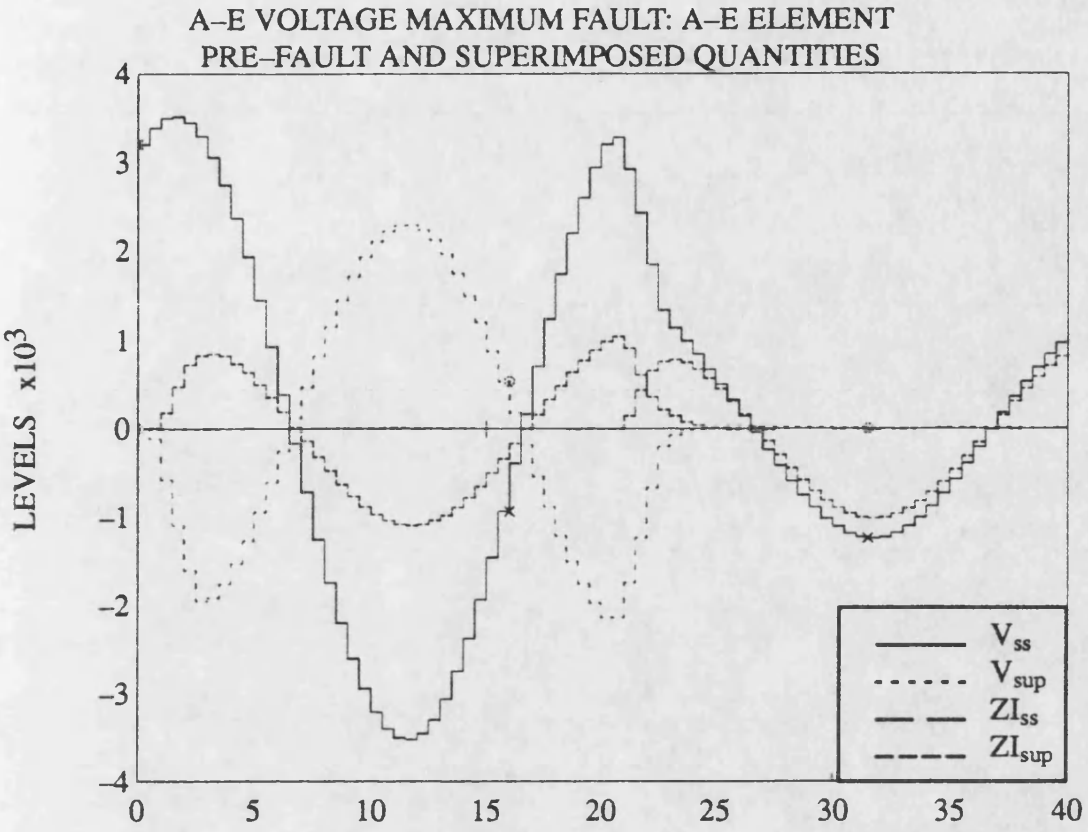

Fig 6.32

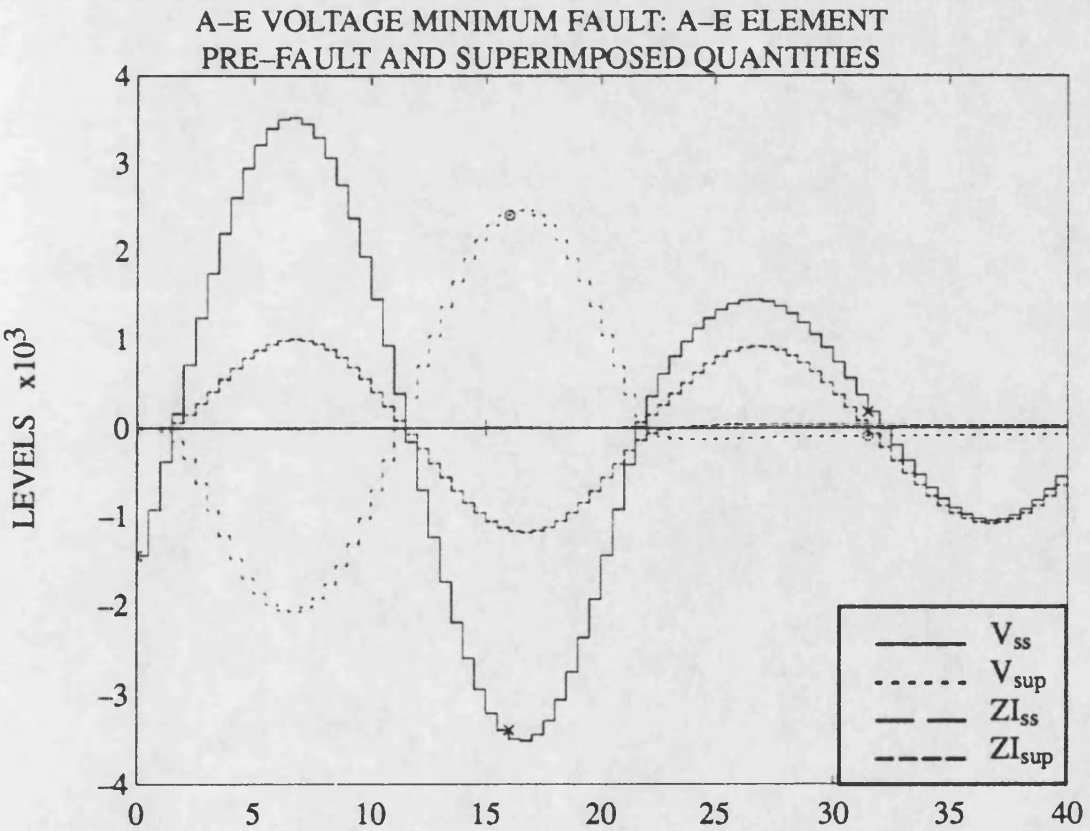

Fig 6.33

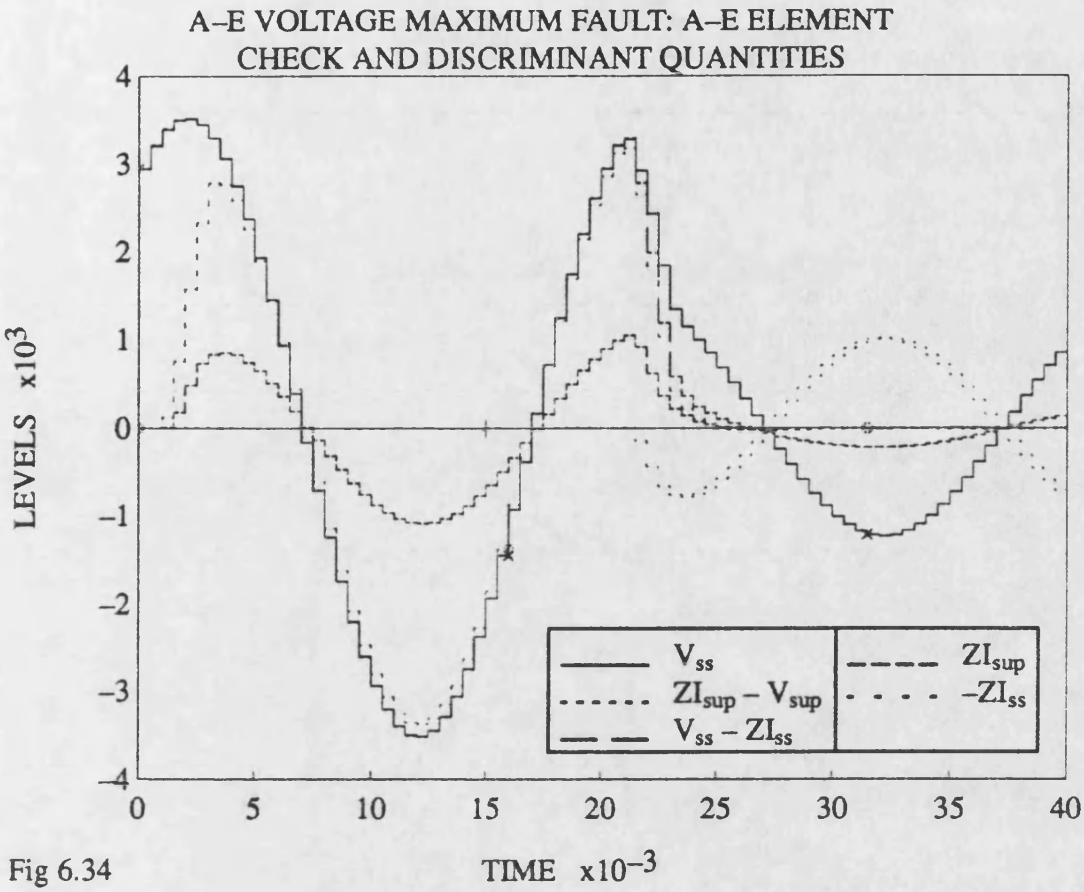

Fig 6.34

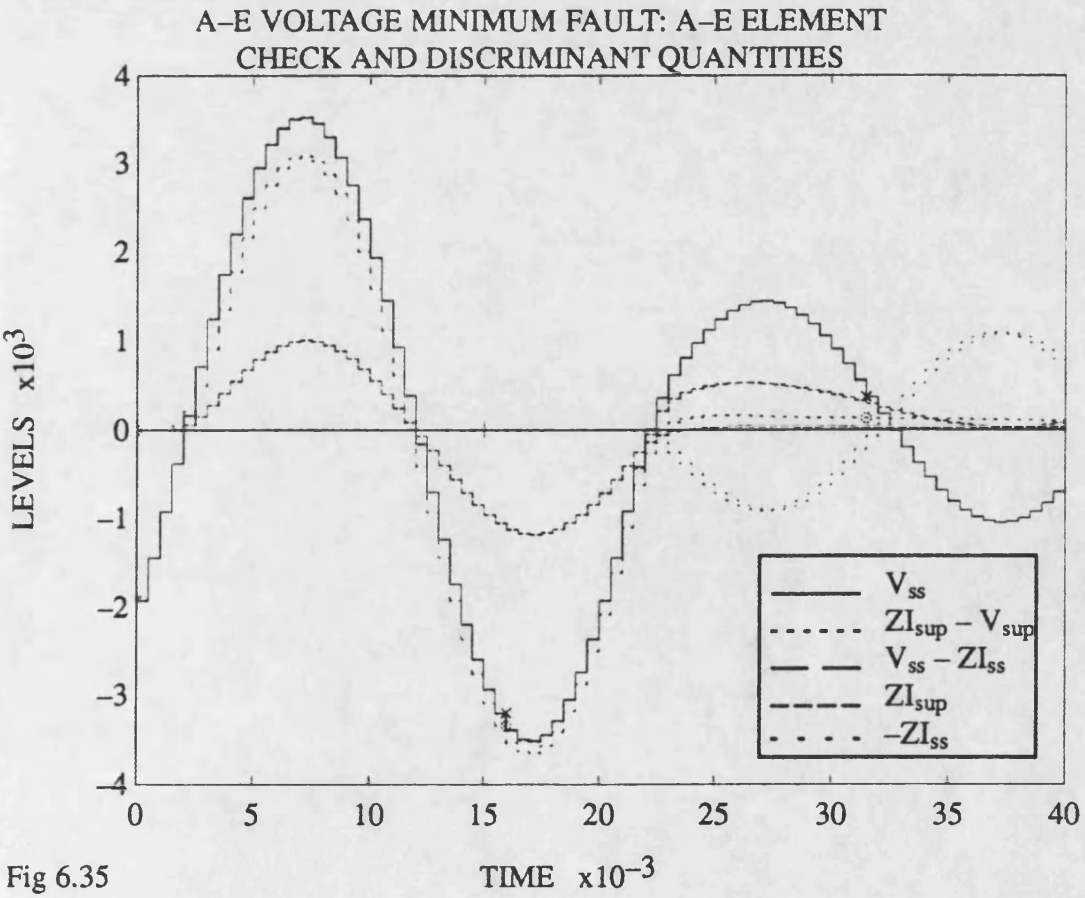

Fig 6.35

A–E VOLTAGE MAXIMUM: CHECKS

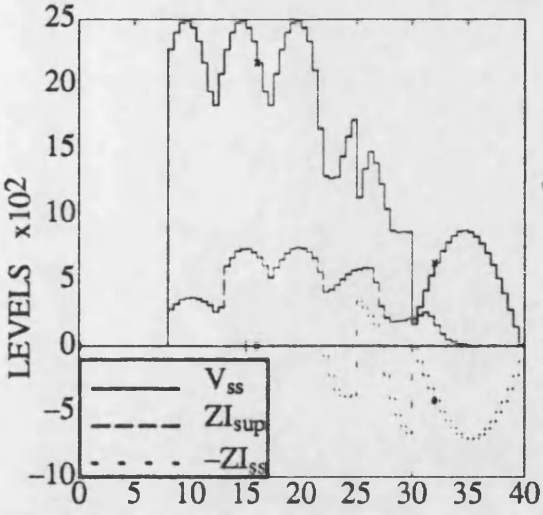

Fig 6.36

A–E VOLTAGE MINIMUM: CHECKS

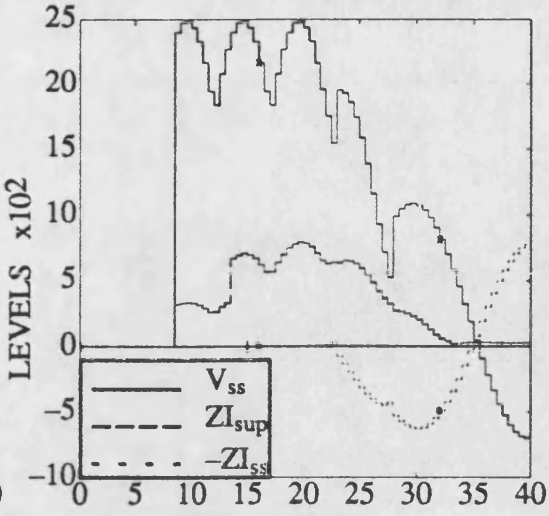

Fig 6.37

PARTIAL REACH DISCRIMINANTS

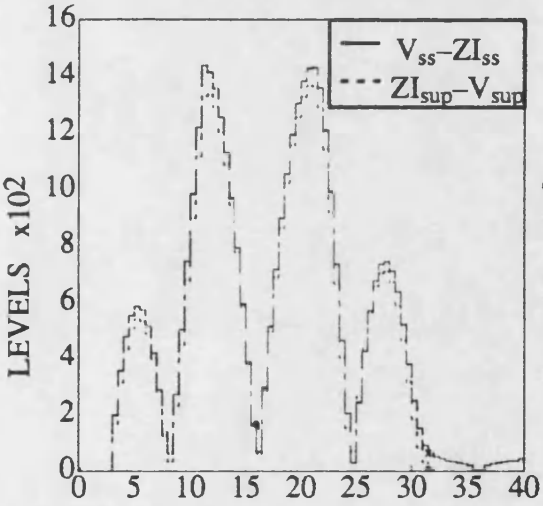

Fig 6.38

VOLTAGE MINIMUM FAULT

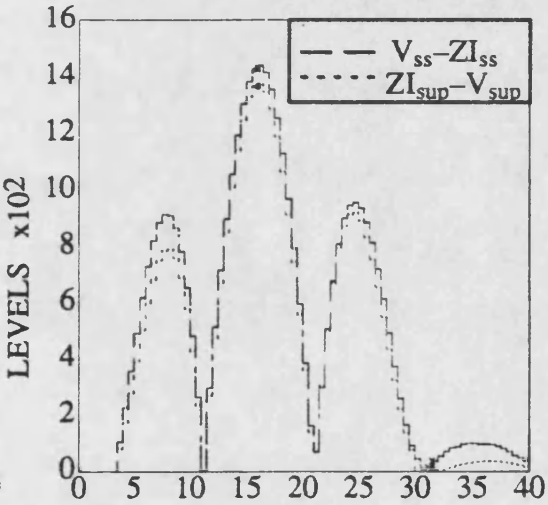

Fig 6.39

FULL REACH POINT DISCRIMINANTS

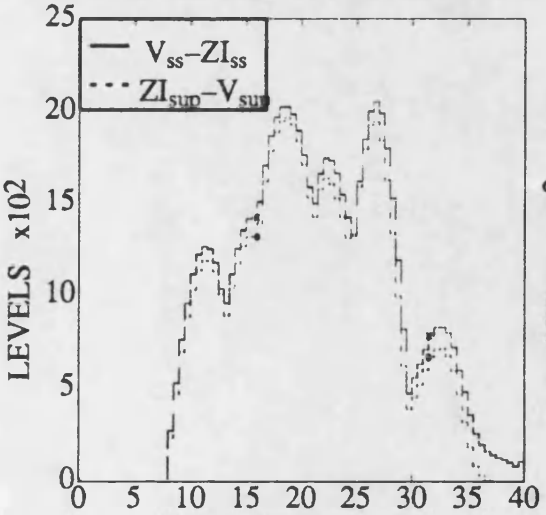

Fig 6.40

VOLTAGE MINIMUM FAULT

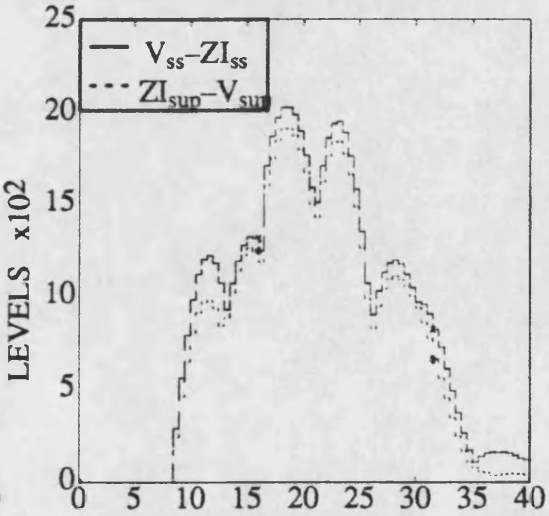

Fig 6.41

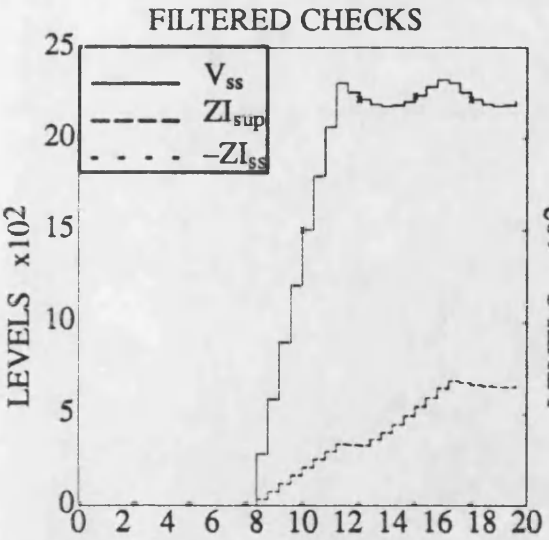

Fig 6.42

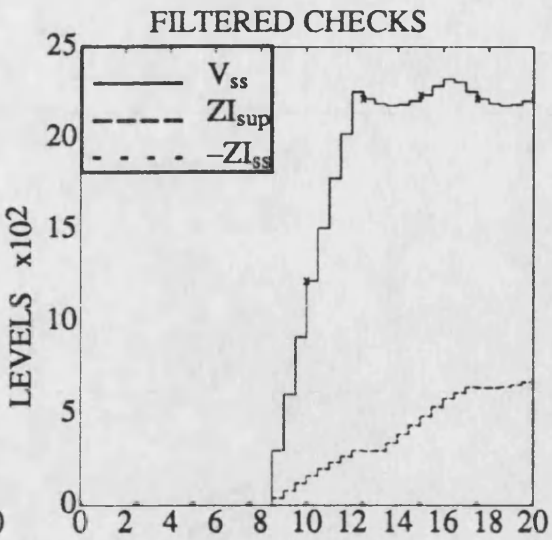

Fig 6.43

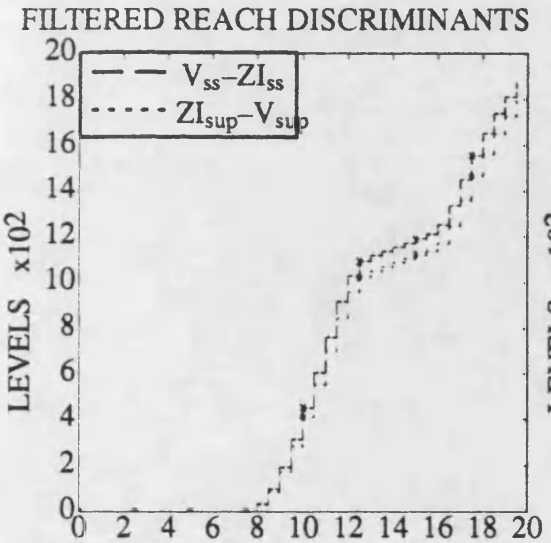

Fig 6.44

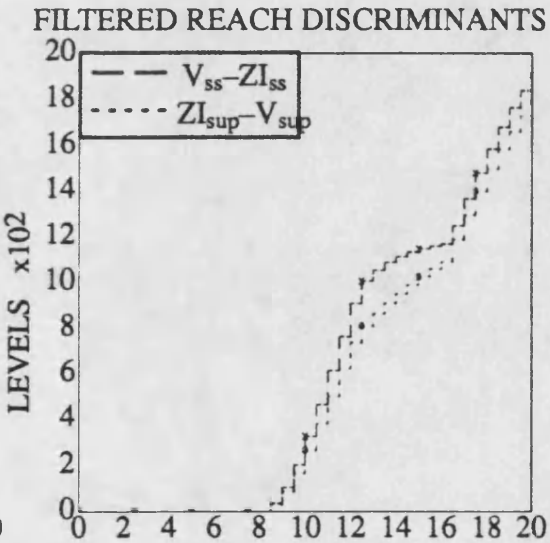

Fig 6.45

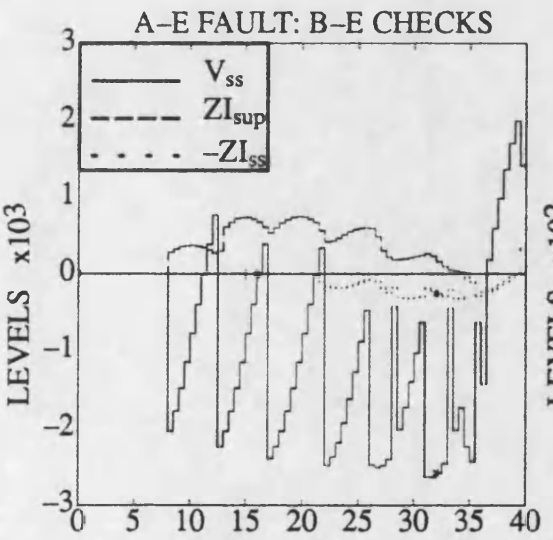

Fig 6.46

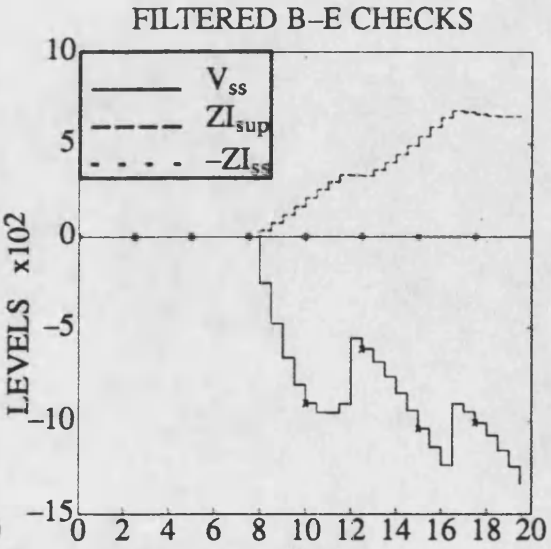

Fig 6.47

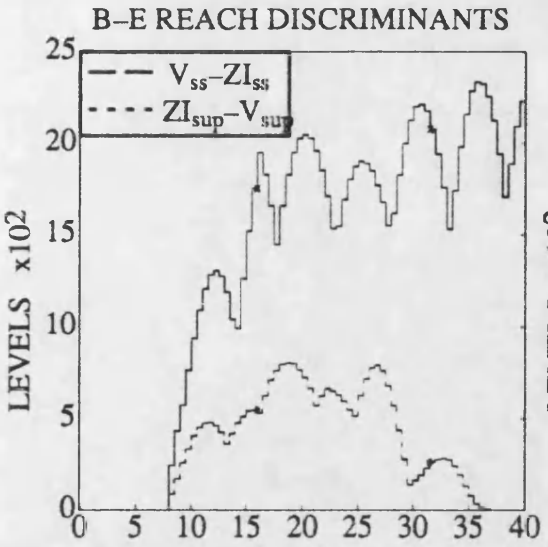

Fig 6.48

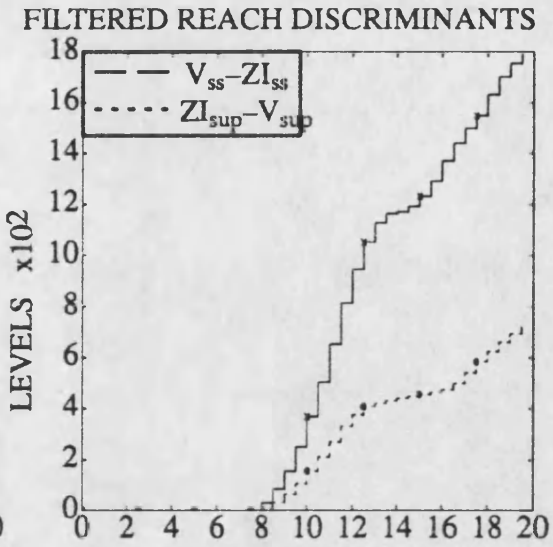

Fig 6.49

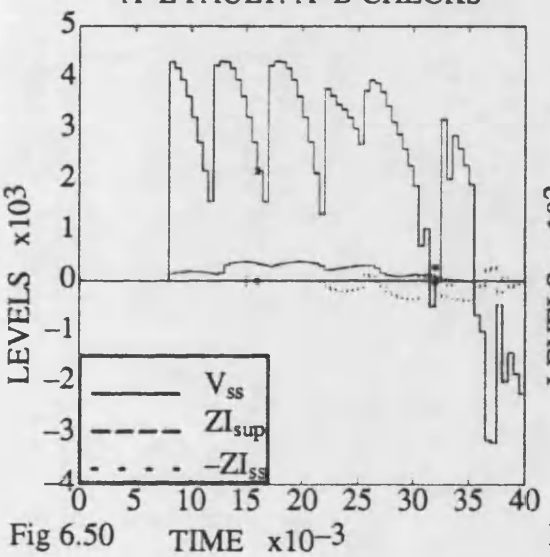

Fig 6.50

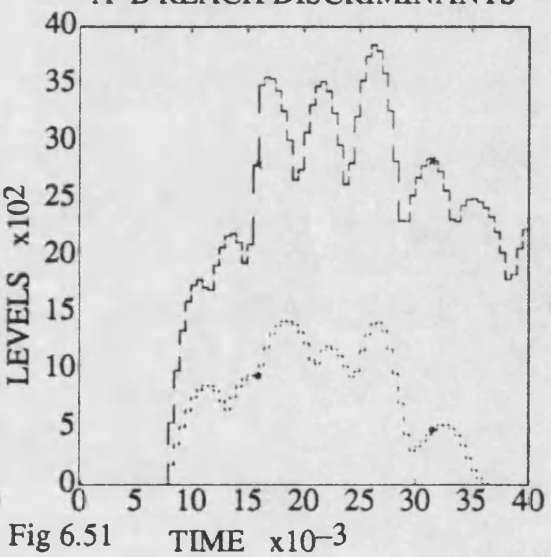

Fig 6.51

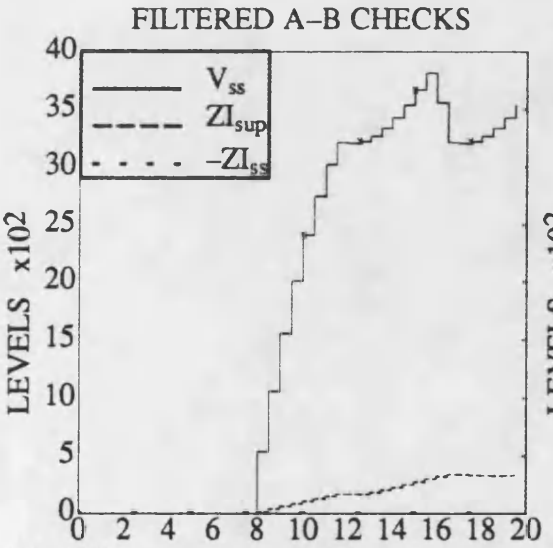

Fig 6.52

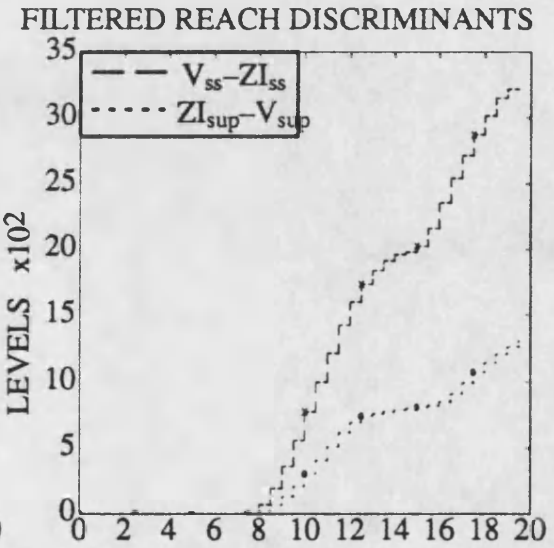

Fig 6.53

DIGITISED a PHASE SIGNALS FOR A–E FAULT WITH POWER FLOW

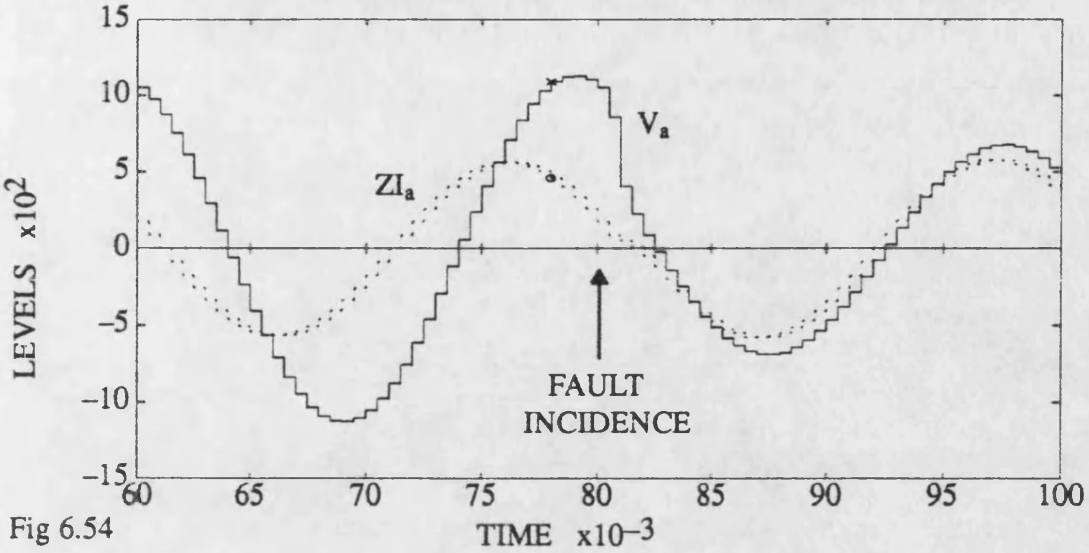

Fig 6.54

PRE–FAULT AND SUPERIMPOSED A–E ELEMENT QUANTITIES

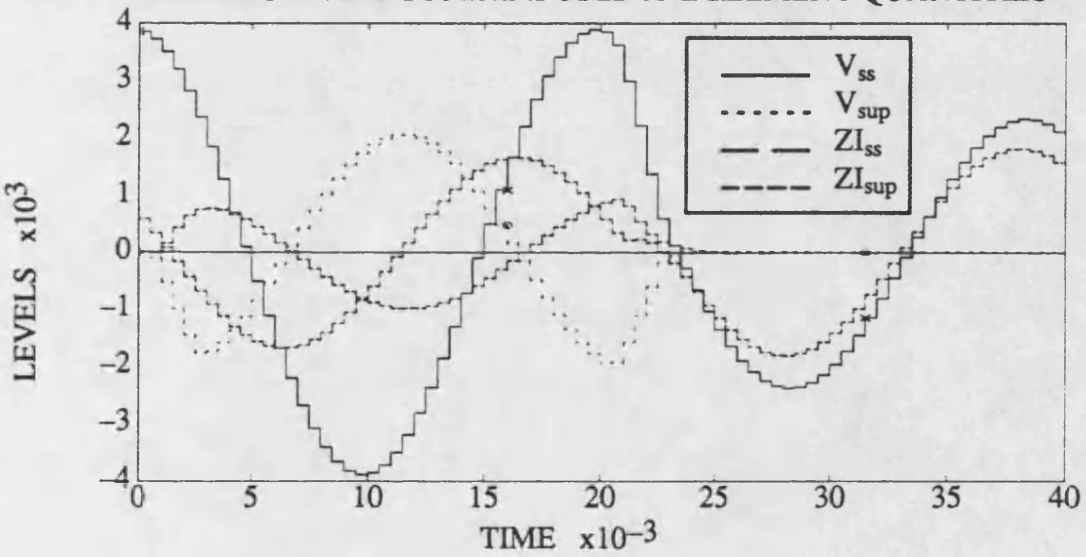

A–E FAULT: CHECK AND DISCRIMINANT QUANTITIES

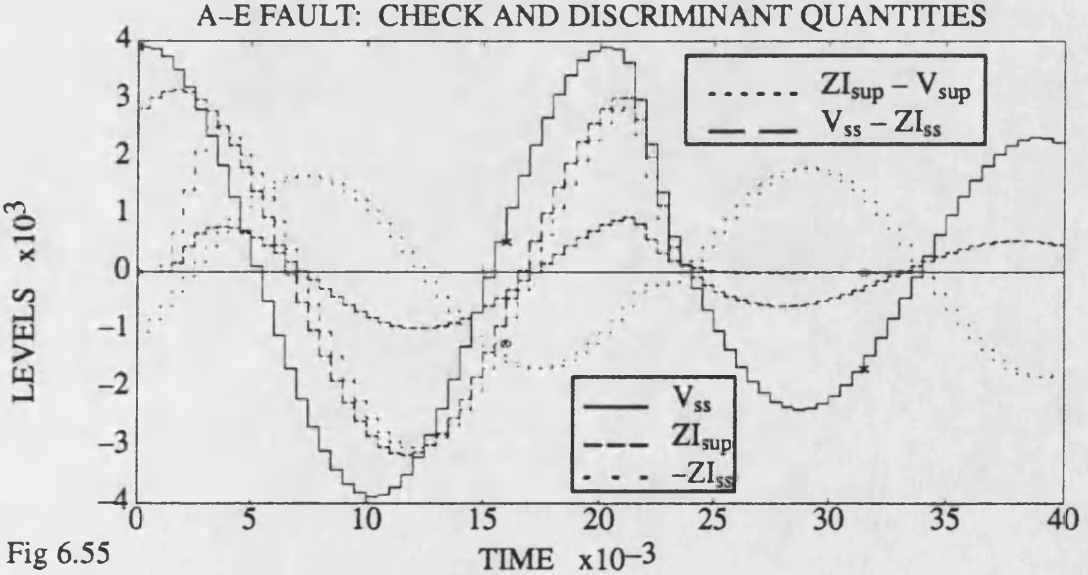

Fig 6.55

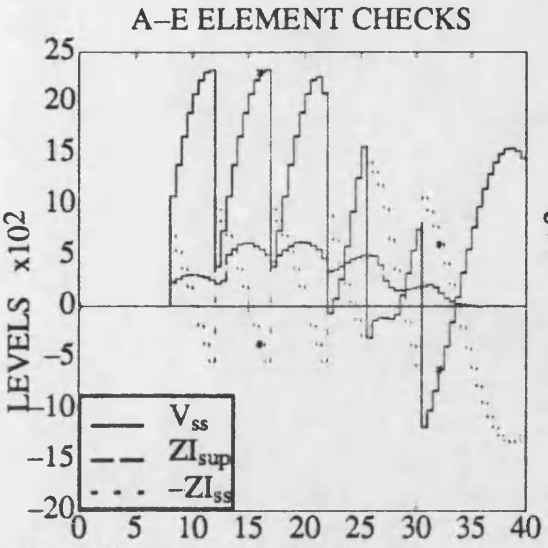

Fig 6.56

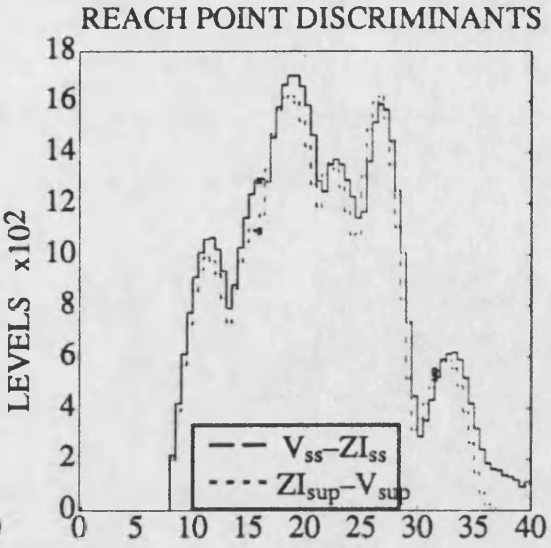

Fig 6.57

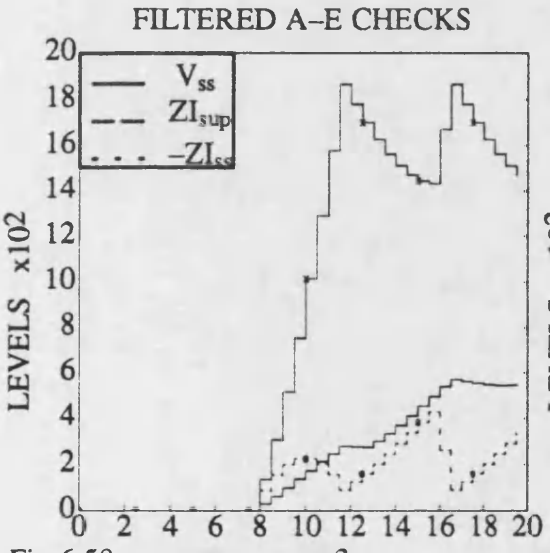

Fig 6.58

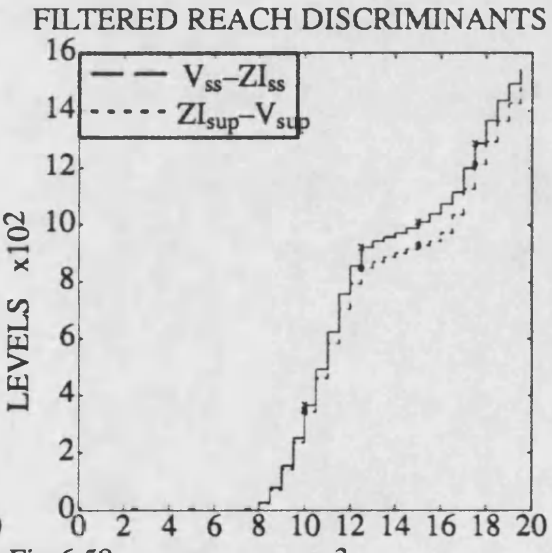

Fig 6.59

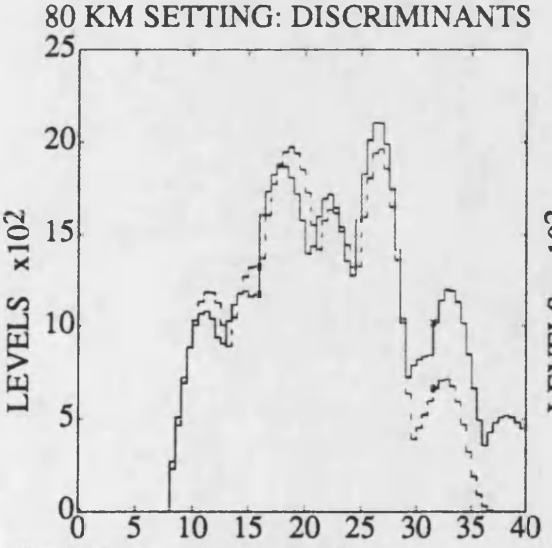

Fig 6.60

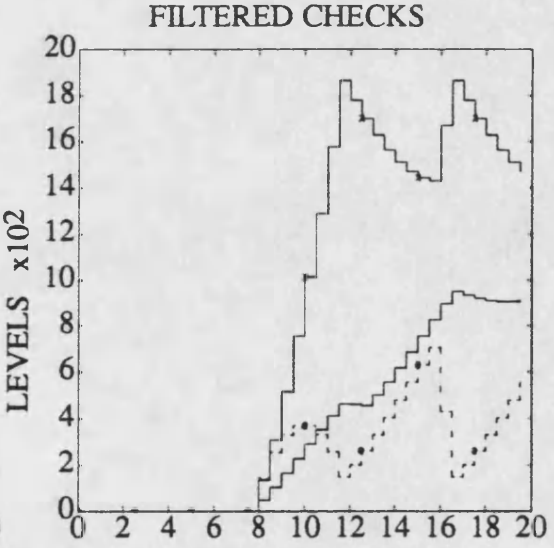

Fig 6.61

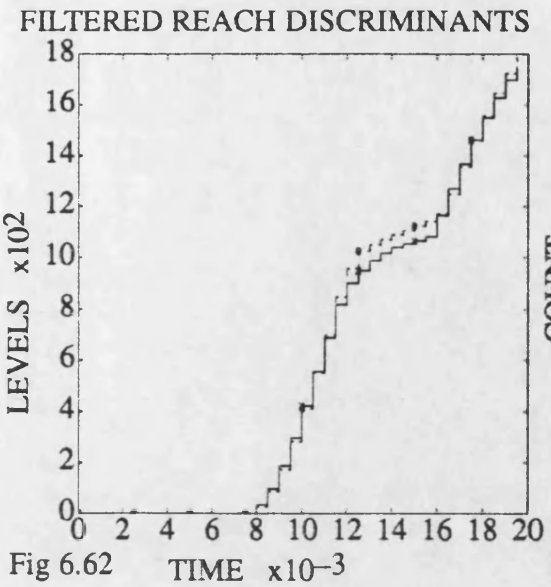

Fig 6.62

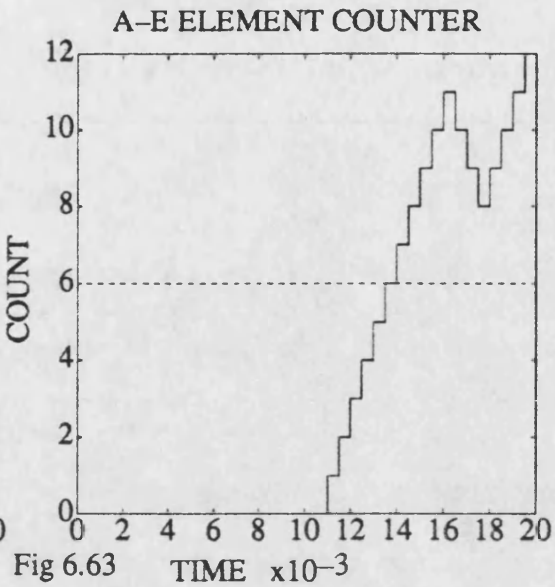

Fig 6.63

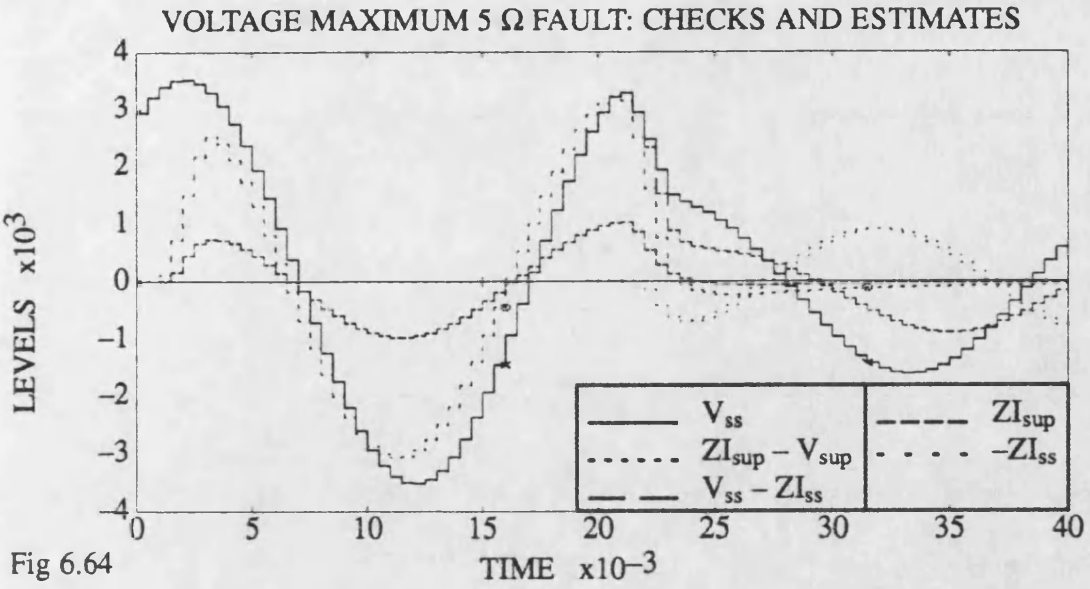

Fig 6.64

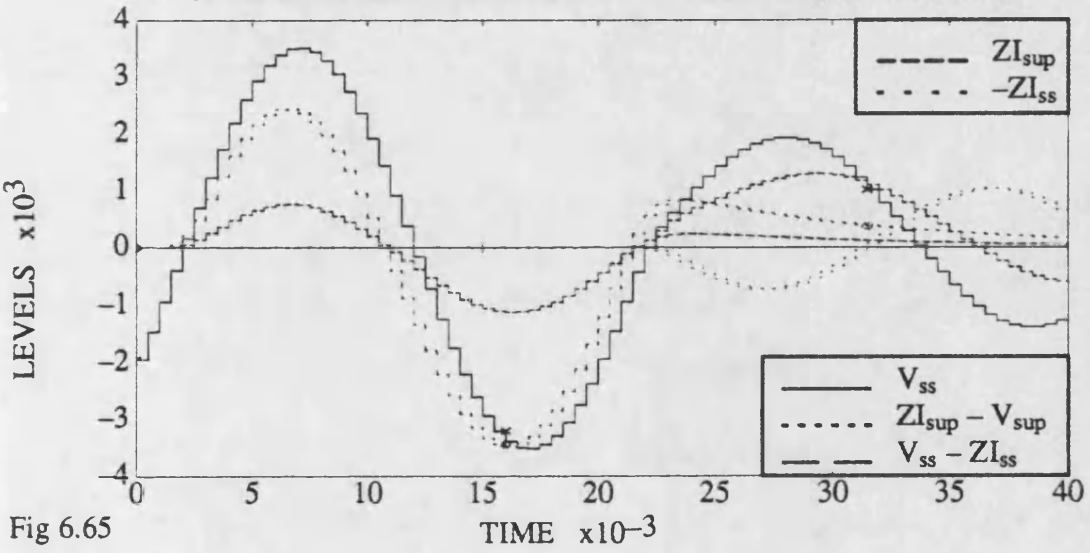

Fig 6.65

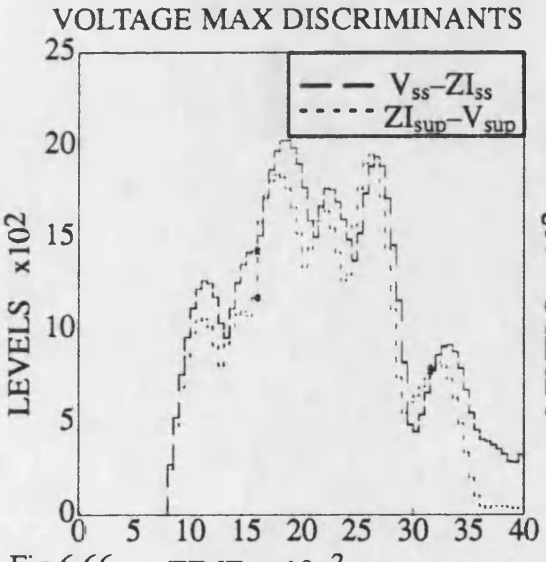

Fig 6.66

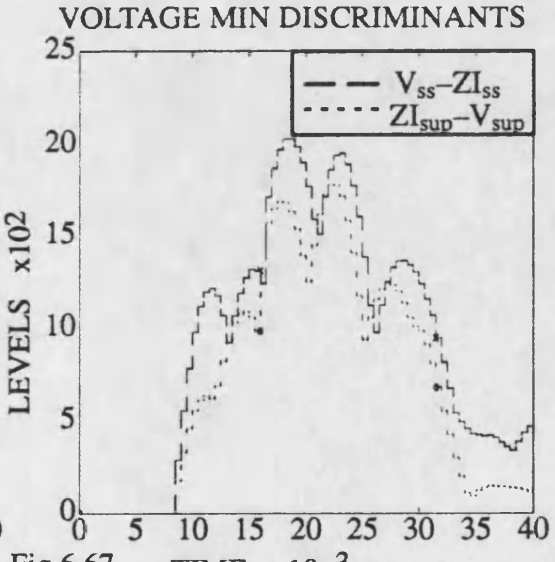

Fig 6.67

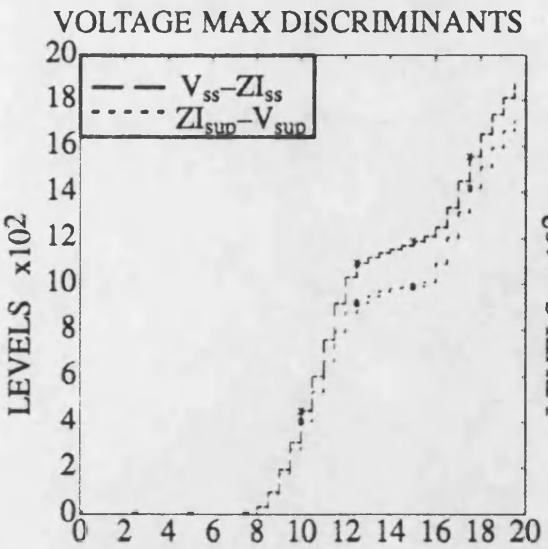

Fig 6.68

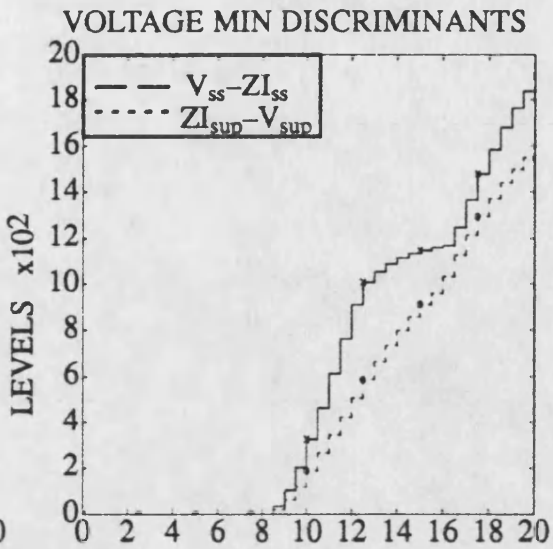

Fig 6.69

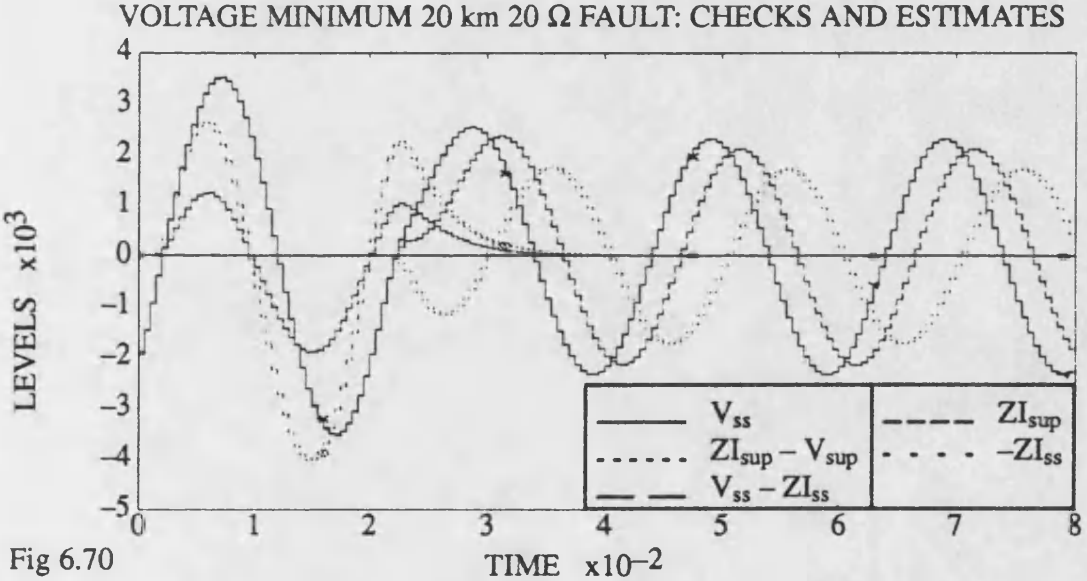

Fig 6.70

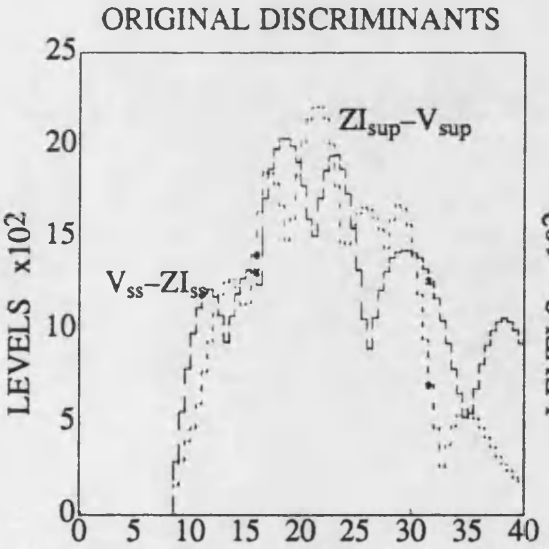

Fig 6.71

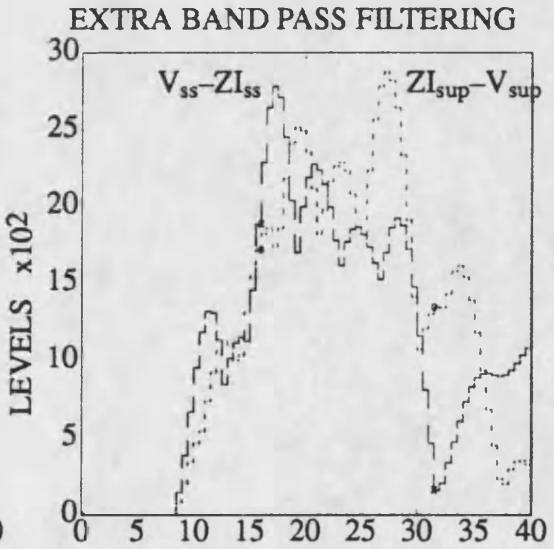

Fig 6.72

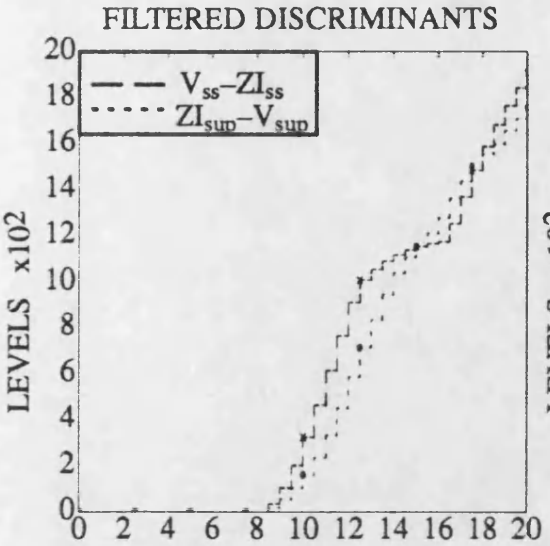

Fig 6.73

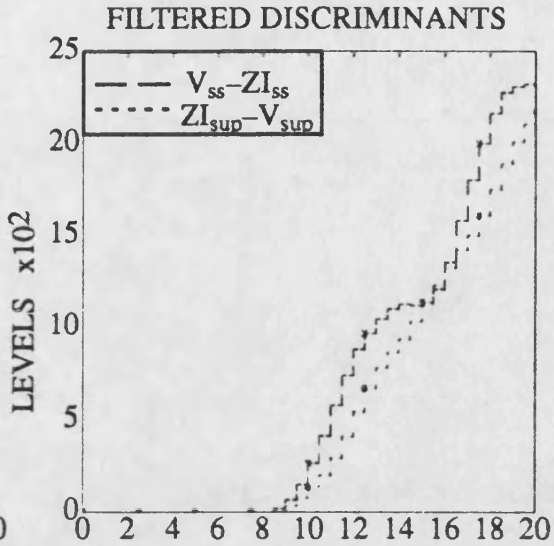

Fig 6.74

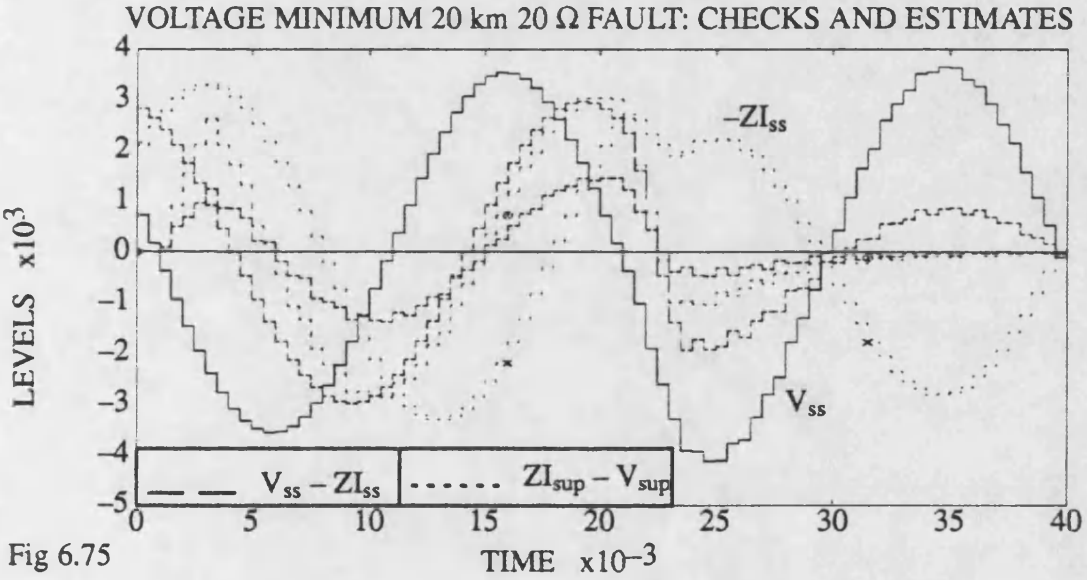

Fig 6.75

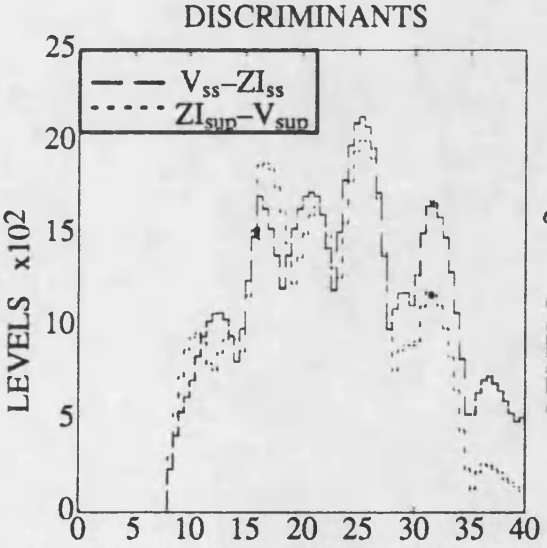

Fig 6.76

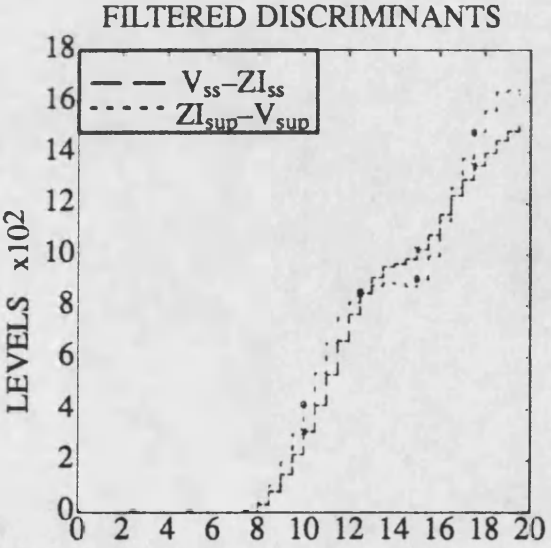

Fig 6.77

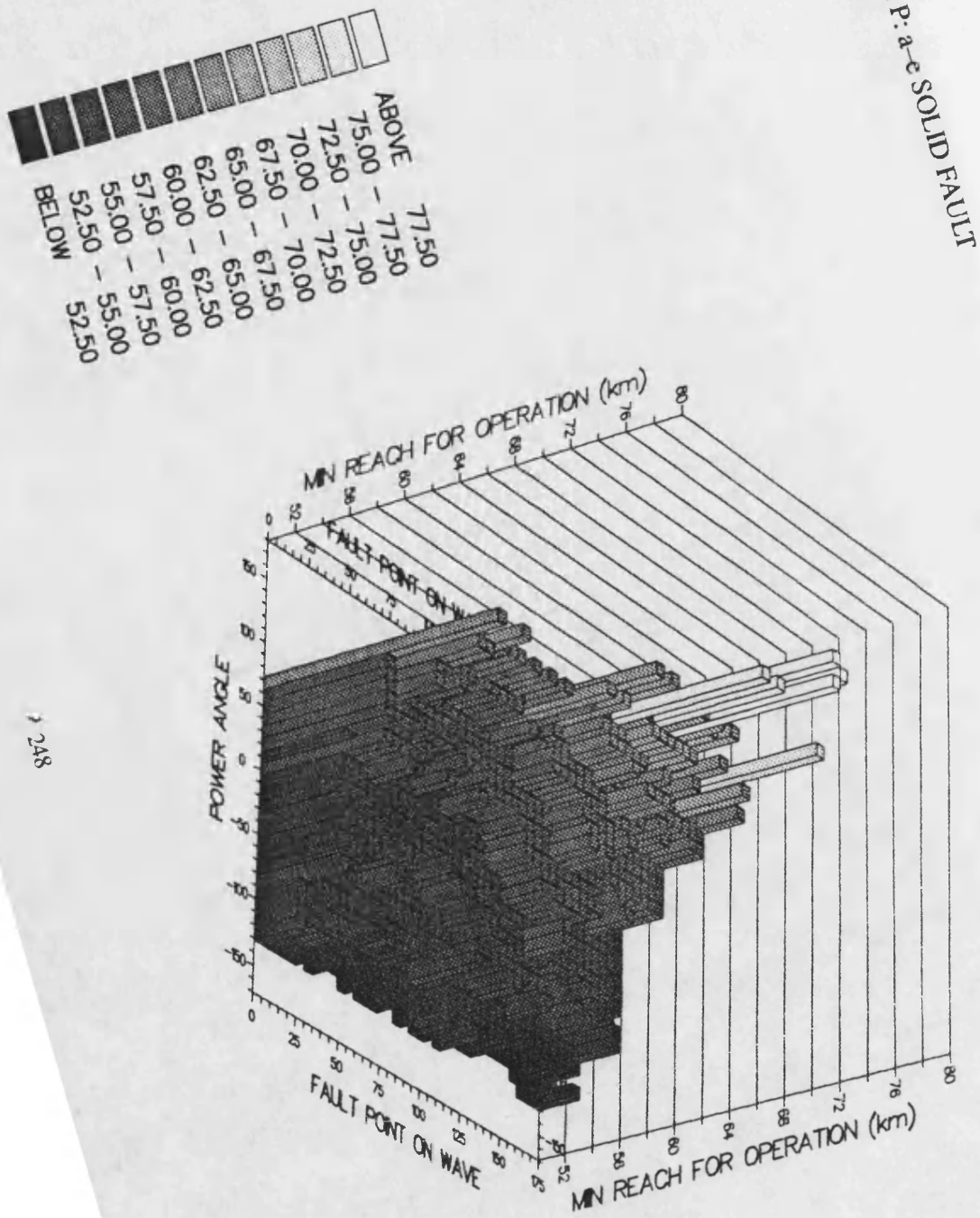

Fig 6.78 IMR AT BUSBAR P: a–e SOLID FAULT

Fig 6.79 IMR AT BUSBAR P : a–e SOLID FAULT

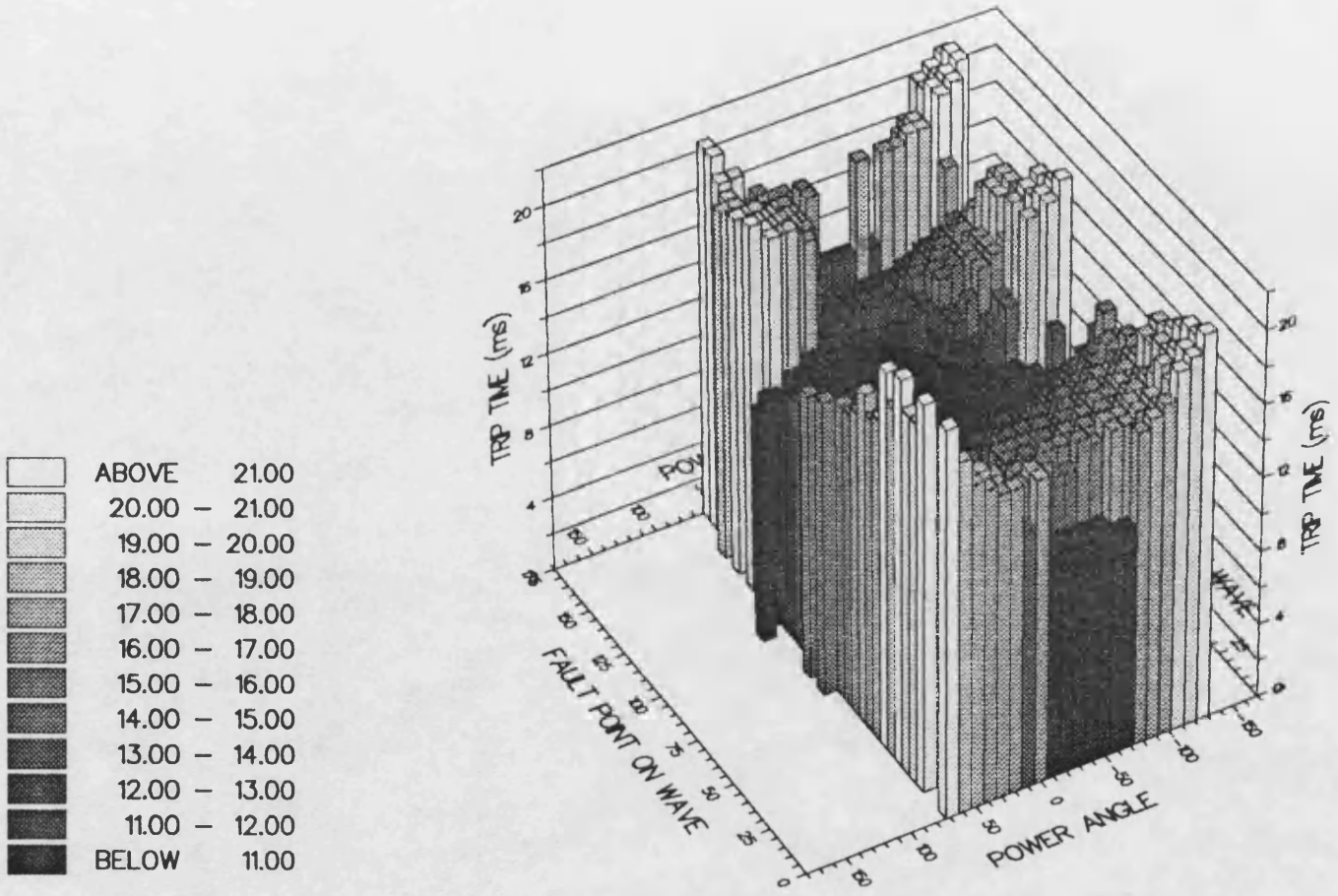

Fig 6.80 IMR AT BUSBAR P: 5Ω a–e FAULT

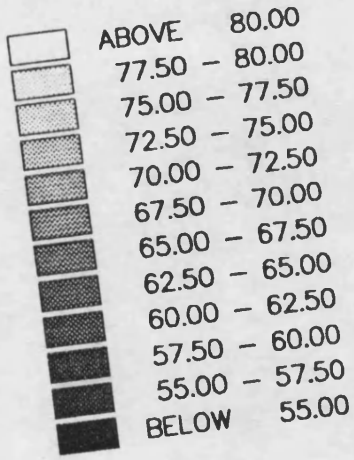

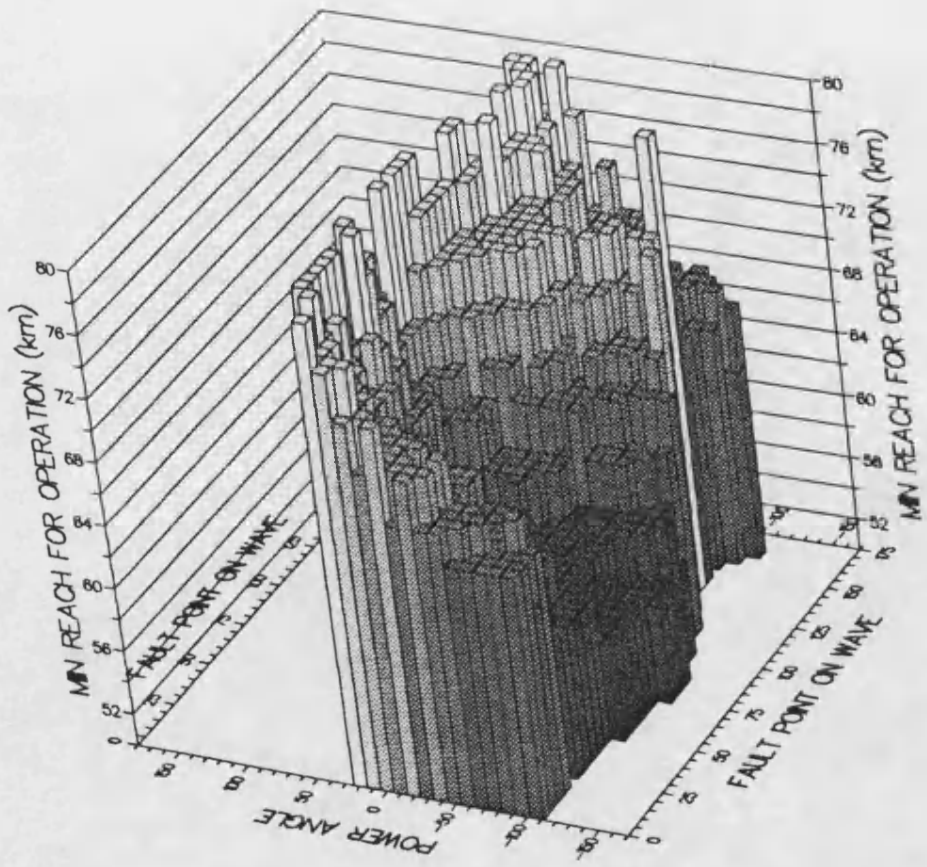

Fig 6.81 IMR AT BUSBAR P: 5Ω a–e FAULT

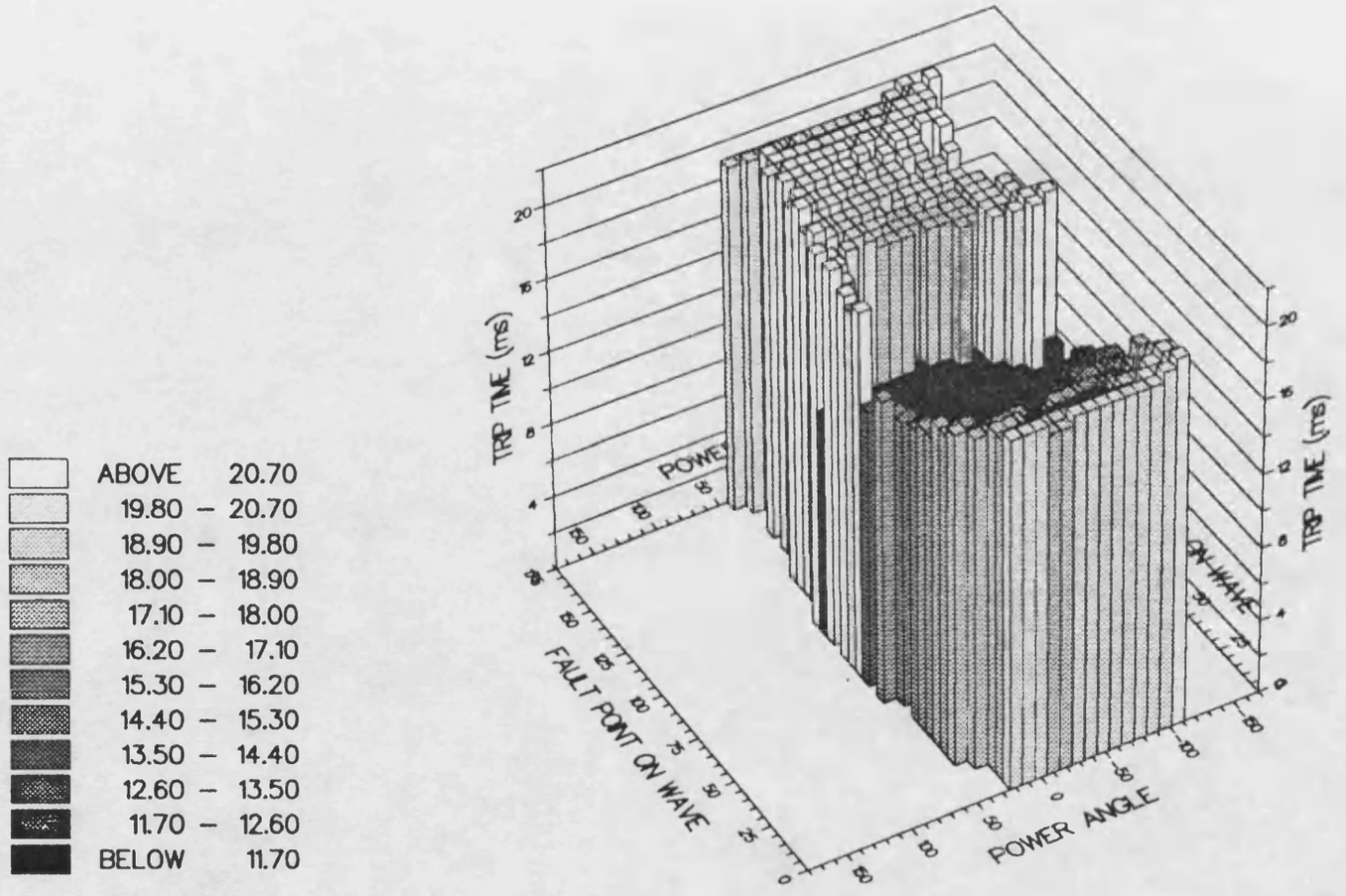

Fig 6.82 IMR AT P: 20 km 20Ω a-e FAULT

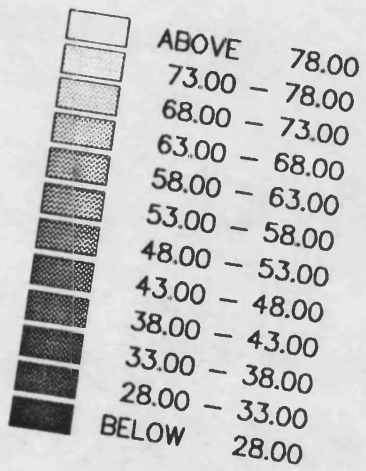

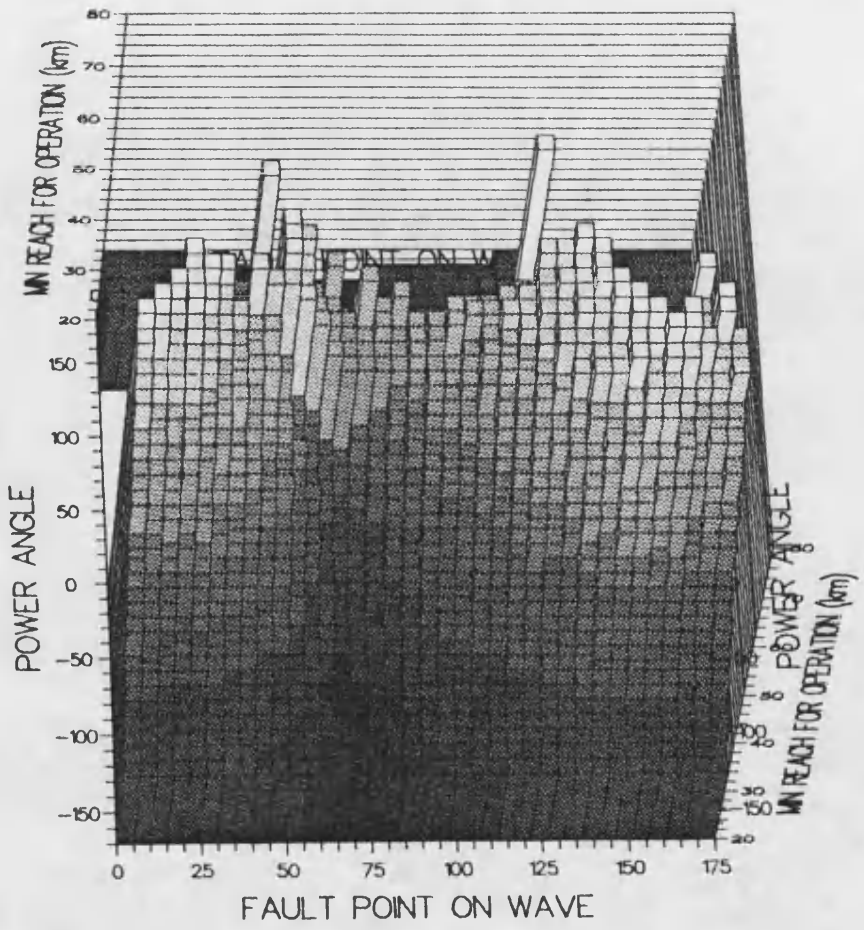

Fig 6.83 IMR AT P: 20 km 20Ω a–e FAULT

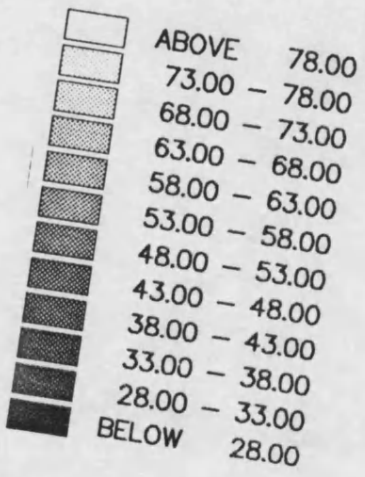

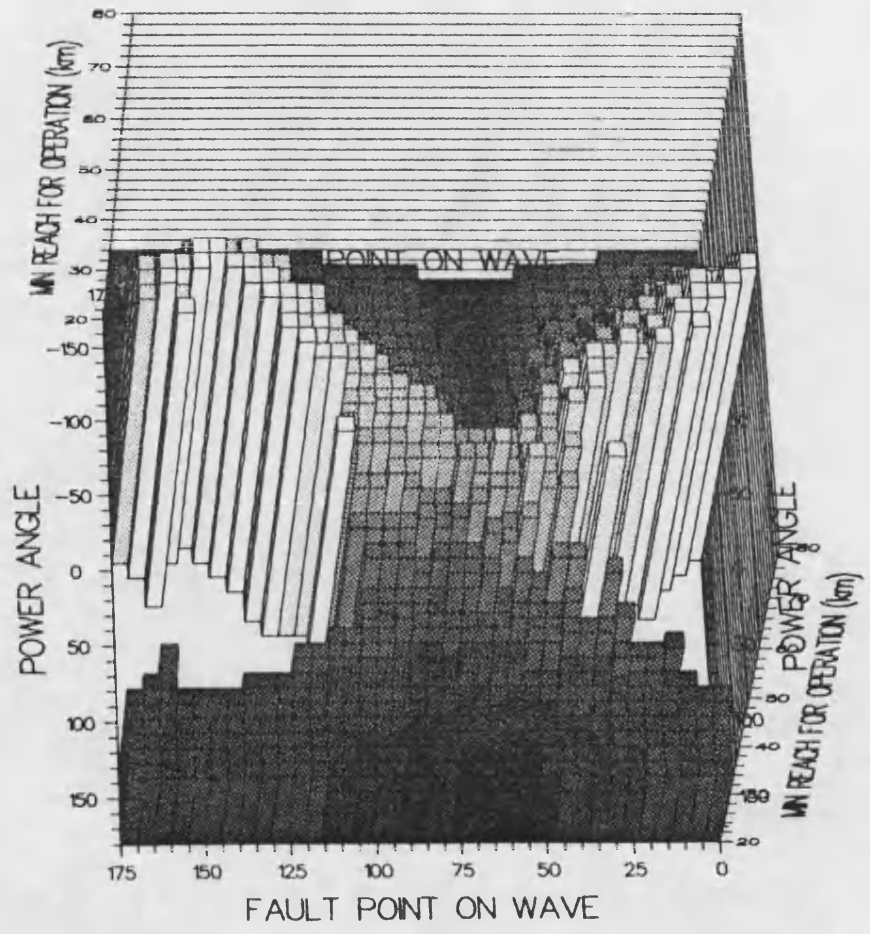

Fig 6.84 IMR AT P: 20 km 20Ω a–e FAULT

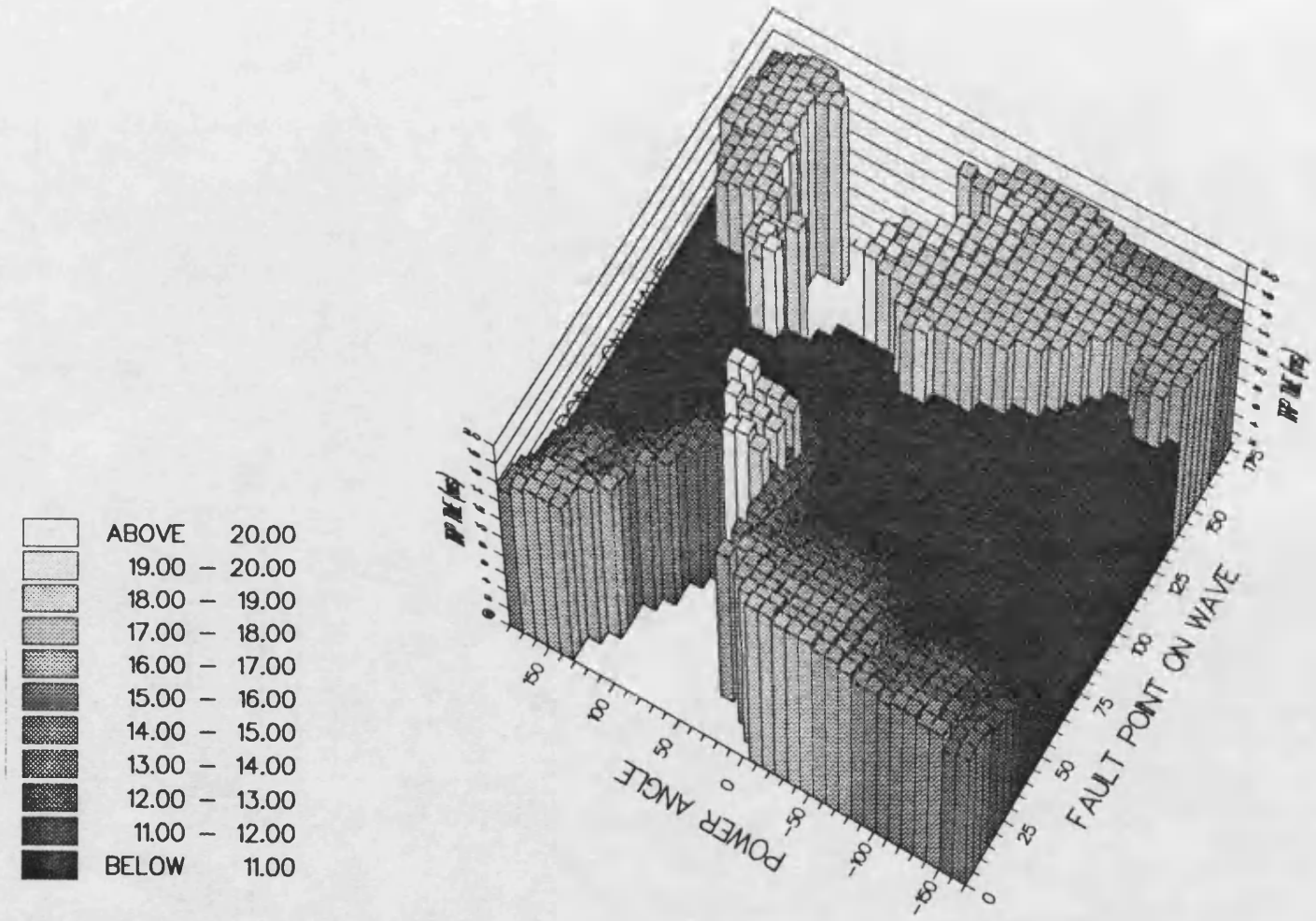

Fig 6.85 IMR AT P: a-e SOLID FAULT; $Z_0/Z_1 = 3$

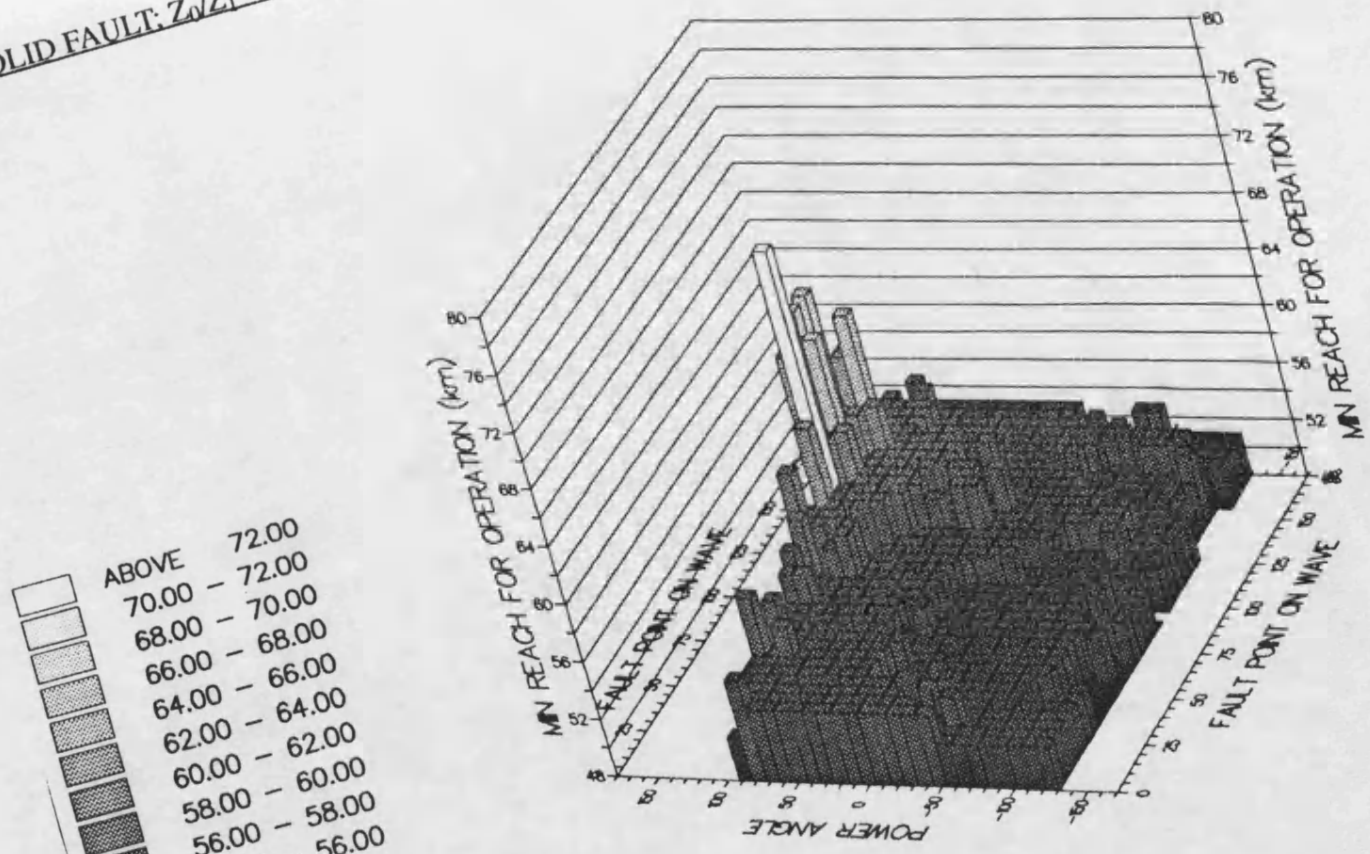

Fig 6.86 IMR AT P: $Z_0/Z_1 = 3$.

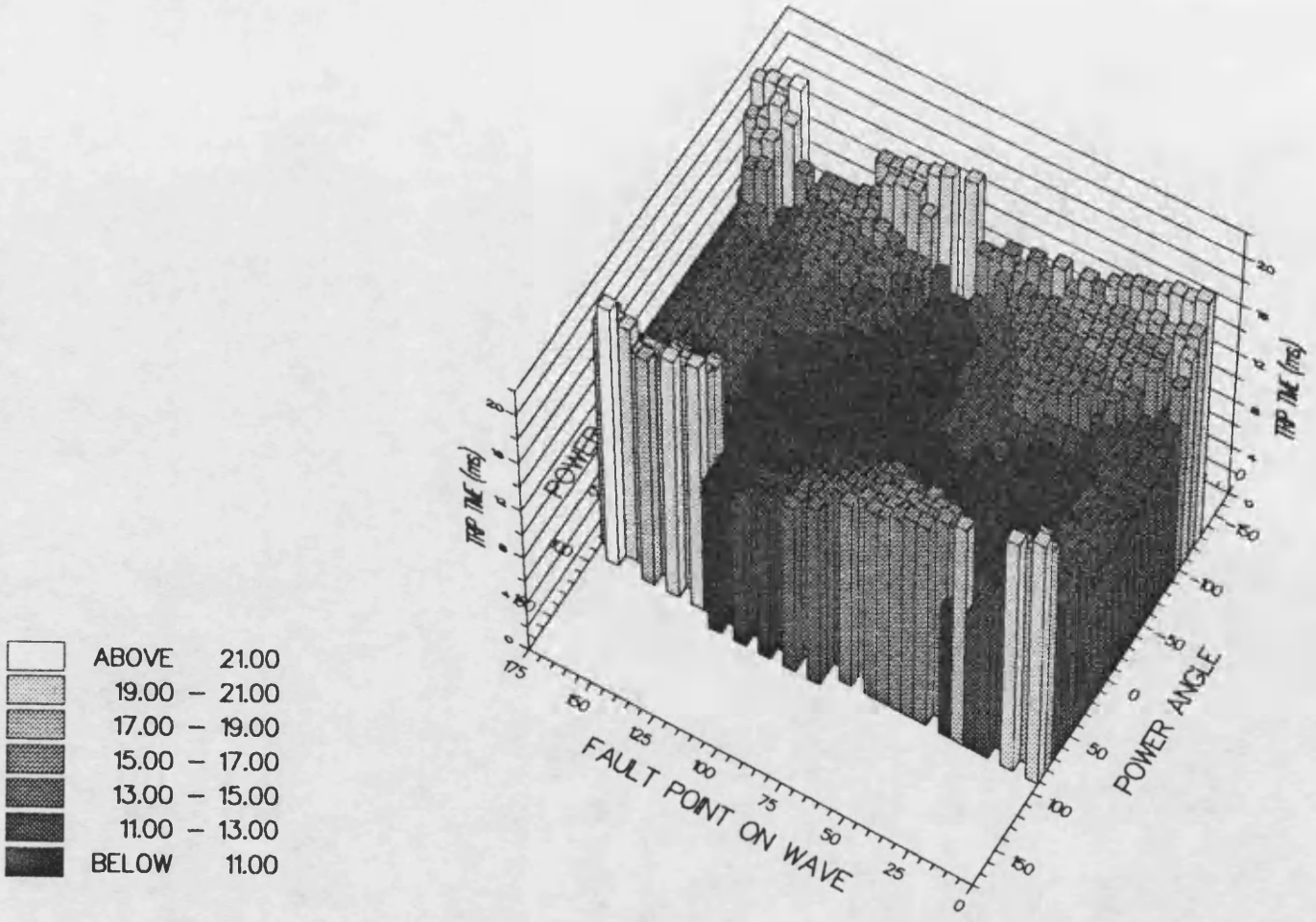

Fig 6.87 IMR AT P; Z_0/Z_1=3; 35 GVA

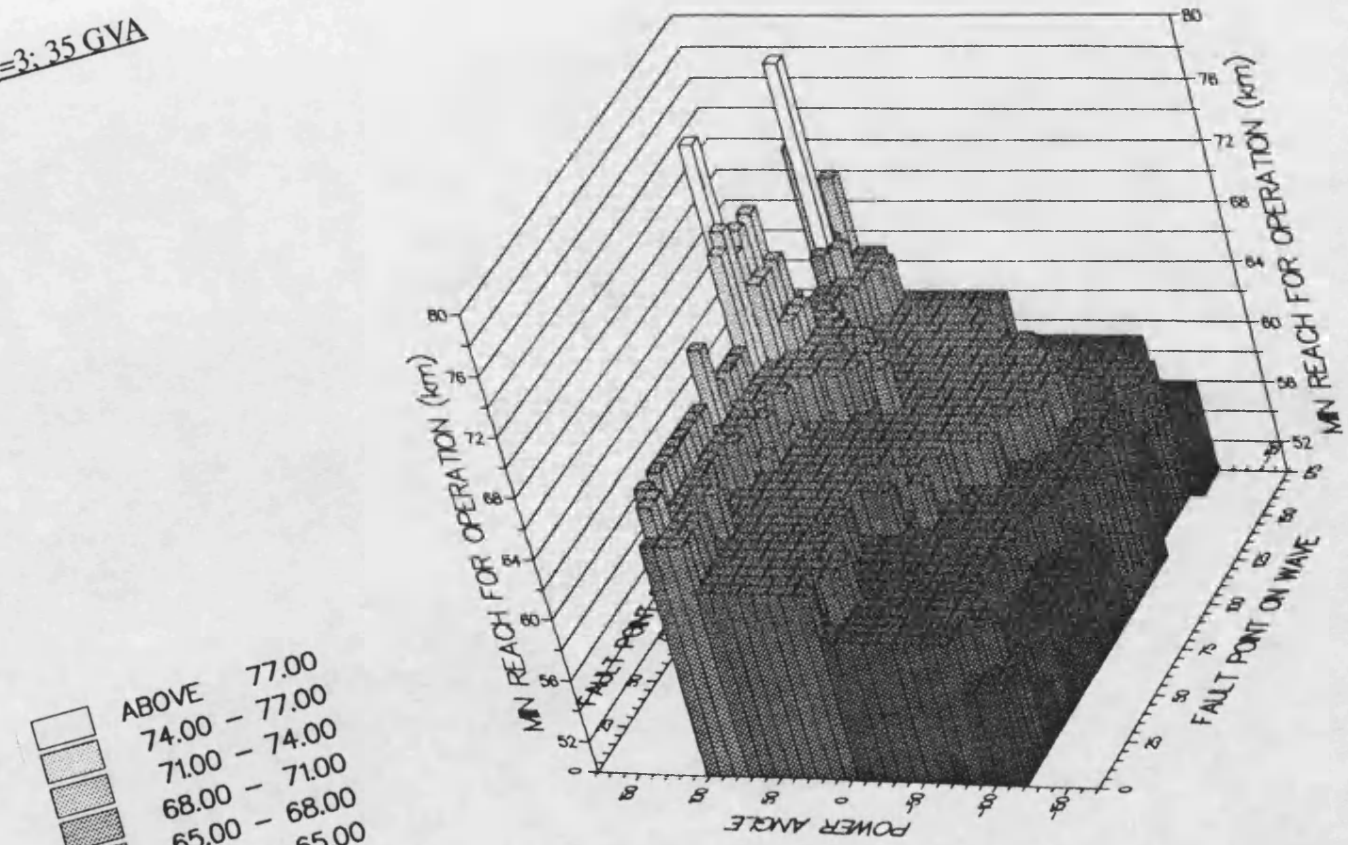

Fig 6.88 IMR AT P: Z_0/Z_1=3; 35 GVA

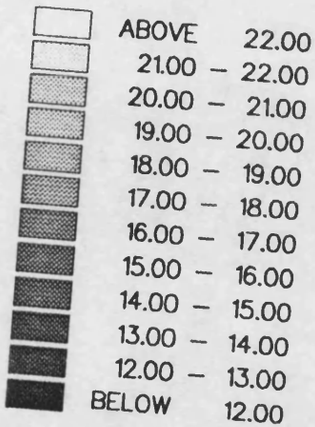

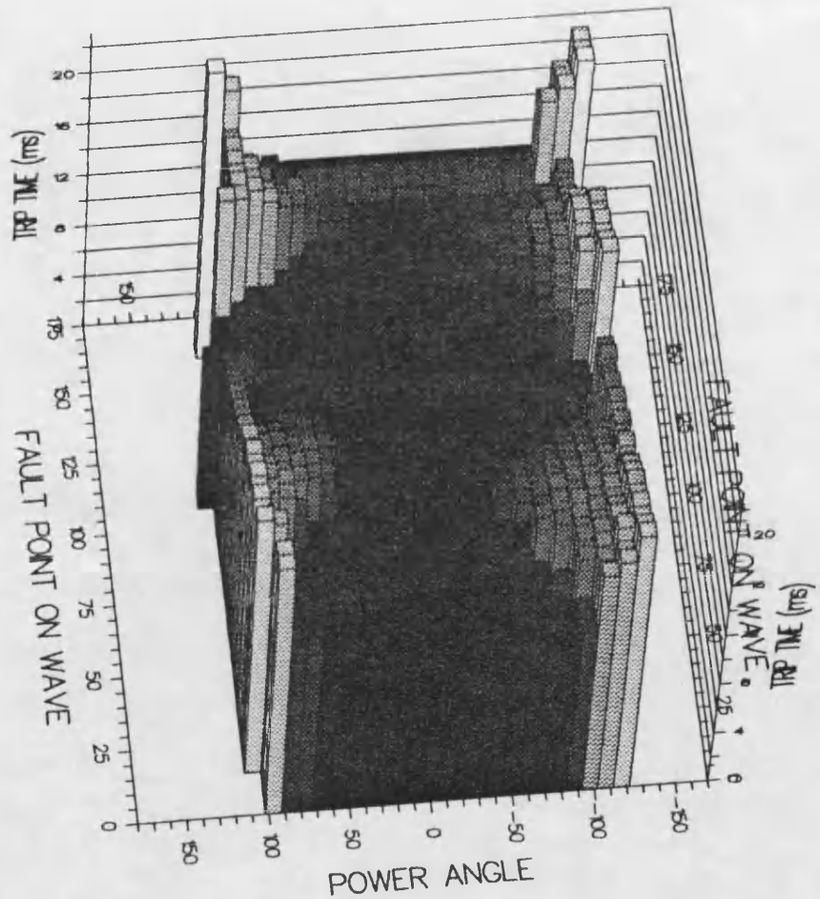

Fig 6.89 IMR AT P; b–e SOLID FAULT; $Z_0/Z_1=1$

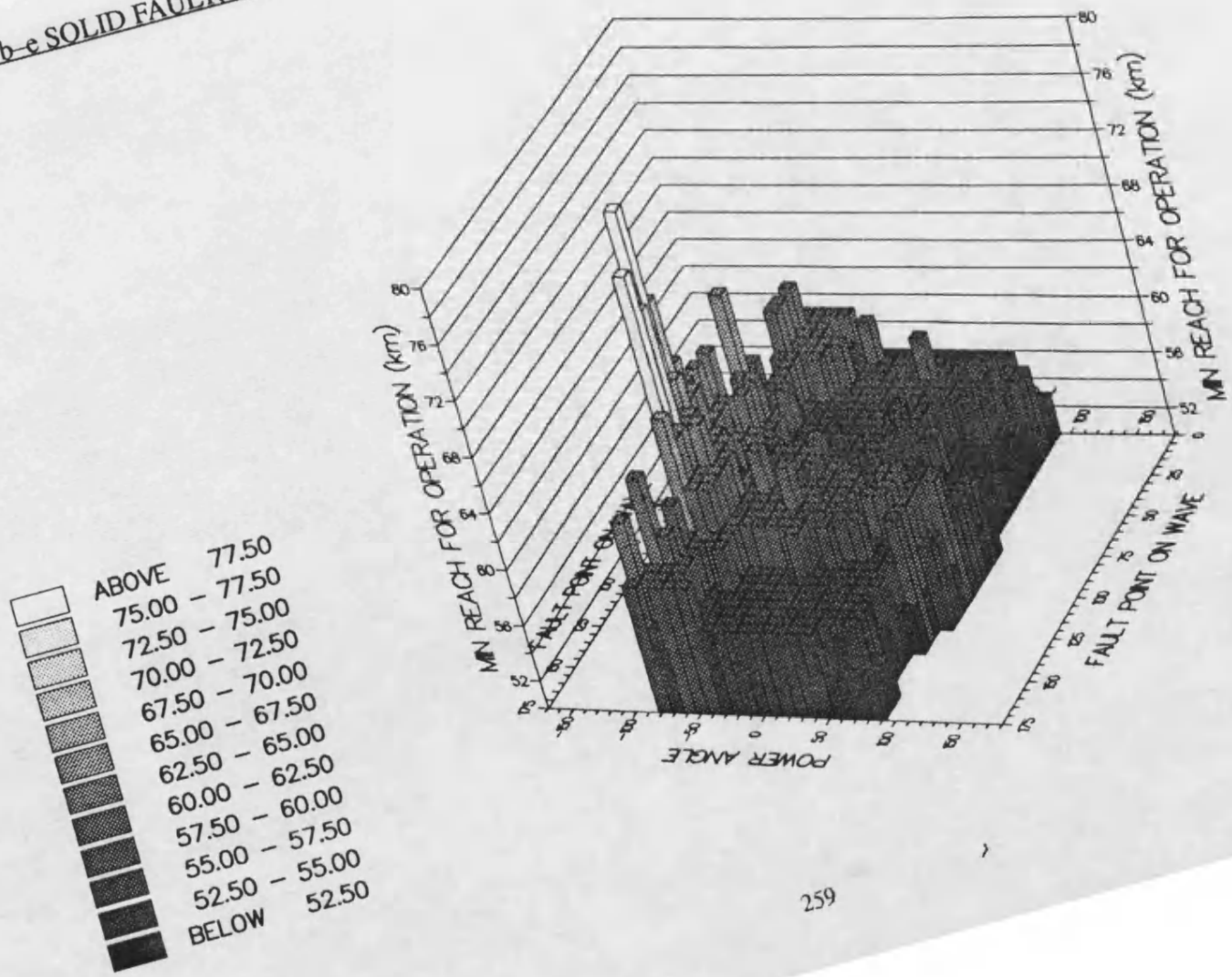

Fig 6.90 IMR AT P: b-e SOLID FAULT; $Z_0/Z_1=1$

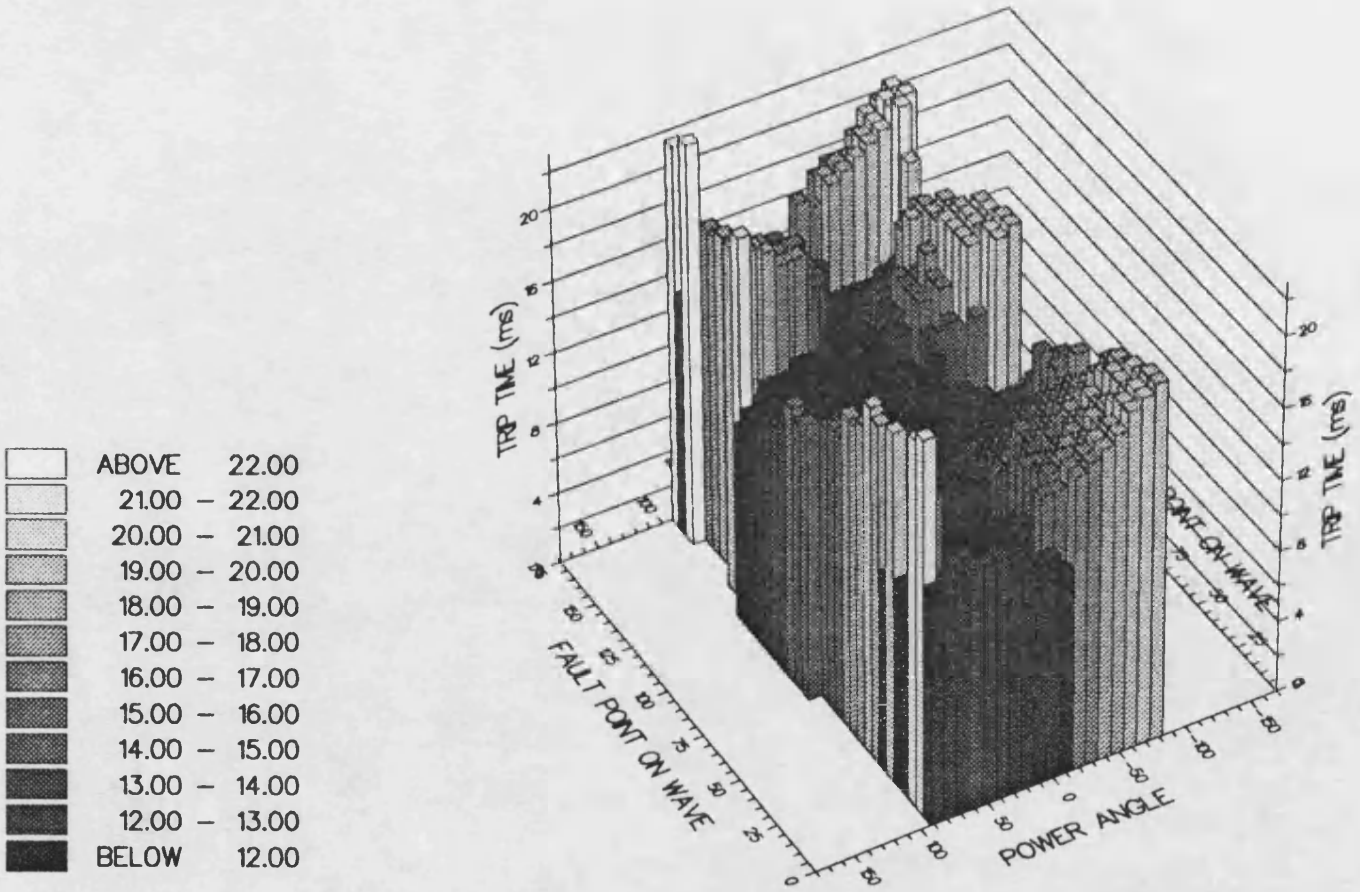

Fig 6.91 IMR AT P; b–c SOLID FAULT

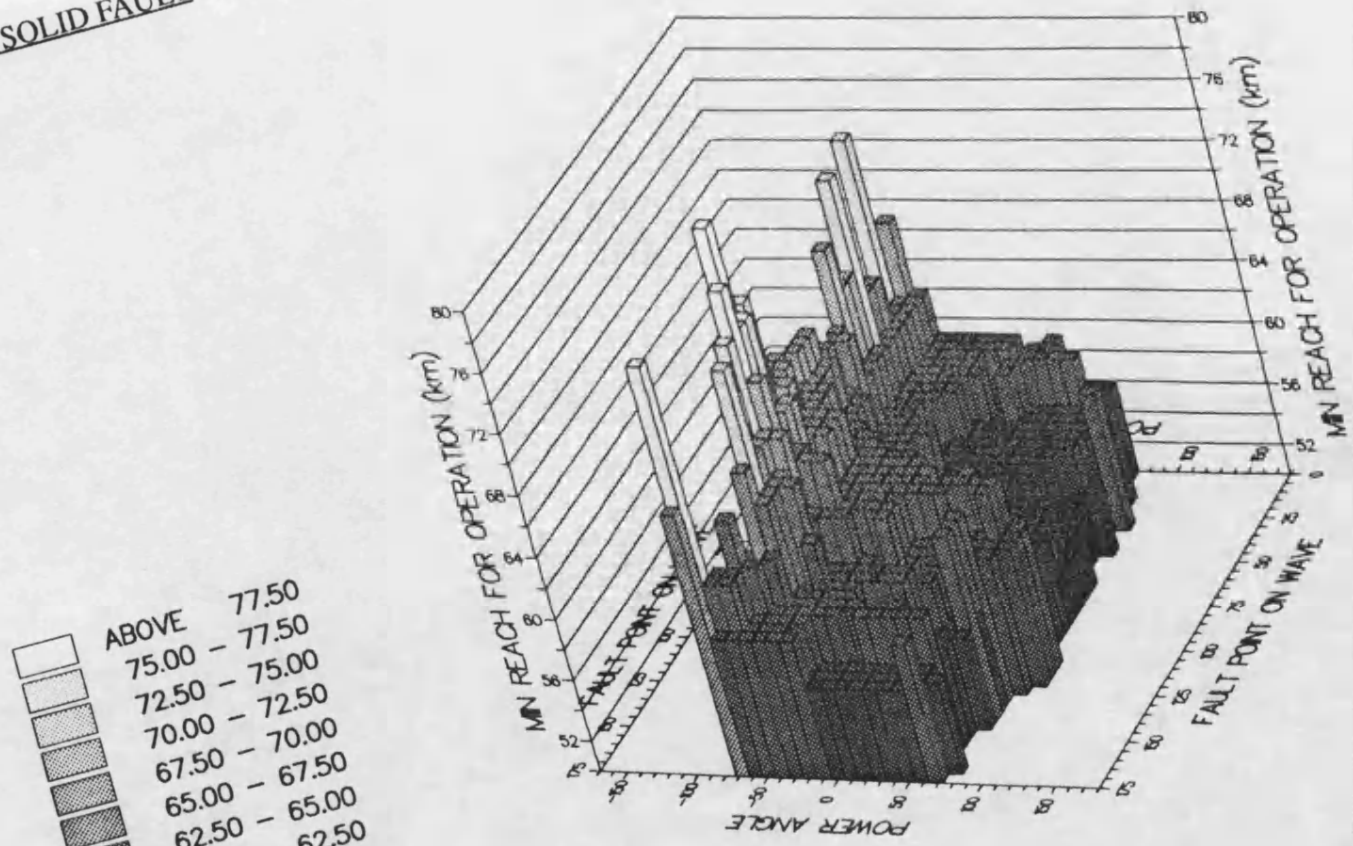

Fig 6.92 IMR AT P; b–c SOLID FAULT

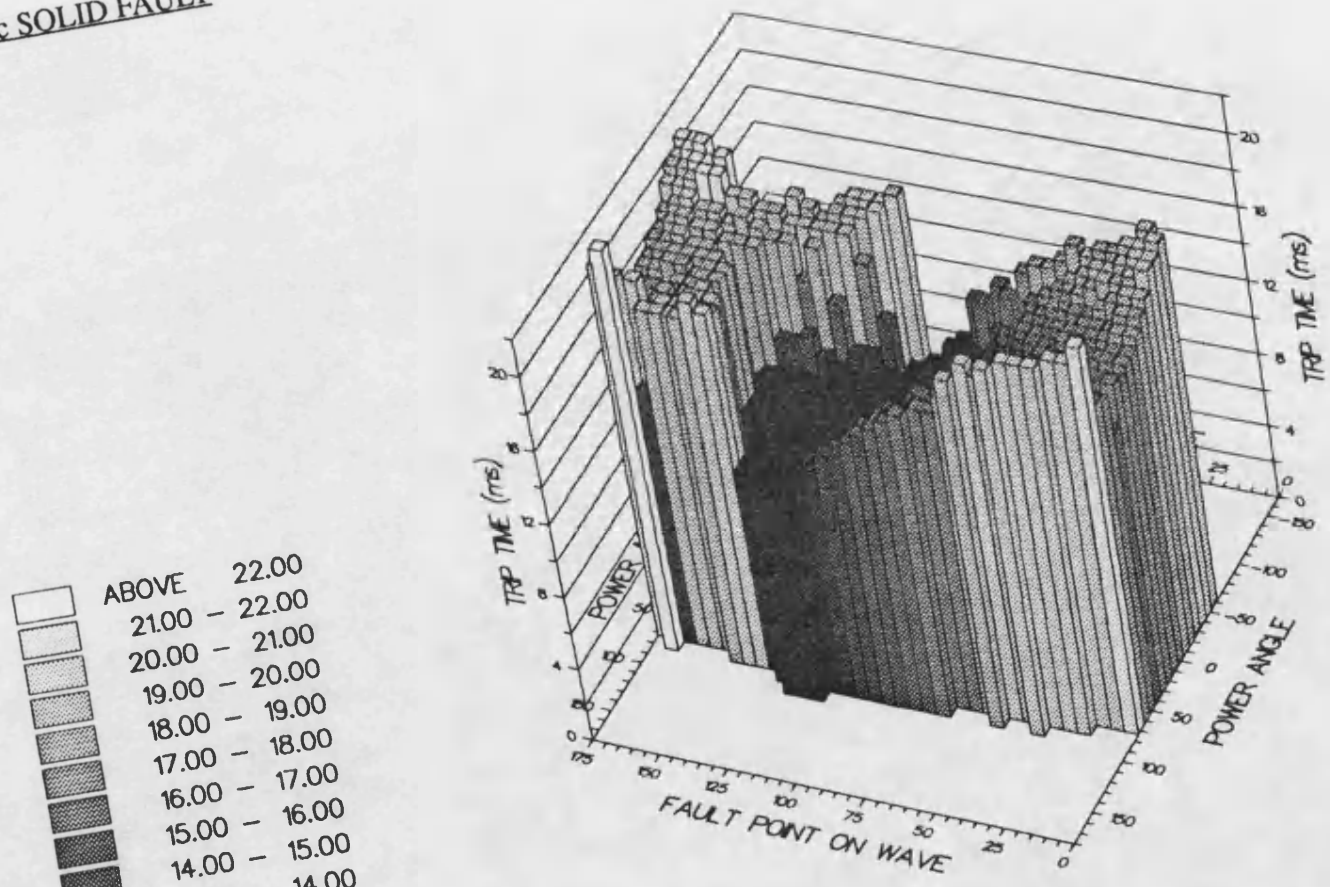

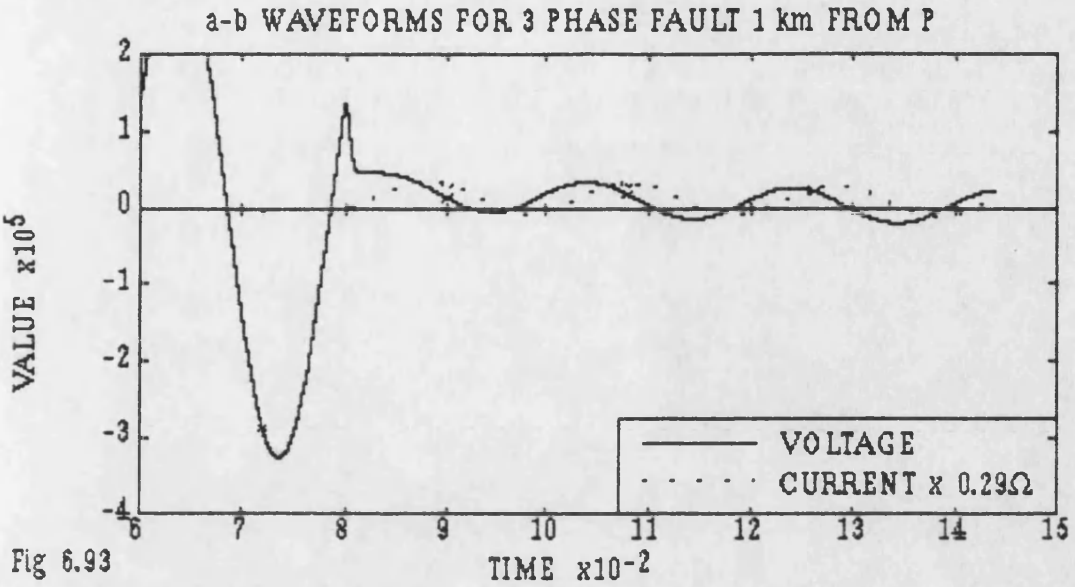

Fig 6.93

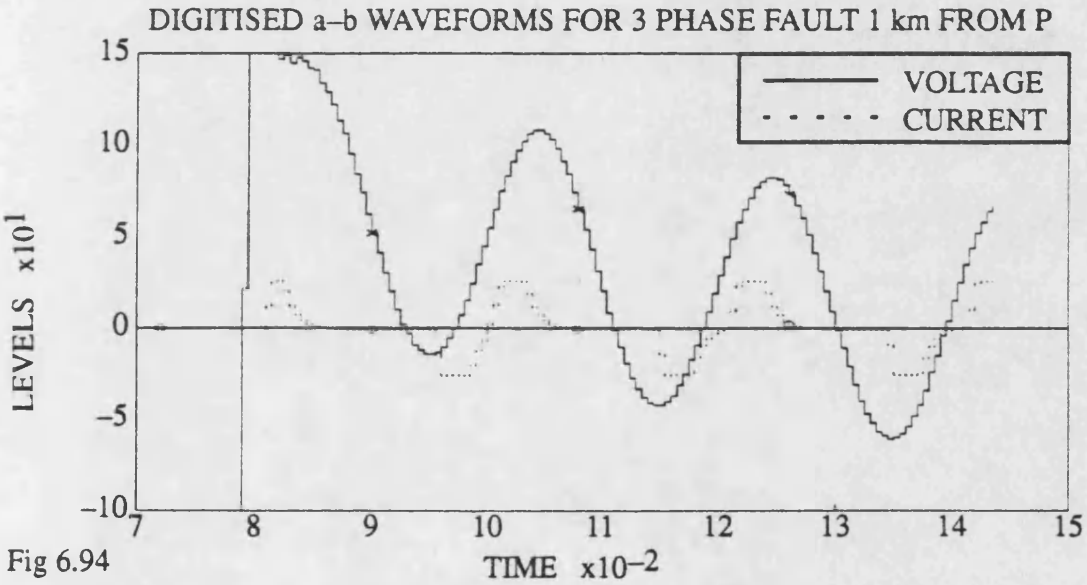

Fig 6.94

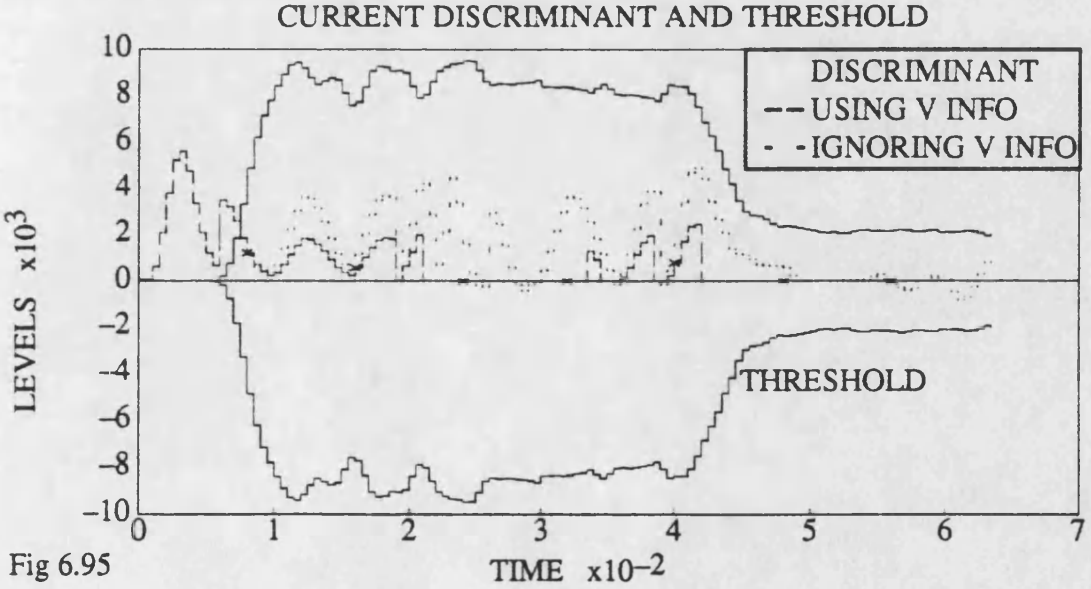

Fig 6.95

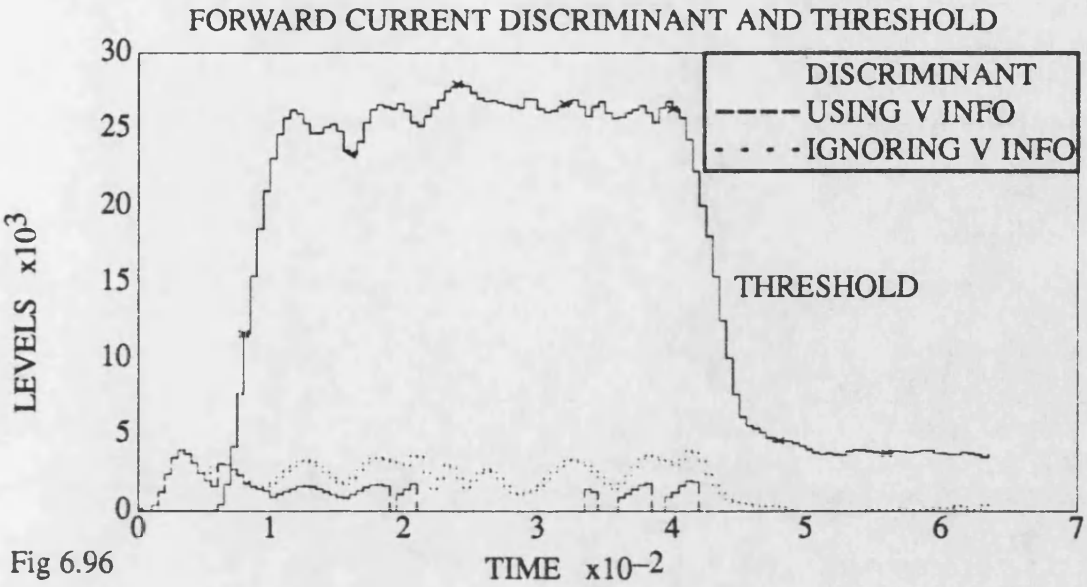

Fig 6.96

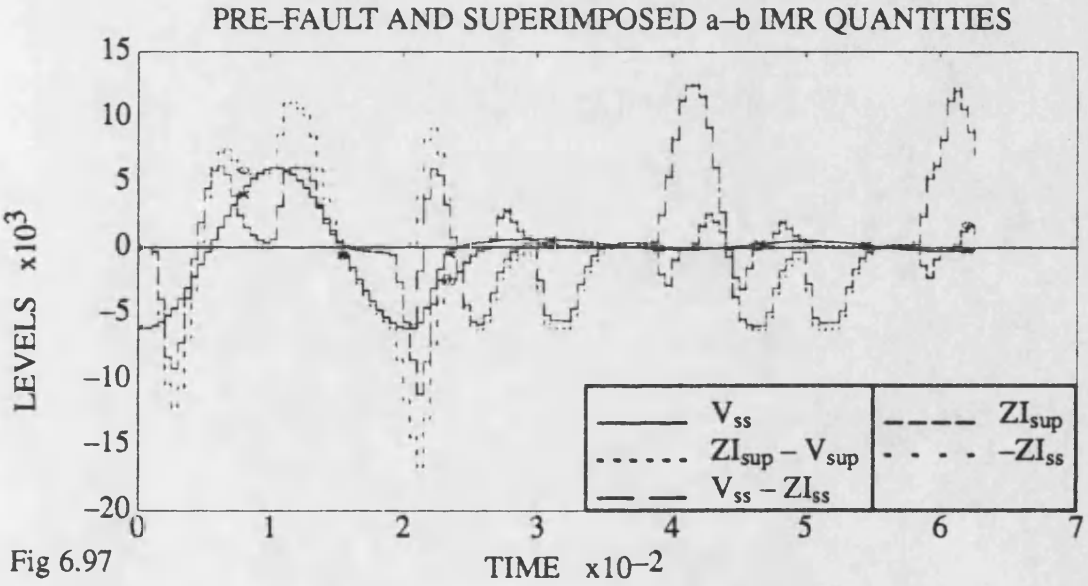

Fig 6.97

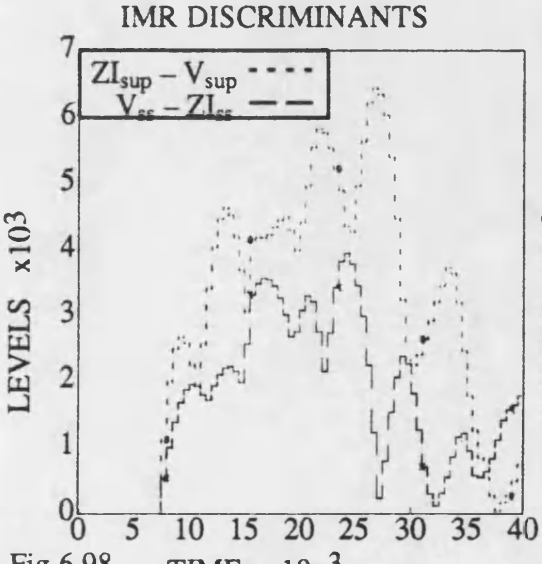

Fig 6.98

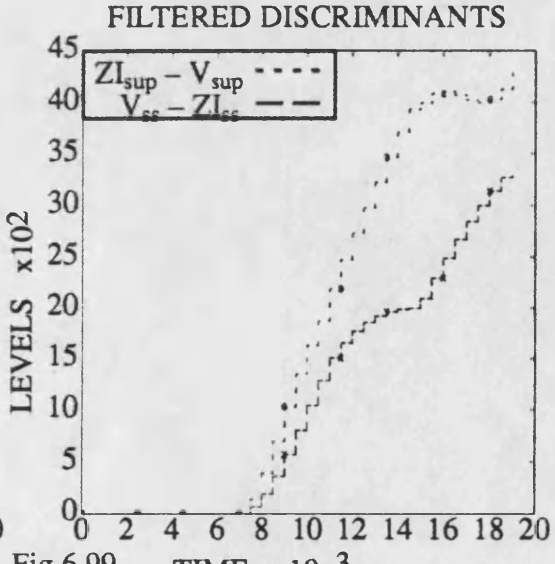

Fig 6.99

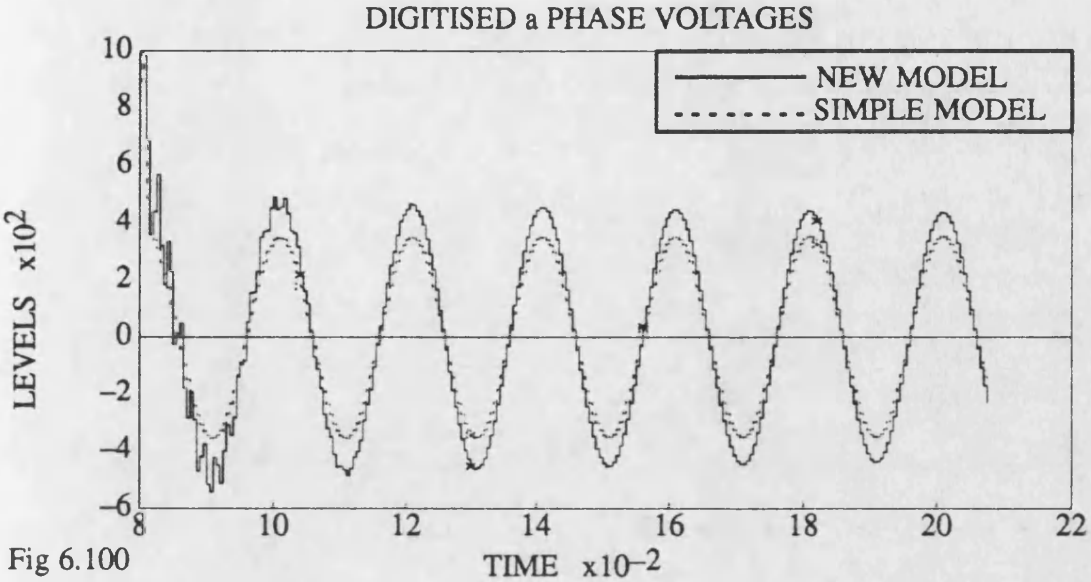

Fig 6.100

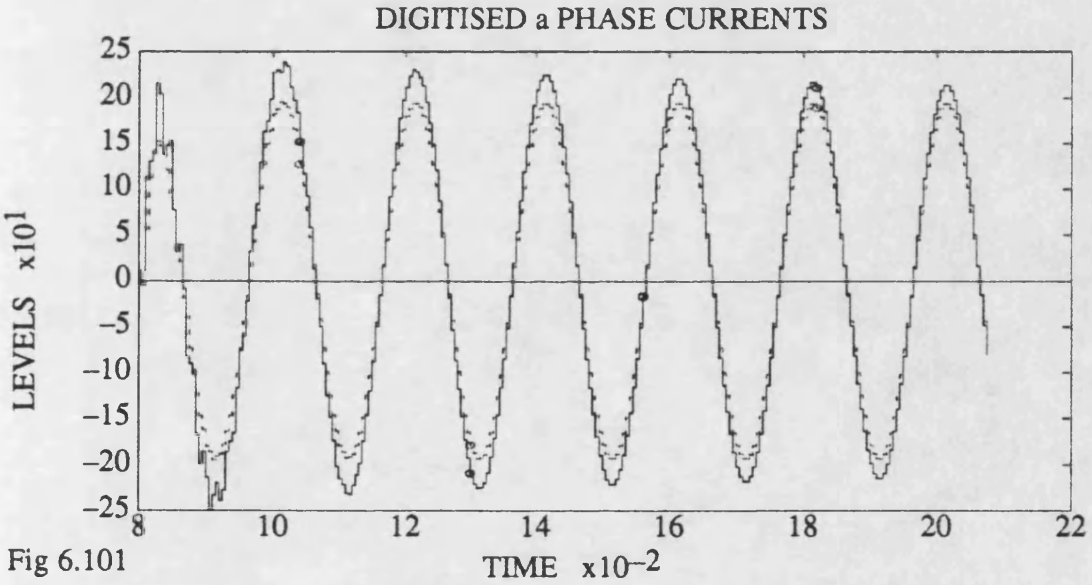

Fig 6.101

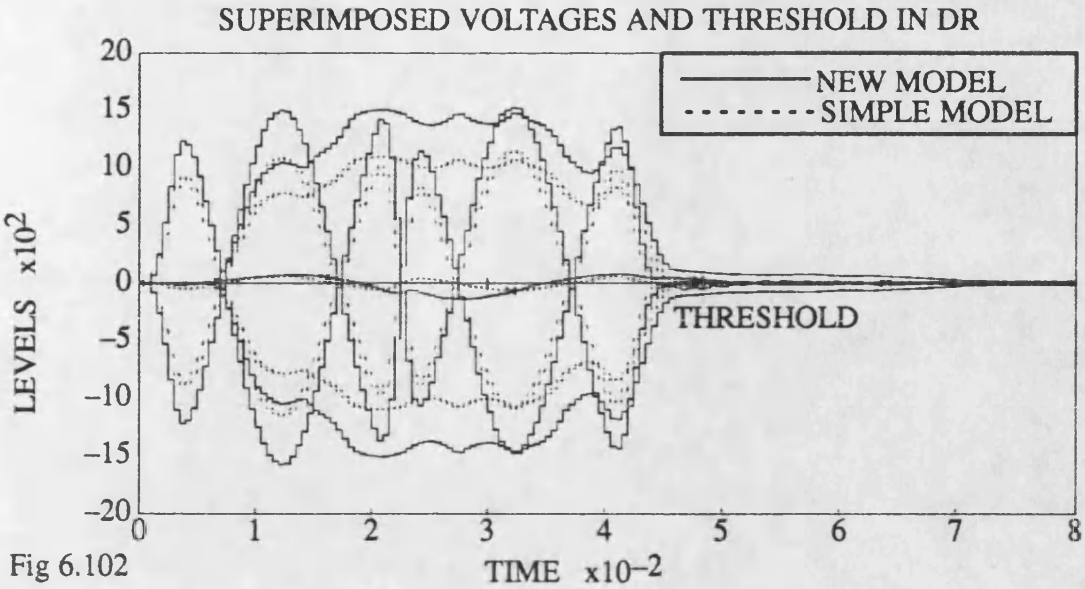

Fig 6.102

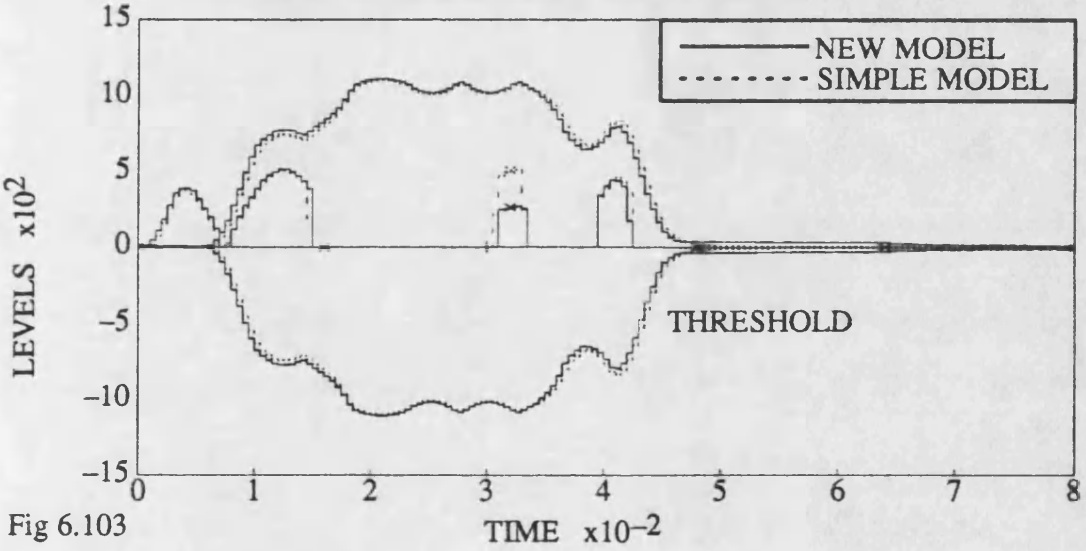

Fig 6.103

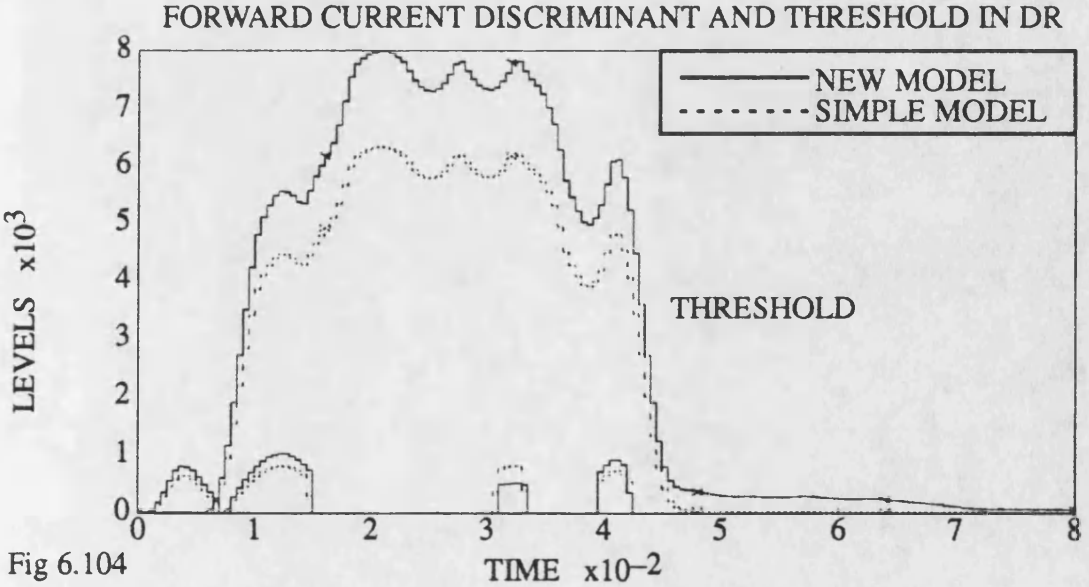

Fig 6.104

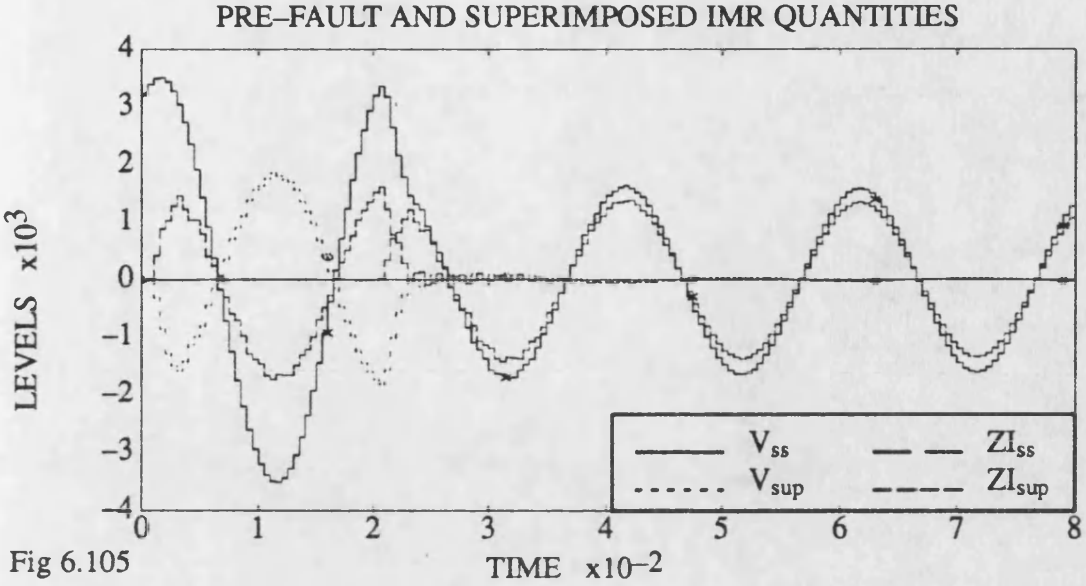

Fig 6.105

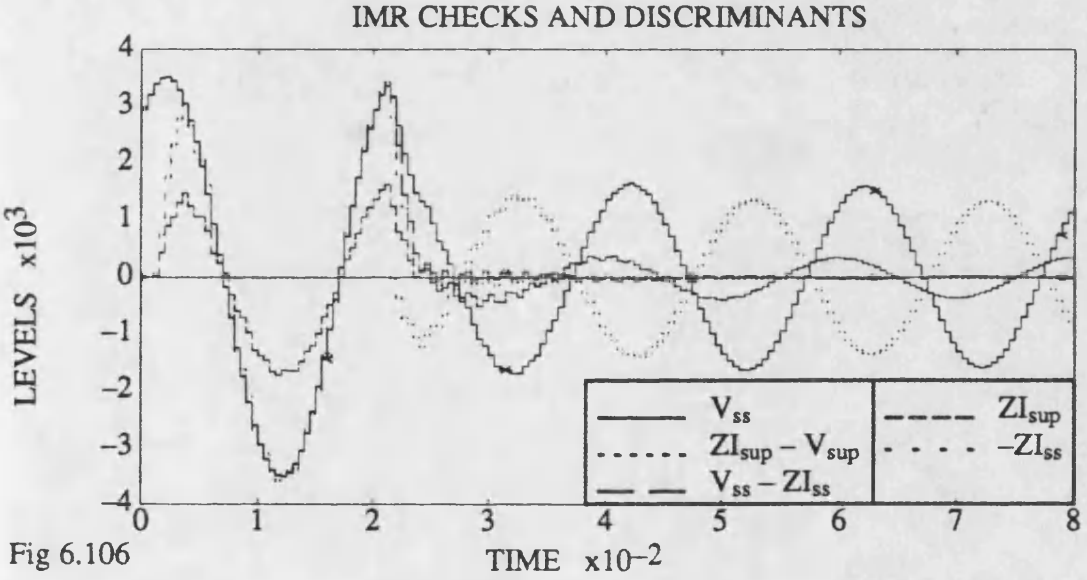

Fig 6.106

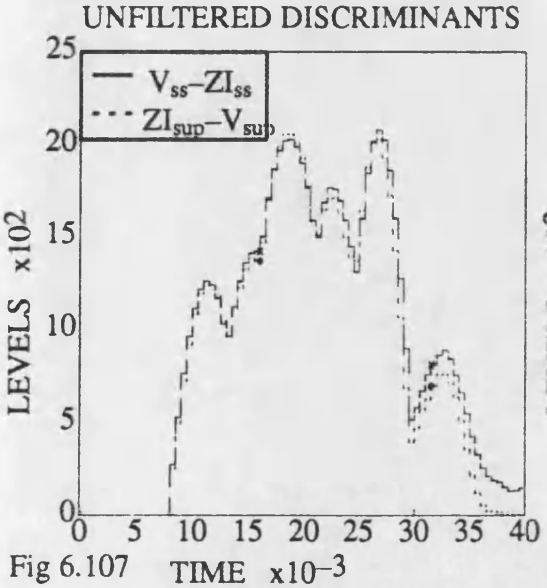

Fig 6.107

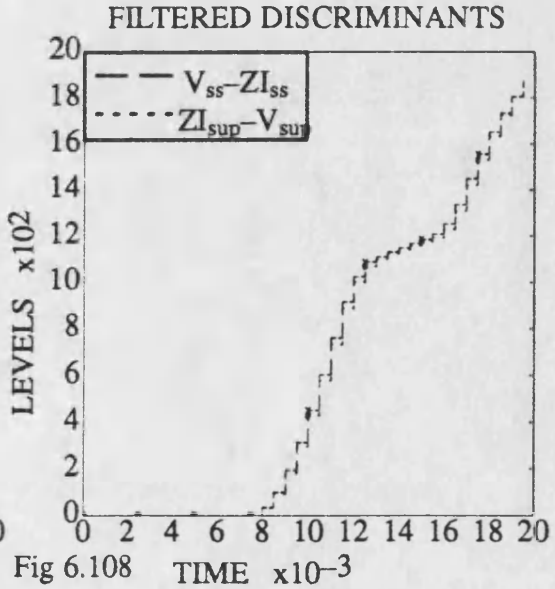

Fig 6.108

CHAPTER 7

CONCLUSIONS

7.1 SIMULATION

7.1.1 FREQUENCY DOMAIN METHOD

The method of deriving and evaluating a frequency spectrum using the Fourier Transform rather than the modified Fourier Transform has proved reliable and accurate. It is less efficient though for the following reasons:

1) More frequency points need to be found: particularly in regions of the spectrum where the value changes rapidly.

2) The Discrete Fourier Transform rather than the Fast Fourier Transform is used to evaluate parts of the spectrum.

However, there are advantages in the use of the the technique:

1) Errors in integration can be quantified (and are used to add further spectrum points in regions of greatest error).

2) The time domain output does not diverge towards the end of the time window.

The inclusion of transducer models in the primary simulation was a success for the CT, but there were initially problems with the CVT. The CT model was a pole–zero model and therefore physically realistic, whereas the CVT model was taken from published data (and the frequency response extrapolated where the data was lacking). However, interpolation in the frequency domain using cubic splines produced output waveforms in the time domain which did not contain any obvious defects.

Comparison of the waveform produced by convolving the power system waveform with the CT model impulse response showed good agreement with the waveform produced when the CT frequency response was included in the system frequency response. It was not found necessary to introduce convergence factors to achieve this result.The comparison was not done for the CVT as there was no reason why the CVT frequency response

should not always be included in the system frequency response. (The non–linearities in the power system to relay voltage transfer function are not modelled).

7.1.2 SIMULATION FEATURES

Several features were introduced to make the simulation more efficient:

1) To generate transient outputs corresponding to the initial fault point on wave and one 90^0 in advance. From these waveforms, the output for any point on wave can be constructed by scaling and addition (provided the system is linear up to that point). If the pair of waveforms are stored, then the simulation can be repeated for any point on wave with only the steady state calculation needing to be done again, which was very useful when relay designs/parameters were being adjusted.

2) For single phase to earth or pure phase faults, the transient output only depends on one voltage, and the stored waveforms for one initial power flow condition can be combined to produce the output of any other. The steady state solutions will be different in each case, but the work in generating them is small in comparison. This feature was used extensively.

3) When power system signals are being generated with the object of convolving them with a transducer impulse response, the upper half of the spectrum must obviously be zero or artificial aliassing will occur. Time will be saved if the matrix is not solved at these frequencies.

4) The solution of the steady state matrix with the assumption that positive sequence sets of currents are injected at the sources rather than positive sequence sets of voltages imposed on the busbars is a necessary improvement. The results for some of the relays tested, i.e. the superimposed component designs, would not have shown to the true extent the problems that lack of transposition produces.

5) The classification of the power system configuration and output options allowed partial automation of results processing, with large files being searched for particular combinations of parameters and graph plots of the cases found being produced automatically.

6) The algorithm for searching for the minimum reach for operation was

found very useful in identifying relay problems, as was information on which element tripped first, as a means of detecting encroachments.

7.1.3 SOURCE SIMULATION

A model of a generator and transformer which was developed was shown to give sub-transient current decay and to produce waveforms in the DR and IMR which were diffrerent to those produced by a simple source model. It is believed that the results more accurately represent the physical system and the models should be considered for use in other simulation studies.

7.2 DIRECTIONAL RELAY

7.2.1 INNOVATIONS

There are three major innovations in this design:

1) The use of one directional detector rather than two or three.

2) The design of the adaptive threshold algorithm produces an output which is close to ideal.

3) The construction of forward current discriminant and threshold which mimic the voltage at the Tee point, simplifies setting of relay sensitivities so that if an external fault can cause a relay to reach a forward directional decision then another relay should always have reached a reverse decision.

7.2.2 INTRODUCTION

This section covers the adaptation of an existing DR design [23] for use in a Teed feeder scheme. The principal difficulty is to maintain the sensitivity of each relay in correct relation to that of the other relays. The requirement may be summarised that a DR may only be allowed to reach a decision indicating a disturbance in a forward direction if, assuming the disturbance were external, one of the other relays could reach a reverse decision. For a plain feeder, a fairly good estimate can be made of conditions at the other end from local quantities. For a Teed feeder, in addition, the estimate requires knowledge of system configuration, source capacities and location of any previous disturbance.

7.2.3 DESIGN DETAILS

1) A sampling frequency of 2 kHz rather than 4 kHz was used, as 2 kHz gives a sufficient number of samples in the desired trip time. A problem was encountered due to travelling waves at a frequency close to 2 kHz being aliassed, which required the power system waveforms to be sampled at 4 kHz, the average of two consecutive samples formed, and the relay fed with that data at a rate of 2 kHz. In effect, the extra stage is acting as a 2 kHz digital notch filter.

2) The current signal is the output of the transactor attached to the CT. No integrating stage is used. The filtering for the current channel is different to that for the voltage to improve the phase match between the signals.

3) Two stages of full cycle superimposed filtering are used as this gives a better shape to the variable threshold than cascaded full and half cycle stages.

4) A single discriminant comprising the sum of the line currents multiplied by the sign of the respective line voltage was chosen to avoid having to co-ordinate the sensitivities of two detectors at each relay.

5) The single current discriminant is compared against a threshold to determine the direction of a disturbance. If this indicates a significant forward disturbance then another check is made by comparing the (separate) forward current discriminant against its threshold. Only if the latter condition is met is the 'forward' counter incremented.

6) The forward discriminant and threshold are composed of superimposed voltage and current in proportions to mimic the voltage at the Tee point. The scaling factor between them reflects the worst case distribution of currents between relays.

7) The current threshold is made to vary according to past values of superimposed current, in order to exclude effects from past disturbances. A new digital algorithm has been developed which enables a faster return of threshold level to normal measurement levels (if appropriate), while not reducing the maximum sensitivity attainable.

8) Separate forward and reverse decision counters are used to allow faster tripping, but suspension of counting for 12.5 ms after a directional decision is needed to prevent the decision process reaching multiple decisions for a single disturbance.

9) Current clipping in Teed feeders is even more troublesome than in plain feeders for DR schemes. The approach adopted is to detect when it occurs at a relay and allow 4 ms. for a directional decision to be reached. If the decision is forward then no action needs to be taken, if reverse, then a reverse signal is broadcast over the communication channel until 50 ms. after clipping was last detected. The local decision counters are reset and local counting is also suspended for this period. This may seem excessive, but the co-ordination of relay sensitivities cannot be achieved when clipping is present at any relay.

7.2.4 PERFORMANCE

Studies to determine the application limits of the DR design are applicable only to the particular Teed feeder configuration studied since the threshold composition and magnitude (which regulate sensitivity) are set using configuration data. In all the studies the initial voltage, current and forward current thresholds were at their minimum permitted levels.

In its final form the DR has a minimum decision time of 2 ms. and a maximum of about 8 ms. The operating time is dependent on fault point on wave and the magnitude of the signals.

In the Tee configuration studied, the main aim was to define the regions for which one relay would detect an internal fault as external. With equal source capacities of 2 GVA at P and R in Fig 1.1b, this region is from the busbar at P to approximately 51 km from P on feeder PT (and similarly on RT). This figure varies by approximately 2 km with fault type and point on wave and always exceeds 40 km even with 50 Ohms fault resistance.

Operation times when the fault on PT is detected as 'forward' by all relays are relatively fast due to a side effect of the composition of the forward current discriminant and threshold. Although the reverse current discriminant may be near a null, the forward current discriminant comfortably exceeds its threshold due to the contribution from superimposed voltage.

7.2.5 APPLICATION TO PREDOMINANTLY CAPACITIVE NETWORKS

Application of the relay design to circuits involving cables and capacitors is likely to prove problematic. In a predominantly capacitative network, a directional criterion which used the relative signs of the superimposed voltage and rate of change of current would give the opposite fault direction to that desired once initial transients had died down. However, once initial transients had died down, the threshold might have exceeded the discriminant and such behaviour would be irrelevant. The initial transient would give the correct directional information, but compared to a directional discriminative process which used superimposed voltage and current, the time during which correct directional information could be derived would be shorter. However for that short initial period the current signal would be changing rapidly, and the rate of change of current would be a more effective discriminant to use.

Problems occur when the directional discriminants do not give the correct directional decision for all time. (They result from the different forward and reverse sensitivities deliberately introduced into the relay, and require additional checks on signal validity as discussed by Barker [23]). Such problems would be worse if the design in this thesis were used in a predominantly capacitive network application, by the same token as they are eliminated for this design in a predominantly inductive network.

7.3 INDEPENDENT MODE RELAY

7.3.1 INTRODUCTION

The IMR described was developed to overcome limitations in DR schemes. From studies done, the main requirements are:

1) No over–reach.

2) Good performance when local source capacity is low.

3) Good fault resistance coverage.

These requirements should be maintained over the whole range of normal operating conditions, and also under power swing conditions, since although the relay would only

make an impedance measurement when the associated DR reach a forward directional decision, it is not inconceivable that such should occur during a power swing.

It will have been noted that issuing of a trip signal in time to allow one cycle fault clearance has not been specified. Although this would obviously be desirable, the author was unable to combine this criterion with the requirements mentioned. Indeed the minimum operating time of the final design is 11 ms comprising 2 ms for the DR operating time, 5 ms delay before counting is permitted and 3 ms counting time. It is certainly possible to achieve reliable relay operation in less than this time using other techniques, which may be more appropriate when operation close to a known high source capacity is anticipated.

The main design problem with any superimposed component impedance measuring technique is pre–fault current which partially determines the voltage(s) at the fault point. This may be illustrated by consideration of a relaying technique which was rejected.

7.3.2 SUPERIMPOSED THRESHOLD TECHNIQUE

It has been found by experiment, that the envelope c.f. 5.7.2 of a relaying waveform which includes a band pass filter (i.e. a transversal filter with m=16) triggered at a certain time, is predominantly determined by the filter characteristics and that time. Hence the maximum value that the filtered output of a unit amplitude waveform applied to the relay can take at any time after triggering may be calculated in advance and stored in ROM. During operation of the relay, the instantaneous value of a filtered quantity could be compared with the value stored in ROM for the time after triggering: if it were greater then a counter could be incremented leading to a possible trip decision.

If the filtered quantity were the fault point voltage, constructed using superimposed relaying voltage and phase shifted superimposed relaying current scaled by a reach factor, then such a scheme would offer potentially very fast tripping, though the operation time would be very dependent on fault point on wave, as discussed in 5.7.1. However, several problems are apparent:

1) A separate threshold would be needed for each fault detector (i.e. a–e, b–e,

c–e, b–c, c–a, a–b) due to the lack of transposition between transmission line conductors.

2) Adjustment of the threshold to take account of the pre–fault voltage at the fault point would inevitably involve either digital multiplication or a very large number of look–up tables in ROM.

3) For a given fault, operation of the relay is only likely at the time when the filtered quantity is maximum. This is a less desirable comparison regime, than one in which one of two quantities is larger than the other for all of the measuring time if a trip is to be issued. The latter would be much less sensitive to noise and signal distortion.

The penalty of ignoring variation of fault point voltage magnitude with pre–fault current and choosing a threshold of say 1.2 p.u. is barely acceptable when high local source capacity is present, and unacceptable (i.e. gross under–reach) when the local source capacity is low.

In view of the implementation problems of the above technique, comparison of the estimate of the value of the fault point voltage constructed using superimposed quantities and that constructed using pre–fault quantities was used as described in the next sub–section.

7.3.3 COMPARISON OF PRE–FAULT AND SUPERIMPOSED QUANTITIES

7.3.3.1 INNOVATIONS

The major innovation is the use of superimposed components, which in turn allows comparison of estimates of fault point voltage and also the different treatment of superimposed current from pre–fault current for earth fault detectors. The reach algorithm is also a new design. It is very stable but slow.

7.3.3.2 INTRODUCTION

The ability to derive superimposed components allows estimates to be formed of the fault point voltage in two ways: using only pre–fault and only superimposed quantities. The relative magnitude of these estimates is used to determine whether a trip counter is to be incremented.

A number of comparison algorithms were investigated and several problems and requirements were identified:

1) Discriminant quantities need to be band pass filtered to reduce the effect of exponential decay in current but also in voltage signals (due to CVT transient).

2) Encroachment between fault detectors was a major problem, particularly for earth fault detectors when phase to phase faults occur in conjunction with large pre–fault power flow.

3) Fault resistance coverage needs to be as large as possible since the DR will operate (detecting an internal fault as external) for large fault resistances. An initial step in this direction is to compare magnitudes of fault point voltage estimates.

7.3.3.3 CHECKS ON SIGNAL VALIDITY

Checks are needed for a number of reasons, some of which are fundamental to distance relaying, and some of which are necessary due to this particular relay implementation:

1) Pre–fault current causes a voltage distribution along the length of a transmission line which can result in the superimposed voltage produced by a fault at one position being larger than that produced by a fault at a closer position. This can lead to over–reaching of the relay. The condition is detected by effectively determining whether the sum of the pre–fault and superimposed currents (scaled and phase shifted) when added to the superimposed fault point voltage increases or decreases the latters magnitude.

2) An obvious requirement is to detect when the voltage magnitude on a line goes through a null due to current flow, since, if the relay reach setting includes the null then tripping would occur. This is fairly easily accomplished by comparing the phase of the superimposed fault point voltage with that of the pre–fault relaying voltage. (In the absence of fault resistance, the phase of the superimposed fault point voltage estimate is reasonably independent of relay setting).

3) The third check is to compare the signs of the superimposed fault point voltage estimate and the (phase shifted) current: if they are in phase then the fault is probably forward, if not, then it is reverse. This is to guard against sequential disturbances.

7.3.3.4 FORMATION OF EARTH FAULT QUANTITIES

One of the main benefits of using superimposed quantities is the ability to prevent earth fault detectors from operating when phase to phase faults occur, by using only zero sequence current in the superimposed fault point voltage estimate. The penalty is a greater tendency for encroachment between earth fault elements, but this does not cause over–reach when it occurs. Encroachment by phase fault detectors for earth faults is not a problem.

7.3.3.5 CORRECTION OF CURRENT PHASE

The effect of untransposition of the line conductors has a large effect on the performance of the relay algorithm, when large pre–fault currents are flowing. This may be effectively corrected by delaying the pre–fault current signals for the fault detector elements by differing numbers of samples, e.g. the a–e element requires a delay of 2 samples, but the b–c element requires no delay. The earth fault detector pre–fault currents need to be zero sequence compensated using the conventional formula.

7.3.3.6 REACH DISCRIMINANT ALGORITHM

In order to reduce point on wave effects, the algorithm combines two versions (90^0 out of phase) of each of the pre–fault and superimposed fault point voltage estimates. This has proved to have excellent performance in terms of reach stability, and freedom from encroachment caused by phase difference between input signals, but the minimum operating time is 11 ms. which is too long for one cycle clearance of faults. However, in Teed feeder applications, reliability of tripping and good performance for resistive faults are higher priorities than speed.

7.3.3.7 EFFECTS OF SOURCE PARAMETERS

Variation of source capacity seems to have small effect on relay performance. At low source capacity, variation of source Z_0/Z_1 does affect relay behaviour, but causes only a slight over–reach. Variation of source X/R (identically for positive and zero sequence capacities) over the range 10 to 30 has a negligible effect.

The correspondence between the pre–fault and superimposed fault point estimates for earth faults at the reach point setting is improved when the new source model is used in simulations.

7.3.3.8 FAULT RESISTANCE PERFORMANCE

Performance for fault resistances of 5Ω and below is acceptable. For resistances of 20Ω and above, the decay of the current offset (for faults other than at voltage maximum) adds an error term which can reduce or increase the likelihood of tripping. With low pre–fault currents, the effect is to cause under–reach, but for high pre–fault currents, the relay will trip for less than the theoretical reach setting (assuming a circular trip zone in the impedance plane centred on zero). Actual over–reach may also be possible during power swings though this did not occur in the results presented.

Since the fault resistance coverage of the IMR design does not equal that of the DR, the addition of IMRs will still leave high fault resistance conditions in which the DR scheme will detect an internal fault as external, but these cases are less common and serious than the ones which would be prevented.

CHAPTER 8

FURTHER WORK

8.1 SIMULATION

8.1.1 POWER ANGLE

One of the most used techniques in this work is the generation of a solution for arbitrary fault point on wave and pre–fault busbar conditions from two stored transient solutions for different points on wave. At present this has only been done for single phase to earth faults or phase to phase faults (which only depend on one voltage at the fault point). This technique could easily be extended to double phase to earth and three phase faults, and would require four and six stored transient solutions respectively.

If it were intended to describe a relay characteristic as a surface with fault point on wave and pre–fault power angle as co–ordinates then the computational savings of using such a technique would be considerable.

8.1.2 GENERATOR MODEL

The generator model developed in this work incorporates several important realistic features, e.g. sub–transient decay of current. This model could easily be used in frequency domain simulation programs using the modified Fourier Transform.

8.2 DIRECTIONAL RELAY

8.2.1 DOUBLE CIRCUIT APPLICATION

The use of a single directional detector rather than three (using phase quantities) or two (using modal quantities) is a great improvement in the concept of directional relaying. The application of this design to double circuit applications should be fairly straightforward and offer the advantage of unambiguous fault direction determination for all types of fault, including inter–circuit faults.

8.2.2 USE OF DIFFERENT CURRENT SIGNAL IN DISCRIMINANT

The construction of a single current discriminant using integrated current signals as in [23] would offer better performance where feeders involving cables were present.

8.2.3 CO–ORDINATION STUDIES

Further work is also needed to validate the co-ordination of relay sensitivities when sequential faults are present. This would require the use of the more sophisticated source models described in this work.

8.3 INDEPENDENT MODE RELAY

8.3.1 PROCESSING OF CURRENT SIGNALS

The results for this relay design have shown how critical it is to produce an accurate estimate of the fault point voltage using pre–fault quantities, and this in turn depends on phase shifting the pre–fault current waveform by an angle which depends on the fault detector element. Since the currents are sampled at 4 kHz, phase shift increments of 4.5^0 would be possible if correction for line untransposition were introduced immediately after digitisation, rather than at a later stage when the effective sampling rate is 2 kHz.

8.3.2 RESISTIVE FAULT COVERAGE

The shape of the protection characteristic of the relay design (excluding the effect of the checks) is theoretically a circle in the impedance plane centred at complex zero. Different combinations of pre–fault voltage quantities and superimposed quantities might be used as in conventional distance relay theory to increase the fault resistance coverage and give a protection characteristic which more closely approached that of a reactance relay.

However the main area of concern is the effect of the fast decay of the current offset for resistive faults which occur at points on wave other than voltage maximum. This effect causes under–reach and has the potential to cause over–reach when large pre–fault currents are flowing. It is difficult to see how this could be overcome using a signal magnitude comparison algorithm.

8.3.3 SUPERIMPOSED THRESHOLD RELAY

The superimposed threshold relay concept (c.f. 7.3.2) might now be considered practicable, since the speed and capability of digital hardware is increasing all the time.

APPENDIX 1

SPECTRUM OF A SWITCHED EXPONENTIAL

This derivation is taken from reference [70].

The function $G(\omega,T)$ may be defined as follows:

$$G(\omega,T)=\int_{-T}^{T} f(t)\exp(-j\omega t)dt$$

Hence the Fourier Transform of function $f(t)$ may be defined:

$$F(\omega)=\lim_{T\to\infty} G(\omega,\ T)$$

However, this process gives a meaningless answer for some signals, e.g.:

$$f(t)=0 \qquad t<0$$

$$f(t)=\exp(jW_0t) \qquad t\geq 0$$

The difficulty may be resolved by redefining ω as the limit of complex frequency $\omega+j\alpha$, as α (which is a small positive real number) tends to zero:

$$\omega=\lim_{\alpha\to 0}(\omega+j\alpha)$$

Where ω approaches W_0, a double limit exists and special care needs to be taken. Writing:

$$u=W_0-\omega$$

For the above choice of $f(t)$:

$$F(\omega)=\lim_{\alpha\to 0}\left(\frac{-1}{ju-\alpha}\right)=\lim_{\alpha\to 0}\left(\frac{u}{j(u^2+\alpha^2)}\right)+\lim_{\alpha\to 0}\left(\frac{\alpha}{(u^2+\alpha^2)}\right)$$

$$\lim_{\alpha\to 0}\left(\frac{u}{j(u^2+\alpha^2)}\right)=\frac{1}{j(\omega-W_0)}$$

Writing:

$$R(\alpha,u)=\frac{\alpha}{u^2+\alpha^2}$$

For any strictly positive α, it is found that:

$$\int_{-\infty}^{\infty} R(\alpha, u)\ du = \pi$$

As α is made smaller, the graph of $R(\alpha,u)$ becomes more and more peaked about the point u=0, but since the area under the graph is constant:

$$\lim_{\alpha \to 0} R(\alpha, u) = \pi\delta(u)$$

The complete spectrum of a complex exponential applied at t=0 therefore consists of two parts:

1) A broad band spectrum:

$$\frac{1}{j(\omega - W_0)}$$

2) An impulse spectrum:

$$\pi\delta(\omega - W_o)$$

From this result the spectra for real sinusoidal signals can be derived.

APPENDIX 2

FAULT RESISTANCE

For complicated fault resistance situations, e.g. an a–b–earth fault with an inter–phase resistance R_{ab} and phase to earth resistances R_a, R_b, the derivation of an equation linking the emf of the superimposed generators with the fault point voltage is not obvious. The first step is to note that the fault point voltage observes the following equation:

$$\mathbf{E_f} = \mathbf{M}\mathbf{V_f} - \mathbf{R_f}\mathbf{C_f}$$

$$\mathbf{M} = \frac{1}{R_{ab}}\begin{bmatrix} R_{ab}-R_a & R_a \\ R_b & R_{ab}-R_b \end{bmatrix} \qquad \mathbf{R_f} = \begin{bmatrix} R_a & 0 \\ 0 & R_b \end{bmatrix}$$

However, to prevent network current flowing in the fault paths (e.g. R_{ab}) before the fault time, the emf of the sources in the fault path have to be increased to E_f' such that they,

rather than the network, supply that current. Setting the network current to be zero gives:

$$\mathbf{E_f'} = \mathbf{ME_f}$$

$$\mathbf{V_f} = \mathbf{M^{-1}(ME_f - R_fC_f)} = \mathbf{E_f - M^{-1}R_fC_f} = \mathbf{E_f - R_f'C_f} \quad \mathbf{R_f'} = \mathbf{M^{-1}R_f}$$

The previous paragraph assumes that the matrix M is not singular, but this may not always be true (physically this means that it is not possible for voltage sources in the fault path to supply the pre–fault fault path current), e.g if R_b is an open circuit in the previous case. The remedy is to add a current source in place of R_b: the first element of the modified source vector E_f" is a voltage, but the second is a current:

$$\mathbf{E_f''} = \mathbf{M'E_f} \qquad \mathbf{V_f} = \mathbf{M'^{-1}E_f - R_fC_f}$$

$$\mathbf{M'} = \frac{1}{R_{ab}}\begin{bmatrix} R_{ab}+R_a & -R_a \\ -1 & 1 \end{bmatrix} \qquad \mathbf{M'^{-1}} = \begin{bmatrix} 1 & R_a \\ 1 & R_a+R_{ab} \end{bmatrix}$$

$$\mathbf{R_f} = \begin{bmatrix} R_a & R_a \\ R_a & R_a+R_{ab} \end{bmatrix}$$

The transforming matrix is now not singular and the desired form of the equation linking V_f' and E_f' can be obtained, with the coefficients of R_f defined above.

APPENDIX 3

PHASE TO PHASE FAULT FORMULATION

A3.1 DERIVATION

For this type of fault there are two faulted phases but only one fault path and current. The source needed in the fault path to prevent pre–fault current flowing is equal to the pre–fault line voltage between those phases. Given the (2*2) admittance equation at the fault point:

$$\begin{bmatrix} C_a \\ C_b \end{bmatrix} = \begin{bmatrix} Y_{aa} & Y_{ab} \\ Y_{ba} & Y_{bb} \end{bmatrix}\begin{bmatrix} V_a \\ V_b \end{bmatrix}$$

Using conditions and definitions:

$$C_a + C_b = 0 \qquad V_f = V_a - V_b \qquad C_f = \frac{C_a - C_b}{2} \qquad V_s = V_a + V_b$$

$$\begin{bmatrix} V_a \\ V_b \end{bmatrix} = \mathbf{M}\begin{bmatrix} V_f \\ V_s \end{bmatrix} \qquad \mathbf{M} = \frac{1}{2}\begin{bmatrix} 1 & 1 \\ -1 & 1 \end{bmatrix} \qquad \mathbf{M}^{-1} = \begin{bmatrix} 1 & -1 \\ 1 & 1 \end{bmatrix}$$

$$\begin{bmatrix} C_a \\ C_b \end{bmatrix} = 2\mathbf{M}\begin{bmatrix} C_f \\ 0 \end{bmatrix} = \begin{bmatrix} Y_{aa} & Y_{ab} \\ Y_{ba} & Y_{bb} \end{bmatrix}\mathbf{M}\begin{bmatrix} V_f \\ V_s \end{bmatrix}$$

This may be rewritten as:

$$\begin{bmatrix} C_f \\ 0 \end{bmatrix} = \frac{1}{2}\mathbf{M}^{-1}\begin{bmatrix} Y_{aa} & Y_{ab} \\ Y_{ba} & Y_{bb} \end{bmatrix}\mathbf{M}\begin{bmatrix} V_f \\ V_s \end{bmatrix} = \begin{bmatrix} Y_{aa}' & Y_{ab}' \\ Y_{ba}' & Y_{bb}' \end{bmatrix}\begin{bmatrix} V_f \\ V_s \end{bmatrix}$$

Where,

$$Y_{aa}' = \frac{Y_{aa} + Y_{bb} - Y_{ba} - Y_{ab}}{4} \qquad Y_{ab}' = \frac{Y_{aa} - Y_{bb} + Y_{ab} - Y_{ba}}{4}$$

$$Y_{ba}' = \frac{Y_{aa} - Y_{bb} - Y_{ba} + Y_{ab}}{4} \qquad Y_{bb}' = \frac{Y_{aa} + Y_{bb} + Y_{ab} + Y_{ba}}{4}$$

Hence,

$$V_s = \frac{-Y_{ba}'}{Y_{bb}'}V_f = Y_{ba}''V_f$$

$$C_f = (Y_{aa}' + Y_{ab}' + Y_{ba}'')V_f = Y_{aa}''V_f$$

If there is no fault resistance then this completes the formulation, since V_f is the spectrum component of the source voltage applied at fault time and V_a, V_b may be recovered by transforming $[V_f, V_s]$ with the matrix M. When fault resistance is present, E_f' rather than V_f is the known quantity, but the two are related by the following equation:

$$V_f = \frac{E_f}{1 + R_f Y_{aa}''}$$

A balanced double phase to earth fault will be modelled if the condition that the sum of the phase currents equal zero is omitted.

A3.2 EXTENSION TO PRINCIPLE

The transformation of the fault point admittance matrix by the connection matrix M has been used to model shunt connections established at fault time. A similar procedure could be used to model the connection of a phase conductor between two points on a network, e.g. reclosure of a single phase.

The principle of inserting voltage sources to make a connection between two nodes and current sources to effect a disconnection was discussed by Johns and Aggarwal [71], but an impedance rather than an admittance system matrix formulation was used.

APPENDIX 4

NOTCH FILTER ANALYSIS

A biquadratic filter function (which approximates a Twin Tee analogue filter) has the following transfer function in the Laplace domain:

$$G(s) = \frac{s^2 + W_0^2}{s^2 + 2\alpha s + W_n^2} = \frac{(s + jW_0)(s - jW_0)}{(s + (\alpha + jW_0))(s + (\alpha - jW_0))} \qquad W_n^2 = W_0^2 + \alpha^2$$

$$\lim_{s \to 0} G(s) = \frac{W_0^2}{W_n^2} \qquad \lim_{s \to \infty} G(s) = 1$$

If α is small, i.e. the notch is sharp, then the low frequency gain should also approximate unity.

Applying a sinusoidal wave form $b(t)$ at t=0 to this filter gives the output waveform $c(t)$:

$$b(t) = \cos(W_0 t + \phi) \qquad t > 0 \qquad B(s) = \frac{s\cos(\phi) - W_0 \sin(\phi)}{s^2 + W_0^2}$$

$$C(s) = G(s)B(s) = \frac{s\cos(\phi) - W_0 \sin(\phi)}{s^2 + 2\alpha s + W_n^2}$$

Hence,

$$c(t) = \exp(-\alpha t)\left[\cos(\phi)\left(\cos(W_0 t) - \frac{\alpha}{W_0}\sin(W_0 t)\right) - \sin(\phi)\sin(W_0 t)\right]$$

$$= \exp(-\alpha t)\left(1 + \frac{2\alpha\sin(\phi)}{W_0} + \frac{\alpha^2}{W_0^2}\right)\cos(W_0 t + \psi)$$

$$\tan(\psi) = \frac{1}{\cos(\phi)}\left(\sin(\phi) + \frac{\alpha}{W_0}\right)$$

Hence for small α, the output is very similar to the theoretical output $b(t)$.

A notch filter similar to this was used by Chamia and Liebemann [2] in their relay design. It can be seen that although there is a zero in the transfer function at power frequency, which rejects the pre–fault steady state component, most of the energy in the output signal is still concentrated about power frequency.

A similar derivation could be carried out in the frequency domain using the results in Appendix 1. The pre–fault spectrum impulses at $\omega=W_0$ and $-W_0$ are removed by the zeros in $G(\omega)$. The continuous part of the spectrum of $B(\omega)$ modified by the notch filter frequency response therefore determines the output, and the shape of the notch around power frequency can be seen to be very significant.

The differences between the Laplace and frequency domain representations of a time domain signal are due to the Laplace variable s having a small negative real part, which allows the conceptual difficulties of the frequency domain approach to be avoided. The restriction that the time domain signal must be zero for $t<0$ means that the pre–fault conditions cannot be included in the formulation. However, the system response to stimuli after that time can be found using either technique, though the Laplace Transform method is more familiar and easier to use for algebraically defined frequency responses.

The difference between the theoretical and practical definitions of superimposed components can be seen in the difference between the spectra $B(\omega)$ and $C(\omega)$: the theoretical definition includes impulses in the superimposed component spectrum; the practical one

does not, but the part of the continuous spectrum removed by the filtering has the form of the function $R(\alpha,u)$ defined in Appendix 1. For small t it is not surprising that the two signals should approximately cancel.

APPENDIX 5

SEQUENCE AND MODAL COMPONENTS

Sequence or modal components rather than phase components are often used when unbalanced currents and voltages (usually caused by unbalanced impedances) exist in three phase networks, as they make understanding and solution of the problem easier.

Sequence components use the fact that in the frequency domain an arbitrary voltage or current distribution between the phases of a three phase system may be resolved into three orthogonal sets of complex phasors:

1) The zero sequence set (with suffix 0).

2) The positive sequence set (with suffix 1).

3) The negative sequence set (with suffix 2).

Each set is dependent on one complex quantity.

The sequence components of e.g. the phase voltages may be found by transforming the spectra of the phase quantities:

$$\mathbf{V}_{012}(\omega) = \begin{bmatrix} V_0(\omega) \\ V_1(\omega) \\ V_2(\omega) \end{bmatrix} = \mathbf{M}^{-1}\mathbf{V}_{abc}(\omega) = \frac{1}{3}\begin{bmatrix} 1 & 1 & 1 \\ 1 & h & h^2 \\ 1 & h^2 & h \end{bmatrix}\begin{bmatrix} V_a(\omega) \\ V_b(\omega) \\ V_c(\omega) \end{bmatrix}$$

The orthogonal transformation matrix M and its inverse are frequency independent. If the phase voltages and currents are related by an impedance matrix, then the sequence quantities are similarly related:

$$\mathbf{V}_{abc}(\omega) = \mathbf{Z}_{abc}(\omega)\mathbf{C}_{abc}(\omega) \qquad \mathbf{V}_{012}(\omega) = \mathbf{Z}_{012}(\omega)\mathbf{C}_{012}(\omega)$$

Since the same transformation matrix is used to transform currents as voltages, the sequence impedance matrix is defined:

$$\mathbf{C}_{abc}(\omega) = \mathbf{M}\mathbf{C}_{012}(\omega) \qquad \mathbf{Z}_{012}(\omega) = \mathbf{M}^{-1}\mathbf{Z}_{abc}(\omega)\mathbf{M}$$

The use of sequence quantities to define generator parameters is related to the physical interpretation that positive and negative currents of angular frequency ω have in a generator: the former produce a magnetic field which rotates in the same direction as the rotor; the latter rotates in the opposite direction. Hence the impedance presented to positive and negative sequence currents is very different, as shown in the respective synchronous and transient inductances. The zero sequence parameters are usually ignored as there is always a delta–star transformer which prevents zero sequence transmission line fault currents reaching the generator.

If the generator rotor is rotating at an angular velocity W_0, then the apparent frequency of a positive sequence set of currents will be $\omega - W_0$, and that of a negative sequence set $-\omega - W_0$ or $\omega + W_0$.

The selection of transformations for power systems problems is discussed in [72].

APPENDIX 6

SEQUENCE NETWORK CONNECTIONS

A6.1 NETWORK CONNECTION FOR AN EARTH FAULT

To satisfy the conditions for an a–e fault that the b and c phase fault currents are zero:

$$C_b = C_0 + hC_1 + h^2C_2 = 0 \quad C_c = C_0 + h^2C_1 + hC_2 = 0 \quad C_0 = C_1 = C_2$$

The sequence networks must be connected in series at the fault point, as shown in Fig 3.1. The following equations define the exciting signal and network impedance:

$$e(t) = \exp(jW_0t) \qquad E(s) = \frac{1}{s - jW_0}$$

$$Z(s) = 2RS1 + 5R1 + Rf + RS0 + s(2LS1 + 5L1 + LS0) = R_x + sL_x$$

Hence the transform of the current is:

$$C(s) = \frac{E(s)}{Z(s)} = \frac{1}{(s - jW_0)(R_x + sL_x)} = \frac{A}{s - jW_0} + \frac{B}{R_x + sL_x}$$

Where,

$$A = \lim_{s \to jW_0} \left(C(s)(s - jW_0)\right) \qquad B = \lim_{s \to \frac{-R_x}{L_x}} \left(C(s)(R_x + sL_x)\right)$$

At this stage the sequence currents should be transformed into phase currents, and the inverse Laplace transform applied to the phase currents. The a phase current will have the form:

$$c_a(t) = \frac{1}{R_x + jW_0L_x}\left[\exp(jW_0t) - \exp\left(\frac{-tR_x}{L_x}\right)\right]$$

The Laplace Transform of the voltage drop across the positive sequence source impedance is:

$$V(s) = \frac{RS1 + sLS1}{(s - jW_0)(R_x + sL_x)}$$

$$= \frac{1}{R_x + jW_0L_x}\left(\frac{LS1R_x - RS1L_x}{L_x(s - jW_0)} + \frac{RS1 + jW_0LS1}{R_x + sL_x}\right)$$

$$VS1 = E(s) - ZS1C(s) = E(s) - V(s) \qquad VS2 = -ZS2C(s) = -ZS1C(s)$$

The voltage drop $VS0$ in the zero sequence source impedance $ZS0$ may be similarly found and hence the busbar sequence voltages and phase voltages.

A6.2 NETWORK CONNECTION FOR A PHASE TO PHASE FAULT

For a b–c fault the a–phase fault current is zero and the sum of the b and c phase fault currents is zero:

$$C_a = C_0 + C_1 + C_2 = 0 \qquad C_b + C_c = 2C_0 - C_1 - C_2 = 0$$

$$C_0 = 0 \qquad C_1 + C_2 = 0$$

These conditions require that the positive and negative sequence networks be connected in parallel as shown in Fig 3.2. The network impedance is defined:

$$Z(s) = 2RS1 + 2R1 + Rf + 2s(LS1 + L1) = R_x + sL_x$$

This has the same form as that for the a–e fault and a similar solution process may be used.

A6.3 NETWORK CONNECTION FOR A DOUBLE PHASE TO PHASE FAULT

For a double phase to earth (b–c–e) fault, the only constraint is that the a phase fault current is zero:

$$C_a = C_0 + C_1 + C_2 = 0$$

This requires that the sequence networks be connected in parallel, as shown in Fig 3.3. If fault resistance is present then there is a choice of using a pi or star fault resistance network. The star connection is used since it makes solution easier and transformations exist between pi and star networks.

If a network consists of three branches in parallel, with branch impedances Z_0, Z_1, Z_2, and a source E in branch 1, then the branch currents may be defined:

$$C_0 = \frac{-EZ_2}{Z_x} \qquad C_1 = \frac{E(Z_0 + Z_2)}{Z_x} \qquad C_2 = \frac{-EZ_0}{Z_x}$$

$$Z_x = Z_0Z_1 + Z_0Z_2 + Z_1Z_2$$

Each of the branch impedances consists of an inductive and a resistive term, and Z_x therefore represents a quadratic in s. Solving this quadratic will give two roots p,q and if the roots are distinct, each of the sequence currents may be expressed:

$$C(s) = \frac{A}{s-p} + \frac{B}{s-q} + \frac{D}{s-jW_0}$$

The coefficients A,B,D may be assigned with the help of the cover up rule , and correspond to a complex time domain output of:

$$c(t) = A\exp(pt) + B\exp(qt) + D\exp(jW_0t)$$

A6.4 NETWORK CONNECTION FOR A THREE PHASE FAULT

For an unbalanced fault, the network could be the same as for the b–c–e fault but with an extra fault resistance across the positive sequence network at the fault point. In view of the infrequent occurrence of these faults on the power system, it was not considered worthwhile to construct and solve this network. (The three decay constants are the roots of a complex cubic polynomial.)

Accidental energisation of the system with earthing clamps in place is a more common occurrence, and may be modelled as a balanced fault, for which the network connexion consists of a single loop (Fig 3.4) of impedance $Z(s)$:

$$Z(s) = R1 + Rf + s(LS1 + L1) = R_x + sL_x$$

Thus it may be solved in the same manner as an a–e fault.

A6.5 EMPIRICAL SOURCE MODEL FORMULATION

The sequence network connections using the simplified source model (Fig 2.14) for an a–e fault are drawn in Fig 3.5. The Laplace Transform of the impedance $Z(s)$ is:

$$Z(s) = 5R1 + 2R_a + RS0 + Rf + s(5LS1 + L1 + LS0)$$

$$+ sL''\left(\frac{s+a+jW_0}{s+b+jW_0} + \frac{s+a-jW_0}{s+b-jW_0}\right) = \frac{P(s)}{Q(s)} \qquad b = \frac{L_d'' - L_l}{L_d' - L_l}$$

Where $P(s)$ is a complex cubic polynomial in s, $Q(s)$ is a complex quadratic).
Hence the current C(s) in the network is:

$$C(s) = \frac{EQ(s)}{(s-jW_0)P(s)} = \frac{A}{s-p} + \frac{B}{s-q} + \frac{D}{s-r} + \frac{F}{s-jW_0}$$

Where p,q,r are the complex roots of $P(s)$, which may be found algebraically [73]. The values of the coefficients A,B,D,F may be found using the cover rule. Hence the Laplace phase currents may be obtained by transforming the sequence currents (which are equal). The impedance of the positive sequence source ZS1 may be expressed:

$$ZS1 = \frac{R(s)}{s+b-jW_0}$$

Where $R(s)$ is a complex quadratic in s. The zero sequence component of voltage at the relaying point may be decomposed into the same partial fractions as $C(s)$, but the other sequence voltages require an extra faction (having the same denominator as that of ZS1) From these, the Laplace domain phase voltages (as in A3.1) and then the time domain phase voltages may then be obtained.

The procedure for a pure phase to phase fault and the balanced three phase fault are similar since only one current loop exists. For a double phase to earth fault, the separation of the expressions for current and voltage in the Laplace domain into partial factors requires the solution of a complex quartic polynomial (Z_x using the notation of A6.3). Quartic polynomials may be solved algebraically [73], but the formulae are rather complicated. Each current and voltage in the time domain has four delaying components and one steady state sinusoidal component.

APPENDIX 7

FILTER POWER FREQUENCY PARAMETERS

A7.1 DEFINITIONS

In the following formulae, the value of the sampling interval T appears frequently. It takes the value 0.5 ms for a sampling rate and 0.25 ms for a 4 kHz sampling rate. The variable z is related to the angular frequency by the following equation:

$$z = \exp(j\omega T)$$

It takes the value unity at zero frequency and –1 at Nyquist frequency.

A7.2 RUNNING AVERAGE FILTER

The frequency response $G(z)$ may be found as follows:

$$G(z) = \frac{1}{m}\sum_{i=0}^{i=m-1}\left(\frac{1}{z}\right)^i = \frac{1}{m}\frac{1-z^{-m}}{1-z^{-1}} \qquad G(1) = 1$$

$$G(-1) = 0, \quad m = 2,4,6,.... \qquad G(-1) = \frac{1}{m}, \quad m = 1,3,5,7,...$$

The filter bandwidth can be calculated from the z transform expression using the formula:

$$\left|\frac{1-z^{-m}}{1-z^{-1}}\right| = \sqrt{2} \qquad \cos(m\omega T) = \mathrm{Re}(z^{-m})$$

The following equation is solved for ω:

$$2\cos(m\omega T) - \cos(\omega T) - 1 = 0$$

The running average filter bandwidths (for 2 kHz sampling rate) are tabulated below, (those for 4 kHz sampling rate are double):

m	wT	bw(Hz)
2	2.4189	770
4	1.3430	427
8	0.7222	230
16	0.3762	120
32	0.1920	61

The gain at power frequency can also be found from the z transform expression. The results are normalised (divided by m) and tabulate below for different sampling rates:

	2 kHz		4 kHz	
m	gain	phase	gain	phase
2	0.9970	-4.5^0	0.9991	-2.25^0
4	0.9847	-13.5^0	0.9961	-6.75^0
8	0.9366	-31.5^0	0.9838	-15.75^0
16	0.7577	-67.5^0	0.9357	-33.75^0
32	0.2341	-139.5^0	0.7570	-69.75^0

The group delay D, (where applicable) is simply:

$$D = 0.5(m-1)T$$

A7.2 RECURSIVE LOW PASS FILTER

The frequency response may be found as follows:

$$G(z) = \frac{z}{1-m+mz} \qquad G(1) = 1 \qquad G(-1) = \frac{1}{2m-1}$$

The recursive low pass filter bandwidth can be calculated from the z transform expression using the formula:

$$\left| m - \frac{m-1}{z} \right| = \sqrt{2}$$

Hence,

$$\cos(\omega T) = \mathrm{Re}\left(z^{-1}\right) = 1 - \frac{1}{2m(m-1)}$$

The bandwidths (for 2 kHz sampling rate) are tabulated below, (those for 4 kHz sampling rate are double):

m	cos(ωT)	ωT	bw(Hz)
2	.75	0.7227	230
4	.9583	0.2897	92
8	.9911	0.1337	43
16	.9979	0.06456	21
32	.9995	0.03175	10

The low pass recursive filter gain at power frequency can also be found from the z transform expression. The results are tabulated below for different sampling rates:

	2 kHz		4 kHz	
m	gain	phase	gain	phase
2	0.976	-8.78^0	0.994	-4.47^0
4	0.879	-24.4^0	0.965	-13.1^0
8	0.648	-45.2^0	0.862	-28.3^0
16	0.380	-63.2^0	0.635	-48.4^0
32	0.198	-74.1^0	0.375	-65.8^0

The group delay D, (where applicable) may be found from the formula:

$$D = \frac{T(m-1)(1-m+m\cos(\omega T))}{1+2m(m-1)(1-\cos(\omega T))}$$

m	2 kHz	4 kHz
2	0.46 ms	0.24 ms
4	1.10 ms	0.69 ms
8	*	1.28 ms

A7.3 DIFFERENCING OVER A DELAY

The power frequency gain and phase are tabulated below:

	2 kHz		4 kHz	
m	gain	phase	gain	phase
1	0.1569	85.5^0	0.0961	87.75^0
2	0.3129	81^0	0.1569	85.5^0
3	0.4669	76.5^0	0.2351	83.25^0
4	0.6180	72^0	0.3129	81^0
5	0.7654	67.5^0	0.3902	78.75^0
6	0.9080	63^0	0.4669	76.5^0
7	1.0450	58.5^0	0.5429	74.25^0
8	1.1756	54^0	0.6180	72^0

A7.4 DIFFERENCING USING A LOW PASS FILTER

The z transform of the gain is:

$$G(z) = \frac{(m-1)(1-z^{-1})}{m-(m-1)z^{-1}}$$

The differencer (using a low pass filter) power frequency and phase are tabulated below:

	2 kHz		4 kHz	
m	gain	phase	gain	phase
2	0.153	76.7^0	0.078	83.3^0
4	0.414	61.1^0	0.227	74.4^0
8	0.712	40.3^0	0.474	59.5^0
16	0.895	22.3^0	0.748	39.4^0
32	0.965	11.4^0	0.913	22.0^0

A7.5 DIFFERENCING USING 2 LOW PASS FILTERS

The filter constants used are (m,4m). The z transform of the gain is:

$$G(z) = \frac{1}{m-(m-1)z^{-1}} - \frac{1}{4m-(4m-1)z^{-1}}$$

$$= \frac{3m(1-z^{-1})}{(m-(m-1)z^{-1})(4m-(4m-1)z^{-1})}$$

The power frequency gain and phase are tabulated below:

	2 kHz		4 kHz	
m	gain	phase	gain	phase
2	0.596	31.5^0	0.404	55^0
4	0.629	-2.2^0	0.578	26.3^0

A7.6 TRANSVERSAL FILTER

The frequency response may be found as follows:

$$G(z) = \sum_{i=0}^{m} b(i)z^{-i} = \frac{m - mz^{-m-2} + (m+2)(z^{-m-1} - z^{-1})}{m\left(1-z^{-1}\right)^2}$$

The power frequency gain and phase are tabulated below:

	2 kHz		4 kHz	
m	gain	phase	gain	phase
4	0.7744	72^0	0.5077	78.75^0
8	2.2438	54^0	1.1380	72.05^0
16	6.6770	18^0	3.8310	45^0

REFERENCES

1 Aggarwal R.K. & Johns A.T.; IEEE PWRD–1 Jan '86 pp 125,134; The Development of a New High Speed 3–Terminal Protection Scheme

2 Chamia M. & Liebermann S.; IEEE PAS–97 Nov/Dec '73 pp 2104–2116; Ultra High Speed Relay for EHV/UHV Transmission Lines – Development, Design and Application

3 Okamura M., Andow F., Mitani I.,Okita Y. & Masui M.; IEEE PAS–99 Jul '80 pp1426,1435; Development of New Relays with Significantly Improved Performance Against Badly Distorted Waveforms

4 Dommel H.W. & Meyer W.S.; IEEE PAS–93 Sep/Oct '74 pp 1401,1409; Numerical Modelling of Frequency Dependent Transmission Line Parameters in an Electromagnetics Transients Program

5a Day S.J., Mullineux N. & Reed J.R.; IJEEE Vol 3 1965 pp 501,506; Developments in Obtaining Transient Response using Fourier Integrals Part 1: Gibb's Phenomena and Fourier Integrals

5b Day S.J., Mullineux N. & Reed J.R.; IJEEE Vol 4 1966 pp 31,40; Part 2: Use of Modified Fourier Transform

5c Day S.J., Mullineux N., Reed J.R. & Battisson M.J.; IJEEE Vol 6 1968 pp 259,265; Part 3: Global Response

5d Mullineux N. & Reed J.R.; IJEEE Vol 10 1972 pp 256,267; Part 4: Survey of the Theory

6 Concordia C. & Brown P.G.; IEEE PAS–90 Sep/Oct '71 pp 2211,2218; Effects of Trends in Large Steam Turbine Driven Generator Parameters on Power System Stability

7 Bozoki B., Benney J.C. & Usas W.V.; IEEE PAS–104 Apl '85 pp 865,872; Protective Relaying for Tapped High Voltage Transmission Lines

8 IEEE Power Systems Relaying Committee; PSRC Special Report No. 79 TH0056–2–PWR 1979; Protection Aspects of Multi–Terminal Lines

9 Hicks K.L, & Butt W.H.; IEEE PAS–99 Nov/Dec '80 pp 2138,2145; Feasibility and Economics of Ultra High Speed Fault Clearing

10 Electricity Council; Power System Protection Vol 2 pp 66,163

11 Griffin C.H.; IEEE PAS–102 Feb '83 pp 420–432; Principles of Ground Relaying for High Voltage and Extra High Voltage Transmission Lines

12 Electricity Council; Power System Protection Vol 2 pp 164,275

13 Johns A.T.; PIEE Vol 127 Pt C Jul '80 pp 228,239; New Ultra–High–Speed Directional Comparison Technique for the Protection of E.H.V. Transmission Lines

13a Disscussion; PIEE Vol 128 Pt C May '81 pp 169,172

14 Thorp J.S., Phadke A.G., Horowitz S.H. & Beehler J.E.; IEEE PAS–98 Jan/Feb '79 pp 246,260; Limits to Impedance Relaying

15 Electricity Council; Power System Protection Vol 3 p 343

16 Electricity Council; ibid pp 376,382

17 Okamura M., Andow F. & Suzuki S.; IEEE PAS–99 Mar/Apr '80 pp 522,527; Improved Phase–Comparison Relaying with Higher Performance

18 Sachdev M.S. & Barabeau: IEEE PAS–98 Nov/Dec '79 pp 2232,2240; A New Algorithm for Digital Impedance Relays

19 Girgis A.A. & Brown R.G.: IEEE PAS–100 Jul '81 pp 3387,3395; Application of Kalman Filtering in Computer Relaying

20 Johns A.T. & Martin M.A.; PIEE Vol 130 Pt C May '80 pp 127,138; New Ultra–High–Speed Distance Protection Using Finite–Transform Techniques

21 Kudo H., Watanabe a., Seo K., Ohura Y. & Matsuzawa K.; IEEE PAS–104 Dec '85 pp 3518,3523; Development of New Distance Relays to Cope with Natural Frequency Transients in UHV/EHV Transmission Systems

22 Wedepohl L.M.; PIEE Vol 112 1965 pp 525.535; Polarised Mho Distance Relay

23 Barker A.; PhD. Thesis University of Bath Jun '84; Wave Differential Protection of EHV Transmission Lines

24 Johns A.T., Martin M.A., Barker A., Walker E.P. & Crossley P.A.; IEEE PWRD–1 Apr '86 pp 24,34; A New Approach to EHV Directional Comparison Protection using Digital Signal Processing Techniques

25 Engler F., Lanz O.E., Haenggli M. & Bacchini G.; IEEE PAS–104 Jun '85 pp 1463,1473; Transient Signals and their Processing in an Ultra High Speed Directional Relay for EHV/UHV Line Protection

26 Dommel H.W. & Michels J.M.; IEEE PES Winter Meeting Paper A78 214–9; High Speed Relaying Using Travelling Wave Transient Analysis

27 Rajendra S. & McLaren P.G.; IEEE PAS–104 Dec '85 pp 3544,3550; Travelling Wave Techniques Applied to the Protection of Teed Circuits: Multi–phase–Multi–circuit System

28 Carson J.R.; Bell System Technical Journal Vol 5 1926 pp 539,554; Wave Propagation in Overhead Wires with Ground Return

29 Wise W.H.; Bell System Technical Journal Vol 27 1948 pp 365,371; Potential Coefficients for Ground Return Circuits

30 Ovick N.L. & Kusic G.L.; IEEE PAS 103 Dec '84 pp 3643,3649; Including Corona Effects for Travelling Waves on Transmission Lines

31 Dommel H.W.; IEEE PAS–88 Apr '69 pp 388,399; Digital Computer Solution of Electromagnetic Transients in Single and Multiphase Networks

32 Budner A.; IEEE PAS–89 Jan '70 pp 88,97; Introduction of Frequency Dependent Line Parameters into an ELectromagnetic Transients Program

33 Snelson J.K; IEEE PAS–91 '72 pp 85,90; Propagation of Travelling Waves on Transmission Lines: Frequency Dependent Parameters

34 Ametani A.; IEEE PAS–95 '76 pp 1545,1549; A Highly Efficient Method for Calculating Transmission Line Transients

35 Semlyen A. & Dabuleanu A.; IEEE PAS –94 Mar/Apr '75 pp 561,571; Fast and Accurate Switching Transient Calculations on Transmission Lines with Ground Return using Recursive Convolutions

36 Semlyen A. & Brierley R.H.; IEEE PAS–103 Dec '84 pp 3579,3586; Stability Analysis and Stabilising Procedure for a Frequency Dependent Transmission Line Model

37 Triezenberg D.M.; IEEE PAS–98 Mar/Apr '79 pp 484,492; An Efficient State Variable Transmission Line Model

38 Marti J.; IEEE PAS–101 Jan '82 pp 147,157; Accurate Modelling of Frequency Dependent Transmission Lines in ELectromagnetic Transient Simulations

39 Semlyen A. & Abdel–Rahman M.H.; IEEE PAS–101 Sep '82 pp 3576,3584; Transmission Line Modelling by Rational Transfer Functions

40 Humpage W.D.; IEE Power Engineering Monograph (Series 3); Z–transform Electromagnetic Transient Analysis in High–Voltage Networks (Published by Peter Peregrinus)

41 Cochran W.T., Cooley J.W. et al.; Proc. IEEE Vol 55 Oct '67 pp 1664,,1674; What is the Fast Fourier Transform?

42 Lego P.E. & Sze T.W.; Trans AIEE Vol 77 Pt 1 1958 pp 1031,1036; A General Approach for Obtaining Transient Response by the Use of a Digital Computer

43 Lanczos C.; Applied Analysis (Published by Pitman) pp 263–267

44a Mullineux N. & Reed J.R.; PIEE Vol 118 Mar?Apr '71 p 602; Frequency Dependent Parameters in Transmission Line Analysis

44b ibid pp 1815,1819; Discussion

45 Ametani A.; IJEEE Vol 10 1972 pp 277,287; The Application of the Fast Fourier Transform to Electrical Transient Phenomena

46 Johns A.T. & Aggarwal R.K.; PIEE Vol 123 Apr '76 pp 353,359; Digital Simulation of Faulted E.H.V. Transmission Lines with Particular Reference to Very–High–Speed Protection

47 Dommel H.W., Yan A. & Wei S.; IEEE PWRD–1 Apr '86 pp 209,215; Harmonics from Transformer Saturation

48 Dick A.F.; IEEE PAS–100 Jan '81 pp 409,419; Transformer Models for Transient Studies

49 German D.W.; IEEE PAS–101 Nov '81 pp 4510,4514; The Simulation of Transformer Feeders Following Switching Operations

50 Avila–Rosales J. & Alvarado F.L.; IEEE PAS–101 Nov '82 pp 4281,4288; Non–linear Frequency Dependent Transformer Model for Electromagnetic Transient Studies in Power Systems

51 Semlyen A. & Avila–Rosales J.; IEEE PAS–104 Nov '85 pp 3189,3194; Iron Core Modelling for Electrical Transients

52 Park R.H.; Trans AIEE Vol 48 Jul '29 pp 716,727; Two Reaction Theory of Synchronous Machines–1

53 Kilgore L.A.; Trans AIEE Vol 50 Dec '31 pp 1201,1214; Calculation of Synchronous Machine Constants

54 Jackson W.B. & Winchester R.L.; IEEE PAS–88 Jul '69 pp 1121,1136; Direct– and Quadrature– Axis Equivalent Circuits for Solid–Rotor Turbine Generators

55 Sharma D., Baker D., Dougherty J., Kankan M., Minnich S. & Shulz R.; IEEE PAS–104 Jul '85 pp 1812,1821; Generator Simulation–Model Constants by Finite Element: Comparison with Test Results

56 Barret P., Colot Y., Herourd M., Meyer J., Michard J. & Monville J.; IEEE PAS–100 Aug '81 pp 3993,4006; Modelling and Tests at Fessenheim Power Station of a 1080MVA Turbo–Alternator and of its Excitation System

57 El–Kateb M.M.T. & Johns A.T.; PIEE Vol 124 Mar '77 pp 223,229; Frequency Domain Digital Simulation of Synchronous Generators Operating Under Faulted Conditions

58 Watson W. & Manchur G.; IEEE PAS–93 May/Jun '74 pp 777,784; Synchronous Machine Operational Impedances from Low Voltage Measurements

59 Hurley J.D. & Schwenk H.R.; IEEE PAS–100 Feb '81 pp 828,826; Standstill Frquency Response Modelling and Evaluation by Field Tests on a 645 MVA Turbine Generator

60 Wright S.H.; Trans AIEE Vol 50 dec '31 pp 1331,1351; Determination of Synchronous Machine Constants by Test

61 Brandwajn V.; IEEE PAS–99 Sep/Oct '80 pp 1918,1926; Representation of Magnetic Saturation in theSynchronous Machine Model in an Electromagnetic Transients Program

62 Warrington A.R. van C.; Protective Relays and their Practice (Published by Chapman & Hall); Section 11.6

63 Jahnke E. & Emde F.; Tables of Functions with Formulae and Curves; (Published by Dover)

64 Morched A.S., Tench G.A. & Kundar P.; IEEE PAS–100 Aug '81 pp 3785,3790; Accurate Calculation of Assymmetrical Fault Currents in Complex Power Systems

65 Galloway R.H., Shorrocks W.B. & Wedepohl L.M.; PIEE Vol 111 Dec '64 pp 2051,2059; Calculation of Electrical Parameters for Short and Long Polyphase Transmission Lines

66 Hammond P.; Applied Electromagnetism (Published by Pergamon); Section 8.9

67 Stalewski a. & Weller G.C.; PIEE Vol 126 Nov '79 pp 1186,1195; Novel Capacitor–divider Voltage Sensors for High Voltage Transmission Systems

68 Hughes M.A.; PIEE Vol 121 Dec '74 pp 1557,1566; Distance Relay Performance as Affected by Capacitor Voltage Transformers

69 Korponey N.E.; IEEE PAS–97 Mar/Apr '78 pp 569,573; Non–gapped Cores, Anti–remanence Gapped Cores or Linear Cores for Current Transformers

70 Mason S.J. & Zimmermann H.J.; Electronic Circuits, Signals and Systems; (Published by Wiley) pp 373,376

71 Johns A.T. & Aggarwal R.K.; PIEE Vol 128 Jul '81 pp 183,195; Digital Simulation of Fault Auto–reclosure Sequences with Particular Reference to the Performance Evaluation of EHV Transmission Lines

72 Long R.W. & Gelopulos D.; IEEE PAS–101 Oct '82 pp 4055,4063; Component Transformations – Eigenvalue Analysis Succinctly Defines Their Relationship

73 Dehn E.; Algebraic Equations; (Published by Dover) pp 11,13